WL-TR-96-3111

FLUTTER PREVENTION HANDBOOK: A PRELIMIARY COLLECTION

D.D. LIU
D. SARHADDI
F.M. Piolenc
ZONA Technology, Inc.
2651 W. Guadalupe Rd, Ste B-228
Mesa AZ 85202

L.S. Wasserman   W. Roberts
Delta Dynamics Inc.

R.E. Donham and G.A. Watts   R.P. Peloubet, Jr.
RED Inc.

MARCH 1997

FINAL REPORT FOR THE PERIOD JAN   1995 - JUNE 1996

DTIC QUALITY INSPECTED 2
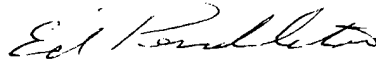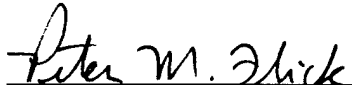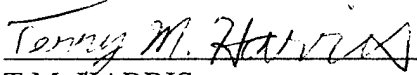
19970730 074

NOTICE

When Government drawings, specification, or other data are used for any purpose other than in connection with a definitely Government-related procurement, the United States Government incurs no responsibility or any obligation whatsoever. The fact that the Government may have formulated or in any way supplied the said drawings, specifications, or other data, is not to be regarded by implication, or otherwise in any manner construed, as licensing the holder, or any other person or corporation, or as conveying any rights or permission to manufacture, use, or sell any patented invention that may in any way be related thereto.

This report is releasable to the National Technical Information Service (NTIS). At NTIS, it will be available to the general public, including foreign nations.

This technical report has been reviewed and is approved for publication.

E.W. PENDLETON
L.J. HUTTSELL
Project Engineers
Vibration & Aeroelasticity Branch

P.M. FLICK
Core Area Leader
Structural Technology Integration

T.M. HARRIS
Acting Chief, Vibration & Aeroelasticity Branch
Structures Division

If your address has changed, if you wish to be removed from our mailing list, or if the addressee is no longer employed by your organization, please notify, WL/FIBV, Bldg 45, 2130 Eighth St Ste 1, WPAFB OH 45433-7542 to help us maintain a current mailing list.

Copies of this report should not be returned unless return is required by security consideration, contractual obligations, or notice on a specific document.

REPORT DOCUMENTATION PAGE

1. AGENCY USE ONLY (Leave blank)	2. REPORT DATE	3. REPORT TYPE AND DATES COVERED
	MARCH 1997	FINAL 01/01/95--06/01/96

4. TITLE AND SUBTITLE
FLUTTER PREVENTION HANDBOOK: A PRELIMINARY COLLECTION

5. FUNDING NUMBERS
C   F33615-94-C-3200
PE   62201
PR   2401
TA   TI
WU   00

6. AUTHOR(S)
D.D. LIU, D. SARHADDI, F.M. PIOLENC, ZONA TECHNOLOGY;
L.S. WASSERMAN, DELTA DYNAMICS INC.; R.E. DONHAM/G.A. WATTS, RED INC.; W. ROBERTS; AND R.P. PELOUBET, JR

7. PERFORMING ORGANIZATION NAME(S) AND ADDRESS(ES)
ZONA TECHNOLOGY, INC
2651 W GUADALUPE RD STE B-228
MESA AZ 85202

8. PERFORMING ORGANIZATION REPORT NUMBER

9. SPONSORING/MONITORING AGENCY NAME(S) AND ADDRESS(ES)
FLIGHT DYNAMICS DIRECTORATE
WRIGHT LABORATORY
AIR FORCE MATERIEL COMMAND
WRIGHT PATTERSON AFB OH 45433-7562
POC: Larry Huttsell/Ed Pendleton, WL/FIBGE, 937-255-7384

10. SPONSORING/MONITORING AGENCY REPORT NUMBER

WL-TR-96-3111

11. SUPPLEMENTARY NOTES

12a. DISTRIBUTION AVAILABILITY STATEMENT

Approved for public release; distribution unlimited.

12b. DISTRIBUTION CODE

13. ABSTRACT (Maximum 200 words)
Four contributions concerning flutter prevention for aircraft are presented. The first author, based on his lifelong experience, discusses three major areas of flutter testing: flutter model design, flight flutter testing and ground vibration testing. For flutter prevention, seven essential flutter cases are selected for discussion in which cause and cure for each case are clearly displayed.

In the second section, the authors discuss six cases of flutter of full scale aircraft or wind tunnel models, as to flutter type, cause and correction. Also included are descriptions of several control surface/tab systems and how they function. Mass and aerodynamic balance types and design rules are also discussed.

In the third section, the author discusses the concurrent development of flutter analysis, numerical modeling techniques, ground vibration testing and in-flight flutter testing at three companies. Airplanes of 18 distinct types serve as illustrative examples, covering subsonic, supersonic and hypersonic regimes.

In the fourth section, the author discusses two cases of aeroservoelastic instability, in which configurations that were flutter-stable without their flight control systems become unstable at certain regimes with the control systems engaged.

14. SUBJECT TERMS
Flutter Model Design, Ground Vibration Testing, Flight Flutter Testing, Control Surface Flutter, Flutter Occurrence, Aeroservoelastic Instability, Military Aircraft, Civil Transport, General Aviation

15. NUMBER OF PAGES

16. PRICE CODE

17. SECURITY CLASSIFICATION OF REPORT	18. SECURITY CLASSIFICATION OF THIS PAGE	19. SECURITY CLASSIFICATION OF ABSTRACT	20. LIMITATION OF ABSTRACT
UNCLASSIFIED	UNCLASSIFIED	UNCLASSIFIED	SAR

FOREWORD

This report was prepared by ZONA Technology, Inc. under the support of the Flight Dynamics Directorate, Wright Laboratory, USAF/AFMC/ASC, Wright-Patterson AFB, Ohio, 45433-7542, for the contractual period of January 01, 1995 through June 01, 1996, *entitled "Flutter Prevention Handbook: A Preliminary Collection"*. Mr Ed Pendleton and Mr. Larry Huttsell of Wright Laboratory (WL/FIB) were the technical monitors under work units 2401TI00 and 2401LE00.

There are four major contributions to this report; these are:

1. *Flutter Model Design and Ground Vibration Testing by* **Lee S. Wasserman**
2. *Aerodynamic and Mass Balance Effects on Control Surface Flutter by* **Roberts E. Donham and George A. Watts**
3. *Flutter Occurrence on Eighteen High Performance Military Aircraft by* **William Roberts**
4. *Aeroservoelastic Instability by* **Raymond P. Peloubet, Jr.**

Because these four articles are rather disjointed from each other, it was decided that each Table of Contents and References should appear with its corresponding article.

At ZONA Technology, the Principle Investigator was Dr. Danny D. Liu; Mr. Darius Sarhaddi and Mr. Marc de Piolenc were the editors.

We at ZONA Technology are grateful to the above authors for their willingness to contribute their lifelong knowledge in flutter technology, wherein the lessons learned throughout the history will be best appreciated by the dynamics engineers for many generations to come. It is hoped that the present report will be a first contribution to a future volumetric Flutter Prevention Handbook collection, complete in its entirety of world aircraft.

Equally, we are indebted to all the reviewers who spent their time and energy to this project in spite of other pressing demands. During the course of the contractual performance, the technical advice and assistance received from Larry Huttsell, Ed Pendleton and Terry Harris of Wright Laboratory; Bob Moore of ASC/EN; Kenneth Griffin of Southwest Research; Thomas Noll of NASA-Langley; Bill Reed of Dynamic Engineering Incorporated; and Victor Spain and Anthony Pototzky of Lockheed Engineering and Sciences Company are gratefully appreciated.

Finally, ZONA would like to acknowledge the USAF's Aeronautical System Center's History Office (ASC/HO) and the Air Force Museum research department (USAFM/MUA) for supplying many of the photographs used in this Handbook.

TABLE OF CONTENTS

Lee S. Wasserman

Flutter Model Design and Ground Vibration Testing
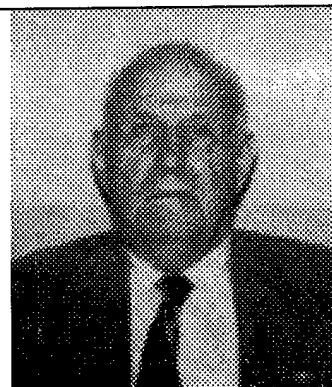
Abstract

In this article, the author presents his in-depth research/development and summarizes his lifelong experience in three major areas of flutter testing, namely, Flutter Model Design, Flight Flutter Testing and Aircraft Ground Vibration Testing.

For flutter prevention, seven essential cases of flutter are selected for discussion in which cause and cure for each case are clearly displayed.

1) *Bending-Torsion Flutter*
   Cause: Lift forces caused by torsional vibration equal to or greater than the damping forces caused by bending vibration.
   Cure: Mass balance, increase in torsional stiffness.
2) *Control Surface Flutter*
   Cause: In most cases by mass unbalance about the hinge line.
   Cure: Mass balance or mass overbalance.
3) *Tab Flutter*
   Cause: Low rotational stiffness and/or free play of the tab about the hinge line.
   Cure: Increase the frequency of tab rotation.
4) *Propeller Whirl Flutter*
   Cause: Wing mounted engines - coupling results from the yawing and pitching motions of the engines.
   Cure: Stiffened engine mounts.
5) *Panel Flutter*
   Cause: Aerodynamic and inertia forces acting on fabric or thin metal surfaces with inadequate supporting structure.
   Cure: Better supporting structure or stiffened skins.
6) *Active controls in some cases have caused flutter but have also been used to prevent flutter.*
7) *Shock Wave/Control Surface*
   Cause: The shock position changes with the control surface angle and the shock causes flow separation.
   Cure: Dampers or a wedge on the wing surface at the shock location to stabilize the shock position.

Lee S. Wasserman

1931-1935 B.A. from Amherst College. 1935-1937 M.S. from M.I.T. 1937 Structural Engineer; Curtiss Wright. 1937-1939 Instrumentation Engineer; Sperry Gyroscope Co. 1939-1953 Wright Patterson Air Force Base; Chief of Flutter Group until 1951 and Chief Scientist of Aerodynamics Research Group from 1951-1953. 1953-1979 President of Dynamic Devices Inc. "The Flutter Model Co." 1979 to present, Chief Consulting Engineer to Delta Dynamics Inc.

Table of Contents

Lee S. Wasserman

Flutter Model Design and Ground Vibration Testing

INTRODUCTION

Bending - Torsion flutter occurs when the lift forces caused by torsional vibrations are equal to or greater than the damping forces caused by bending vibrations. In most cases, the bending stiffness will be too low to balance the inertia forces at the flutter frequency, so some lift due to torsion will be required. In addition, the torsional frequency will have to be reduced to the flutter frequency by a twisting moment consisting of the lift at the quarter chord and the inertia force at the center of gravity. The damping moments about the quarter chord produced by torsional vibrations will also have to be balanced. The balance will be supplied by the acceleration of the center of gravity caused by bending vibrations. Low flutter speeds will occur with low torsional stiffness and with the center of gravity location of most sections substantially behind the aerodynamic centers. Reductions in the flutter speed will also occur when a surface like an all-movable stabilizer has a low pitch stiffness. If the bending-to-torsion frequency ratio at zero airspeed is increased and the elastic axis is well ahead of the center of gravity of each section, a substantial reduction in flutter speed can occur. However, the flutter speed will reach a minimum value and then increase as the bending to torsion frequency ratio increases.

Control surface flutter occurs when the control surface vibrations about the hinge line provide the lift and/or moment required to cancel out the damping caused by bending and torsion of the supporting surface. Control surface flutter is caused in most cases by mass unbalance about the hinge line. However, when the fixed surface vibrates in torsion as well as in bending, the moment of inertia of the control surface adds to the moments caused by mass unbalance, so in such cases, mass overbalance will be required for flutter prevention. The frequency ratio effect for control surfaces is similar to the effect in bending torsion flutter in that flutter can be prevented by control surface frequencies which reduce the response of the control surface below the value required to cancel the damping of the supporting surface.

Tab flutter is similar to control surface flutter since mass unbalance and low tab frequencies cause the tab to move in the direction to balance the damping due to control surface rotation and torsion. Symmetrical control surface rotation is restrained by the stiffness of the control system. Most trim tab flutter is caused by low rotational stiffness and/or free play of the tab about its hinge line. Geared tabs are more likely to flutter if the tab rotation leads the control surface rotation since the moment acting to rotate the tab is in the same direction as the moment caused by mass unbalance. Tabs used in the control system to rotate the control surface (spring tabs) are the most critical to flutter because the control system dynamics limits the frequency of tab rotation.

Metal structures have raised the bending-torsion flutter speeds above the limit diving speeds of most aircraft except when engine nacelles, bombs and fuel tanks are attached to the wing structure. The reduction in the torsional frequency and the possibility of critical bending-to-torsion frequency ratios have resulted in flutter in the operating range.

Propeller whirl flutter has occurred in airplanes with engines mounted on the wing. The instability is caused by both the gyroscopic and aerodynamic coupling of propellers resulting from yawing and pitching motions of the engines.

Panel flutter has occurred due to the aerodynamic and inertia forces acting on fabric and or thin metal surfaces with inadequate supporting structure.

Active controls have caused flutter in some cases, but have also been used to prevent flutter.

Shock waves have caused flutter of control surfaces because the shock position changes with the control surface angle and the shock causes flow separation which produces unstable moments about the control surface hinge line. In most cases, mass balance will not prevent this type of flutter and dampers must be used. In one case, it has been reported that the problem has been solved by a wedge located on the wing surface at the shock location.

1. Vibration Modes and Frequencies

a) Calculations of influence coefficients, including finite element analysis
b) Calculations of mass distribution
c) Calculation of frequencies and mode shapes
d) Measurement of frequencies and mode shapes

There are a number of methods that have been used to measure the frequencies and mode shapes at zero airspeed. The problems include the suspension of the aircraft, the location of the shakers, the wave form of the excitation, the instrumentation, and the method of evaluating the test data. (*A report covering the above items will be provided in a later version of the Flutter Prevention Handbook.*)

e) Use of vibration data to indicate the probability of flutter

Vibration data have been used as an indication of the probability of flutter. For example, if the data showed highly coupled motions of bending and torsion of fixed surfaces, a low bending-to-torsional flutter speed is possible. In the case of control surfaces, a lagging motion of large amplitude with a large response of the fixed surface indicates the probability of a low flutter speed. A similar situation exists for control surfaces and tabs.

f) Use of vibration data in flutter calculations

Flutter calculations can be conducted using measured coupled modes, (i.e. with no mass or elastic coupling). If uncoupled modes are used, agreement between the predicated and measured coupled modes obtained during ground vibration tests indicate that the amount of coupling is correct.

2. Flutter Prevention

a) Mass Balance

Mass balance has been the most widely used method to prevent control surface flutter. A frequently used method is uniform mass balance with distributed weights. Overbalance can be required when the supporting structure vibrates in both bending and torsion. In this case, the increase in the moment of inertia caused by the balance weight must be limited or a reduction in the flutter speed can occur.

b) Changes in stiffness

When mass balance is not practical, stiffness changes may be necessary. For control surfaces and tabs, raising the rotational frequency is often the most practical method of preventing flutter. Stiffness changes as well as mass balance are frequently used to prevent flutter due to the mounting of nacelles, external fuel tanks and weapons on the wing structure. Center of gravity locations near the quarter chord have prevented flutter of tip tanks. Fins to stabilize the tanks in pitch have also been used.

c) Dampers

Hydraulic dampers have been used to prevent shock induced flutter of control surfaces.

d) Tailoring of composites

e) Active controls

Active controls have been used to prevent flutter in cases where dampers as well as changes in mass and stiffness are either not effective and/or not practical.

3. Flutter Models

a) Need for models

Flutter models are needed because of the difficulty of accurately predicting flutter with existing theory. The occurrence of flutter after the airplane has been constructed can result in very large increases in costs.

b) Scaling rules

Geometric scaling with the same materials in the model and aircraft results in the same flutter speeds.

c) Design and construction of low speed models

Low speed models are constructed by reductions in the scaled stiffness of the model. Since geometric scaling of the structure with reduced thickness of the materials is normally impractical, the usual construction consists of a spar which provides all of the stiffnesses and rigid sections attached to the spar which provide the aerodynamic shape and the scaled mass distribution. At least six separate sections are used with small gaps between each section. The space between these gaps can be closed with a flexible material.

d) Design and construction of transonic models

Transonic models have been constructed in two ways. One method is to use hollow spars to keep the weight down and to cover the spars with balsa sections that add a limited amount of stiffness. Chordwise low density balsa has been found to be acceptable. The second method is to use geometric scaling with the materials having the same stiffness properties required to provide the scaled stiffness values.

e) Structural tests of models

The use of mirrors on the model to reflect light beams projected from a side projector has been used to measure the slopes of the model structure under loads. The slide in the projector produces vertical lines for torsion measurements and horizontal lines for bending measurements. A measuring board with vertical and horizontal scales is used to read the slopes in bending and torsion. The bending stiffness EI and the torsional stiffness GJ are determined from the formulae $EI(d/dx)$ and $GJ(d/dx)$. Influence coefficient measurements with electronic or mechanical dial gages have also been used.

f) Inertia tests of models

In sectionalized models, the weight center of gravity (c.g.) and moment of inertia of each section is measured. The spar weights are calculated from the spar geometry and the combined spar and section weight and inertia are computed. For models with scaled structures, the total weight, center of gravity and moment of inertia are measured and compared with theoretical values. Where costs will permit the destruction of a model, the model can be cut into sections and the weight center of gravity and moment of inertia of each section is measured.

g) Model instrumentation
h) Wind tunnel test programs
i) Evaluation of test data

More detailed information concerning flutter models will be supplied later.

4. Flight Flutter Testing

a) Excitation methods
b) Instrumentation
c) Interpretation of test data

5. Flutter Cases Which Were Not Predicted by the Theory and Flutter Models

a) Errors in the mechanical forces
b) Errors in the aerodynamic forces
c) Errors in the stability equations
d) Method used to fix each case flutter

6. Flutter Research Areas

a) Computation of the aerodynamic forces at transonic speeds including shock waves
b) Nonlinear systems
c) Active controls
d) Thermal effects on structures
e) Tailoring of composites

7. Aeroelasticity

a) Control surface reversal
b) Divergence
c) Stability effects caused by structural deformation
d) Effects on aeroelasticity caused by active controls

FLUTTER MODEL DESIGN

Scale Factors

One approach which will lead to an understanding of the scale factors is to become familiar with geometric scaling and the applicable scaling rules. If all of the dimensions of a structure are reduced without changing any of the materials or methods of construction, the resulting structure is said to be geometrically scaled. The frequencies of the resulting structure multiplied by the length scale factor will be equal to the frequencies of the full scale structure. For example, a geometrically scaled model with a length scale factor of 1/10 will have frequencies equal to 10 times the full scale frequencies. To prove this key point with a simple example, consider a cantilever beam with a weight attached to the end. The elastic constant is $3EI/L^3$ and the mass is proportional to L^3, so the frequency is proportional to the square root of $3EI/L^6$. For geometric scaling EI is proportional to L^4, so the frequency is proportional to $1/L$ or the frequency times L is a constant.

The structural velocity is the frequency times the scaled amplitude. For a tenth scale geometrically scaled model, the scaled amplitude is 1/10 and since the frequency is 10 times full scale, the velocity ratio is unity. The ratio between the air velocity V and the structural velocity is usually specified as $V/b\omega$, where b is the semichord of an airfoil and ω is the frequency. The scaling rules require that $V/b\omega$ be the same for the model and full scale structure. This rule implies that $V/L\omega$ is a constant.

The other key model scale factor in addition to the length ratio and the velocity ratio is the density ratio. The values of the density and velocity ratios are established by the conditions in the wind tunnel. For example, if the density of the air in the wind tunnel is twice the density of the air in the flight condition being simulated, the scaled weight of each model component must be doubled. In addition, if the air velocity in the wind tunnel is half of the velocity of the full scale flight condition, the velocity ratio of the model must be reduced to one half, which requires that the frequency ratio be halved because $V/b\omega$ is fixed. If the model weights are doubled, the velocity ratio will remain unchanged, provided that the stiffness is also doubled, since the frequency ratio will not be changed. If the stiffness is reduced to half and the weight is doubled, the frequency ratio will be halved and therefore the velocity ratio will be halved.

The ratio q equals the density ratio multiplied by the square of the velocity ratio, which is 2 x 1/4 or 1/2 for the above case. To obtain the model stiffness, the geometrically-scaled stiffness is multiplied by the ratio q.

There are a number of reasons why geometrical scaling is not used for flutter models. One major reason is that the typical aircraft structure is so complicated that scaling each element of the structure as well as the geometric tolerances would be completely impractical. In addition, the scale factors must be changed to simulate the velocity, density and (in transonic and supersonic testing) the Mach number of the full scale flight conditions in the wind tunnel.

The concept of geometric scaling is mainly useful for calculating the scale factors to be applied in designing the model. For example, the weight is proportional to L^3, the static unbalance proportional to L^4, and the moment of inertia proportional to L^5 for a density ratio of unity which is true for geometric scaling. The bending and torsional stiffnesses EI and GJ are proportional to L^4 for the density and velocity ratios of unity applicable to geometric scaling. For other density ratios, all the scale factors are multiplied by the density ratio. For other velocity ratios, EI and GJ are also multiplied by the square of the velocity ratios.

It was mentioned previously that the density ratio multiplied by the square of the velocity ratio is proportional to the ratio q so that the EI and GJ are proportional to L^4q where q is the ratio defined earlier. The angle of twist or bending due to a moment is proportional to $1/(L^3q)$ while the angle of twist due to a load is proportional to $1/(L^2q)$. The deflection due to a moment is the same as the angle of twist due to a load. The deflection due to a unit load is proportional to $1/Lq$. The scaled weight is proportional to L^3 multiplied by the density ratio so

1-8

that the static deflection under gravity is proportional to $(L/V)^2$ and the static deflection divided by the scale is proportional to L/V^2. To obtain scaled model deflections under gravity, the velocity ratio must equal the square root of the inverse of the scale. V^2/L is sometimes defined as the ratio g.

The physical significance of the scaling rules may be determined from the equations of equilibrium. The same equations of equilibrium must apply to the model and full scale aircraft, if the model test results are to be directly applied to predict the full scale results. All the forces or moments involved in the equations of equilibrium must therefore change by the same percentage as the scale is changed.

For example, the mass times the acceleration must change by the same percentage as the spring constant times the displacement or $L^3\omega^2L$ must be proportional to L^2 or $(AE/L)L$. For this reason, L^2W^2 or $L\omega$ equals a constant as indicated above for geometric scaling. The aerodynamic forces are proportional to q multiplied by L^2 so $L^4\omega^2$ multiplied by the density ratio which is proportional to the inertia force must be proportional to L^2q or $L^2\omega^2/V^2$ or $V/(L\omega)$ must be constant. The concept of maintaining the force and/or moment ratios independent of the scale is useful in checking the scaling rules for other types of forces or moments such as damping and/or friction.

Low Speed Flutter Models

The technical difficulties and high cost of designing, building and testing models in transonic and supersonic tunnels has led to the use of flutter model tests in low speed tunnels. The test results have proven to be useful at transonic speeds because the mechanism of classical flutter is relatively independent of Mach number up through the transonic range. Mach number effects have been obtained with the concept of Mach number corrections. The shift in the center of pressure and the change in the lift curve slope have been used in the past to estimate such corrections. However, more accurate corrections can now be obtained with the use of compressible subsonic and supersonic theory.

The usual low speed flutter model component consists of a skeleton made up of metal spars which simulate the stiffness distribution of the full scale structure including the control surfaces plus a number of balsa sections fastened to the spars. The balsa sections are used to transmit the airloads and some of the inertia loads to the spars. (See Figure 1).

The design problems are as follows:

1) Spar Design
2) Spar Joints
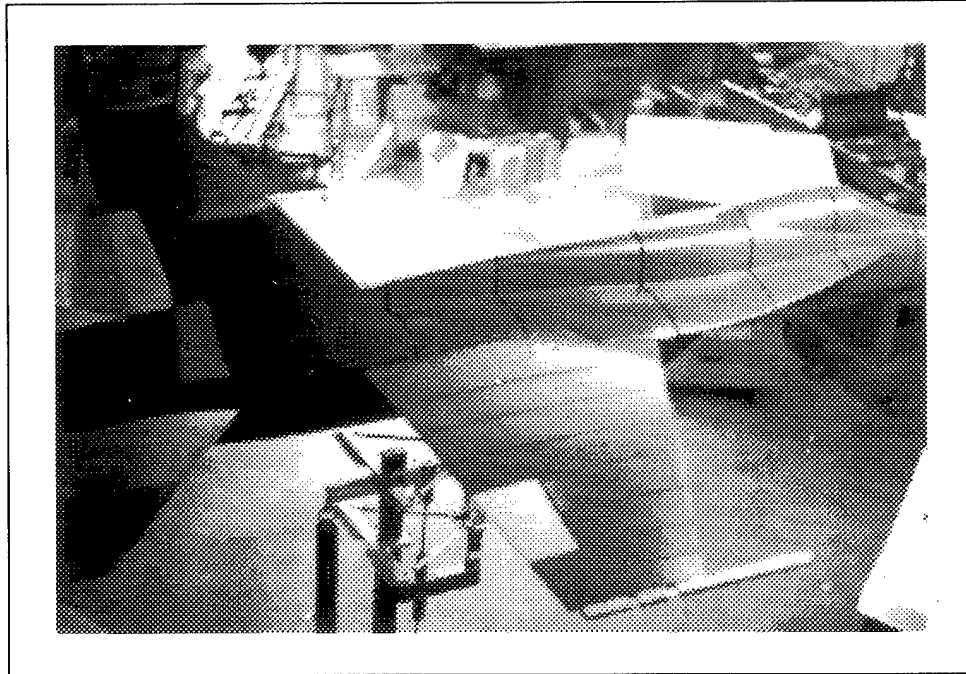3) Attachments of Balsa Sections, Control Surfaces, Actuators and Pylons to the Spars

Figure 1: Low Speed Flutter Model

4) Balsa Sections
5) Control Surfaces
6) Actuators
7) Pylon Design
8) External Stores
9) Model Mounting Systems

1) Spar Design

A key requirement of spar design is to obtain the scaled stiffnesses with adequate strength within the allowable weight. The first step is to obtain the required model values of the vertical and fore and aft bending stiffnesses EIV and EIL, the torsional stiffness GJ and the allowable weight. Deflections perpendicular to wing, horizontal tail and vertical tail surfaces are usually defined to be in vertical bending. Deflections in the planes of these surfaces toward the leading or trailing edges are defined to be in fore and aft bending. For the fuselage, lateral bending stiffness is used instead of the fore and aft bending. If full scale data are supplied, the full scale EI and GJ are multiplied by L^4 times the ratio q to obtain the model EI and GJ values and the full scale weight per inch of span is multiplied by L^2 times the density ratio to obtain the model weight per inch. The model weights are usually converted to grams per linear inch because of the light weights of certain model components. The weight of the balsa covering can in most cases be held to 40% of the total section weight and the weight of the ballast weights about 10%, so that not over 50% of the model section weight can

be used for the spar weight. Since the spar strength will increase as the spar height is reduced and the area and thus the weight is increased, it is good design practice to use the maximum allowable spar weight. Nevertheless, the maximum spar weight will be less than 50% of the total weight in model sections having high densities.

Solid spars milled from 2024-T3 aluminum (see Figure 2) are usually used, although magnesium alloy is substituted in those cases where the aluminum spars will equal or exceed the 50% weight limitation. In very few cases will hollow spars be required in low speed flutter models. The wing and tail spars are normally rectangular in cross section with a fore and aft flange while the fuselage spars may be similar or may be shaped like tees, crosses or tubing to which vertical or horizontal flanges are fastened depending on the values of *EIL*, *EIV* and *GJ*. Obtaining the correct values of *EIL* in the fuselage spar is usually but not always more important than obtaining the correct values of the fore and aft stiffness in the airfoil surfaces. The ratio of the width *b* of the spar to the height *a* of the spar is determined by the ratio of *GJ* and *EIV*. (The use of *b* for the width and *a* for the height was selected arbitrarily by Dynamic Devices, the predecessor of Delta Dynamics.) Curves of *J/IV*, *IL/IV*, J/A^2, and IV/A^2 vs. *b/a* were computed using the formulas for *J* in Timoshenko's *"Theory of Elasticity"* or Roark's *"Formulas for Stress and Strain"*. The values of *I* are the area moments of inertia according to the elementary theory of bending.
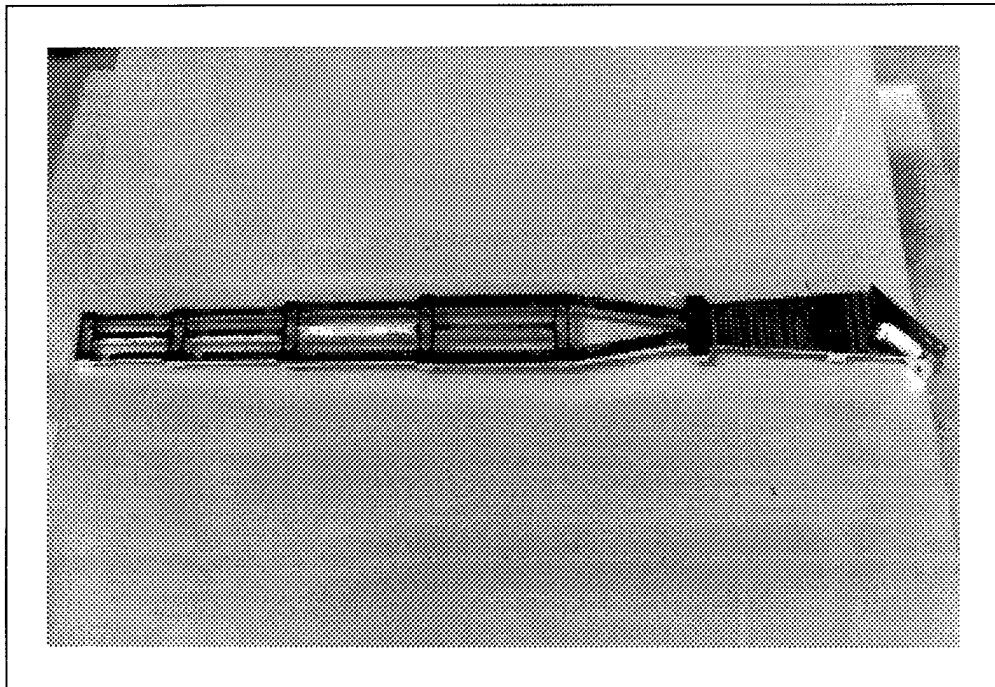

Figure 2: Control Surface Spar Design

The value of b/a determined from the graphs using the required $J//V$ value also determines the cross sectional area A and thus the weight per inch which is obtained by multiplying A by the density if the material. If the fore and aft EI is too low, then a thin fore and aft flange may be machined integrally at the center line which will increase the fore and aft EI with minimum changes of the other stiffnesses but with a small increase in weight. In some cases however, the fore and aft flange is moved above the center line to increase the bending EI without adding weight. The other problem which occasionally shows up is a higher required ratio of $J//V$ than can be obtained with a rectangular spar. Some designers have added thin webs at plus and minus 45 degrees to the elastic axis on the top and bottom spar surfaces to obtain the increased $J//V$ ratio. The other possibility is the addition of an auxiliary spar which adds more to GJ than EIV because the chordwise connecting strips between the spars are more flexible in transmitting bending moments than in transmitting twisting moments.

The graphical solutions mentioned above were used to solve spar design problems before the availability of low cost personal computers. Simple programs for solving spar design problems on personal computers have now eliminated the need for such graphs. One approach in such programming is to input the scale factors, the full scale EI and GJ values and the elastic moduli and density of the material and use the computer to provide the spar dimensions and the weight distribution. If the spar weight distribution exceeds the allowable values, magnesium alloys may be substituted for 2024-T3, or a hollow spar may be used. The use of model values of EI, GJ and weights as computer inputs is another possibility and has some advantage because model values for different aircraft tend to be similar regardless of the full scale values.

2) *Spar Joints*

Joints in the spar skeleton (see Figure 3) must be carefully designed to provide adequate strength and rigidity without any slippage. The joints should be as strong as the spars being connected together and as rigid as practical. Joints made with machine screws which balance the applied moments by tension loads in the screws have proven to be satisfactory in most cases while bolts in shear are usually unsatisfactory because of slippage. Blocks machined into the end of spars to be joined together is one design concept but a lot of material must be removed. Machine screws through the blocks between two spars will resist vertical and fore and aft bending moments with tension loads on the screws as long as the initial tension on each screw is high enough to prevent load reversal. The torsion moment will be resisted by friction unless the flanges are locked together over a key or a pin or an additional block is bolted perpendicular to the other blocks or machined integral with one of the blocks and bolted to the other block. Another concept involves tapering the spars at a joint and using four screws to balance out vertical bending and torsion moments. Fore and aft moments would have to be balanced by a key, additional blocks or friction.
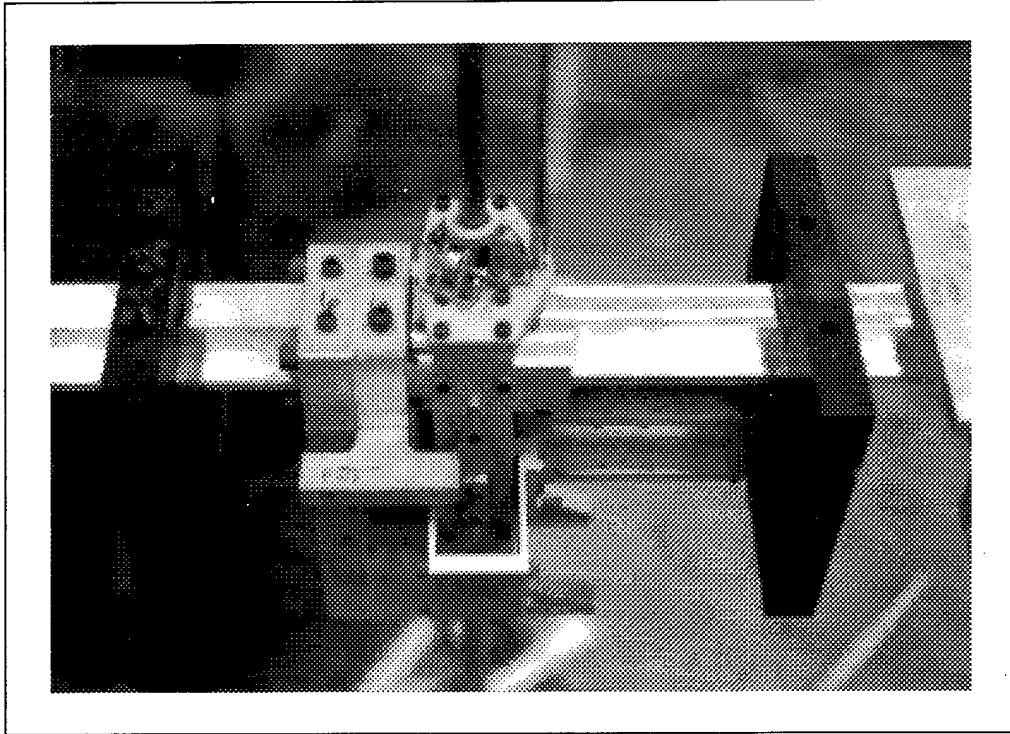
Figure 3: Fuselage Spar Joints

3) Attachments to the Spar

The balsa covering is fastened to the spars in sections so that the balsa does not increase the spar stiffness. The attachment is usually made with machine screws and small blocks machined integrally with the spar. Other attachments to the spar including control surfaces, actuators and pylons are made in a similar manner. The blocks are perpendicular to the spar elastic axis and extend over a short length of spar so that a minimum amount of spar strain energy will be stored in the blocks. Nevertheless, it is a good design practice to include some increase in the spar stiffnesses due to the blocks, particularly for those in torsion. The spar between each block supporting a balsa section may be of constant cross section with average stiffness values or may be tapered to represent the scaled stiffness distribution.

4) Balsa Sections

The number of balsa sections may be as high as 10 for each wing and 12 for the fuselage. Six sections are used for tail surfaces and four to six for control surfaces. The balsa sections must be designed to transmit some of the inertia and all of the aerodynamic loads to the spars at the highest flutter frequencies expected in the wind tunnel tests. Since there will be some flexibility in the attachment between the spar and the sections, the ratio of the section motion to the spar motion will increase as the frequency and the air loads increase. This flexibility

between the spar and the sections can introduce substantial errors in the results. The key section design problem is therefore to minimize such errors by making the sections and attachment as rigid as possible within the allowable weight. For this reason, the sections are usually built with most of the balsa grain running perpendicular to the spar or streamwise if the sections are built in the streamwise direction. The sections are usually built in halves, split at the spar centerline. The grain at the leading and trailing edge is usually spanwise to increase the rigidity. The balsa section halves are glued together and at the same time are glued to 2024-T3 aluminum alloy plates called bridges. Each balsa section is slid over to the spar to the correct position and the bridges are fastened to the spar blocks with machine screws and nuts. To improve the glue joints between the balsa and the bridges, holes are sometimes drilled through the bridges before assembly to the balsa.

The sections are covered with fiberglass or silk if weight permits or otherwise are covered with paper for increased strength and rigidity (see Figures 4 and 5). Each section including the bridge plates can be removed as a unit from the spar to check the weight, c.g. location and the moments of inertia.

Other types of bridges have been used in an effort to increase the rigidity of the balsa sections. One bridge design has four hardwood or metal shear webs forming a sort of "X" frame to provide stiffness in both roll and pitch. The shear webs are mechanically fastened to a block containing holes for bolting the section to the spar blocks or in the case of metal webs may be integral with the section block. Hollow balsa sections consisting of ribs covered with balsa planking have been used with these bridges. For thick airfoils, this type of construction may weigh less than the solid balsa sections although the weight of the glue will frequently be more than the weight saved by reducing the volume of the balsa wood. In addition, the contours of solid balsa sections may be machined eliminating the need for most of the hand work required on built up sections.

In cases where the spar weight is much less than 50% of the section weight, some of the extra weight should be used to increase the strength and stiffness of the balsa sections. However, heavy concentrated weights such as fuel weights should not be carried by the balsa sections but should be fastened directly to the spar.

At one time sample balsa sections were built for measuring the weight, strength and rigidity before the final section design was approved. However, the use of computer programs to compute the weight, rigidity and the strength has reduced the need for such samples. Nevertheless, strength tests on the completed model are still considered desirable to evaluate the effectiveness of the glue joints. The spar strength may be used to compute the required strength of the balsa sections although the maximum wind tunnel dynamic pressure or some substantial percentage of the pressure may also be used.
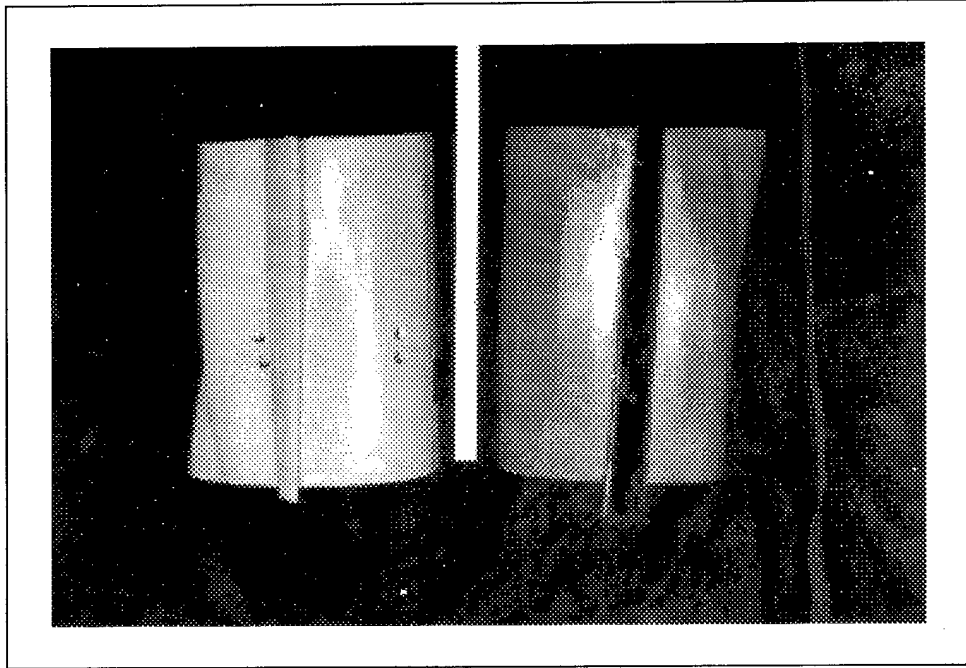
Figure 4: Balsa Sections Mounted to Sheet Metal
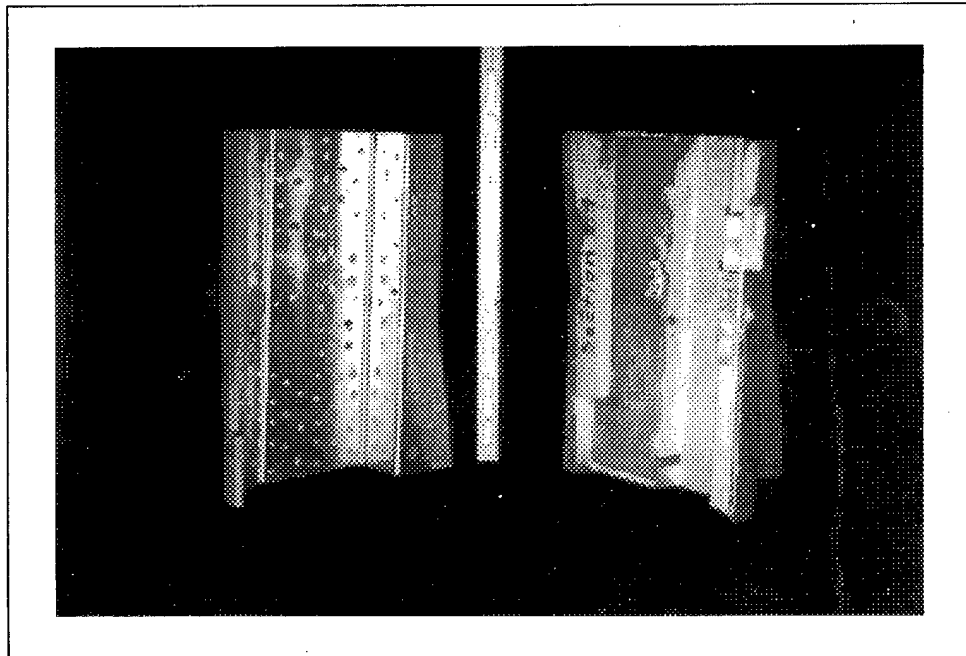Frame and Covered with Fiberglass (Top View)

Figure 5: Balsa Sections Mounted to Sheet Metal
Frame and Covered with Fiberglass (Bottom View)

5) Control Surfaces

The design of control surfaces is similar to the design of fixed surfaces except that the scaled stiffnesses may be only the torsional stiffness or in some cases the torsional and vertical bending stiffnesses. In addition, scaling the static unbalance and moment of inertia about the hinge line is usually more important than scaling the weight since excess weight may be used as part of the ballast weights of the supporting surface. However, the weight must be kept within tolerance in low density sections.

The design of the hinges for control surfaces is a key problem because the friction torques should be reduced to a minimum or at the very least should be reduced in proportion to the reduction in the scaled inertia and aerodynamic torques. If the friction torques on the model are excessive, the results will not be acceptable. Flexure hinges usually work much better than ball bearing hinges because the ball bearing hinges can not be easily aligned when there are more than two hinges unless the model design provides a definite procedure for aligning each bearing. Flexure hinges using silk or nylon threads have been tried but usually fail after a single flutter point so flexure hinges using beryllium copper or spring steel have proven to be superior. Another possibility is to use plastic strips made from nylon to obtain low hinge stiffnesses. Since flexure hinges are somewhat fragile, a single ball bearing hinge is sometimes used to prevent the loss of a control surface due to flexure hinge failure. In lieu of the bearing hinge, other safety devices should be installed to prevent loss of control surface when flexure hinges are used. The other problem with hinges is the transmission of loads or moments across the hinges due to flutter. In some cases, it is desirable that each hinge be mounted on a torsion flexure to reduce the moments transmitted across the hinge due to bending of the fixed surface and/or the control surface.

6) Actuators

The simulation of actuators is another key problem. Torsion bars have proved to be the best solution in most cases since the bars do not load up the hinges and the bars fit into the space between the control surface leading edge and the fixed surface trailing edge. The bars are usually designed to withstand plus or minus five degrees of rotation without yielding. In some cases a double torsion bar will be necessary to store enough energy. For some actuators, a strip of beryllium copper is bent to form a "U" shape representing two bars connected together with actuator arms at the other ends of the "U" connected to the fixed and movable surfaces. Single or double torsion bars can be formed from spring steel before heat treating or can be machined from 2024-T3. The formula for J can be determined from the graphs mentioned above or from a computer program.

7) Pylon Design

Pylon design is one of the more difficult problems encountered in low speed flutter models. The pylons may be used for mounting external stores or engines. The objective is to obtain the required stiffnesses or influence coefficients with a structure consisting of beams machined

from solid stock as a one piece unit or with a series of beams assembled together with machine screws. In addition to the bending and torsion deflections due to the beams, shear deflections using double cantilevers must occasionally be added.

In general, it will be helpful to follow the full scale load paths in the model but high stresses may prevent this approach. In some cases stops can be used to prevent failure of the pylon due to high stresses.

Computer programs based on beam theory have proven to be quite useful for establishing the final design. In general, there will be two three by three matrices of stiffness of influence coefficients that must be matched. One for symmetric and one for anti-symmetric motion of the pylon. To start the analysis, a system of three beams is setup that appears to simulate the real structure. The location and/or angle of the beams is along the axis that reduces the vertical and fore and aft loads to loads perpendicular to the beams and axial loads so that by ignoring the axial deflections, a two-by-two matrix is obtained. The three unknowns, are the *EI* values of each beam and the three conditions are the pitch angle due to a pitching moment, the vertical displacement due to a load and the pitch angle due to a load or the displacement due to a moment which are the same. On the first try, the solution may yield unacceptable results such as negative values of *EI*. The lengths of the beams may be changed or shear deflections may be added until an acceptable design is achieved. For the anti-symmetric case, the approach is to select an elastic axis that separates out the effects of *GJ* and gives values for *EIL* for the three beams. The final step is to determine the values of *GJ* for each of the beams or the total value of the torsional stiffness. Care must be used in attaching balsa sections to pylons to avoid stiffening the pylon and interfering with pylon deflections. (See Figure 6).
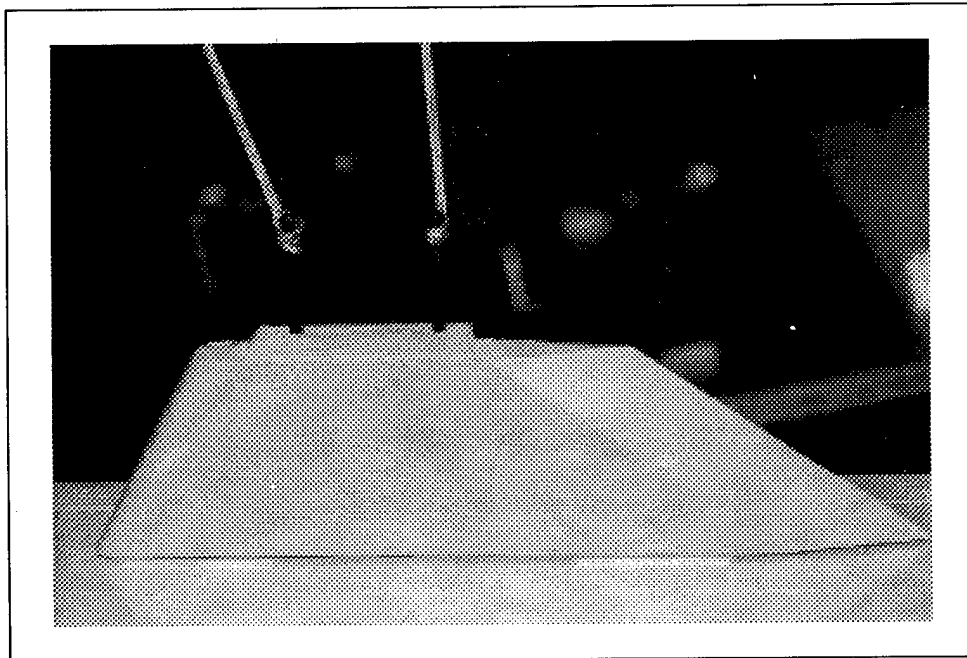

Figure 6: Pylon Design

8) External Stores

Computer programs have been developed for store design. For a rigid store (the store is broken up into seven or more sections - see Figure 7) the inputs are the radius and coordinates at the ends of each section. The program calculates the volume, c.g. and radius of gyration of the assembly about the c.g. as well as the density required for the total weight. If the density is much higher than the density of hard wood, the weight, moment of inertia and unbalance about the c.g. are computed for a hard wood covering. The program then computes the changes in the weight, static unbalance and moment of inertia that must be added to meet the design requirements. The distance of the added weight from the c.g. is then computed to correct the unbalance. The moment of inertia due to the added weight is then subtracted from the total moment of inertia that must be added.
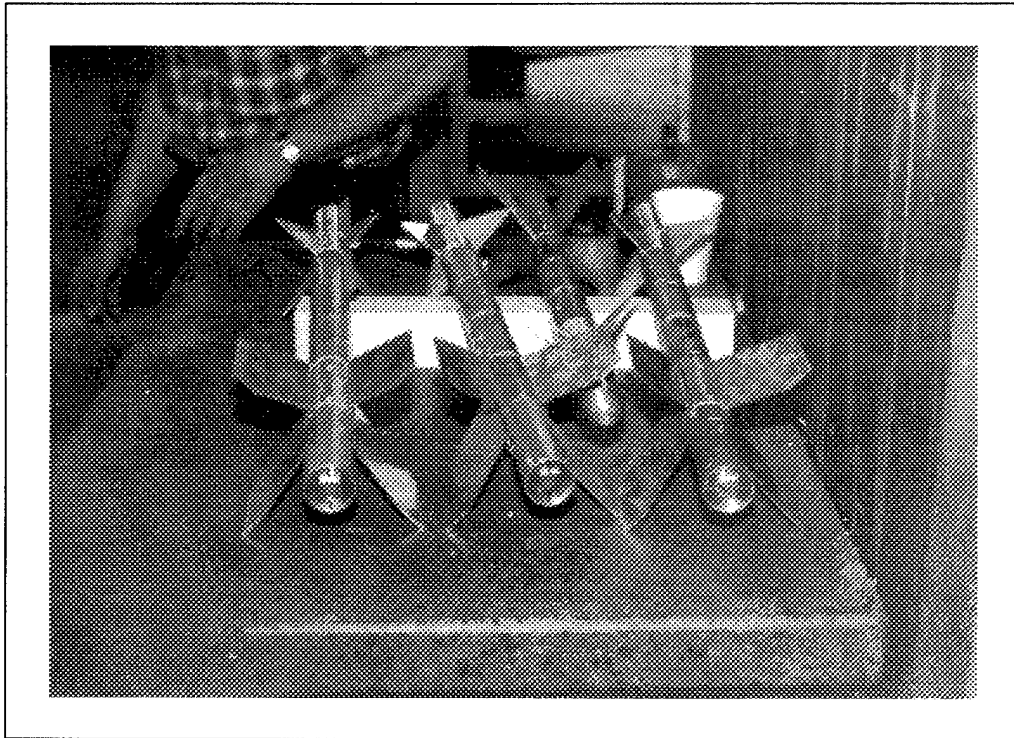
Figure 7: External Stores

The next step is to design a metal bar that will add the correct weight and moment of inertia. The radius of gyration to provide the additional moment of inertia is used to establish the length of the rod and the area of the rod is determined from the weight that must be added and the corrected density of the material in the rod. The corrected density is the difference between the density of the rod and the density of the hard wood. The rod is usually drilled with holes for the attachment of the store to the pylon.

If the store density is about the same or lower than the density of hard wood, balsa wood may have to be used for the outside contour. In this case, 2024-T3 may be used for the rod or no rod will be used if the area is too small. It this case, a 2024-T3 plate will be cemented to the balsa for mounting the store to the pylon. In addition, the weights required to properly balance the store will be calculated using a computer program with the locations of the ballast weights as additional inputs.

The design of flexible stores is somewhat similar to the design of fuselages although the spar in many cases will be a solid or hollow aluminum alloy cylinder with a tapered or stepped wall thickness. Rings will be machined around the cylinder to support the ballast weights and balsa or hard wood sections. The external sections and ballast weights are either clamped around the rings or held to the rings with machine screws if the thickness of the rings is sufficient.

9) Mounting Systems

The mounting system (see Figure 8) should provide three symmetrical and three antisymmetrical rigid body degrees of freedom with frequencies 1/3 or less of the lowest flutter frequency. While this requirement can be satisfied with many different mechanical systems including cable systems and four bar linkages, the rod mount has been used in more low speed flutter model tests than any other type of mount. The rod mount consists of a slider, a gymbal and a vertical rod. The slider rolls up and down on the rod on ball bearings or ball bearing rollers to provide the vertical translation degree of freedom. Three bearings located at 120 degree angles are fastened to each end of a cylinder which fits with ample clearance around the rod. The front bearings at each end of the cylinder take out the drag loads. The other two bearings are spaced just to touch the surface of the rod. In most cases, one of the bearings will be adjustable to reduce the play. Two shafts machined integrally or bolted at the center of the slider cylinder fit ball bearings mounted in a rectangular gymbal to provide the pitch degree of freedom. The gymbal in turn will have bearings or shafts mounted at 90 degrees from the pitch direction to provide the roll degree of freedom. Springs are installed in the gymbal mechanism to provide stability of the model in roll and pitch in the wind tunnel. The bending of the rod provides the fore and aft and lateral translation degrees of freedom. The yaw degree of freedom is provided by the rotation of the model around the rod.

The mounting system must be designed to provide the flutter model with static and dynamic stability during wind tunnel operations. Static stability will be obtained if the aerodynamic center is behind the elastic axis. While this situation is almost always the case in yaw, the pitch elastic axis is placed behind the c.g. to prevent dynamic instability in the pitch and translation degrees of freedom. If the aerodynamic center is ahead of the pitch elastic axis, sufficient pitch stiffness must be supplied to prevent static divergence of the model. The other instability that has shown up in wind tunnel tests is Dutch roll. One solution that has been satisfactory in most cases is to use a strong roll spring. In most rod mounts, the yaw frequency will be zero at zero airspeed and will increase as the tunnel q is increased. If the yaw frequency approaches the roll frequency, Dutch roll is likely to occur if the dihedral effect

and the roll-yaw product of inertia are both of the same sign and are of sufficient magnitude. Positive dihedral causes the wing which is yawed to the forward position to produce upward lift and thus an up rolling moment while positive product of inertia causes a rolling moment in the opposite direction for the same yaw position. In some rod suspension systems, there are no roll bearings and the roll degree of freedom is provided entirely by the flexibility of the rod.
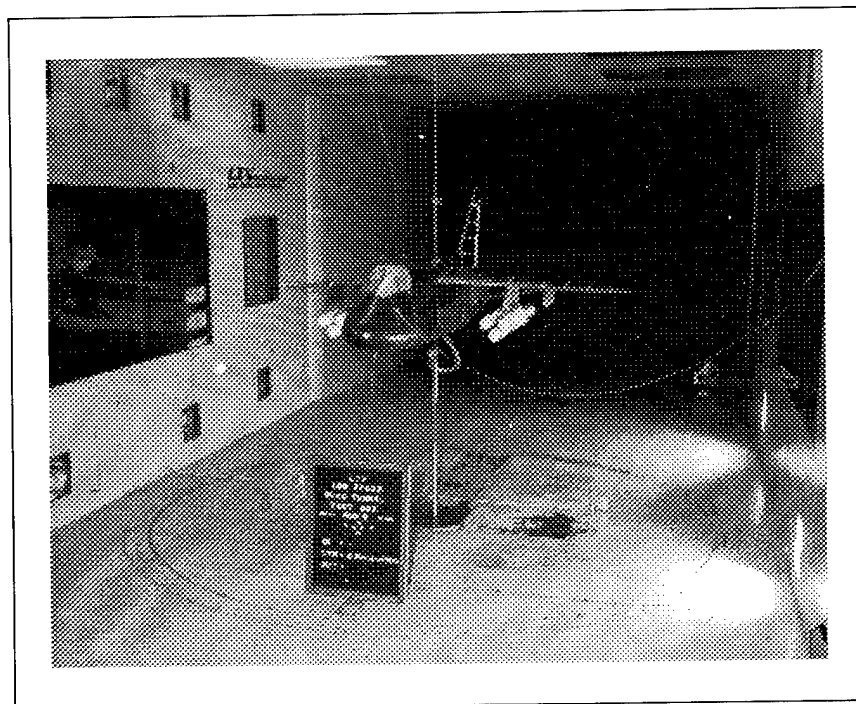

Figure 8: Mounting Systems

The model should be positioned near the center of the tunnel with the wings level during the wind tunnel tests. One method involved the use of electric motors to drive the control surfaces for trimming the model in pitch and roll. This method is satisfactory but complicates the model design. It was noticed, however, that the trim settings changed very little during a test program so setting the trim manually was tried. In this case, the model was positioned in the center of the tunnel by supporting the model on a spring connected to a cable which in turn was connected to a winch. The latest design involves two cables connected to the fuselage forward and aft of the rod and one cable connected to the slider on the rod. The spacing of the front and rear cables is about twice the radius of gyration. The angle of attack and the position of the model can be changed by adjusting both the front or rear cables and the cable connected to the slider is used to pull the model up against the stops. At the present time, the three-cable system cannot be used for balancing large unsymmetrical loadings. It appears that a fourth cable connected to the model through a spring to apply a moment about the roll axis will have to be added if balancing large static rolling moments is desired. Otherwise, the rolling moment will be balanced by the roll spring and bending of the rod.

The mounting system should be designed to prevent destruction of the model due to violent instability or flutter. It is essential that the rod must not fail regardless of what happens to the model. This criterion requires a stress analysis of the rod with conservative loads and moments and the use of high strength material in the rod. The rod is usually installed with some initial tension to keep the stresses down. Since the rod will not be stiff enough to limit the angle of attack, external cables and/or stops in the suspension system should be used to limit the angles of yaw and pitch to safe values at the top q of the wind tunnel tests. If the model is flown with a c.g. substantially behind the rod, the initial contact should be with a stop behind the c.g. so that if the model hits a stop, the airloads caused by model pitch will tend to hold the model against the stop.

High Speed Models

High speed models (see Figures 9 through 12) are designed to be tested at the same Mach number as the full scale airplane as well as at the same density ratio. The velocity ratio is therefore the same as the ratio of the speed of sound in the wind tunnel to the speed of sound at the flight condition being simulated. For air tunnels, the speed of sound ratio is proportional to the square root of the ratio of the absolute static temperature on the wind tunnel to the absolute static temperature of the atmosphere at the altitude being simulated. Since the speed of sound ratio is about 0.85 to 0.9 for air tunnels, the velocity ratio is much higher than for low speed models and thus the model frequencies, stiffnesses (*EI* and *GJ*) and strengths must be much higher than for low speed models. The key problem is to obtain the scaled stiffness and strength without exceeding the scaled weight.

High Speed Wind Tunnels

High speed flutter models have been tested in blowdown tunnels, continuous flow pressurized air tunnels and the continuous-flow pressurized Freon tunnel at Langley Field. The blowdown tunnel has the advantage of higher density ratios at transonic and supersonic speeds than either of the other types of tunnels, but the test section sizes are smaller to limit the amount of air that is used in each run (or blow) to the amount that is available at the required pressure in the compressed-air tanks. Continuous-flow high-pressure air tunnels are usually limited to sea-level density at Mach one and thus will be above sea-level at the higher Mach numbers. In Freon, the speed of sound is only about one half of the speed of sound in air, which means a stiffness ratio of about 0.25 at sea-level density. In this case, the stiffness ratio is not low enough for the normal low speed flutter model design procedure and not high enough for a high speed design based on an approximate simulation of the full scale structure.

Model Design for Transonic Blowdown Tunnels

In the transonic blowdown tunnels which are used for flutter model testing, the usual density ratio ranges from 1.5 to 2.0 and the velocity ratio is the square root of the static temperature ratio which equals about 0.79 at a Mach No. of unity. The static temperature in the test
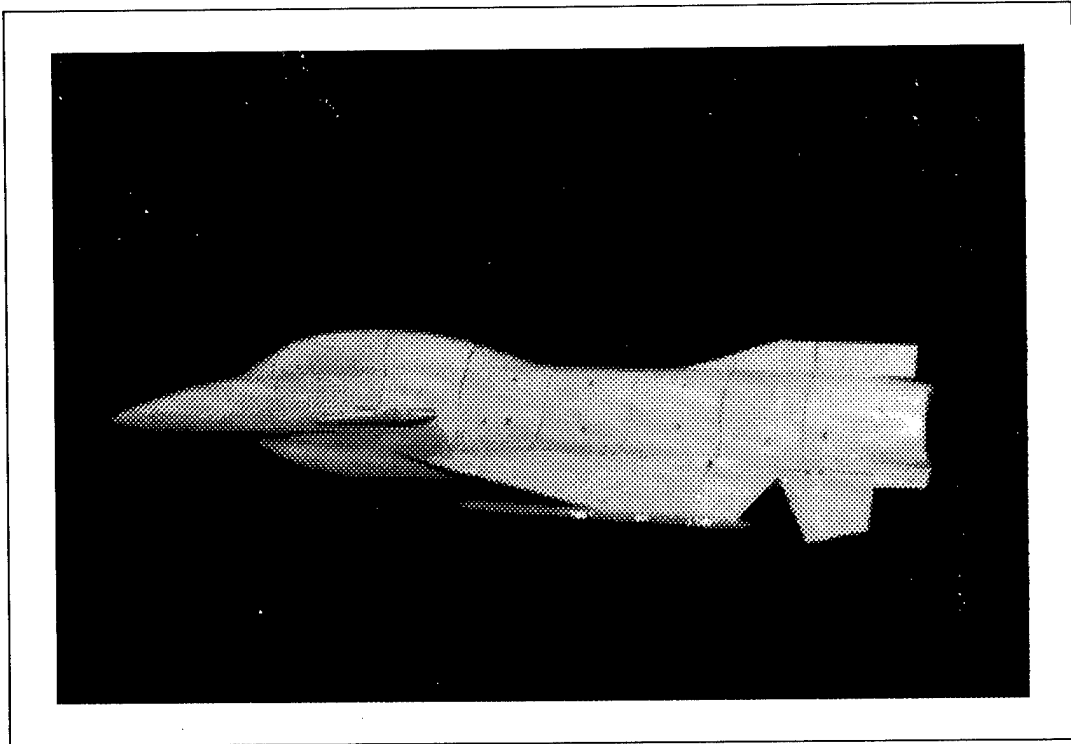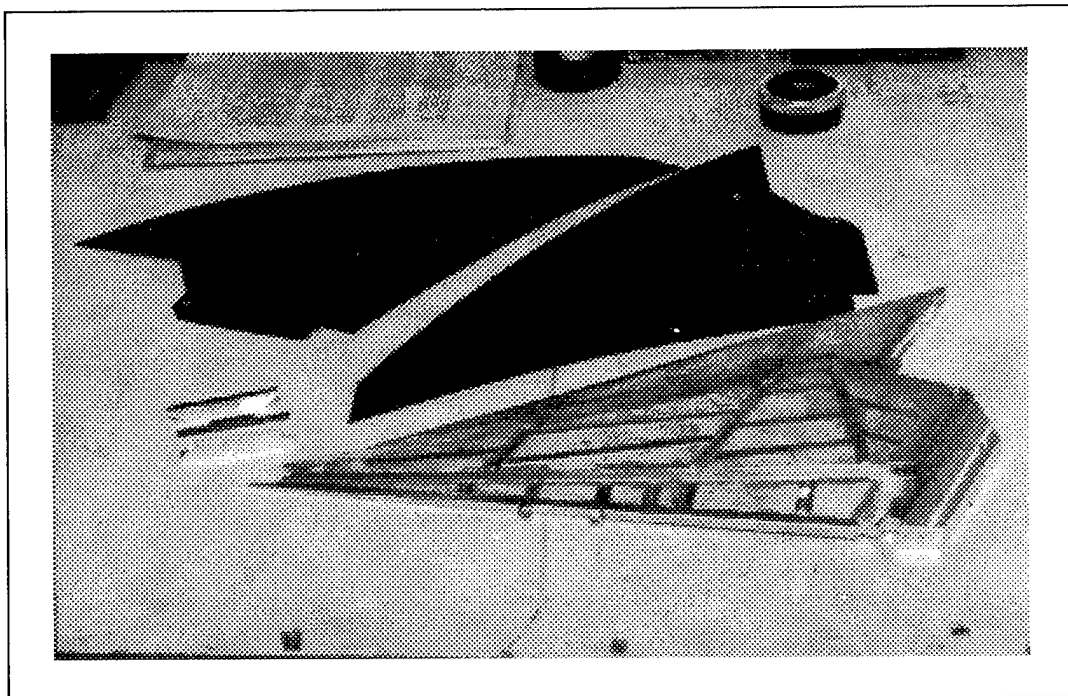
1-21

Figure 9: High Speed Flutter Model
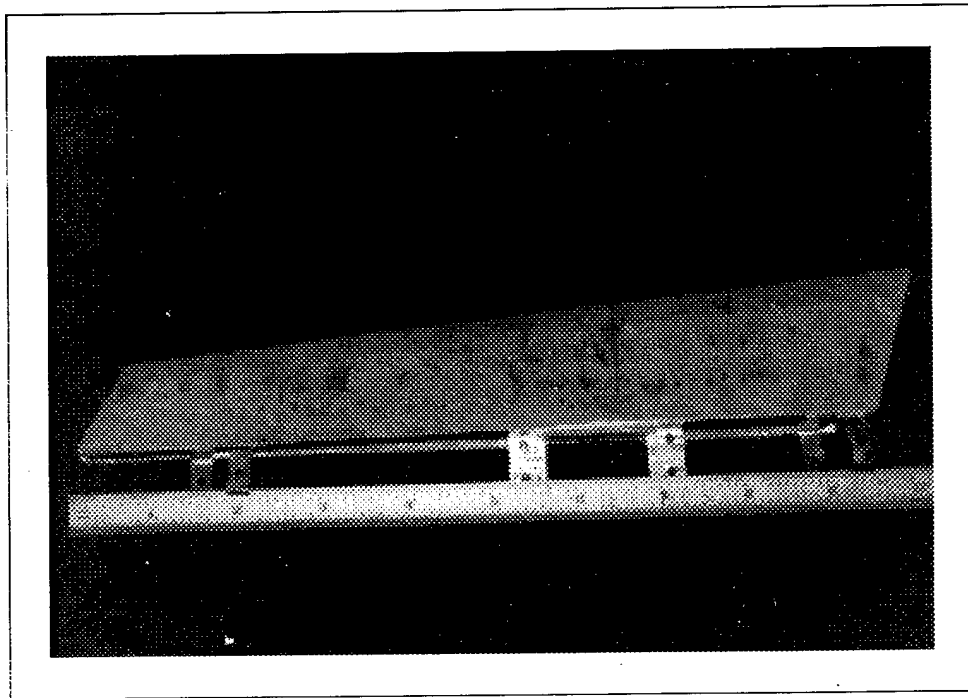

Figure 10: Cabon Graphite Skin Model

Figure 11: Leading Edge Flap Design Showing Actuator and Flexure Hinges
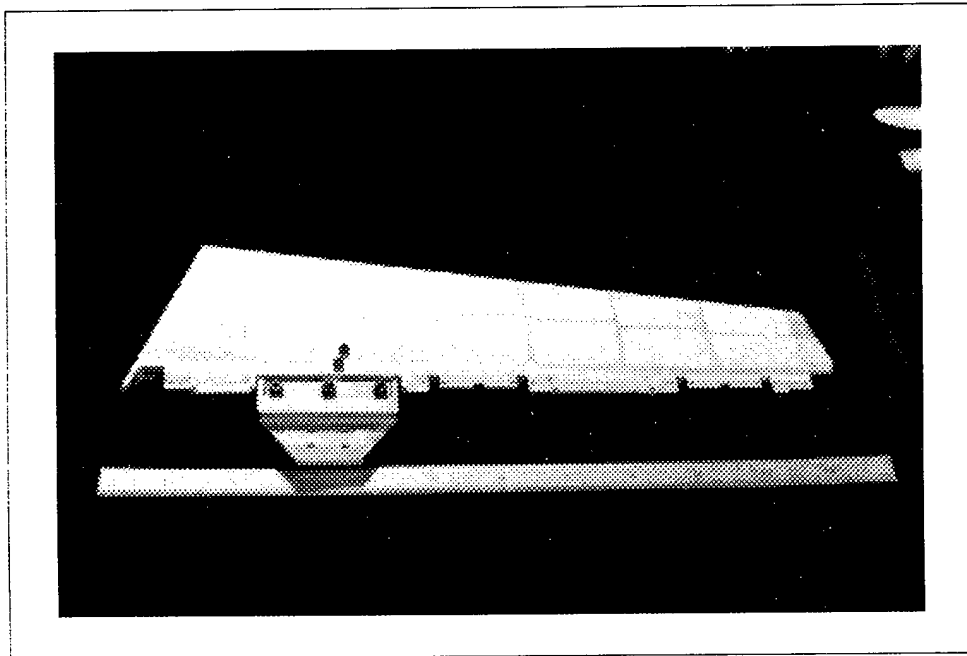

Figure 12: Flaperon Design Showing Actuator and Hinge Points

section is related to the temperature in the high pressure tank by the quantity $1/(1+0.2\ M^2)$ which equals about 0.833 at Mach one. The high pressure tank usually starts at the ambient temperature but the temperature will drop as the air is used which gives an average ratio of about 0.79 to the ambient temperature. This ratio will change with the flight condition and also if the tank is equipped with heaters. The temperature ratio times the density ratio is the q ratio for transonic model design. However a 30% - 40% stiffness reduction is usually used to provide the model with a margin of safety in stiffness. The resulting q ratio for a transonic model with a density ratio of 1.5 will therefore be about 1.5 x 0.79 x 0.71 or about 0.85. To obtain the full scale flutter q at the simulated altitude, the model flutter q may be divided by 0.85 but the resulting full scale q will not include the margin of safety. However, if 1.185 which equals 1.5 x 0.79 is used as the divisor, the resulting lower value of the full scale q will include the margin of safety. The full scale frequency is obtained for the above case by multiplying the model frequency by the scale and dividing by the square root of (0.79 x 0.71).

It has been shown above that geometric scaling will provide unity ratios of the velocity and $V/b\omega$. Multiplying the stiffness by 0.79 reduces the frequency ratio to the square root of 0.79 but $V/b\omega$ remains unchanged since the velocity ratio is reduced by the same factor. Increasing the density ratio to 1.5 does not change the $V/b\omega$ if the stiffness is also increased by 1.5. Incorporating the margin of safety reduces the frequencies and increased the $V/b\omega$ values for the model, since V is fixed by the Mach number and the tunnel static temperature. The increased $V/b\omega$ value means that the angle of attack due to the vibration velocity is reduced in comparison to the angle of attack due to the vibration amplitudes of twist and bending slope or control surface rotation. The smaller damping forces resulting from the lower frequencies will in general increase the probability of flutter for control surfaces and other flutter cases which have a limited positive damping range. Despite this violation of the scaling laws, this situation is considered acceptable when the definite flutter points which are needed for verification of the theory cannot be obtained in the wind tunnel with the correct $V/b\omega$ values or the design and/or fabrication of a model with the correct $V/b\omega$ values is not practical with available flutter model technology.

Although higher $V/b\omega$ values for the model than for full scale will lead to conservative results, it is well known that the flutter q is relatively insensitive to changes in $V/b\omega$ for classical bending-torsion flutter as long as the $V/b\omega$ values are in the range where the slope of the lift curve remains relatively constant. The unsteady aerodynamic pressures include the inertia pressures which are proportional to ω^2, the damping pressures which are functions of $V/b\omega$ and proportional to $V\omega$ and the lifting pressures which are also functions of $V/b\omega$ and proportional to V^2. In classical bending-torsion flutter, the lifting pressures must raise the bending frequency to the flutter frequency and, in combination with the inertia forces, must provide the couple that twists the structure. The flutter q therefore tends to be a function of the slope of the lift curve, the torsional stiffness and the distance between the aerodynamic center and the center of gravity, and is affected much less by changes in the $V/b\omega$ ratio. For other types of flutter, a more detailed analysis should be used to evaluate the effects of violating the $V/b\omega$ scaling rule.

In the blowdown type of transonic tunnel, the usual test procedure is to start with low density at a selected Mach number and increase the density until flutter occurs. The value of q as a function of Mach number is given by the formula $0.7M^2P$, where M is the Mach number and P is the static pressure. Using P equal to 14.7 psi at sea level, the full-scale value of q at a Mach number of unity will be about 10.29 psi or 1482 psf. In the tunnel at 1482 psf and a temperature ratio of 0.79, the density ratio will be 1/0.79 or 1.26, which means that the weight of each model component should be 1.26 times the geometrically-scaled weight to simulate the sea-level test condition. If the model density ratio is 1.5, the altitude at 1482 psf in the wind tunnel corresponds to a density ratio of 1.5/1.26, or about 6000 ft. The sea-level value of q in the tunnel for a density ratio of 1.5 is 12.26 psi or 1764 psf. It is clear that this value equals 1.5 x 0.79 times the sea level q. Higher altitudes which are critical in testing for certain cases of control surface flutter or buzz may be simulated by adding weights to the model without increasing the model stiffness. However, the effects on flutter of the increased values of $V/b\omega$ for the model should be evaluated in most cases by analysis.

The higher EI and GJ values required for transonic models can be achieved in many cases within the allowable weight by the substitution of hollow box spars in place of the solid spars used on low speed models. Initially the spars were made in two halves milled from 6061-ST or a magnesium alloy and then welded together and heat treated.

More recent models have been constructed from chemically-etched 2024-T3 sheet attached to channels formed from either 2024-T3 or 6061-ST or 6061-O. In this latter case the channels are heat treated after forming. End grain balsa with grain running normal to the top and bottom plates is cut to precise dimensions using a sanding disc on a milling machine or a grinding wheel on a surface grinder to control the heights of the box beams. The top and bottom sheets are cemented to the spars and the balsa using 3M 3813 adhesive and a clamping fixture to maintain the proper pressure on the glue joints until the adhesive sets up. In addition, aluminum 2014 alloy brads 0.035 inch in diameter and 3/16 to 1/4 inches long are added as required across joints to prevent tension failures of the adhesive. In this assembly, holes are drilled across the joints with diameters about 0.035 inches, the brads are dipped into an epoxy adhesive such as EA956 or REN and are driven into place in the holes. The brads are grooved on the outside diameter to improve the holding power. Care must be taken not too fail the joint adhesive in the process of nailing the structure together.

The spar weight per inch is still maintained at 50% or less than the total weight, as is the case for low speed models. The combined weights of the top and bottom sheets per inch should not exceed about 40% of the total weight per inch. From this calculation the area of the skins can be determined by dividing 40% of the weight per inch by the density of 2024-T3 or about 45.4 grams per cubic inch. The scaled value of $I(EI/E)$ is used to determine the mean height required between the skins from the formula

$$a_m = \left(3.6\,\frac{I}{A}\right)^{0.5} \tag{1}$$

where

A is the total skin area, and

a_m is the mean distance between the top and bottom skins.

In the formula, 90% of the required I is assumed to be provided by the top and bottom skins, and the rest by the spars. The skin thickness is normally less than 0.032, but is selected to obtain the spar width necessary for GJ, or from the fore and aft stiffness, whichever is larger. The usual formula for the torsional stiffness, i.e.

$$J = \frac{4AB^2}{\int \frac{1}{t} ds} \tag{2}$$

is used to determine the width of the box required for J since AB is the mean area enclosed by the box and the width of the box is AB divided by the mean distance between the skins. Since this formula gives too high a value of GJ for tapered beams, and if solid balsa covering is to be used, the torsional stiffness is increased further, so the spar is usually designed to provide from 75% to 90% of the required GJ. The 90% value is used when the J/I ratio is 3.5 or more. The value for I is computed without correction as the area moment of inertia about the neutral axis including the spars. The above approach is facilitated by the use of computer programs.

Detailed flutter model design is similar to conventional mechanism design except that the weight, stiffness and strength of each component must be computed as part of the design process. In general, the structural or spar weight should not exceed 40% of the total allowable weight in each model section or the section cannot be properly mass balanced. Mass balancing usually means obtaining the correct weight, c.g. location and moment of inertia of each section. A computer program is used to compute the masses which must be added to satisfy these mass balancing requirements.

In addition to the spar design, the other model design problems are the hinges and actuators for the control surfaces, the pylons and external stores, and the connections between major components such as the fuselage and the wings and the fuselage and the tails. Beam theory is normally used to solve the majority of the model structural design problems for which computer programs have been written by Delta Dynamics. The design objective is to have each part perform its required function with the correct stiffness as well as with an acceptable static strength and weight and a minimum of friction and hysteresis. In addition the design should be as simple as possible to minimize the cost of machining and inspection.

Since many engineering man hours must be spent converting the engineering calculations described above into the drawings and instructions which a shop needs for the fabrication of the model hardware, advanced design techniques involving the use of CAD systems would

appear to offer substantial savings in cost and time. The objective sought by Delta Dynamics is to make use of CAD systems which will provide disks which can be used to control the Bridgeport CNC mill through the Bridgeport EZCAM computer system.

The models must be tested to determine the actual mass and stiffness distributions. Most of the stiffness tests are made by fastening mirrors to the model and reading the changes in the slope angles of the mirrors under external loads or moments applied to the model (see Figure 13). Cross wires projected from a slide projector are reflected by the mirrors and focused on a scale. The motion of the cross wires on the scale are approximately proportional to the change in angle of the corresponding mirror on the wall. Using the rule that the angle of incidence equals the angle of reflection, it can be seen that the motion of the cross hairs equals the change in angle multiplied by twice the distance between the mirror and the scale. It the light beams are nearly perpendicular to the mirrors, the above rule can be used without applying corrections.
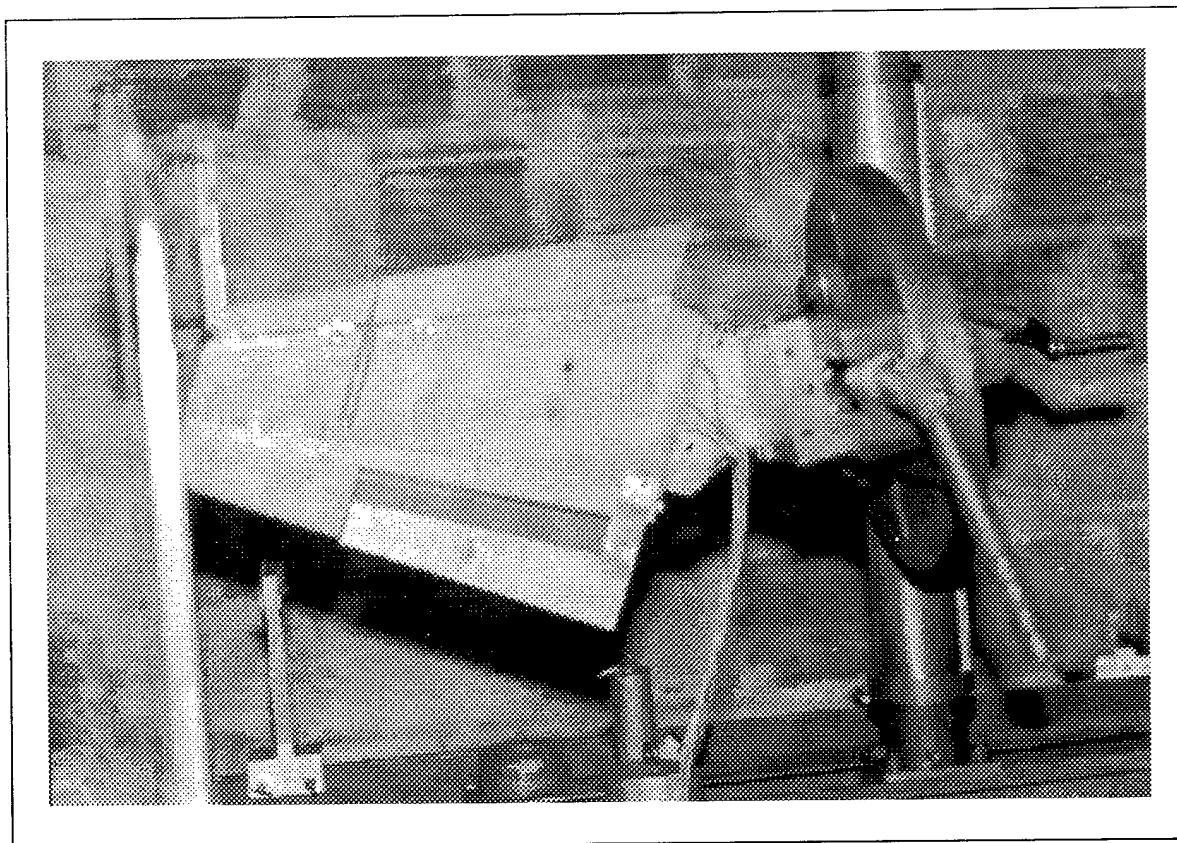

Figure 13: Mirror Deflection Testing

The mirror test technique has proven to be fast and quite accurate. The major problem is hysteresis in the model structure which causes the readings not to return to the zero positions when the loads are removed.

Computer programs are available to compare the measured readings with the required readings. The change in angle with respect to distance along a beam equals *M/EI* or *T/GJ*, where *M* is the bending moment and *T* is the twisting moment. For a given distance along the spar, the angle changes equal the integrals of the above quantities.

To locate the center of gravity of a model component, the component is balanced at two angular positions on a knife edge or the edge of a triangular scale. Lines are drawn on the model for the two positions and the intersection of these lines is the center of gravity. To obtain the moment of inertia, the model component is fastened to a bifilar pendulum with the c.g. at the center of rotation of the pendulum. The period of the oscillation is measured and the ratio of the moment of inertia to the weight is computed using the formula:

$$\frac{I}{Wt} = \left(\frac{g}{l}\right)\frac{d^2}{\omega^2} \tag{3}$$

where

g is the acceleration due to gravity,

d is half the distance between the strings,

l is the length of the strings and

ω is the frequency in radians per second.

The frequency in radians per second is equal to $6.282/T$ where T is the period in seconds. The formula for the bifilar pendulum includes the increase in the effective mass when the radius of gyration is greater than d. When I/Wt equals d^2, the formula reduces to the case of the simple pendulum for which ω equals the square root of g/l. At the present time, the period is measured with a stop watch which is somewhat slow since 10 or more cycles are counted to improve the accuracy. It is possible that an electronic timer in combination with a optoelectronic device could be used to save test time since only a small number of cycles would have to be measured.

FLIGHT FLUTTER TESTING

Flight flutter testing is used to demonstrate safety from flutter for the airspeeds and altitudes at which flutter analyses, wind tunnel flutter model tests, and past experience with flutter problems indicate that the margins of safety are the lowest. A second reason for such testing is to produce flight test data that can be used to show that the margins of safety against flutter meet or exceed the values in the specifications for the aircraft. If the aircraft carries fuel in the

wing, wing mounted engines, external stores on the wing including weapons and/or tip tanks, additional flight flutter testing will be required if the flutter prediction program indicates a number of loading conditions that will produce flutter within the flight envelope.

In the years of flight flutter testing before 1940, a number of such tests with vibration excitation equipment resulted in structural failures and deaths to the flight crews. Although this result slowed up this method of testing, there has been a substantial increase in the number of such tests because of requirements established by the government to obtain approval for high performance passenger and military aircraft. This increased emphasis on flight flutter testing has also led to improvements in flutter prediction methods including unsteady aerodynamics, flutter calculations using digital computers, wind tunnel tests of flutter models and ground vibration testing. Modifications of the flutter analyses are carried out if the mode shapes and frequencies measured during ground vibration testing are substantially different from the values used in predicting flutter before completion of construction of the first aircraft of each new design.

The advantages of flight flutter testing with vibration excitation equipment are as follows:

1) If flutter occurs, the airspeed required to initiate flutter will almost always be reduced if the amplitudes of vibration of the structural components involved are increased well beyond the amplitudes encountered by random air disturbances during dives by test pilots.

2) The decrease in airspeed at the start of the flutter will usually cause flutter to be less violent when it does occur because of the decreases in the aerodynamic forces and moments.

3) Substantial vibration responses will tend to prevent nonlinear forces and moments from producing false indications of safety from flutter. Such non-linearities include static hinge friction, excessive boundary layer thicknesses and preloaded springs. If the skins of the structure of a wing, stabilizer or fin is close to buckling due to static loads, substantial vibration responses will result in reduced frequencies.

4) Explosive types of flutter such as bending-torsion of fixed surfaces can often by detected before flutter occurs by the reduction in the gains of the amplifiers that is required to prevent overloading. In one case involving the excitation of bending-torsion flutter with a rotating weight vibrator, the gains of the amplifiers had to be reduced several times due to the decreases in damping and increases in the vibration responses that occurred as the flight speed approached the flutter speed.

Some warning of the approach to flutter has been obtained without the use of vibration excitation equipment. In one case of spring tab flutter with a preloaded tab spring, the neon bulbs that were used to indicate overloading of the amplifiers started flashing well before the vibrations could be detected by the members of the flight crew. Another method for detecting the approach to flutter involves the use of an oscilloscope for detecting the phase and amplitude relationships between bending and torsion. An electrical output signal proportional

to the torsional vibration amplitude is connected to move the spot, produced by the electron beam, along one axis (either vertical or horizontal), and the electrical output signal proportional to bending vibration is connected to cause the spot to move along the other axis. The gains are adjusted to keep the motions of the spots within the limits of the scope. At speeds well below the flutter speed, the motion of the spot is random, indicating that the phase angles and amplitude ratios between bending and torsion are changing with time. As flutter is approached, the spot will move in an ellipse or circle for a small number of cycles. This display, which indicates a definite phase angle and amplitude ratio between bending and torsion, can be used by the flight crew as a warning not to increase the airspeed unless approval is obtained from the engineering department.

The equipment suitable for flight flutter testing is as follows:

1) Vibration excitation equipment - A single rotating weight or counter-rotating weights are driven by D.C. shunt motors. The connection between the motor and the rotating weights can be through a reduction gear or by means of a flexible shaft connected to the reduction gear. In this case, the reduction gear must be mounted on separate bearings. Two type of aerodynamic vibrators have been used; conventional oscillating vanes, and the combination of a flat plate with a variable speed rotating slotted cylinder at the trailing edge. Sketches of the various types of excitation equipment are shown in Figures 14 through 16.
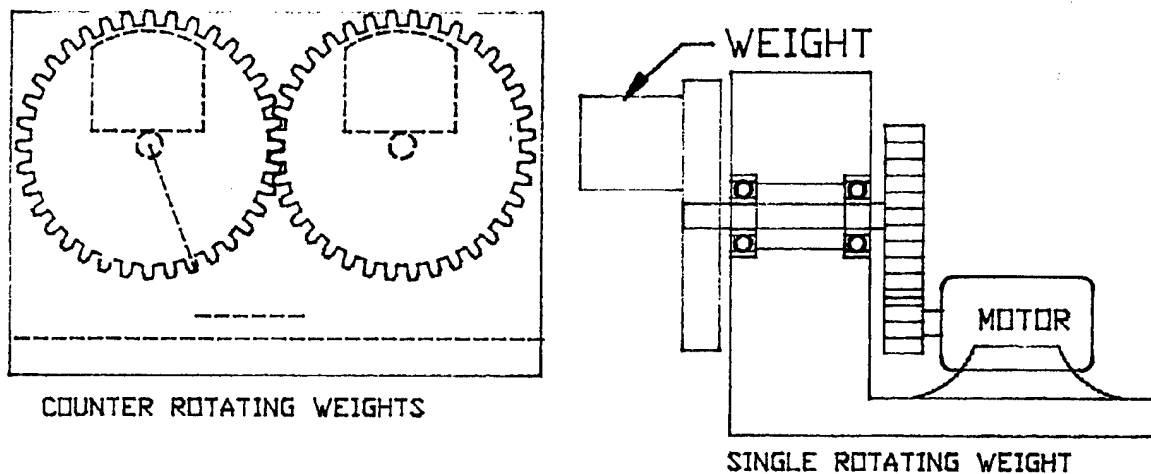

COUNTER ROTATING WEIGHTS
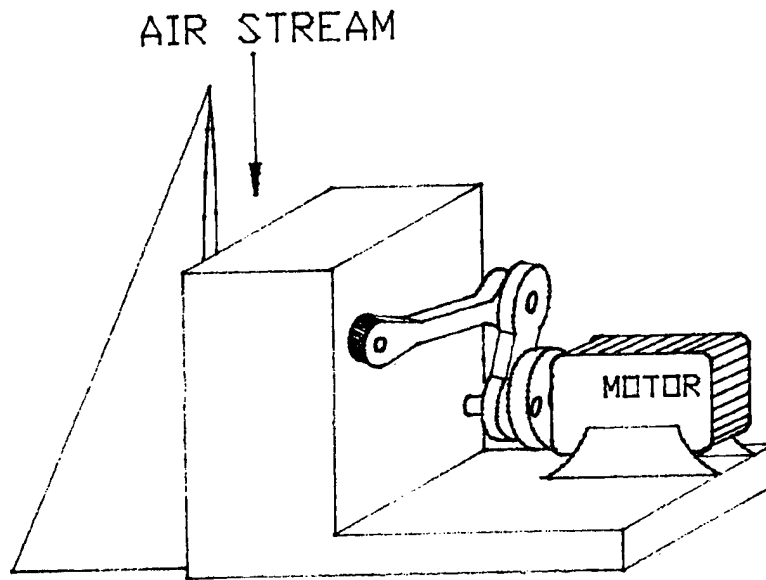
SINGLE ROTATING WEIGHT

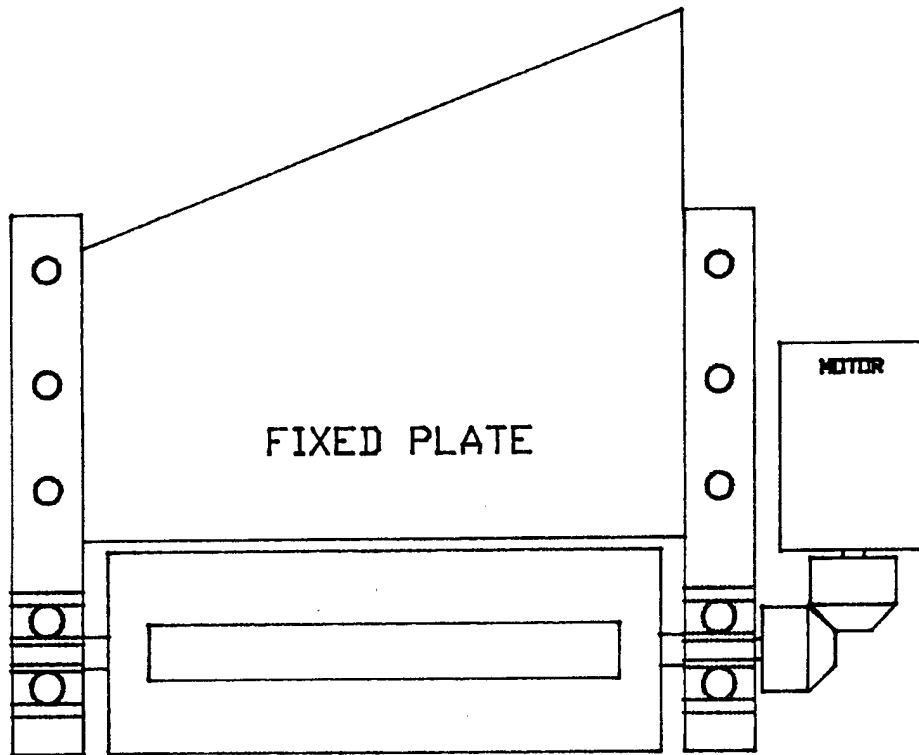Figure 14: Rotating Weights

Figure 15: Oscillating Vane

Figure 16: Slotted Cylinder

2) Vibration measuring instruments for use during flight flutter testing include strain gages, accelerometers and velocity pickups. Vibrations of control surfaces and tabs have been measured by using a magnet attached to the control surface and a coil attached to the supporting surface with an output proportional to the rotational velocity of the control surface and/or tab relative to the supporting surface. Strain gages on a torsion beam attached between the control surface and supporting surface, and photoelectric devices, have also been used. Sketches of some of the measuring devices are shown in Figures 17 through 19.
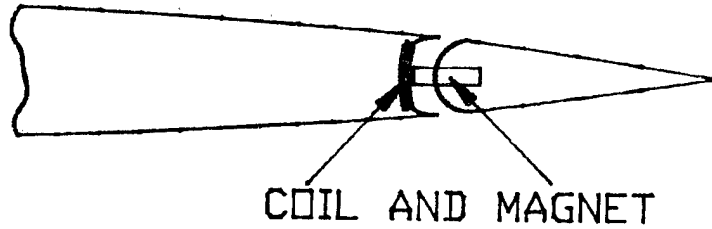
COIL AND MAGNET

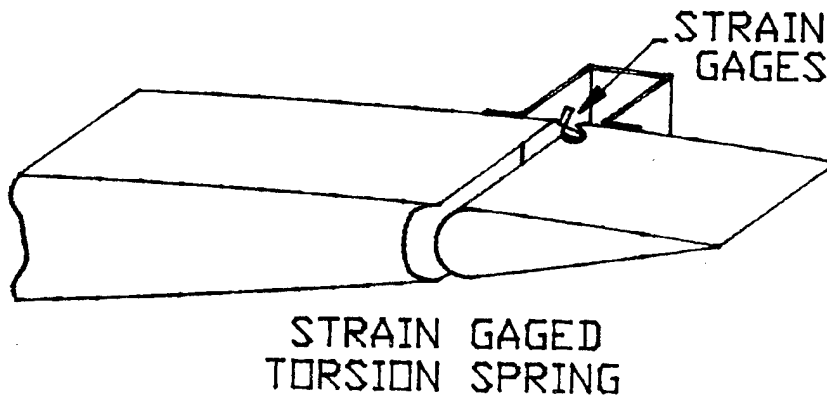Figure 17: Coil and Magnet

STRAIN GAGES

STRAIN GAGED
TORSION SPRING

Figure 18: Strain Gauged Torsion Spring
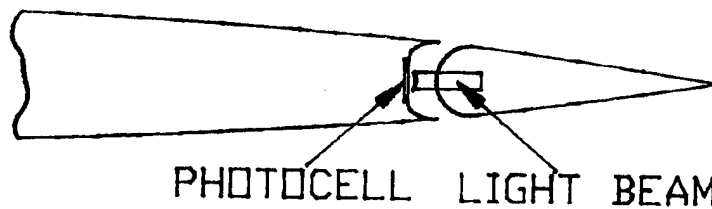
PHOTOCELL LIGHT BEAM

Figure 19: Photocell Light Beam

The installation of suitable vibration excitation and measuring equipment should be determined by the mode shapes indicated by the flutter analysis. For fixed surfaces including wings, stabilizers and fins, the oscillating aerodynamic vanes are usually located at the tips of the surfaces and the airfoils with rotating cylinders are located just inboard of the tips. Mechanical shakers consisting of rotating weights are usually located near the leading edge inboard of the tip to produce a substantial torsional response. The vibration measuring equipment should be located to indicate the type of flutter that is expected. However, practical difficulties in locating the measuring equipment, such as no removable cover plates in the structure at the desired locations, must be considered. This problem can be solved by making the installation of test equipment in the test airplane during construction.

In certain cases, vibrations in flight have been caused by separated air flow. Such flow separation may be detected by pressure measurements on the on the external surfaces at high speeds and by means of yarn tufts attached to the surface at airspeeds low enough that the tufts will remain attached to the surface. Flow separation induced by shock waves has been encountered in a number of high performance aircraft. One method for preventing such separation has been to use vortex generators. Another method that has been used successfully in one case is to install a wedge at the location of the shock on the wing. It is believed that the wedge stabilizes the position of the shock wave. Dampers have been used on many aircraft to prevent excessive vibrations of control surfaces due to shock-induced flow separation. Typical vortex generators are shown in Figure 20 and the wedge is shown in Figure 21.
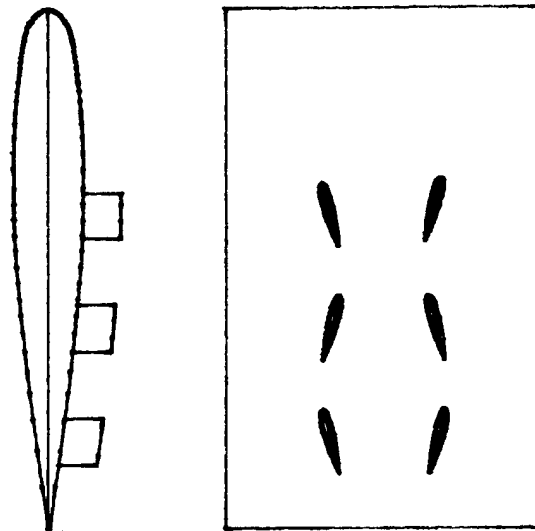
VORTEX GENERATORS

Figure 20: Vortex Generators
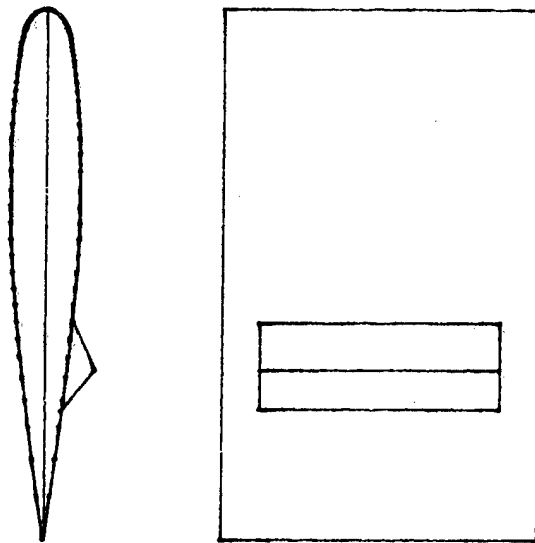
WEDGE

Figure 21: Wedge

When flutter is encountered during high speed flights by test pilots, an extensive effort is made by the engineering department to determine the cause of the problem and to test modifications of the airplane such as mass balance and/or dampers, if the control surfaces are involved. Since extensive modifications of the structure after the airplane has been constructed can be extremely expensive, the actual modification is determined by the joint effort of the flutter, structural and manufacturing groups under the supervision of the chief engineer. Major structural modifications are often evaluated by means of wind tunnel tests of flutter models before the changes are made and additional flight flutter tests are conducted.

Although aircraft with top speeds well below the speed of sound are less likely to flutter, it is recommended that companies and individuals who design and build such aircraft consider employing an experienced flutter engineer as a consultant to prevent flutter problems that might result in the destruction of the airplane and injury or death to the pilot. Although the exact causes of deaths or injuries in home built aircraft are not known, ground vibration testing and simple flutter analyses may uncover structural and flutter problems. In some low speed aircraft, the structural frequencies involved in flutter can be low enough so that suitable excitation of the structure in flight can be made by oscillating the control pedals or control column. The control wheel can also be used for the unsymmetrical excitation of the ailerons. If flutter is approached, the forces required to move the control surfaces will be reduced because of the reduction in damping. Low frequency vibration responses can usually be observed and/or felt by the test personnel so that the installation of vibration measuring equipment may not be necessary.

AIRCRAFT GROUND VIBRATION

Test Techniques

One objective of ground vibration testing is to obtain the vibration amplitude distributions, (mode shapes) and the frequencies of the structure for use in the prediction of flutter problems. Most flutter problems involve two or more of the following types of vibration: bending and torsion of fixed surfaces, rotation and/or torsion of control surfaces and rotation of tabs. Flutter occurs when the aerodynamic damping due to motions in one vibration mode such as wing bending is balanced by the lift due to the angle of attack in another vibration mode such as wing torsion. Figure 22 illustrates two of the vibration modes of a wing-aileron combination.

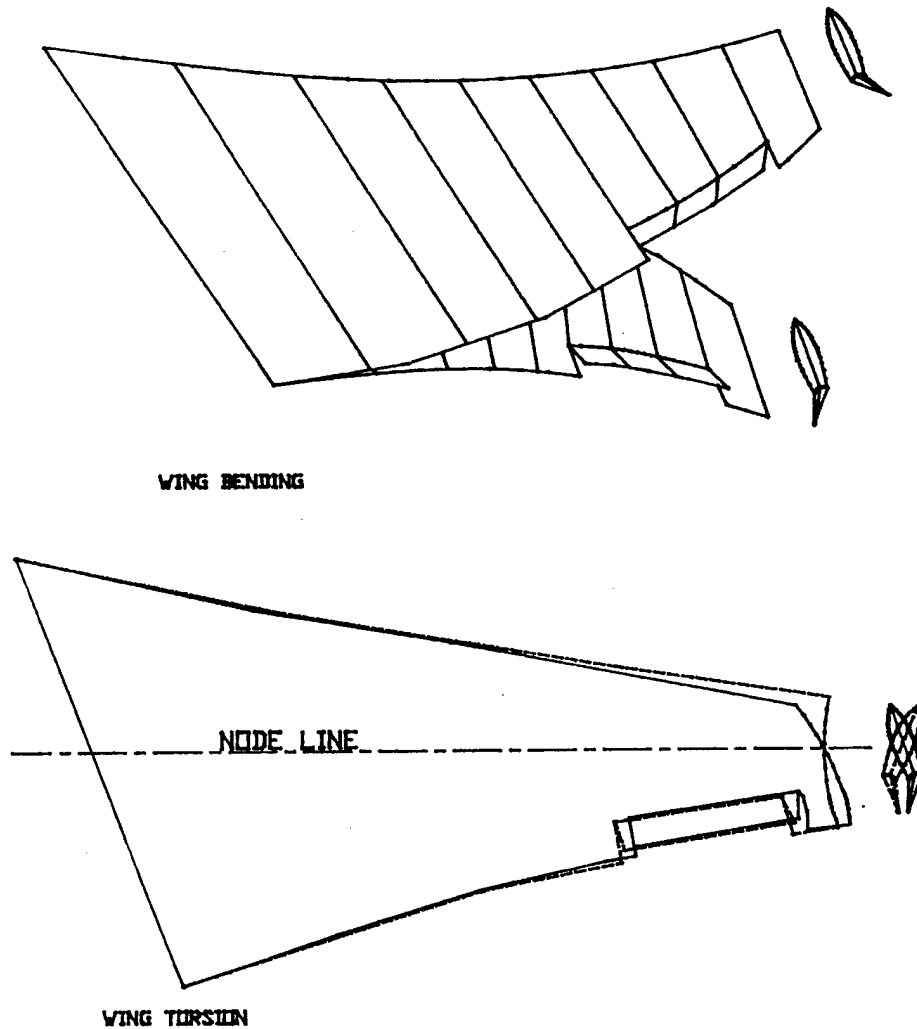WING BENDING

WING TORSION

Figure 22: Wing-Aileron Vibration Modes

The primary causes of flutter are as follows:

1. Insufficient torsional stiffnesses with center of gravity locations of spanwise sections substantially behind the quarter chords on wings, stabilizers and fins.

2. Control surfaces with center of gravity locations of spanwise sections behind the hinge lines and inadequate rigidities in the control systems.

3. Trim tabs with inadequate stiffnesses in the rotational restraints and/or excessive free play.

4. Spring tabs with inadequate stiffnesses in the rotational restraints coupled with motions of the control systems.

5. External stores on the wing including engines, tip mounted fuel tanks, and heavy wing mounted weapon systems which produce unstable coupling between bending and torsion.

6. Wing mounted engines with propellers which produce unstable gyroscopic and aerodynamic couplings between pitch and yaw.

7. Horizontal tails mounted on the tops of vertical tails which produce unstable coupling between fin torsion and stabilizer yaw with fin bending and stabilizer roll.

8. Rotational flexibilities at the roots of all movable horizontal tails which substantially lower the torsional frequencies.

9. Active control systems.

Although theoretical predictions of the frequencies and mode shapes before construction of the aircraft can be subject to significant errors, such predictions are very useful in the planning of ground vibration testing as will as in flutter calculations and flutter model programs which are completed before the aircraft has been constructed.

The equilibrium conditions applicable to dynamic analysis require that the internal inertia, damping and spring forces acting on each mass must balance any external forces which are applied or the internal forces must be in balance at locations in the structure where there are no external forces. It is obvious that the equations of equilibrium apply for all vibration testing no matter how nonlinear or highly damped the structure may be or what types of force inputs are applied. However, the usual analytical procedures for dynamic analysis make use of the normal modes of vibration which can only exist in structures that are linear.

The following problems encountered in the ground vibration testing of aircraft should be considered in order to obtain the required normal mode information with sufficient accuracy and with the efficient use of the manpower available to conduct the tests.

1. Providing rigid body frequencies which are low compared to the structural frequencies

2. Locating the shakers
3. Selecting the wavefoms used for inputs to the shakers
4. Measuring the responses
5. Processing of the test results

1. Providing Low Rigid Body Frequencies

Some success has been obtained in meeting this objective by supporting the aircraft on the landing gear with reduced pressures in the tires. In this case, there will be some linear damping caused by motions of the shock struts. However, such damping forces will usually be small compared to the inertia and elastic forces in the structural frequency range.

Air springs beneath the tires have been used to improve the isolation. Although, retracting the landing gear might be desirable to simulate flight conditions, the support system is likely to be too complicated to be used. If such a support system is desired, the aircraft could be supported from above using three cables to provide the yaw, lateral and fore and aft degrees of freedom and tension springs connected between the cables and the aircraft to provide the vertical, pitch and roll degrees of freedom. The cables should be eliminated if the tension springs would provide all six degrees of freedom within the allowable frequency range. Compression springs located beneath the aircraft would be another potential mounting system.

2. Locating the Shakers

The vibration modes involved in potential flutter problems should be considered when determining the most useful locations of the shakers. All shaker locations which produce substantial vibration amplitudes of the components of the aircraft whose motions can cause flutter would be satisfactory. For wings without stores, engines and tip tanks, as well as for stabilizers and vertical tails, the usual practice has been to locate the shakers near the tips of the structures and phase the shakers on wings and stabilizers to obtain symmetric and antisymmetric modes. To excite the torsional modes, the shakers should be installed well ahead of behind the torsional nodal lines. Such locations would be just ahead of the trailing edge control surface or near the leading edge or just behind the leading edge control surface if such a surface is used. While two shakers could be installed near each wing tip and phased to produce forces for bending excitation and torques for torsion, this installation is only required if the torsional response is not adequate with one shaker installed near each tip. If the vibration responses of control surfaces are not adequate, direct attachment of the shakers to the control surfaces should be used. However, if dampers are attached to the control surfaces, tests should be run with and without the dampers. For spring tabs, the response of the control system as well as the response of the tab should be measured. In this case, it will be necessary to attach a shaker to the control system if the response is inadequate with a shaker attached to the control surface. The vibration amplitude of the tab should be large enough to overpower tab restraints caused by preloaded springs.

For wings with external stores, direct attachment of shakers to each of the stores which might cause flutter would be required if the response of the store is too small to overcome non-

linearities as well as for accurate measurements when the shakers are attached near the wing tips.

Direct attachment of the shakers to the control surfaces should be made if the surfaces are used for active control. The active control system should be energized during such tests.

The methods of attaching shakers to the above structures include: a) attaching the shaker rods to a plate with machine screws where threads are available on the surfaces of the aircraft structure to mount the plate with a bolt, and b) holding the shaker rod against the structure using a vacuum inside a rubber vacuum cup attached to the shaker rod. Another possibility is to glue a mounting plate to end grain wood which is attached to the structure with fast drying glue which can be easily removed after the test has been completed. It is desirable that bending moments at the end of the shaker rod be reduced with a universal joint with minimum free play and low friction.

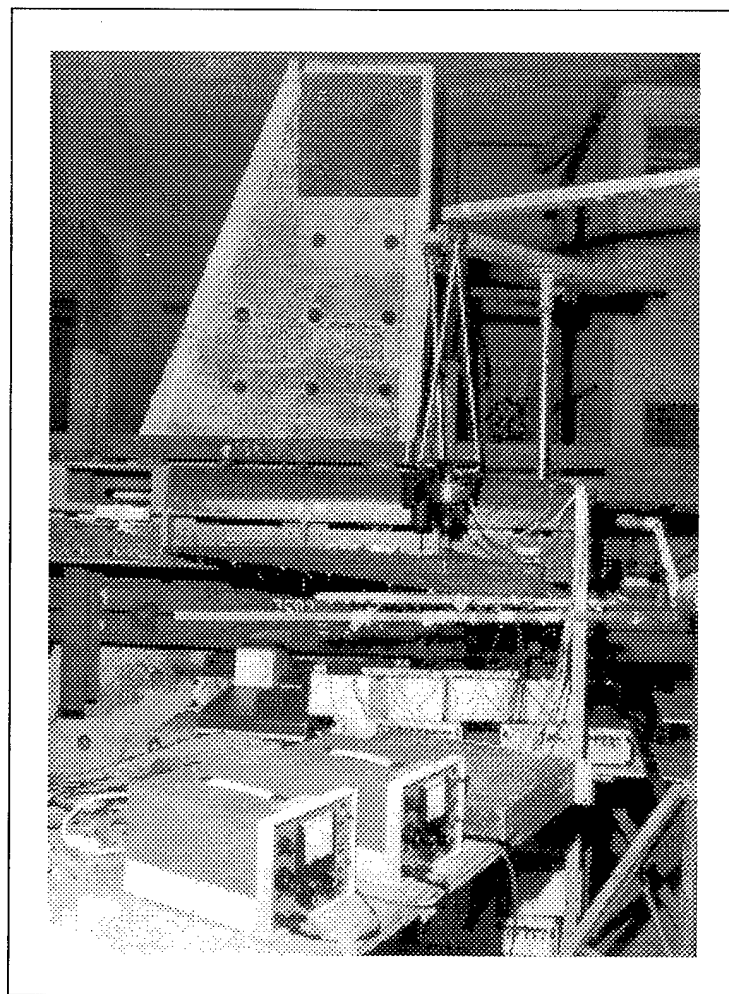Figures 25 through 28 demonstrate different placements of shakers:
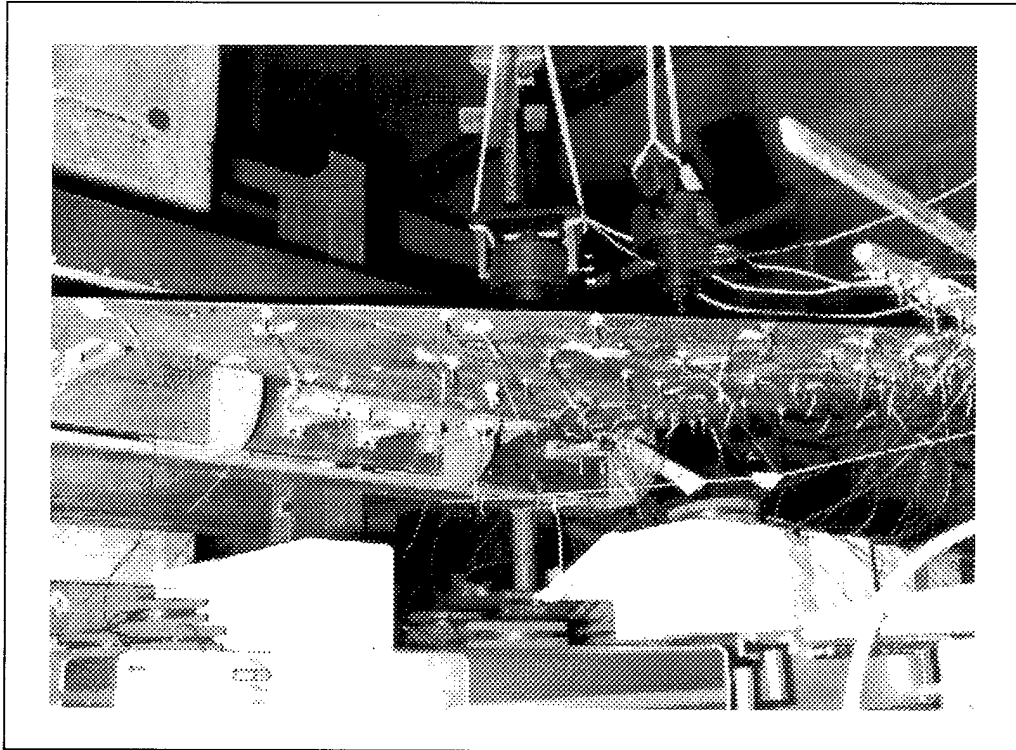

Figure 25: Shaker Location (View #1)

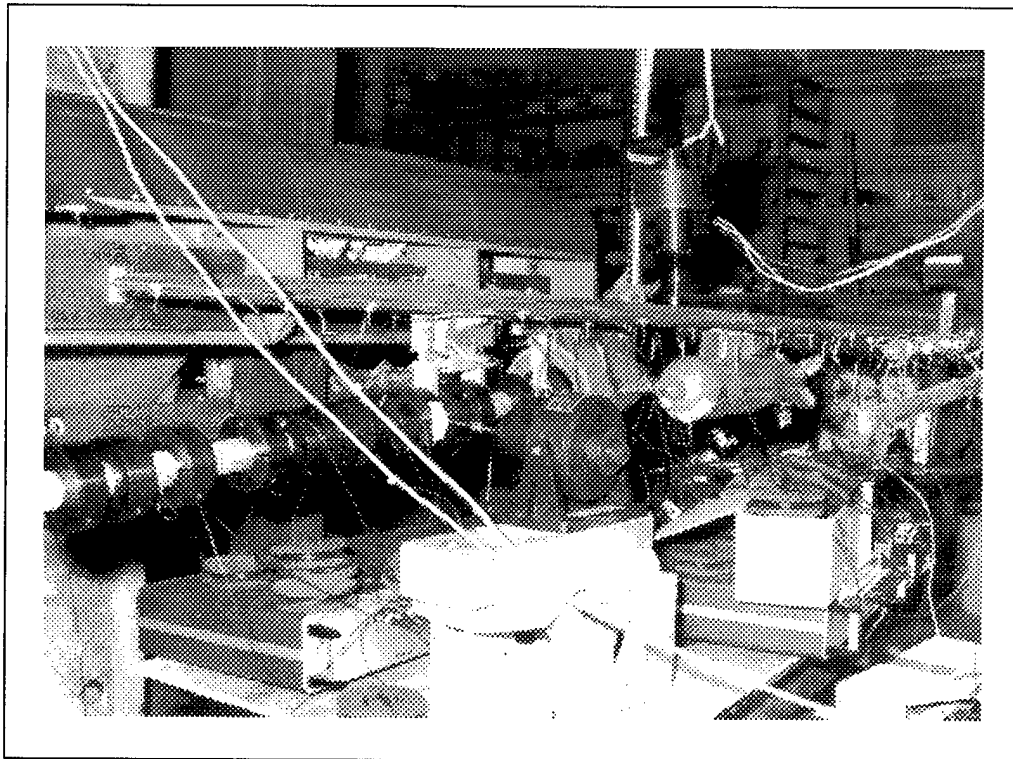Figure 26: Shaker Location (View #2)

Figure 27: Shaker Location (View #3)
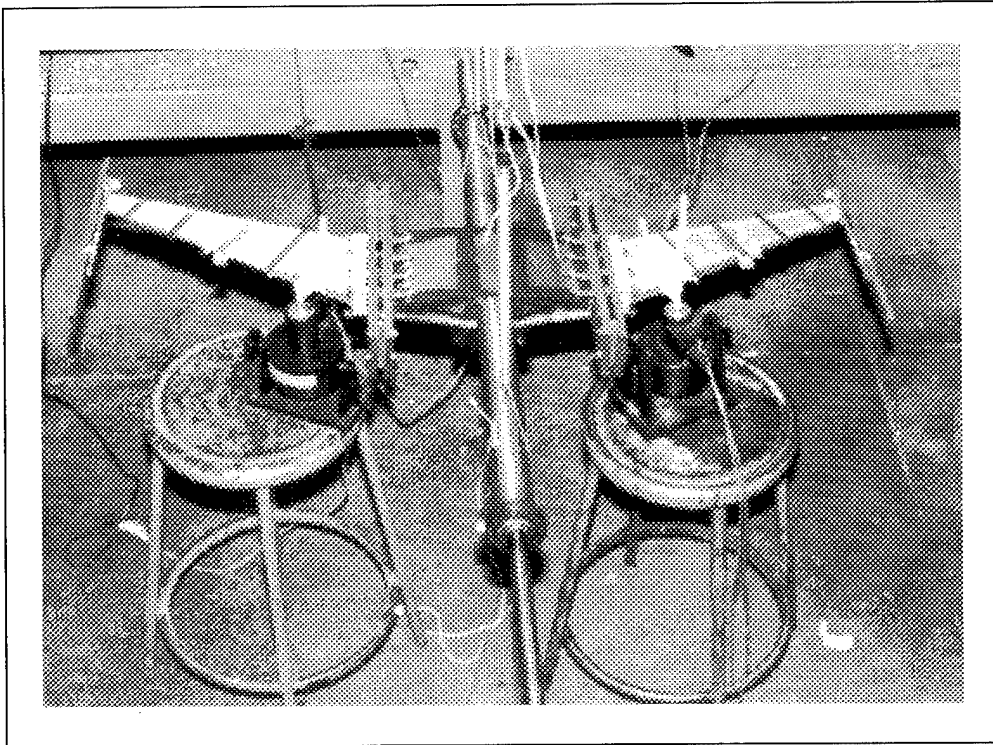
Figure 28: Shaker Location (IORN Bird)

3. *Shaker Inputs*

It is recommended that sine dwell be used as the shaking force since the mode shapes and frequencies can be measured directly from the outputs of accelerometers or other vibration measuring devices. Although more complicated shaker inputs have been used to save test time, the calculations of the mode shapes and frequencies are based on the assumptions of linear theory which will not be applicable at certain locations in the actual structure. In addition, the concentration of the input forces at one frequency with sine dwell provides the high energy excitation which is often necessary to overcome friction, free play and other non-linear effects including structures using skins which buckle at high loads. Nevertheless, where accurate theoretical predictions have been made and previous experience with similar structures using complicated vibration inputs has been satisfactory, an input waveform containing all the frequencies of interest could be tried to save test time. The following figures demonstrate some typical shaker inputs:
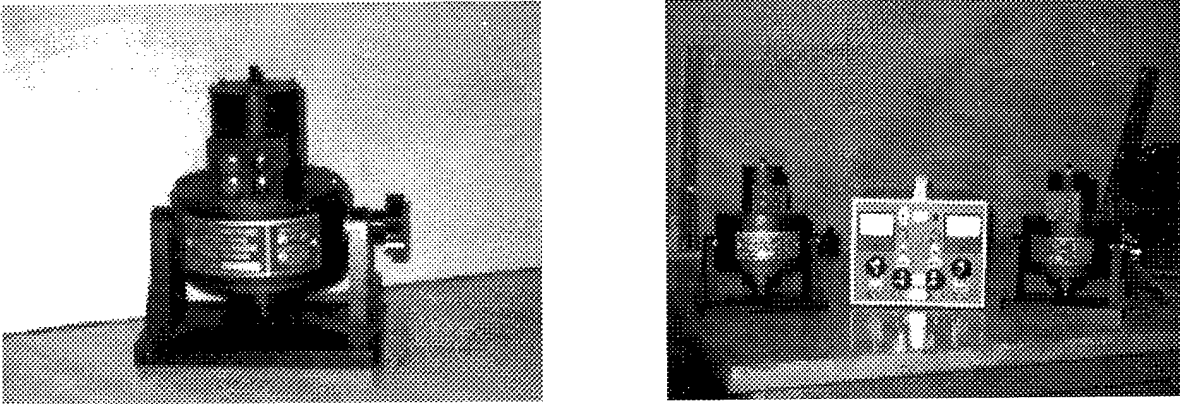
Figure 29: Shaker Input

4. *Instrumentation*

Roving vibration measuring pickups (accelerometers or devices which respond to vibration amplitude or velocity) have been used by some test engineers.

In this case, one vibration pickup should be mounted on the structure to provide a reference amplitude and the roving pickup should be held against the structure with a restraint which will not affect the frequency and damping. In some cases, test personnel can use one hand to hold the pickup against the structure. In other cases, the pickup can be mounted on a spring restrained light weight four bar linkage which test personnel can use for the same purpose. A typical design for such a linkage is shown in Figure 30.
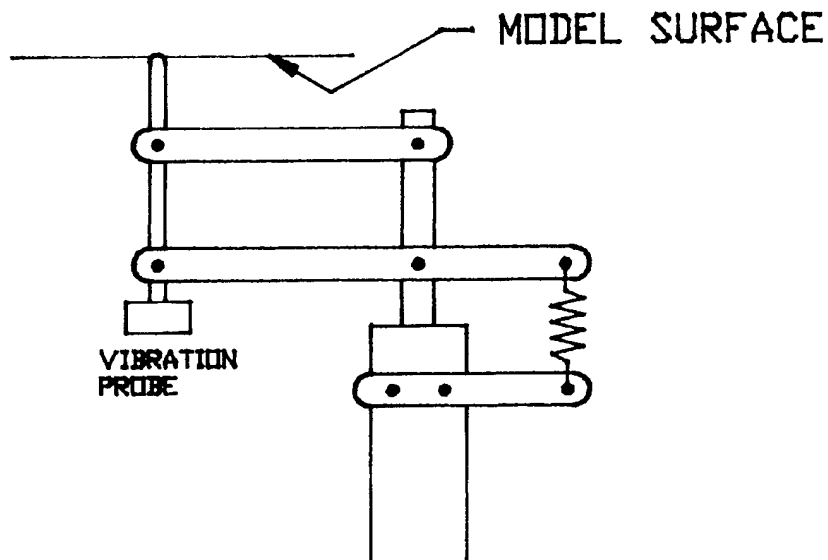
Figure 30: Four Bar Linkage Vibration Probe Support

Improved data processing is possible with the installation of a large number of pickups. However, the use of a good math model can be used to reduce the number. Tests should be made with a sufficient number of pickups to determine if the correlation with theory appears to be acceptable. If the agreement is satisfactory, additional pickups will not be required. Sine dwell should be used in cases where a large number of pickups have been installed, since the amount of test time that might be saved with more complex inputs will usually be small compared to the time required for calibrating and installing the pickups.

Fast drying glue can be used to install lightweight pickups directly to the structure where the external surface is flat. In other locations, the pickups should be fastened to thin metal plates glued to end grain wood pads which are contoured to fit the surface and can be glued with fast drying glue. For heavier pickups, thicker metal plates should be used so that the pickups can be mounted with machine screws.

5. *Data Processing*

Measuring the response using a multichannel oscilloscope or recorder with an adequate frequency response has been widely used to obtain the amplitudes, frequencies and phase angles excited during ground vibration testing. However, some of the digital systems in use at the present time might be almost universally used in the future to save engineering hours. In this case, the data would be digitized and stored on disks for later processing. However, enough data should be processed during a vibration test to insure that the results are sufficiently accurate so that the test will not have to be repeated.

Engineers with sufficient flutter experience can usually make this decision correctly by studying the vibration amplitudes and phase angles in the vibration modes that might result in flutter.

ADDITIONAL INFORMATION CONCERNING MODAL ANALYSIS

Orthogonality between two natural modes is computed by multiplying each mass by the product of its displacements in the two modes and summing the results over all the masses. If the displacement of each mass in the two modes are in different directions, each product is multiplied by the cosine of the angle between the directions. A zero result from the summation indicates that the modes are orthogonal. The advantage of using orthogonal modes is that the response in each mode can be computed using the equations for a single degree of freedom system.

For each normal mode, the generalized coordinate is the displacement of the structure at a reference station. This displacement is multiplied by a function (mode shape) giving the ratio of the displacement of each point in the structure to the displacement at the reference station. The effective mass in each normal mode is computed by multiplying each mass by the square of the ratio of the amplitude of the mass to the amplitude at the reference station and summing the results for all the masses. The effective spring force is computed by multiplying the

effective mass by the square of the undamped natural frequency and the effective damping can be computed from the amplitude ratio at resonance or from decay records. the effective input force is the actual force multiplied by the amplitude of the structure in the direction of the force at the point where the force is applied.

The amplitude and the phase angle of vibration in a single degree of freedom system caused by a force P is given by the formula

$$P = m\omega^2 x - kx(1 + jg) \tag{4}$$

in which m is the mass, k is the spring constant, ω is the frequency in radians per second and g is the damping coefficient. A vector plot may be drawn to determine the response. $m\omega^2 x$ is located along the positive x-axis, kx is located along the negative x-axis and $-kxjg$ is located on the negative y-axis. A low frequencies, P is located a few degrees above the x-axis since $m\omega^2 x$ is small compared to kx and kg is usually small compared to k. At resonance, $m\omega^2 = k = m\omega_n^2$ where ω_n is the natural frequency, so the force P leads the displacement by 90 degrees.

At high frequencies, $m\omega^2$ is much greater than k, so P leads the displacement by slightly less than 180 degrees. A typical vector diagram is shown in Figure 31.
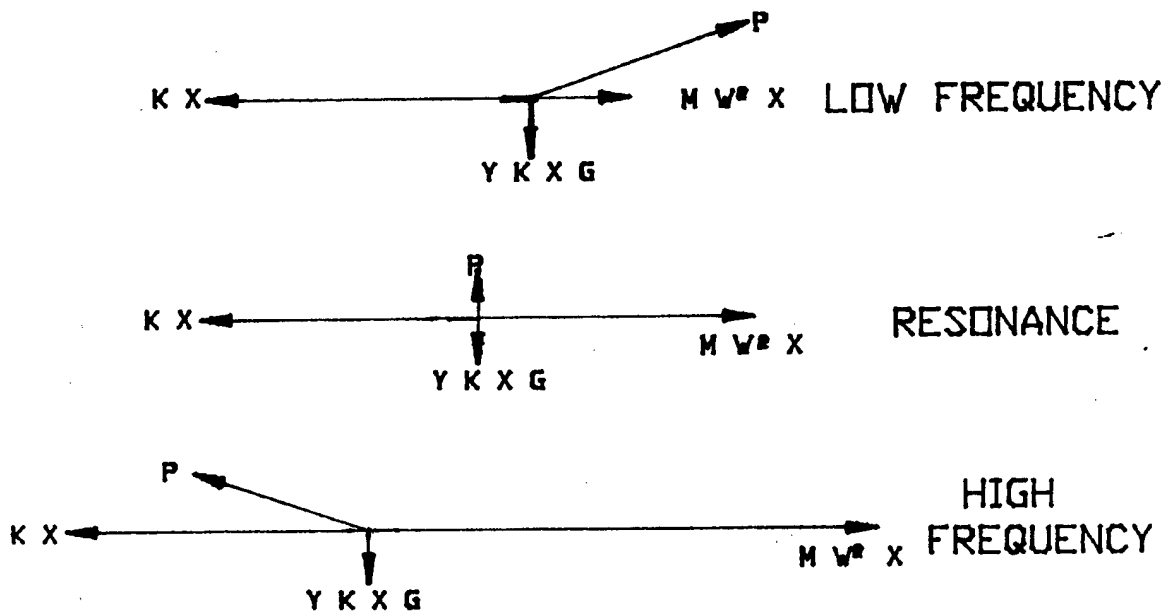
Figure 31: Typical Vector Diagram

If the force inputs of the shakers are known, the effective mass in each natural mode might be calculated from the value of the effective force, the amplitude of the reference station at resonance and the decay of free vibrations. The effective force must be large enough to produce a substantial response in the mode for which the effective mass is being computed. The response at resonance is P/kg and if g is determined from the damping of free vibrations, k can be computed. The effective mass is then equal to k / ω^2. One problem with this method is that the value of g obtained from the decay of the amplitude of a mode excited during a ground vibration test may vary with the amplitude. For this reason, the measured effective mass should be compared with the effective mass computed from the measured vibration amplitudes and the computed weights.

Robert E. Donham and George A. Watts

Aerodynamic and Mass Balance Effects on Control Surface Flutter

Abstract

Six cases of flutter of full scale aircraft or wind tunnel models, shown in the table below, are discussed as to flutter type, cause and correction. Also included are descriptions of several control surface/tab systems and how they function. Mass and aerodynamic balance types and design rules are also discussed.

| Case	Flutter	Cause	Cure
1	aileron/wing torsion	stores distribution	relocate stores or placard
2	vertical fin/rudder	excess rudder aerodynamic balance	placard
3	vertical fin/rudder	concentrated mass balance	mass balance redistribution
4	stabilator rotation/bending	rotation/bending mode coupling	mass balance redistribution
5	wing/aileron	excess control surface rotational inertia	reduced inertia + static mass overbalance
6	elevon/wing torsion	wing torsion/aileron rotation coupling	not applied

Robert E. Donham

Engineering Specialist in flutter and dynamics with more than forty years (Lockheed, Burbank, retired Engineering Department Manager Flutter, Vibration, and Acoustics) experience in aircraft design, analysis and manufacturing. Includes FAA certification of fixed wing airplanes and helicopters, as well as military patrol, transport and fighter aircraft; 41 types in all. FAA Designated Engineering Representative (DER NM-483), Structures.
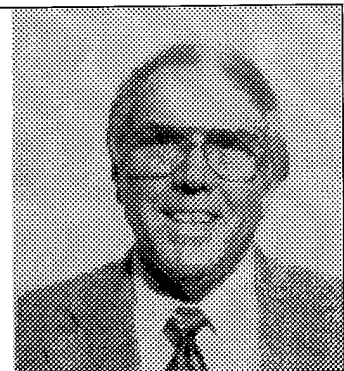
George A. Watts

Has conducted research in unsteady aerodynamics, predicted vibration modes in aircraft, spacecraft and helicopters and planned and executed ground vibration tests. He has participated in flight flutter testing of aircraft and whirl and wind-tunnel testing of helicopter rotors. He has analyzed aircraft flutter and response to atmospheric turbulence. This has been part of 45 years experience in aerospace engineering supported by three degrees in aeronautical engineering and one in physics.

Table of Contents

Robert E. Donham and George A. Watts

Aerodynamic and Mass Balance Effects on Control Surface Flutter

It is imperative that flutter not occur within the useable flight envelope of an aircraft and that a safe-speed margin beyond envelope boundaries be maintained. Furthermore, flutter margins must be attained efficiently, to forestall the accumulation of excessive structure or ballast weight that could compromise payload.

A companion consideration to flutter in flight vehicle design is the provision of sufficient structure stiffness to prevent static aeroelastic divergence, control reversal and excessively large stability derivatives. Though not the primary subject of this handbook, static aeroelasticity methodology can be useful in the analysis of certain types of flutter and this is briefly discussed.

The common features of classical flutter phenomena and means of detecting them theoretically and experimentally are explored. Standard rules for designing aerodynamic geometry, internal structural arrangements and mass balance distributions to minimize the possibility of flutter without large weight penalties are discussed.

The cases cited are of flutter encountered, during the design/development phase of actual aircraft, in flight or in dynamically scaled wind tunnel model tests. In some cases flutter occurred despite application of the rules of good design for flutter prevention.

INTRODUCTION

The term "flutter" is applied to many differing dynamically unstable mechanisms produced by fluid flowing past structures and their mass distributions. Flutter implies unexcited (or self-excited) structure vibration amplitudes that increase exponentially in time without limit, (or to a limit fixed by some nonlinearity of the system). Among these are types not currently amenable of theoretical analysis such as: smokestack and bridge flutter induced by shed bluff-body vortex streets and the closely related highly-swept-wing flutter caused by leading-edge vortex shedding at high angle-of-attack at subsonic speed. At transonic speed, single degree-of-freedom aileron buzz induced shock boundary-layer interaction is another form of flutter. These nonanalytic forms and panel flutter (of aircraft skin panels) are not discussed in this handbook.

This contribution discusses types of aircraft flutter predictable through the use of linear attached-flow unsteady aerodynamic theories. These instabilities result from the interaction of two or more fundamental vibration modes. Such modes may include the overall vehicle "rigid" body and other mechanical modes as produced, for example, by hinged control

surfaces and rotating propellers. In some cases, largely non-aerodynamic, natural modes of vibration such as: wing fore and aft motions coupled with fuselage yaw (wing scissors motion); vertical fin pitch coupled with fuselage vertical bending; and horizontal yaw coupled with fuselage lateral modes (horizontal stabilizer scissors) must be included.

Some Types of Flutter

Despite this limited view, the list of mechanisms that lead to "catastrophic" flutter continues to grow. A few are as follows:

- *Wing/Aileron Flutter* -- An interaction of wing bending, wing torsion and aileron rotation. Found in both swept and unswept wings. Can be symmetric or antisymmetric. Is similar to fin-rudder and horizontal tail-elevator flutter. Full distributed static mass balance prevents bending/control surface flutter but may not prevent torsion/control surface flutter. This is discussed in Case 5.

- *Fixed Surface/Control Surface/Tab Flutter* -- Tab rotation induces a control surface rotation that in turn creates a fixed surface aerodynamic force. Freeplay or lack of adequate tab actuator stiffness can lead to flutter when the tab is not mass balanced.

- *Wing/Body Flutter* -- Low-frequency interaction of wing bending and "rigid-body" plunge and pitch modes. Low body pitch inertia, as found in flying wings, for example, can lead to this form of flutter. Short period mode can couple with wing bending and in some cases with wing torsion, especially when large tip tanks are in use.

- *Hump-Mode Flutter* -- One of several flutter mechanisms produced by the interaction of podded engines and wing vibration modes. Found in transport aircraft. Similar effects can be seen when control surfaces couple with fixed surface modes.

- *External Stores Flutter* -- Induced by added mass, can be affected beneficially by a lack of symmetry of the spanwise mass distribution. In fighter aircraft, use of wing pylon MER (Multiple Ejection Racks) and TER (Triple Ejection Racks) external store configurations might still become critical for unsymmetric intermediate combinations of stores. An example involving a twin turbofan aircraft is presented in Case 1.

- *Propeller Whirl-Flutter* -- A precessive oscillation of the propeller and engine relative to the airframe. Affected by low structural stiffness of the engine-propeller system mounting. Involves cross coupled yaw and pitch degrees of freedom driven by propeller aerodynamic and gyroscopic moments.

Objectives

This contribution addresses the following aspects of the classical forms of flutter found in aircraft:

- Aircraft design to minimize the possibility of catastrophic flutter.

- The definition, mathematical description and theoretical analysis of aeromechanical systems employed in flutter analysis.

- Ground vibration testing to verify the mathematical model of the aircraft inertia-elastic system.

- Wind tunnel flutter testing.

- Flight testing procedures that lead to minimum risk during flutter exploration.

The diversity of the flutter situations encountered in actual aircraft is illustrated by six examples. Each flutter mechanism and how it was found are discussed. The corrective actions taken and success or lack of success of steps on the way to a safe configuration are noted.

AIRCRAFT DESIGN FOR FLUTTER SAFETY, STRUCTURAL AND BALLASTING EFFICIENCY

Flutter Mechanisms -- General Discussion

All mechanizations of flutter depend on the interaction of aerodynamic, inertia, and elastic forces. Structural elastic (or spring) forces react with inertia (or accelerated mass) forces to create the oscillatory character of flutter seen in the orthogonal (or independent) natural vibration modes of the system. Aerodynamic forces modify the elastic forces to change the frequencies of the fundamental natural modes. They also act to couple certain of the modes together. This creates timewise phase lags between them and results in positive or negative damping of the new combined modes of the total system. Aerodynamics may thus lead to strong damping, of the otherwise conservative (or nondissipative) system, or to the divergent oscillation, known as flutter.

Configuration Effects on Flutter

An aircraft typically consists of a slender body of small lift effectiveness but large forward-located mass and pitch and yaw moments of inertia. To this body are attached surfaces of great lift effectiveness and relatively little weight, such as the wings and tail surfaces. Engine, fuel and external pylon mounted store weights, however, may be distributed spanwise across the wing.

Wing Mass Distribution Effects

The chordwise location of the wing spanwise mass distribution plays a major role in the flutter stability of the wing-body system. Two dimensional unsteady aerodynamic theory shows that motions with node lines aft of the leading edge to about fifty percent of chord are stable. Location of the mass centroid distribution aft of the elastic axis tends to be destabilizing. (The elastic axis is the spanwise locus of chordwise points along which concentrated normal forces may be applied without inducing wing elastic twist, usually near forty percent of chord).

Control Surface Effects

Trailing-edge control surfaces, unless irreversibly actuated, complicate the behavior of wing-body systems. This is due to the large aerodynamic forces delivered to the wing modes by such surfaces. At subsonic speeds, for example, a one degree rotation of a control surface of 30% chord produces lift equivalent to a 2/3 degree rotation of the whole wing section, across the span of the control surface. The centroid of the section lift added to the wing will be located 15% of the chord length aft of that produced on the wing by an equivalent AOA change.

Any oscillation of a manually controlled (or essentially free floating) control surface therefore causes very large lift and twisting moments on the supporting surface with attendant vertical and rotational accelerations.

A control surface displacement producing a force or moment in phase with (or in the direction of) an elastic rate of change of deflection of the main surface promotes flutter. A flutter occurrence, however, requires a coupling between the control and the main surface degrees of freedom.

An example of such coupling is provided when the first moment of the mass of a control surface is located aft of its hinge line. If a wing tip, oscillating in plunge is at the top of its stroke and accelerating downward, an aileron with its mass center aft of the hinge line will rotate trailing-edge upward. This produces a downward aerodynamic force, in the direction of the wing tip velocity. Any lag in the control surface displacement or its aerodynamic force buildup, relative to the wing tip displacement can result in flutter.

Mass Balancing

The above problem is usually solved by shifting the mass centroid of the control surface to the hinge line by the addition of counterweights forward of the hinge line. This is called *mass balancing*. It is very effective in suppressing bending mode coupling but overbalance is required for torsion mode decoupling. This is discussed in Case 5.

Federal airworthiness requirements impose arbitrarily large design loads on mass balance support structure to make sure weights do not fall off. The supporting structure and attachment of concentrated mass balance weights used on control surfaces on small aircraft must withstand inertia limit loads normal to the control surface imposed by accelerations up to 24g.

Effects of Control Surface Tabs

A further complication to the flutter dynamics of an airplane with a free-floating (or manually operated) control surface occurs with the addition of a tab (a small hinged surface) to the control surface trailing-edge. This results in three surfaces in tandem with two intermediate hinges connecting them.

The purpose of a tab is to reduce the control surface hinge moment to make manual control easier. It does this by rotating in the opposite direction to that desired of the control surface. Its position at the trailing-edge of the control surface allows its small force, in the wrong direction, to produce a large control surface hinge moment in the direction desired. Thus the system of three surfaces can provide the desired net lift force with a zero net hinge moment.

A trim tab is usually rotated to a fixed displacement relative to its elevator, for example, to produce a required steady tail lift force with zero hinge moment and stick force. It does not affect the rate of change of hinge moment application per unit deflection of the elevator. In some aircraft, tab rotation is, in addition, geared to elevator deflection for the purpose of reducing "stick force per g". It is then referred to as a *geared tab*. Another variation consists of allowing the control surface to float free about its hinge axis while the stick force is applied directly to the tab. The tab then supplies the required hinge moment to the control surface with little force feedback to the stick. Tabs are usually not mass balanced unless free, as are spring tabs. All tabs must be irreversible, frequency criteria and free play requirements must be met, unless the tab is properly balanced and has no unsafe flutter characteristics.

Effects of Control-Surface Aerodynamic Balance

A more common way of reducing the stick force per g is through the use of *aerodynamic balance*. This is accomplished by tailoring the control surface planform geometry so that some lifting area lies ahead of the hinge line. This area provides hinge moment in a direction opposite to that provided by regions aft of the hinge line. Two methods are in common use: the *aerodynamic horn* -- an area projection well forward of the hinge line near the surface tip and the *set-back hinge* -- that distributes the forward projected area uniformly along the control surface span by placing the control surface hinge line well aft of the leading-edge.

Aerodynamic balance partially balances the hinge moment produced by normal pressure aft of the hinge-line. The designer must be careful not to overbalance the control surface or it will statically diverge to full throw (to the mechanical stop).

Aerodynamic balance reduces the hinge moment per unit control surface rotation at a given dynamic pressure. This reduces the aerodynamic *spring* constant and frequency of the control surface rotational degree of freedom. Flutter of a wing and aerodynamically unbalanced aileron, for example, may take place when the rigid rotational frequency of the aileron approaches that of a higher frequency bending or torsion mode of the wing. The effect of aerodynamic balance is to raise the airspeed at which the frequency coalesces and flutter will occur.

In addition, movement of the hinge-line to a position aft of the control surface leading-edge progressively reduces damping of the surface rotation mode.

These two effects can convert a mild low-speed flutter into a severe flutter problem at high speed.

Control Surface Dampers

Control rotation-mode dampers may be employed when surfaces are too thin to house mass balances. They are also useful in the suppression of transonic *buzz*. Dampers may also be employed beneficially in wing-store cases of marginal stability.

AIRCRAFT FLUTTER ANALYSIS

Flutter analysis has evolved from the consideration of two or three degrees of freedom, at a time, by a hand calculation, prior to about 1950, to the analysis of the interaction of thirty or more vibration modes today through the use of large digital computers. The lack of computing capability in the early days forced the flutter engineer to carefully study the degrees of freedom available to him to ascertain which small group would likely lead to flutter, before undertaking the tedious task of finding the unstable roots. He postulated flutter mechanisms and investigated them analytically.

With the computer resources available today there is a tendency to include all possible modes in an analysis of flutter safety. This sometimes leads to difficulty in identifying the dominant physical mechanism causing flutter and in finding the most efficient way to modify the design to effect a solution.

Inertial-Elastic System

The theoretical analysis of flutter usually begins with a consideration of the dynamic behavior of the aircraft structure and its mass distribution in a gravity-free airless environment. An eigenvalue analysis provides the system resonant frequencies and the corresponding modes of natural vibration. These may be verified by direct experimentation on the completed aircraft by a ground vibration test.

Elastic Properties

The elastic properties of the free-free aircraft may be expressed as a flexibility matrix. (Each column of which is the distribution of deflections produced by a unit load applied at one loading point and reacted by rigid body inertia forces at all points. All deflections are measured relative to a common point or set of points in the physical structure). A flexibility matrix is the inverse of a stiffness matrix and may be calculated by finite element structural analysis methods.

Inertia Properties

The aircraft weight distribution is discretized into local masses and moments of inertia at the points employed in the flexibility matrix. (This may require the use of interpolation schemes).

Vibration Mode Analysis

The above flexibility and inertia information is substituted into the matrix equation describing the dynamic oscillation of the conservative system. It is a set of unforced coupled second-order ordinary differential equations. The eigenvalues of its characteristic equation are extracted computationally and become the natural frequencies of the system. The eigenvectors (or mode shapes) associated with the eigenvalues then follow directly.

Coordinate Systems For Flutter Analyses

The theoretical vibration modes above are often employed in flutter analyses as the representative degrees of freedom of the system since they are orthogonal to each other and to the rigid body modes (or they are inertially uncoupled, i.e., inertia forces in one mode produce zero generalized forces in the others). They may not, however, be orthogonal to a control surface rotation degree of freedom when it is added as a general coordinate to describe control surface relative motion.

It is not necessary to employ the natural vibration modes as the describing degrees of freedom of the airplane, and in fact were not available in the early days of flutter analysis since they were then impossibly tedious to calculate. It is only required that the deflection describing modes be general enough to reproduce the important motions of the inertia-elastic system and the static aeroelastic system.

Notes: 1. It may not be feasible to employ a sufficient number of natural vibration modes to adequately describe the static aeroelastic behavior of some low frequency flutter modes. In such cases it may be necessary to employ a smaller number of nonorthogonal modes specially tailored to include such effects.

The static aeroelastic deflection shapes due to AOA, pitch rate and control surface deflection make good candidates for inclusion with a set of elastic modes in analyses of flutter in which rigid-body motions are important, for example.

If coordinates are employed that are not orthogonal, cross-coupling flexibility and inertia terms are present. Modern computers have no problem calculating and including these.

2. Static aeroelastic problems are usually analyzed in terms of the unreduced stiffness, (or flexibility), matrices of all load and deflection points on the aircraft structure rather than in terms of the reduced set of orthogonal elastic modes employed in flutter analysis. Though a small number of lower frequency elastic modes may adequately represent the dynamic motions involved in flutter, they will often not represent the elastic twist of the wing adequately for static aeroelastic analyses.

Unsteady Aerodynamics

Aircraft unsteady aerodynamics, at one value of nondimensionalized or reduced frequency, may be expressed as a matrix of complex aerodynamic forces on the set of contiguous elemental areas making up the thin lifting surfaces of wings, tails, control surfaces, etc. The differential pressures generating the forces are produced by the surface element motions: angular displacement and linear velocity normal to freestream flow.

The time lag between surface motion and pressure development is accounted for by the real and imaginary elements of the complex matrix.

The aerodynamic pressure distribution due to the motion of each mode, at one reduced frequency, is applied to all modes and integrated over the aircraft surface to yield the aerodynamic coefficients of a reduced set of flutter equations. This is the general procedure utilized with any general coordinates.

Detailed lifting surface computer programs are employed in generating the basic unsteady aerodynamic matrices, above. The primary methods in use today, for both steady and unsteady matrix prediction, are Strip Theory and Doublet Lattice for the subsonic flight regime and ZONA51 for the supersonic. In the transonic regime specialized codes are applied.

The analytical investigations of aircraft reported in this note, however, made use of MSC NASTRAN for the dynamic models, (structure-inertia systems), and unsteady Strip Theory and Doublet Lattice with steady-state weighting for the unsteady aerodynamics.

In discussing flutter prevention, however, a simpler implementation of unsteady aerodynamics has been employed in this note: incompressible two-dimensional unsteady aerodynamics operating on the plunge, pitch and control rotation degrees of freedom. This methodology provided the key to flutter analysis during the first fifty years of powered flight through its utilization in Strip Theory. Despite the lack of spanwise interference between sections in this theory it has been surprisingly effective. This may be due to the high aspect ratio of lifting surfaces common during this period.

FLUTTER EXPERIENCE

The following cases of flutter have been chosen to illustrate the diversity and complexity of flutter mechanisms occurring in actual flight, encountered in wind-tunnel testing of new aircraft designs or found by analysis and corrected prior to flight.

Case 1: Effect of Wing-Store Distributions on Aileron/Wing Torsion Flutter

Aircraft Description

The twin-turbofan aircraft, see Figure 1, has its engines mounted on the aft fuselage. Its swept low-wing has upper surface fences at 47% semi-span. Wing thickness varies from 10.5% at the root to 8% at the tip and sweep of the quarter-chord is 30 degrees. Conventional ailerons are actuated hydraulically with artificial feel and are almost irreversible.

The swept vertical fin has a swept tailplane mounted at its semi-span.

- Maximum Mach Number = 0.80
- Maximum Cruise Speed = 461 knots TAS at 40,000 ft altitude

Though originally designed as a light commercial transport, it is currently employed in the military services of several countries. Two of its uses are as an aerial refueling trainer and maritime reconnaissance.

The configurations investigated, employed symmetrically-arranged inboard and outboard external store attachment points under the wing as is shown in Figure 1 and Table 1. Twenty-seven store configurations were considered.

The ailerons were not mass balanced and thus depended on a high irreversibility frequency and rotation mode damping to maintain aileron/wing coupled flutter margins. Ground vibration tests showed the following values:

Hydraulic Power	Left Aileron		Right Aileron	
	Frequency Hz	Damping g	Frequency Hz	Damping g
On	49.3	0.06	50.3	0.05
Off	47.6	0.07	48.2	0.07

(Note: Vibration peak width at the half power point divided by the center frequency furnished the measured damping value, *g*).
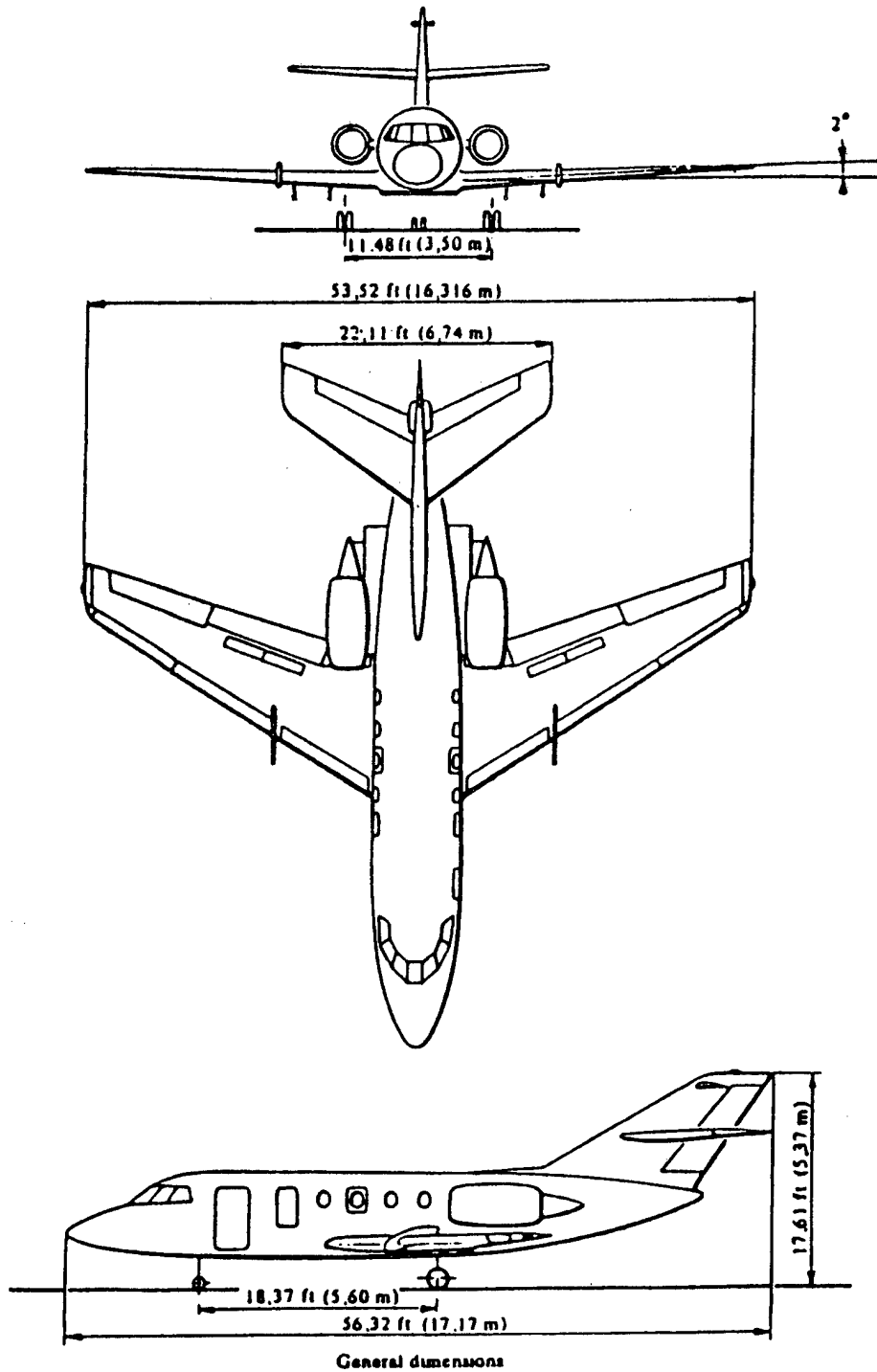
Figure 1: Test Aircraft For Wing-Store Effect On Aileron/Wing Torsion Flutter

Table 1: Symmetric Vibration Modes Of The Test Aircraft

Fuel Tanks Empty (Symmetric Modes)

Frequency (Hz)	Vibration Mode Description
5.51	Wing 1st bending, A/P pitching
6.12	Wing 1st bending, A/P pitching
7.57	Stabilizer bending coupled with wing bending
10.57	Fuselage vertical bending-stabilizer bending
12.99	Fuselage vertical bending-engine pylon bending
15.77	Stabilizer bending
18.34	Wing 2nd bending-engine pitching
18.34	Engine pitching
31.23	Wing torsion
32.19	Wing torsion-aileron rotation
36.53	Wing 3rd bending
37.75	Elevator rotation (1 hydraulic system)
40.30	Elevator rotation (2 hydraulic system)
--	Higher-order wing torsion
55.01	Higher-order wing bending-torsion
--	Stabilizer 2nd bending
--	Stabilizer torsion

A twin hydraulic booster system rotated each aileron at its spanwise center. Each system also included a viscous damping circuit to prevent flutter.

Ground vibration tests also provided symmetric and antisymmetric overall vibration modes and natural frequencies for the aircraft with no fuel or stores, as described in Tables 1 and 2. Note the outer wing torsion mode frequency identified during the antisymmetric tests as approximately 51 Hz. The above ground measured aileron rotational modes for the various booster conditions range from 47.6 Hz through 50.3 Hz and exhibited g-damping levels of 0.05 to 0.07.

In the one configuration that was predicted to be flutter critical, near a frequency of 51 Hz, two unsymmetrical stores only were carried: of 300 and 140 lb weight respectively. These stores were carried on the outboard pylon stations.

Flutter Experience

Four flutter clearance programs were conducted on 27 store configurations. Most were symmetrical mixes of inboard and outboard stores on the four pylons. Analyses, ground and

Table 2: Antisymmetric Vibration Modes Of The Test Aircraft

Fuel Tanks Empty (Antisymmetric Modes)

Frequency (Hz)	Vibration Mode Description
5.58	Fuselage torsion
6.33	Fuselage torsion-stabilizer rocking
7.43	Stabilizer rocking
9.62	Fuselage side bending-stabilizer rocking
12.23	Wing bending
13.85	Wing bending-fuselage side bending
17.05	Fin bending
20.66	Engine pitching
23.49	Rudder rotation (1 hydraulic system)
26.11	Rudder rotation (2 hydraulic system)
28.66	Wing 2nd bending
31.76	Wing torsion
40.47	Stabilizer bending
42.20	Elevator rotation (1 hydraulic system)
42.20	Elevator rotation (2 hydraulic system)
50.70	Higher order wing torsion
68.97	Stabilizer torsion

flight tests indicated no flutter within flight operational boundaries with all but one configuration, the only unsymmetrical one.

It consisted of one store per side located on the outboard pylon stations but of different weights (300 lb and 140 lb) and moments of inertia.

Analyses

This configuration was analyzed as a complete aircraft, i.e., with each side described independently, using NASTRAN with Doublet Lattice unsteady aerodynamics. The analyses were conducted with aileron damping set at $g=0.03$ and with the measured aileron rotation springs. Analyses were run with the full predicted unsteady aerodynamic aileron hinge moments and with hinge moments reduced to 50% of full value. Solutions were found for $M=0.76$ over a range altitudes from sea level to 40,000 ft.

The clean aircraft was entirely free of flutter with acceptable margins. With the unsymmetric stores on the outboard pylons only, the outer wing torsion mode coupled with the aileron rotation mode and resulted in flutter at approximately 51 Hz primarily involving motions on

the light side, within the flight envelope, even though $g=0.03$ had been included in the analysis.

Flight Tests

The unsymmetrical stores configuration was the first of the 27 configurations flight tested in each of the four test periods.

The instrumentation, see Figure 2, emphasized wing structural strains and pylon store accelerations and recorded all control surface displacements.

Horizontal and vertical tail elastic strains were also recorded to permit the monitoring of any loss of empennage stability.

The strain monitoring gauges were added to give some indication of excessive load over a wide range of frequency and to make up, to a certain extent, for the lack of the large number of instruments usually found on prototype aircraft. Strains are proportional to structural deflection while accelerations are proportional to the product of deflection and frequency squared. Hence if an accelerometer is chosen to measure high frequency vibration, it will not pick up even large amplitude low frequency oscillations that could indicate large loads.

Since strain is directly indicative of structural damage, strain gauges can provide a limited but quantitative indication of excessive dynamic loads.

At the extreme edge of the flight envelope at 25,000 ft altitude the aileron rotation mode damping reduced from $g=0.06$ to $g=0.02$ over the last 50 Kts EAS, as determined by RDMDEC (random decrement) analysis of the test data. The test was repeated and gave the same result, thus in the interest of flight safety the aircraft was placarded (restricted) against flight with damping below the ground measured value.

With the stores, described above, on the outboard racks aileron/wing torsion flutter was predicted to occur. On the inboard racks the flutter disappeared.

Postulated Flutter Mechanism

The presence of the light store on the outboard pylon led to the observed instability. Its light weight but significant moment of inertia produced a change to the outer wing torsion mode without significantly changing its frequency. This substantially increased the unbalanced mass/inertia coupling between the aileron rotation mode and outer wing torsion mode without increasing the frequency separation. The opposite side of the aircraft with the heavier store remained stable due to its increased frequency separation. A symmetric configuration of light stores on each side, had it existed, would have had a much lower flutter speed.

STRAIN GAGE BRIDGE LOCATIONS
AND
ACCELEROMETER LOCATIONS

VERTICAL TAIL BENDING

AILERON ACCEL. (FSI)

OUTBD PYLON VERT. & LAT. (RIGHT WING)

INBD PYLON VERT. & LAT. (RIGHT WING)

HORIZONTAL TAIL BENDING

(RIGHT SIDE)

VERT. OUTBD PYLON LEFT WING

RIGHT WING BENDING

RIGHT WING TORSION

/ STRAIN GAGE
● ACCELEROMETER

LEFT WING BENDING

RUDDER DISPLACEMENT

AILERON DISPLACEMENT

ELEVATOR DISPLACEMENT

● POSITION INDICATORS

AILERON DISPLACEMENT
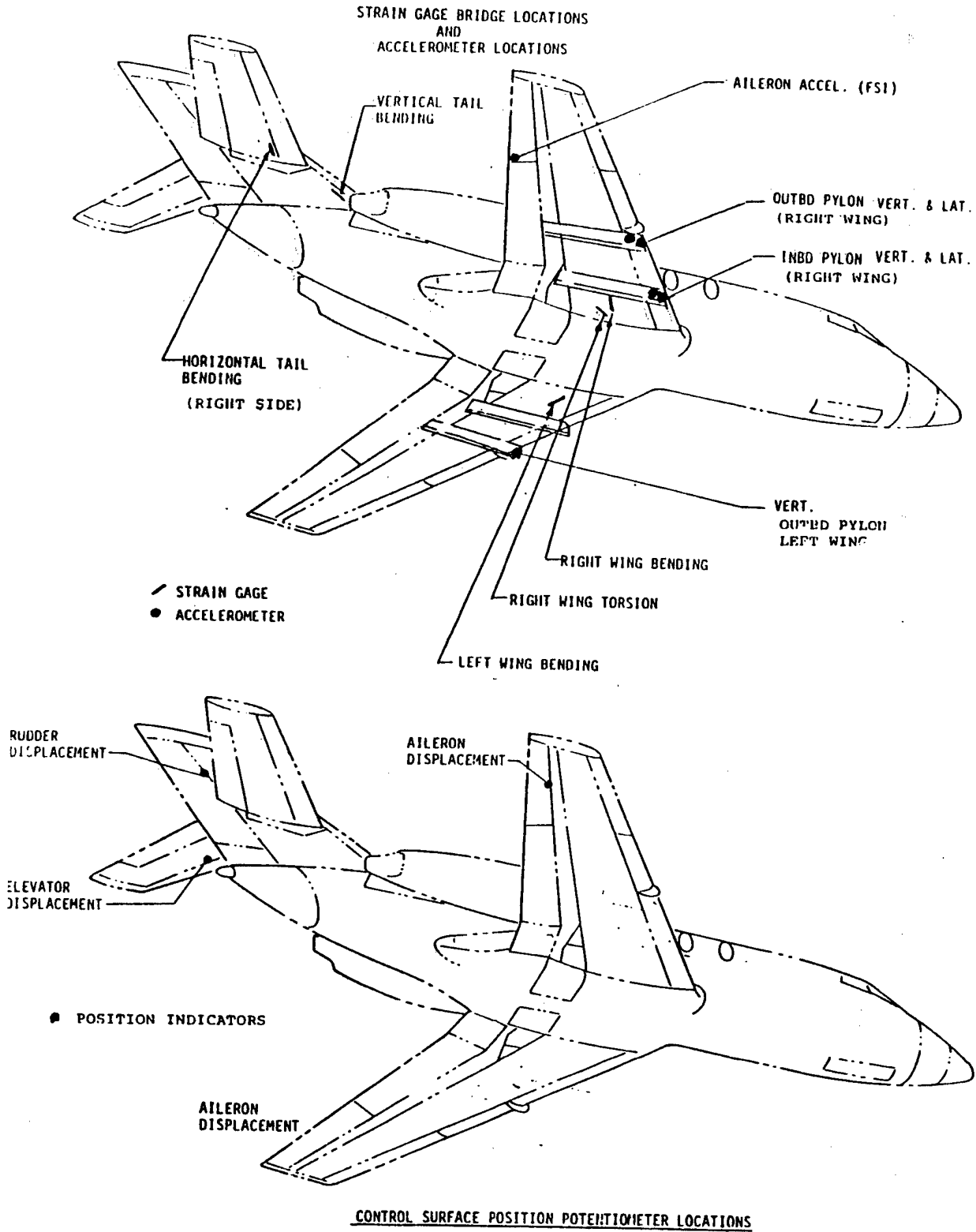
CONTROL SURFACE POSITION POTENTIOMETER LOCATIONS

Figure 2: Instrumentation Layout For Store-Induced Flutter Flight Tests

2-16

Corrective Action Taken

The simple remedy to this problem was to restrict the airspeed for this configuration. The second choice was to move the stores to the inboard pylons where the problem did not exist.

Choice of arrangement made it possible for all 27 configurations in four subsequent programs to meet the full flight envelope of this aircraft without wing stores. The predicted most critical flutter cases were all flight flutter tested to the full design envelope, supported by FM telemetry and lattice filter analysis of the test results. These configurations, approximately ten aircraft, were FAA STC'd and are now operating under CAA regulations in the UK.

Case 2: Effect of Aerodynamic Balance on Vertical Fin/Rudder Flutter

Aircraft Description

A WWII light bomber with twin radial piston engines and an unswept shoulder-mounted wing of high aspect ratio ($AR=9.5$) is the subject aircraft of Case 2. (See Figure 3). The aircraft was of metal monocoque construction except for the rudder and tabs which were fabric covered. The unswept fin and rudder and horizontal stabilizer and elevator were of conventional geometry.

Originally developed as an attack bomber during World War II, served in both the Korean War and the Southeast Asian conflict.
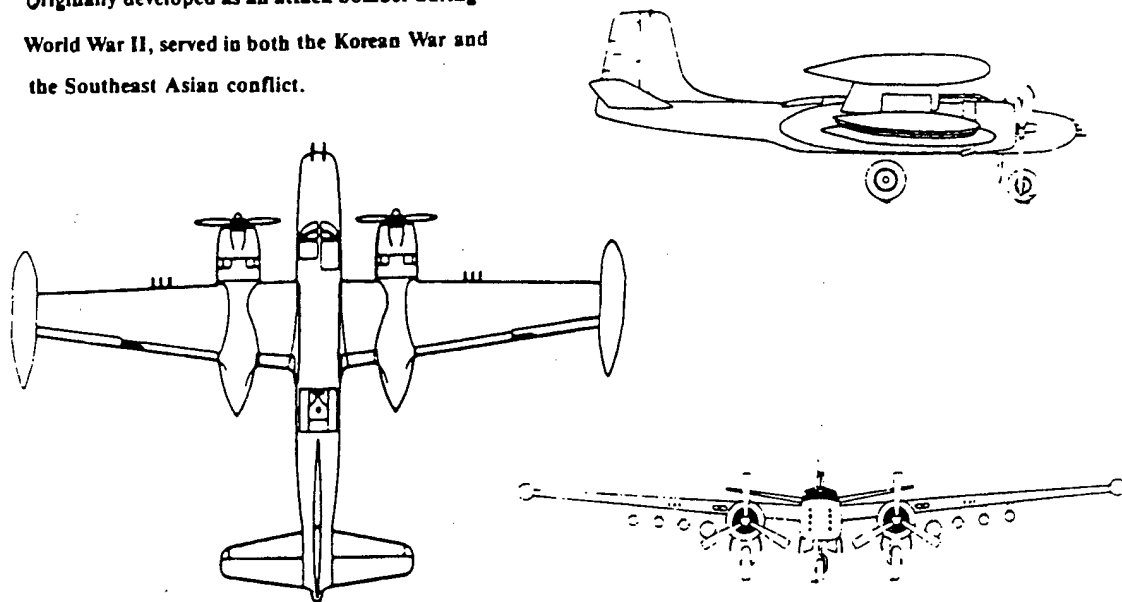

Figure 3: Aircraft Flight Tested For Effect Of
Aerodynamic Balance On Vertical Fin/Rudder Flutter

The rudder, of approximately 35% chord, was marked by a very large distributed aerodynamic balance of approximately 8% of the fin and rudder chord.

The particular aircraft flutter tested was retrofitted for counterinsurgency service. Eight wing pylons were added for rocket and gun pods, bomblet dispensers and other external stores. The tip tanks were not installed during the reported test.

Maximum speed at 10,000 ft was 323 KTAS (knots, True Air Speed). The design dive speed was 370 KEAS (knots, Equivalent Air Speed).

Flutter Experience

The fin and rudder exhibited a limited amplitude flutter at 375 KEAS that did not induce structural failure and the aircraft landed normally. The flutter, at 5 KEAS faster than the design dive speed, oscillated at 12 Hz, and was of the fin bending/rudder rotation type.

The flight test had been conducted to examine the clean aircraft prior to the addition of external wing stores outboard of the propellers. The test was considered perfunctory, a test of the instrumentation, since no changes were known to have been made to the fuselage/empennage system. The test, however, did include tail instrumentation and was conducted so as to provide a slow build-up in airspeed.

Postulated Flutter Mechanism

With little inertial coupling between the fin bending and rudder rotation modes, the mechanism of Case 3 is not likely to be the major cause of this unexpected flutter. With inertia coupling out of the picture aerodynamics became suspect.

The large distributed aerodynamic balance is somewhat unusual, but may be investigated by two-dimensional unsteady aerodynamics theory. Aerodynamic stiffness and damping of the rotation mode as the hinge-line progressively moves aft of the leading-edge of a control surface is provided by the equation in Figure 4 on the following page. The real part becomes the aerodynamic stiffness and the imaginary is proportional to the damping.

At $k=0.16$, and $e=0.4$ the aerodynamic stiffness (real part) reduces to zero at $c=0.58$ and the aerodynamic damping (imaginary part) reduces to approximately 1/3 the value it had with the hinge line at the rudder leading-edge. The distance from the leading-edge to the hinge line is $c-e = 0.18$ in terms of the half chord, b; that is, the hinge-line is 9% of the fin and rudder chord behind the control surface leading-edge.

The hinge-line on the bomber rudder is approximately at that chord station; thus it appears that the rotation mode frequency increase with airspeed will be relatively small. Furthermore, its modal damping is also quite small relative to that of a leading-edge hinged control surface.
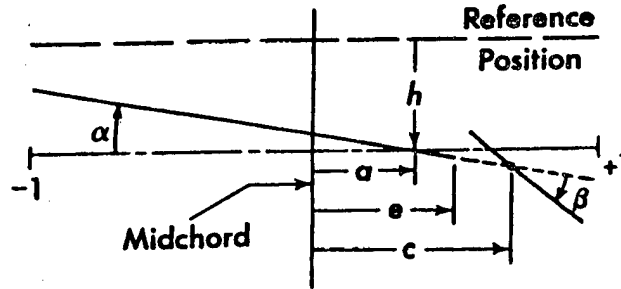
Hinge moment, T', due to control surface deflection, β, is given by:

$$\lambda = \frac{Kb}{SI} < T' = \pi\rho b^4 \omega^2 \left\{ \left[T_\beta - (c-e)(P_\beta + T_z) + (c-e)^2 P_z \right] \beta \right\}$$

The reduced frequency $k = \dfrac{b\omega}{v} = 16$ at 12 Hz at the design dive speed gives the real and imaginary parts plotted below. Values for T_β, T_Z, P_β in the table below are adapted from Scanlan and Rosenbaum, Reference 1.

e=0.4				
k	T_β	T_Z	P_Z	P_β
0.16	-1.94111-0.29845i	0.00851-0.31053i	-0.01542-1.55072i	-9.7045-1.0184i

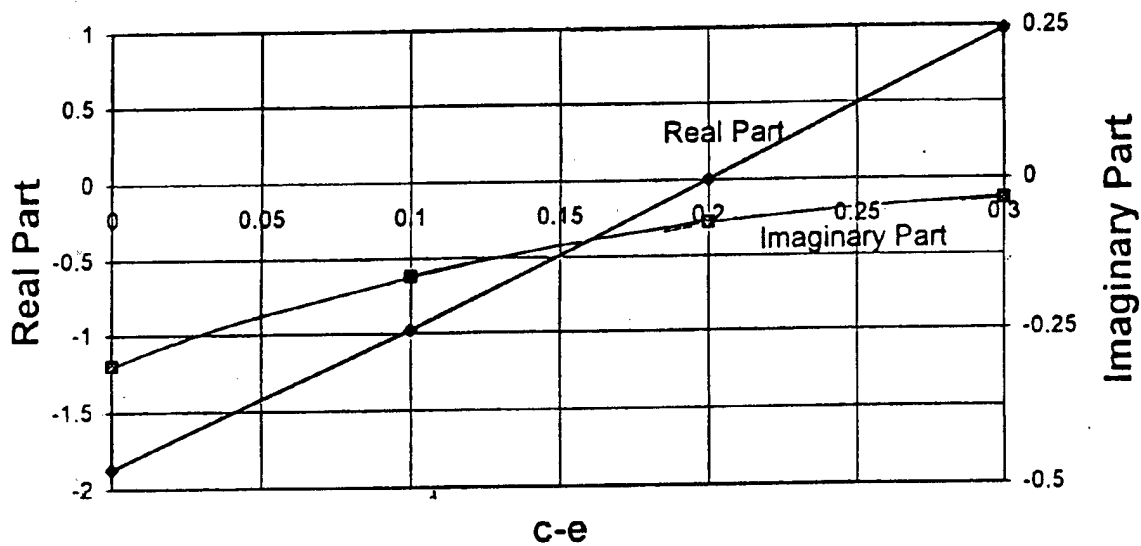
Figure 4: Rudder Unsteady Aerodynamic Hinge Moment, T', Due To Rudder Deflection At $k = 0.16$

It is postulated that a very slow growth of rotation frequency with forward speed led to a coalescence with the fin bending mode frequency just above the design dive speed. This coalescence, in conjunction with reduced rotation mode damping, led to the observed flutter.

Flutter Corrective Action

The flutter took place at a speed almost outside of the operational overspeed envelope. A simple airspeed restriction would therefore be sufficient to meet airworthiness requirements. The nature of this flutter, however, is such that an increase in mechanical rotation-mode torsion spring stiffness would cause the flutter to occur at a lower airspeed, that could be well within the flight envelope.

This dangerous condition is a consequence of large aerodynamic balance and should be avoided.

Case 3: Vertical Fin/Rudder Flutter Despite Meeting Flutter Prevention Design Criteria

Among the rules that guide designers toward flutter-free configurations are those provided by the US CAA (Civil Aeronautics Administration) in the early 1950s. Some are presented in Airframe and Equipment Engineering Report 45, "Simplified Flutter Prevention Criteria for Personal Type Aircraft," by Rosenbaum and Vollmecke.

Its empennage design criteria for rudders recognize that flutter will most likely result from a coupling of rudder rotation with either the aft fuselage lateral bending or torsional natural modes.

It specifies a parallel axis criterion to prevent rudder coupling with aft fuselage lateral bending and a perpendicular axis criterion to prevent rudder coupling with aft fuselage torsion (see Figures 5 and 6).

The parallel axis criterion requires that the ratio, $\gamma = \dfrac{bS_\beta}{I}$, not exceed a value given in Figure 5. Its parameters are as follows:

S_β, rudder static unbalance.
b, fin and rudder semi-chord.
I, rudder moment of inertia about the hinge axis.

The maximum allowable ratio is a function of the flutter speed factor (the inverse of a reduced frequency based on the aft fuselage natural bending frequency, f_h , the semi-chord and the design dive speed, V_d).
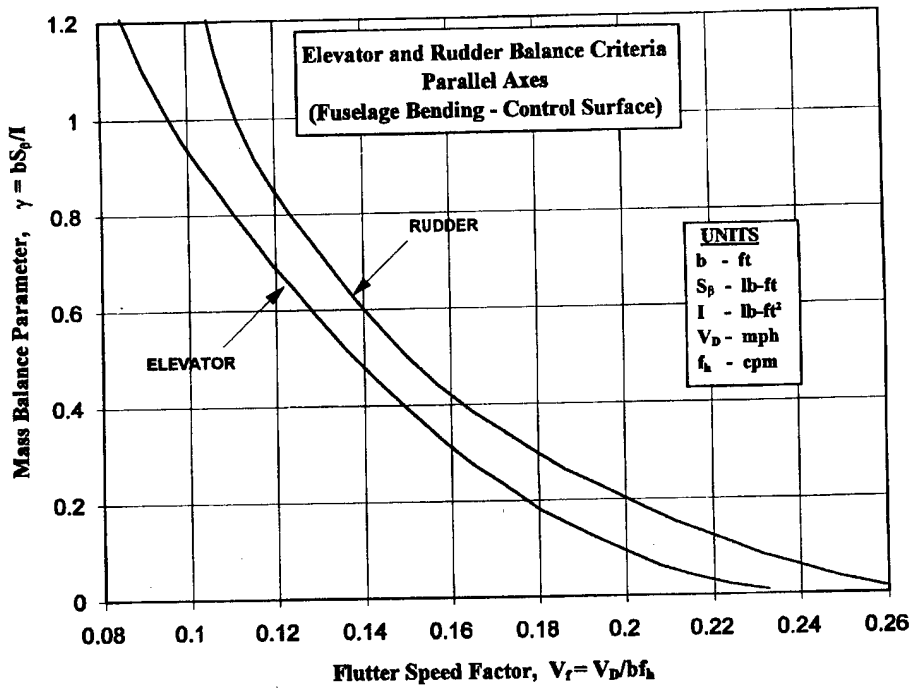
Figure 5: Rudder Mass-Balance Criterion For Freedom From
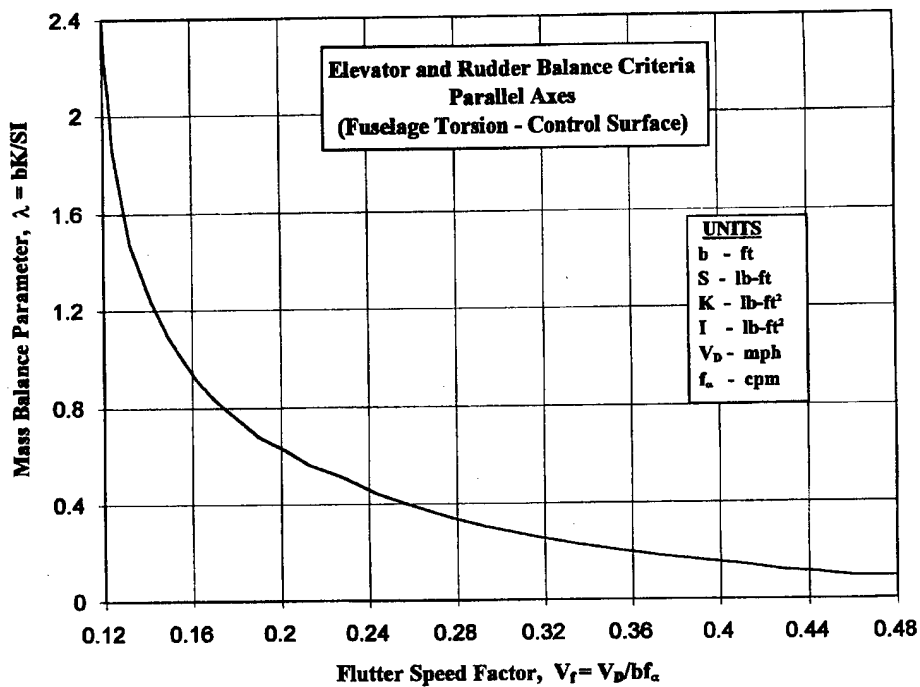Rudder Rotation/Fuselage Side-Bending Flutter

Figure 6: Rudder Mass-Balance Criterion For Freedom From
Rudder Rotation/Fuselage Torsion Flutter

The perpendicular axis criterion is similar but requires the ratio, $\lambda = \dfrac{kb}{IS}$, to be less than a value given in Figure 6. Its parameters are as follows:

K, product of inertia of the rudder mass about the torsion and hinge axes.
b, fin and rudder semi-chord.
I, rudder moment of inertia about the hinge axis.
S, the distance from the torsion axis to the tip of the fin.

The maximum allowable ratio is dictated by the flutter speed factor (or inverse of the reduced frequency at V_d based on the fuselage torsional frequency, f_α, and the fin and rudder semi-chord).

The present case indicates that even though the flutter design criteria, above, are met, flutter may still be possible.

Aircraft Description

A two-seat, twin-engined light aircraft, see Figure 7, is the test aircraft in Case 3. The all metal unswept low-wing is of semi-monocoque construction. Its external skin surfaces are formed by chem-milling and stretching. The aircraft has a conventional tail with swept vertical surfaces and an conventional horizontal fixed stabilizer and elevator.
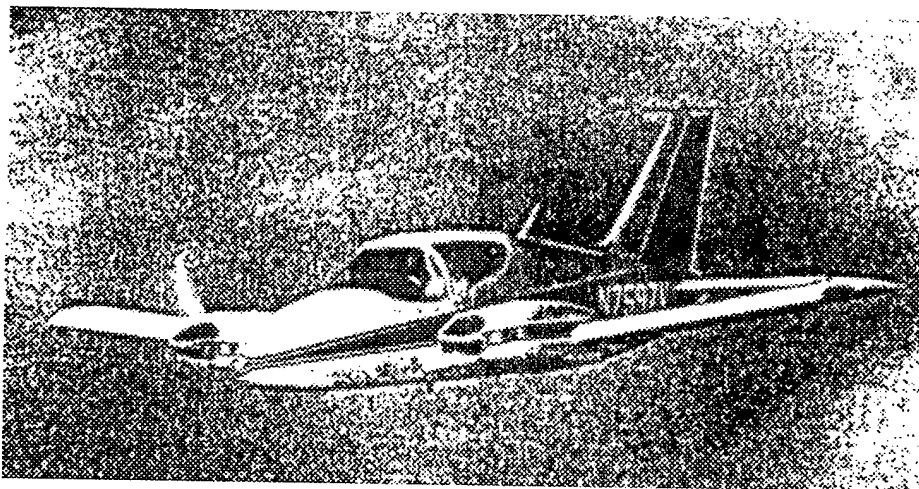
Figure 7: Test Aircraft For Vertical Fin/Rudder Flutter
Despite Adherence To Flutter Design Criteria

The swept fin and rudder are shown schematically in Figure 8. Rudder mass balance was concentrated at the rudder tip to minimize the product of inertia of the rudder about the fuselage torsion and hinge axes with the smallest possible balance weight that would meet the perpendicular axis criterion.
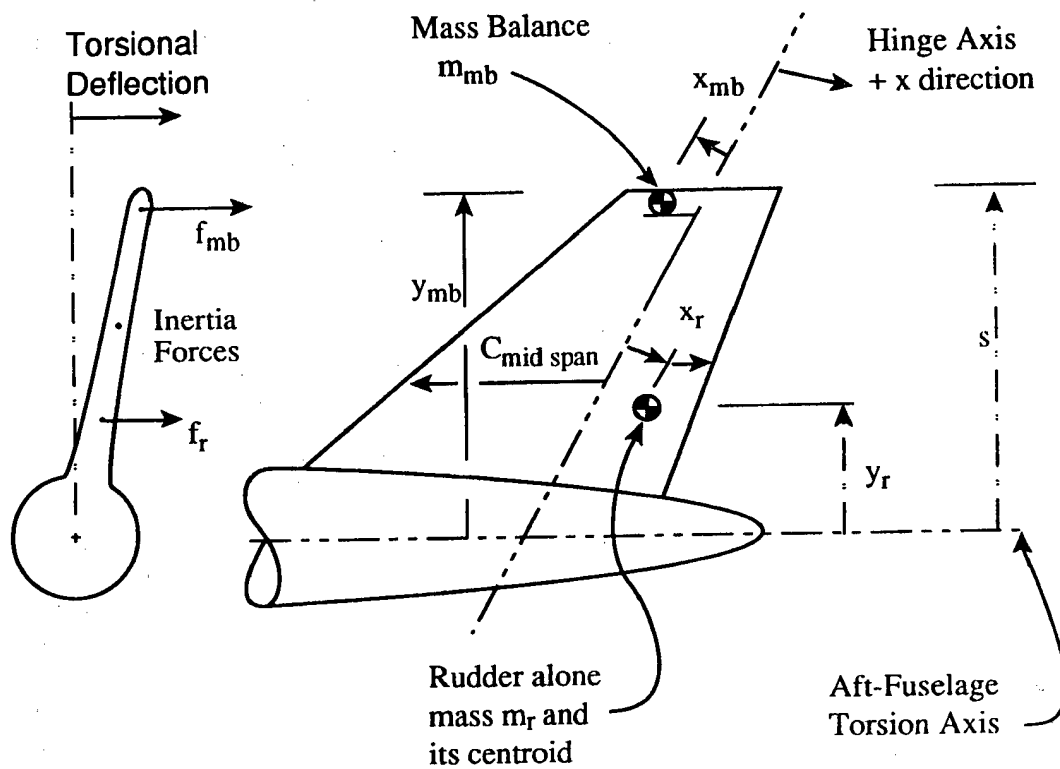
$$K = m_r x_r y_r + m_{mb} x_{mb} y_{mb} \quad \text{(lb ft}^2\text{)}$$

K must be such that $\lambda = \dfrac{Kb}{SI} <$ the value from Figure 6 for $V_f = \dfrac{V_D}{bf_\alpha}$,

where:

I = mass moment of inertia about the hinge line (lb ft²)
b = $c_{midspan}/2$ (ft)
c_α = fuselage torsion mode *natural* frequency (cps)
V_D = design *dive* speed (mph)
S = effective fin span (ft)

Figure 8: Rudder Rotation/Fuselage Torsion Mode Flutter Prevention Design Criterion

Flutter Experience

Vertical fin/rudder flutter was experienced in flight despite adherence to the flutter design criteria of CAA Rept 45.

Ground vibration testing disclosed a fin and rudder bending node line at approximately 60% fin span at a natural frequency near the inflight measured flutter frequency.

Postulated Flutter Mechanism

In a rudder rotation/aft fuselage torsion flutter, locating a single rudder mass balance at the maximum distance from the fuselage torsion axis, i.e. at the rudder tip, yields the maximum compensating product of inertia per unit distance forward of the hinge line for that weight. (See Figure 8). The rudder was balanced in accordance with this logic.

In the flutter observed, however, the mode participating with the rudder rotation was not aft fuselage torsion but vertical fin and rudder lateral bending. The mode possessed a node line at 60% of the fin span as shown in Figure 9. The tip located mass balance inertia force, in this case, is in a direction opposite to that of the inertia force on the rudder aft of the hinge line. Thus, instead of canceling the inertial hinge moment as it would in the case of fuselage torsion, it adds to it, and thereby strongly couples the bending mode to the rudder rotation mode. In other words, fin bending motion induces rudder rotation that in turn induces lateral airloads on the fin that amplify the fin bending motion. Thus, the precondition for flutter is in place.
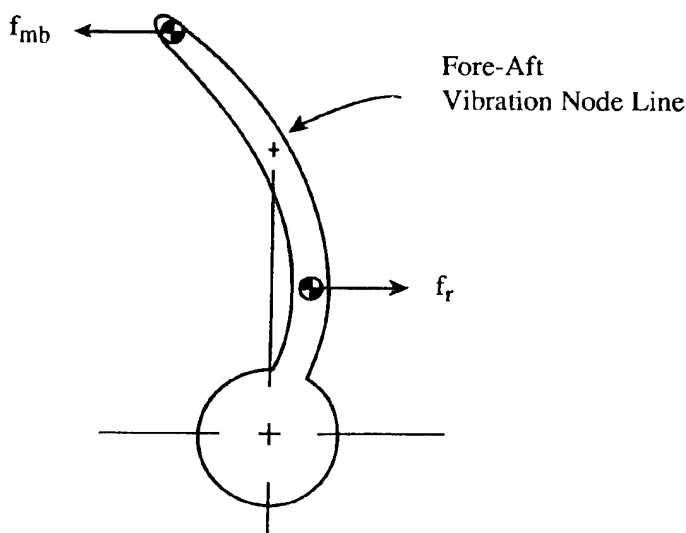
Figure 9: Vertical Fin and Rudder Bending Mode

Flutter Corrective Action

With the flutter mode identified it became possible to neutralize it. Reducing the tip weight until it just balanced the fraction of rudder weight above the node line and adding a second weight near the bottom of the rudder to balance the rudder weight below the node line, as shown in Figure 10, decoupled rudder rotation from fin and rudder bending.

Decoupling was due to the fact that bending mode induced accelerations produced balanced, (or zero), hinge moments separately both above and below the node line.

In the subject airplane, the balance weights were distributed 1/3 to the rudder tip and 2/3 to the rudder base. This redistribution of mass balance weights was slightly heavier than the original that covered only fuselage torsion coupling.

This exercise, in addition, illustrates the "flutter design rule" that control surface spanwise inertial hinge moment should be balanced locally at each span station by distributed balance weights when possible.
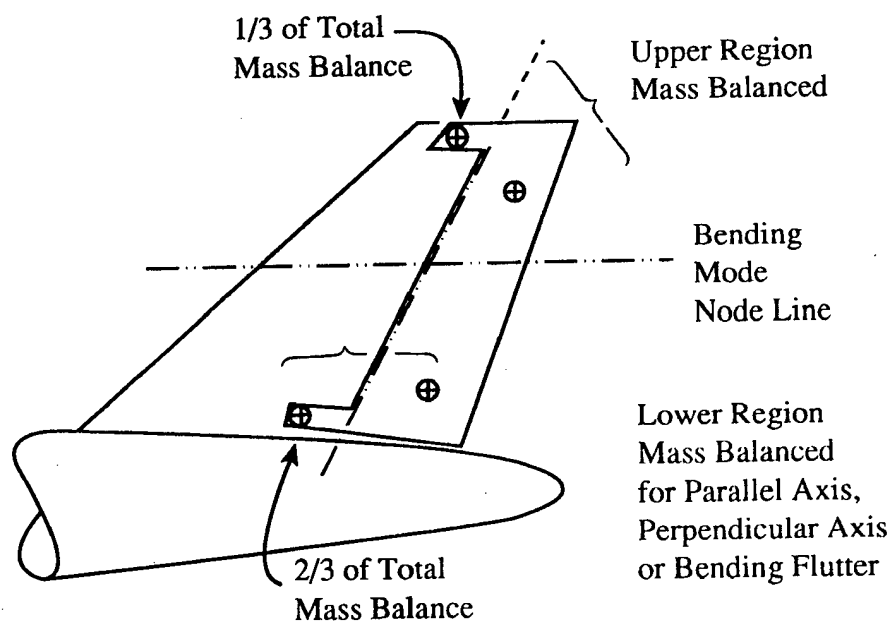
Figure 10: Rudder Rotation/Vertical Fin Bending Flutter Cured By Distributing Mass Balance

Case 4: Flutter of a Stabilator

Aircraft Description

The aircraft in Case 4 is a high-performance, single engine, two-seat (side-by-side), low-wing homebuilt monoplane of all-metal semi-monocoque construction and a conventional fin and rudder. (See Figure 11). The design employed a *stabilator* (all moving tailplane hinged to the aft-fuselage with no elevator). The stabilator contained a *servotab* (trailing-edge tab geared to stabilator rotation).
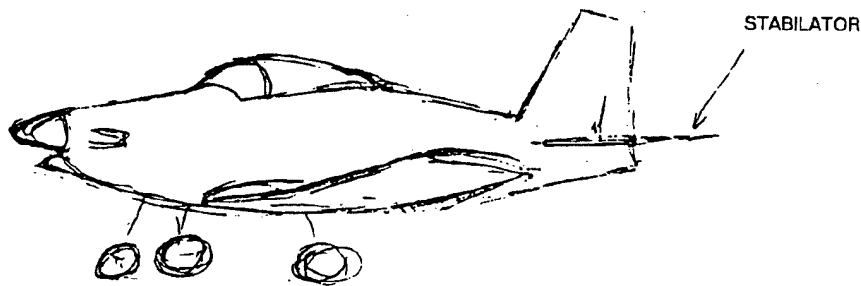
Figure 11: Amateur Built Sport Aircraft Suffered Stabilator Flutter

To prevent flight-normal acceleration from producing inertia hinge moments, the first moment of the stabilator mass about its hinge-line was brought to zero by the use of a single centerline counterweight. (See Figure 12).

The maximum sea-level speed was 200 miles per hour. Flight tests were conducted to 230 miles per hour.
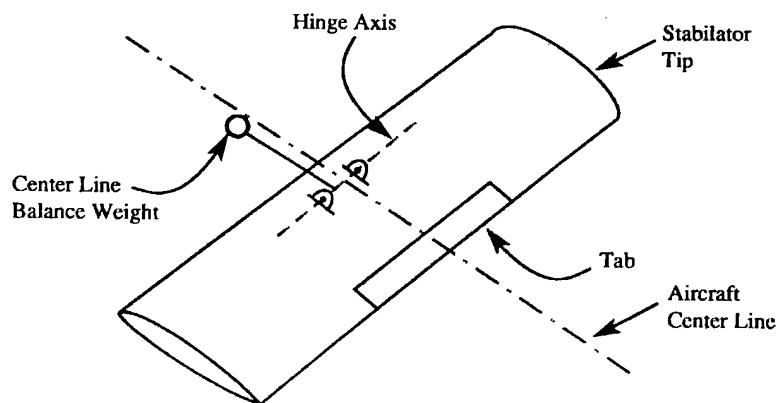
Figure 12: Simplified Schematic Of Stabilator, Central Balance Weight And Tab

Flutter Experience

Following an in-flight failure, without witnesses, a speed placard of 180 mph was applied to all aircraft of this type. A second accident at very high speed produced similar damage and this time the flutter and departure of the stabilator were witnessed.

A flutter investigation, initiated by the designer, began with flight tests to calibrate flutter instrumentation. These were terminated at 190 MPH despite the fact that the configuration had previously been flown to 230 MPH. Dynamic results recorded at 160, 170, 180 and 190 MPH showed a mode, consisting of symmetric pitch, stabilator rotation and first bending, to be losing damping with airspeed and to be approaching instability.

An apparent cause of this was the center-line installed balance weight arm that supported the only balance weight on the stabilator. It was an L-shaped structure attached to the stabilator with its short side pointed down and long side, with the lead balance weight attached, pointed forward. (See Figures 12 and 13).

In the approaching flutter mode, at 31 Hz, the central mass-balance arm took on a cantilever bending oscillation reacted by an almost rigid rotation of the stabilator. (See Figure 13).

The flutter specialist suggested, based on ground vibration tests, that the balance arm be stiffened by a gusset across the L. Stiffening the support arm changed the rotation mode ground vibration frequency from 16 to 20 Hz.

Following the modification, in planning the flight tests with the stiffened balance arm, it was thought possible that the change might have made the flutter situation more critical, since it had been based on limited data and no analysis. The test series was therefore conducted in an orderly manner with a gradual build-up in flight speed.

During the flight tests, with the stiffened balance arm, the symmetric rotation mode coupled with the symmetric stabilator first bending mode and became unstable at 175 MPH, or at a 15 MPH lower speed than with the unstiffened balance arm. Fortunately, though the damage was severe, the aircraft remained flyable and made a safe landing.

The flutter specialist then advised the designer that the single central mass-balance configuration should be replaced by a more conservative, distributed balance, arrangement.

Following the logic outlined in the next section, the final modification moved one-third of the centerline mass balance to the stabilator tips, i.e. one-sixth to each tip. This cured the flutter problem and no flutter was experienced in flight tests to 231 mph. The aircraft was cleared to a never-exceed-speed of 210 mph.
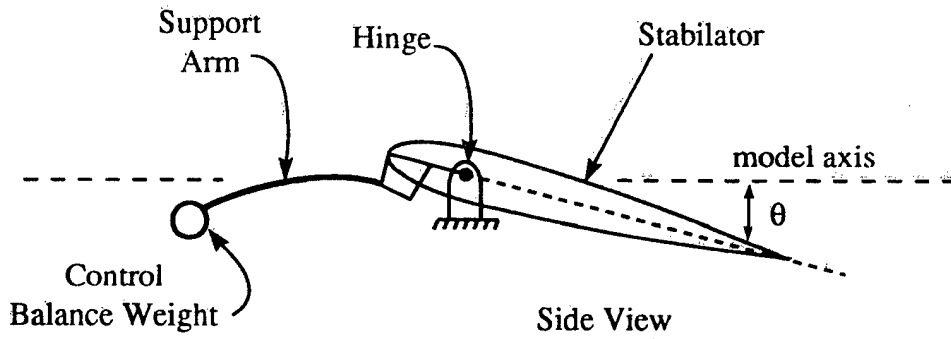
Stabilator Rotation (Torsion) Mode
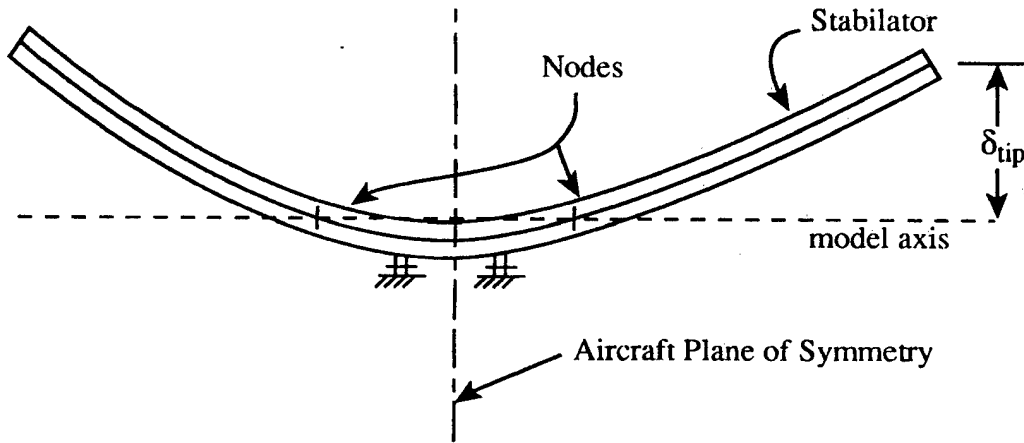
Figure 13: Principal Stabilator Modes Participating In The Observed Flutter

Postulated Flutter Mechanism

The rotation mode, described above, changed frequency with aircraft forward speed due to the aerodynamic hinge moment acting as a spring-to-ground. That is, the hinge moment due to surface unit rotation increased as the square of the forward speed. The stabilator bending mode, on the other hand, did not twist significantly with deflection and therefore did not encounter a spring-to-ground. Its frequency did not change significantly with aircraft forward speed.

Aside: Because surface vibration velocities normal to the wind are small in the rotation mode, its modal damping would be small if unaffected by other modes. Bending-mode surface normal velocities, however, are much larger and produce modal damping that grows linearly with aircraft forward speed increase, if not influenced by other modes.

It is clear that in streaming air the lower rotation-mode frequency will approach that of the bending mode at some forward speed. In addition, the oscillating rotation mode should be able to produce an aerodynamic force distribution that excites the bending mode. This is illustrated in Figure 14.

For one mode to influence another, its motion-produced force distribution must apply a nonzero *generalized force* to the other. The generalized force is defined in Figure 14. It is clear from the figure that oscillations of the rotation mode will excite the bending mode at high forward speed.

If the rotation mode supplies an input generalized force to the bending mode at a frequency well below the bending-mode resonance, the responding bending-mode displacement will be essentially in phase with the input force and of amplitude dictated by bending-mode flexibility. (See Figure 15).

If the rotation mode supplies the input force at a frequency well above the bending-mode resonance, the bending mode-displacement response will be 180 degrees out of phase with the input force or will be in the opposite direction. Its amplitude is then dictated by the *generalized mass* of the bending mode resisting the input force.

The **generalized mass** of a mode is defined as follows:

$$G.M. = \int_{-y_{tip}}^{y_{tip}} m(y)\varphi^2(y)dy \qquad\qquad m = \text{distributed mass, slugs/ft}$$

If, on the other hand, the rotation-mode-induced bending-mode generalized force has a frequency equal to the bending-mode resonant frequency, the bending-mode displacement will respond with a 90 degree lag to the input force, as shown in Figure 15. Its amplitude will be dictated by the *viscous damping* reactive force in the bending mode. (The bending-mode viscous force is proportional to and opposes mode velocity.)

In other words, the rotation-induced generalized force in bending will be in phase with, not bending displacement, but bending velocity. By this means energy is input to the bending mode. The bending-mode amplitude will increase until its viscous resisting (or damping) force equals the bending generalized force input by the torsion mode.

Bending Mode Displacement $\phi(y)$ ft

Aircraft Plane of Symmetry

δ_{tip}

y, ft
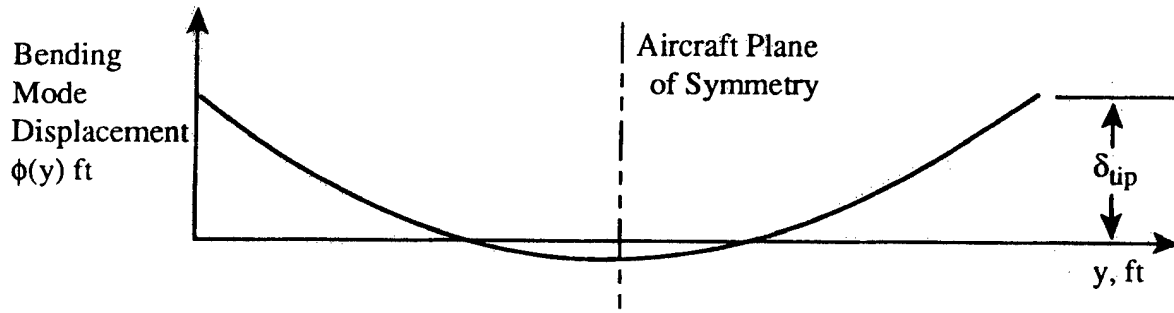
Bending Mode Shape $\phi(y)$
for Unit Tip Displacement , δ_{tip} = 1.0 ft.

Spanwise Loading $\omega(y)$ lb/ft

Airload Distribution lb/ft

y, ft
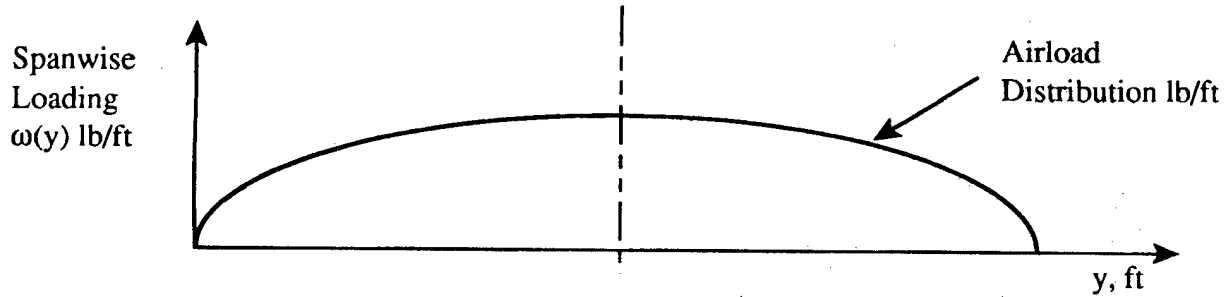
Spanwise Airload Distribution, $\omega(y)$
due to Unit Torsion Mode Displacement, θ = 1 rad

$\omega(y)\, \phi(y)$

y, ft
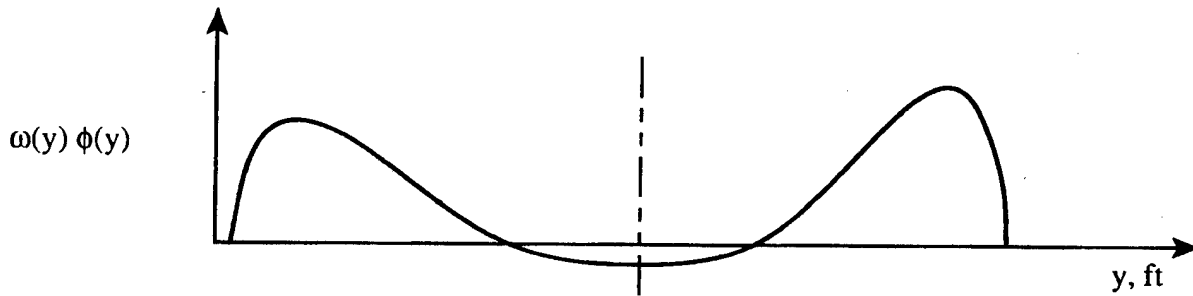
Product of Bending Mode Shape and
Torsion Mode Induced Spanwise Load Distribution

Figure 14: Bending Mode Generalized Force Applied
By Rotation, (Torsion), Mode Aerodynamics
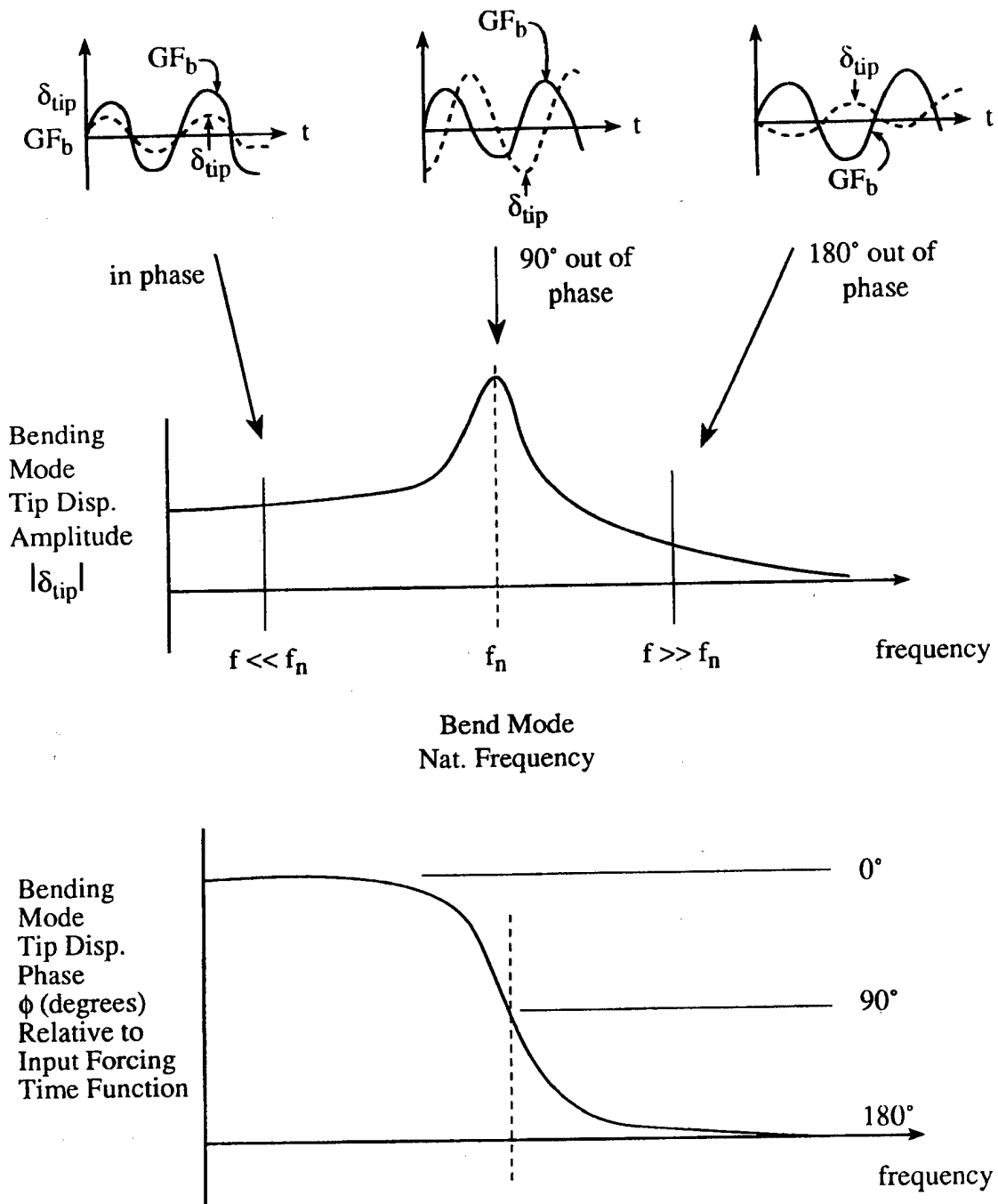
Figure 15: Bending Mode Response To Rotation, (Torsion), Mode Generated Forcing Function, GF_b

An input force to a mode near its natural frequency from a driving mode is **not** sufficient to cause flutter (a dynamic instability). Instability requires the responding degree-of-freedom, in turn, to *feed back* a generalized force to the driving mode. In this way the increasing amplitude of the responding mode causes a continual increase in the driving-mode motion. The mutual reinforcement results in increases, without limit, of displacements in both modes, or a *dynamic divergence* or flutter.

In the present case of stabilator flutter the primary feedback was provided by the unbalanced first moment of section inertia about the hinge line produced in the outboard region of the tail surface by the bending mode. Due to the small normal acceleration of the centerline mass balance at its location in the bending mode, in this case, it could not react to this large inertial hinge-moment.

The feedback hinge-moment is in-phase with the rotation-mode angular velocity or in the direction to add energy. Thus the ingredients are in place to cause flutter. It is only necessary that the destabilizing energy being added to the system be larger than the bending-mode damping energy being removed.

Flutter Corrective Action Assessment

The movement of one-third of the mass balance to the stabilator tip effectively balanced the inertial hinge-moment generated in the bending mode. This essentially zeroed the feedback generalized force thereby neutralizing the flutter instability. This is another application of the *distributed mass balance* design rule.

Case 5: Wing-Aileron Flutter Due to Excessive Control Rotational Inertia

Aircraft Description

The subject aircraft of Case 5 is a low-wing, long-range naval patrol aircraft with four tractor propellers driven by turboprop engines mounted on an unswept wing of high aspect ratio. (See Figure 16). The all metal aircraft of semi-monocoque construction had a conventional unswept tail.

Control surfaces were hydraulically actuated with a reversion to manual control in the event of a failure. This meant that the control surfaces could be restrained by a rotation spring or treated as rotationally unrestrained in wind tunnel flutter tests.

The *never exceed speed*, V_{ne}, was 405 KEAS.

Note: This was a proposed new aircraft of increased capability based on an existing aircraft. Comparisons of characteristics with those of the original aircraft were therefore possible.

Flutter Experience

A 1/12 scale flutter model of the aircraft experienced violent wing tip torsion-mode flutter with aileron rotation participation. This took place at an equivalent full scale frequency of 17.1 Hz at a full scale flight speed of 417 KEAS.

A flutter analysis by the p-k Method, employing Doublet Lattice unsteady aerodynamics and making use of the FAMAS-MADOL computer system, confirmed the observed behavior. Free-free natural vibration modes of the aircraft that participated in the flutter are shown in Figures 16 and 17.

The variations with flight speed of the aileron rotation and wing tip torsion-mode frequencies are shown in Figure 18. The corresponding dampings of the coupled modes are shown in Figure 19.

Flutter occurred despite the use of aileron mass balance to reduce the static unbalance to zero. The configuration included full wing fuel tanks and no external stores.

A number of distributions of mass balance weights along the aileron span were examined analytically, and it was concluded that the flutter problem could not be corrected solely by the use of mass balance. The moment of inertia of the basic aileron about the hinge line was so large that it became impractical even to overbalance the surface to uncouple the rotation mode. It became necessary to recommend a completely new lightweight aileron design to reduce rotational inertia.

Postulated Flutter Mechanism

Inertial coupling of the plunge, pitch and control surface rotation degrees of freedom can be shown for rigid body motions as indicated in Figure 20.

Control mass balancing (static balance) is accomplished by reducing the control surface mass offset arm to zero, $\bar{x}_\beta = 0$, so that $S_\beta = 0$. Examination of Figure 20 then indicates that control rotation acceleration no longer produces vertical (or lift, L) inertia force and plunge acceleration, $\ddot{h}$, contributes no hinge moment (HM) to the control surface. Thus static balance uncouples the plunge and control rotation modes.

Control surface static balance, however, still permits control rotation acceleration to contribute pitching moment (M) to the section by virtue of the I_β term in the 2,3 matrix position and section pitch acceleration to produce hinge moment through the 3,2 term. Thus the pitch and control rotation degrees of freedom remain coupled even with statically balanced control surfaces. Control rotation/section pitch flutter thereby remains a possibility.
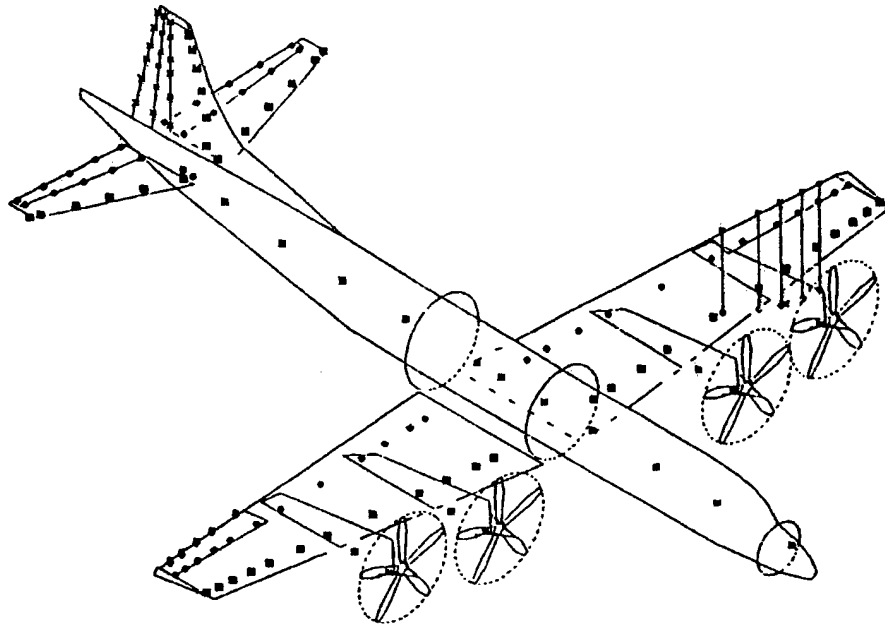
Figure 16: Test Aircraft Model For Wing/Aileron Flutter
Due To Excessive Control Rotational Inertia
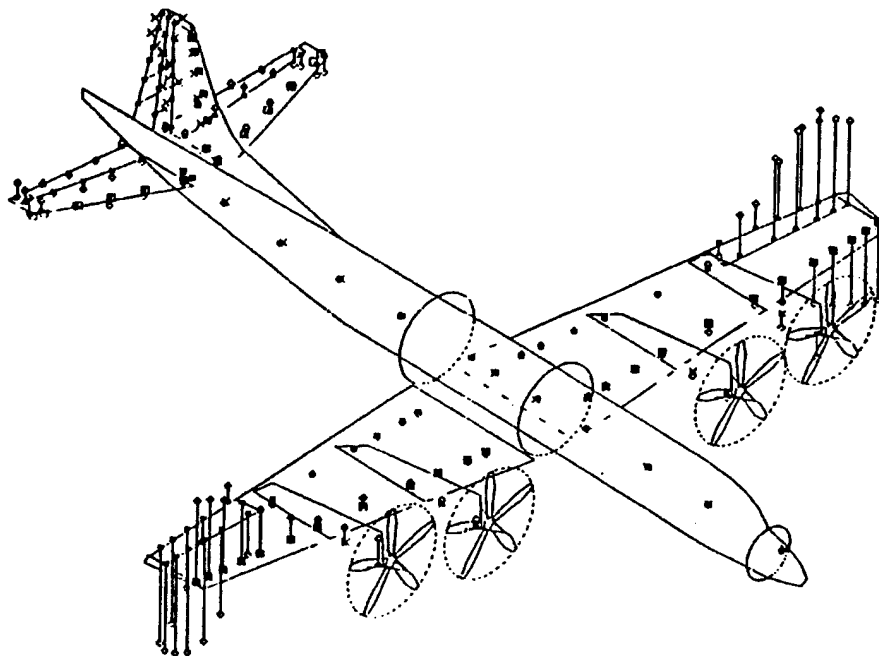
Figure 17: Wing Torsion Mode That Interacts With
Aileron Rotation To Produce Flutter
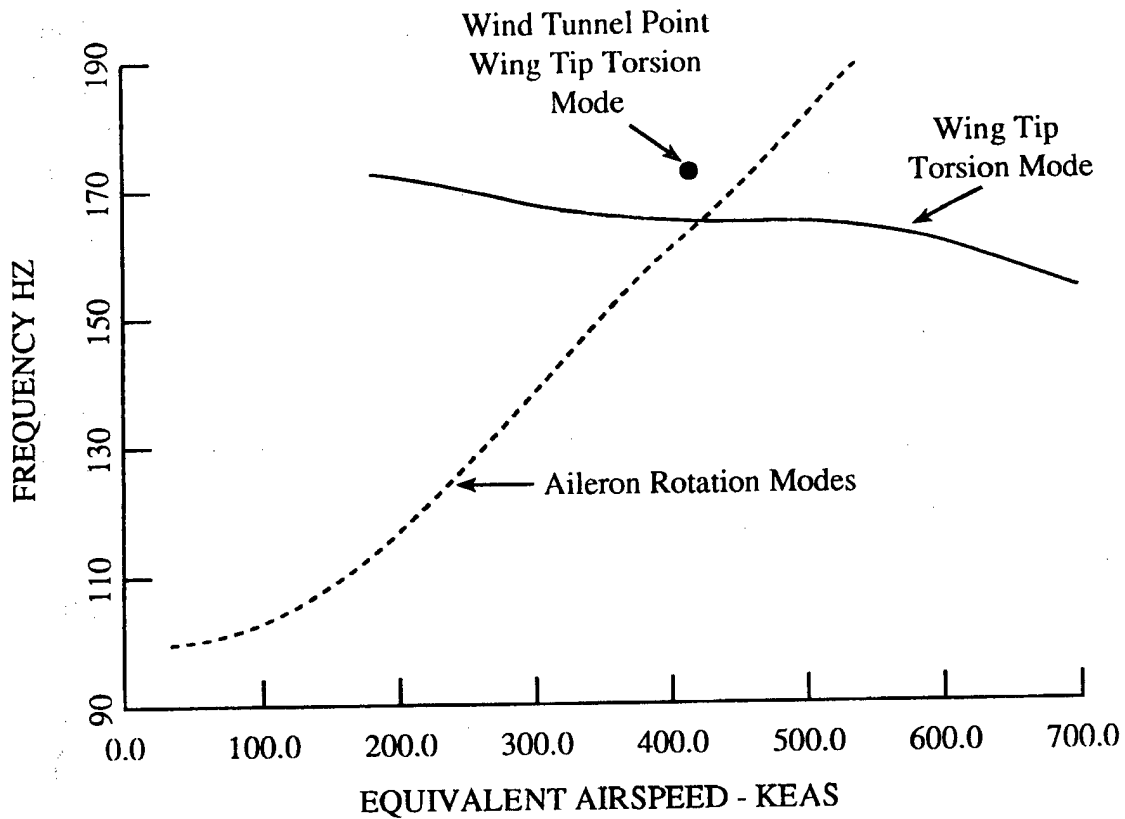
Figure 18: Frequency Versus Airspeed Prediction
For The Wind Tunnel Model

Overbalancing the control surface, i.e., by employing negative $\bar{x}_\beta$, may allow

$$c_1 S_\beta + I_\beta = 0$$

and this uncouples the pitch and control surface rotation modes. Such a remedy may, however, introduce coupling of the control surface and plunge modes that leads to a different form of instability.

If this occurs it may be necessary to redesign the control surface to reduce its moment of inertia about the hinge line.
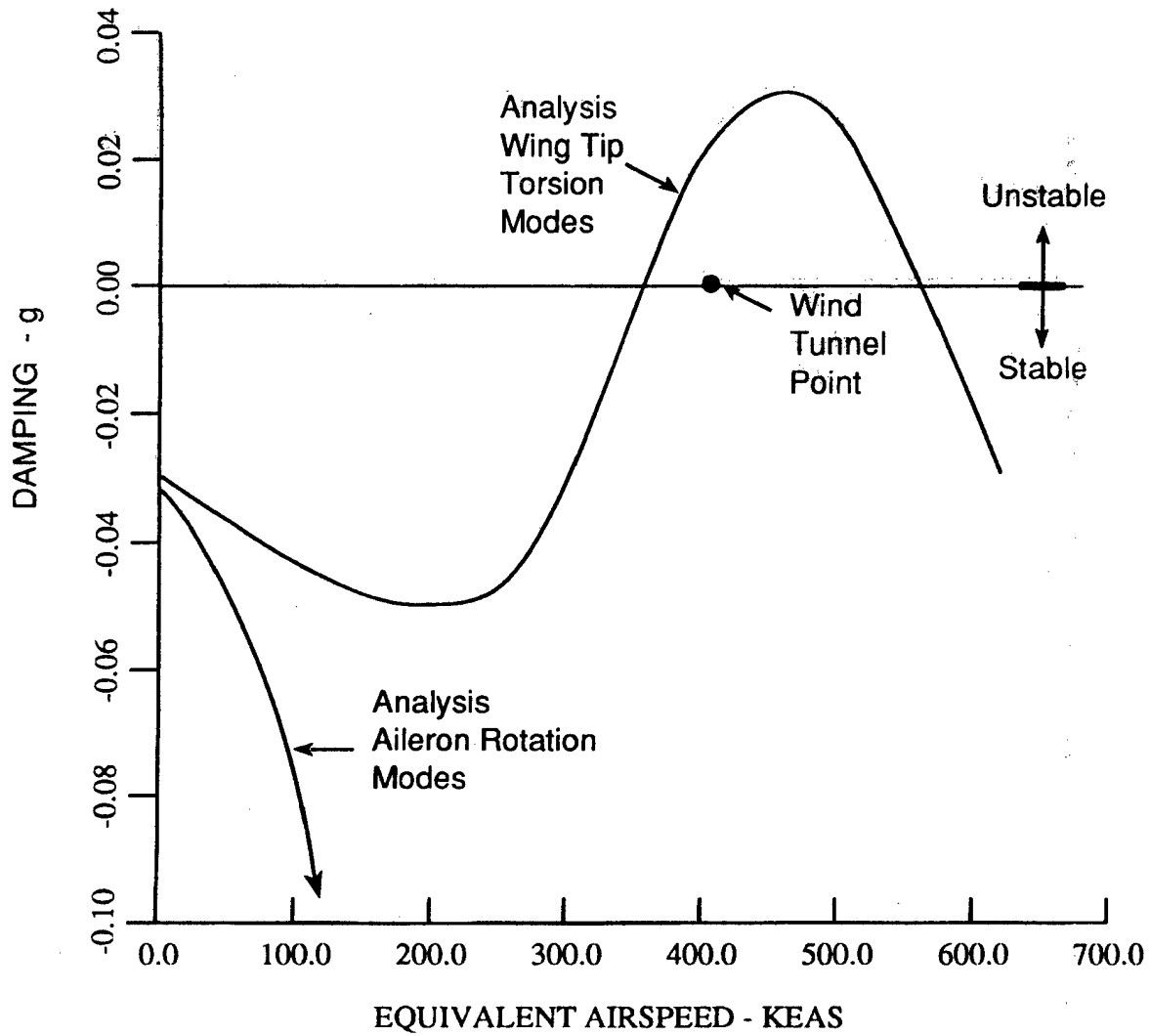
Figure 19: Damping Versus Airspeed Prediction
And Wind Tunnel Result

Flutter Corrective Action Assessment

A region of unacceptable flutter stability with the original aileron design is shown in Figure 21. Analysis of an aileron of reduced moment of inertia and 110% overbalance static first moment is shown in Figure 22. The second design was judged to be marginally satisfactory.

Overbalance, in this case, is defined as an additive nose-heavy balance equal to 110% of the original tail-heavy balance without counterweights.
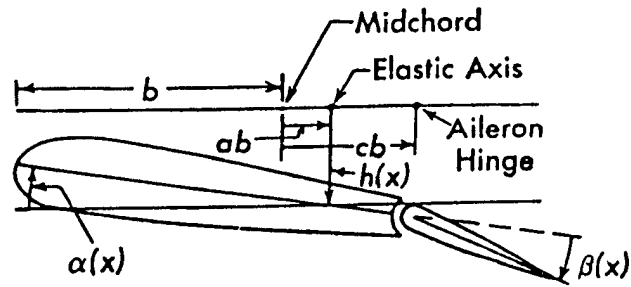
$$\left\{\begin{matrix} L \\ M \\ HM \end{matrix}\right\}_{\text{Inertia}} = \begin{bmatrix} M_W & S_W & S_\beta \\ S_W & I_W & c_1 S_\beta + I_\beta \\ S_\beta & c_1 S_\beta + I_\beta & I_\beta \end{bmatrix} \left\{\begin{matrix} \ddot{h} \\ \ddot{\alpha} \\ \ddot{\beta} \end{matrix}\right\}$$

where:

$c_1 = c - a$

$S_\beta = W_\beta \bar{x}_\beta$

$S_W = W \bar{x}_W$

W_β is aileron weight

$\bar{x}_\beta$ is c.g. location measured from the hinge line, positive aft

W is wing section weight

$\bar{x}_W$ is c.g. location measured from the elastic axis, positive aft

Figure 20: Inertia Coupling Of The Plunge, h, Pitch, α,
And Control Rotation, β, Degrees Of Freedom

2-37

X	MACH NO. = 0.200
◇	MACH NO. = 0.500
+	MACH NO. = 0.711
□	MACH NO. = 0.818
△	1.00° (VELOCIY/MACH LIMIT) ENVELOPE
○	1.15° (VELOCIY/MACH LIMIT) ENVELOPE
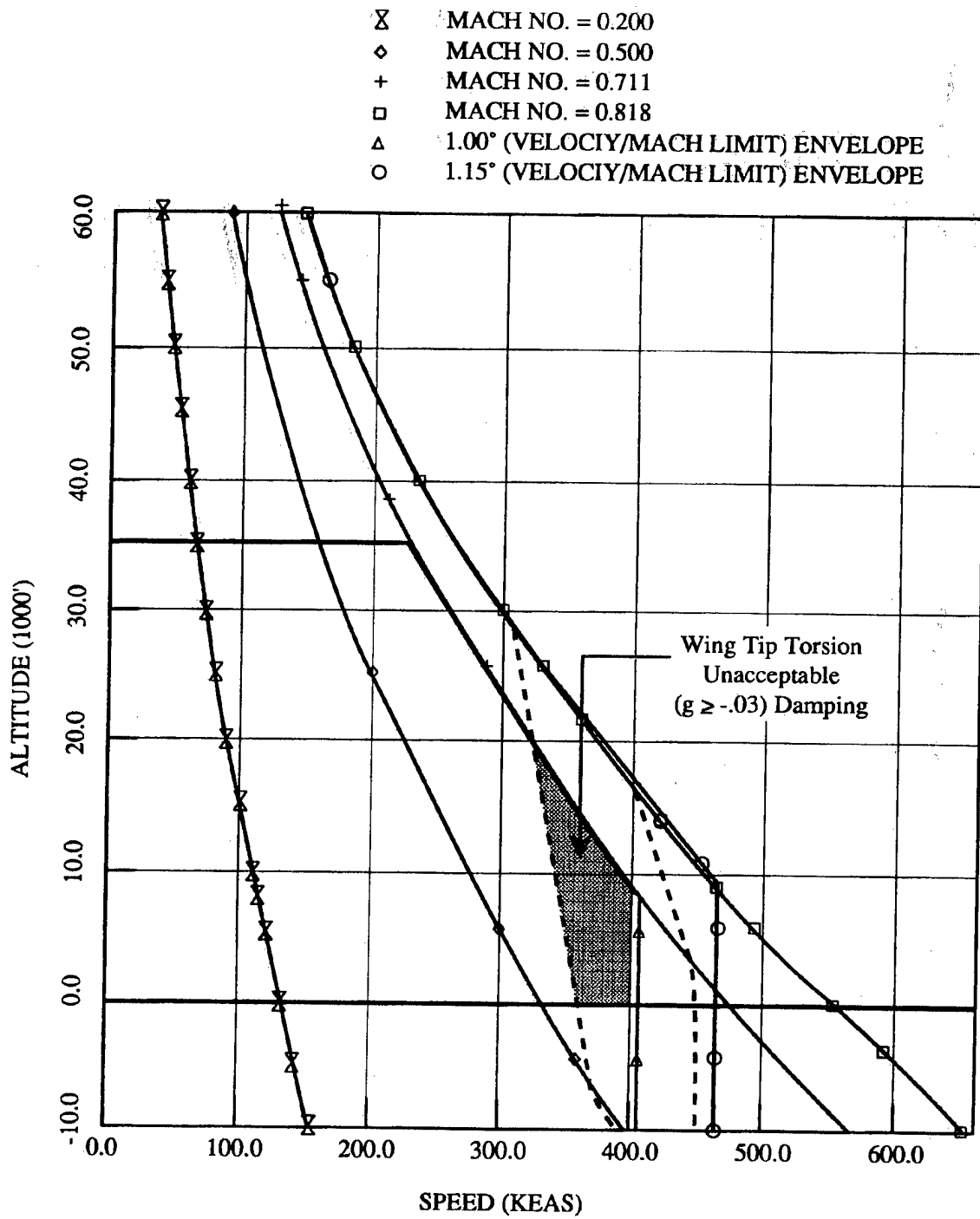
Figure 21: Unacceptable Flutter Enclave For The Nominal Aileron
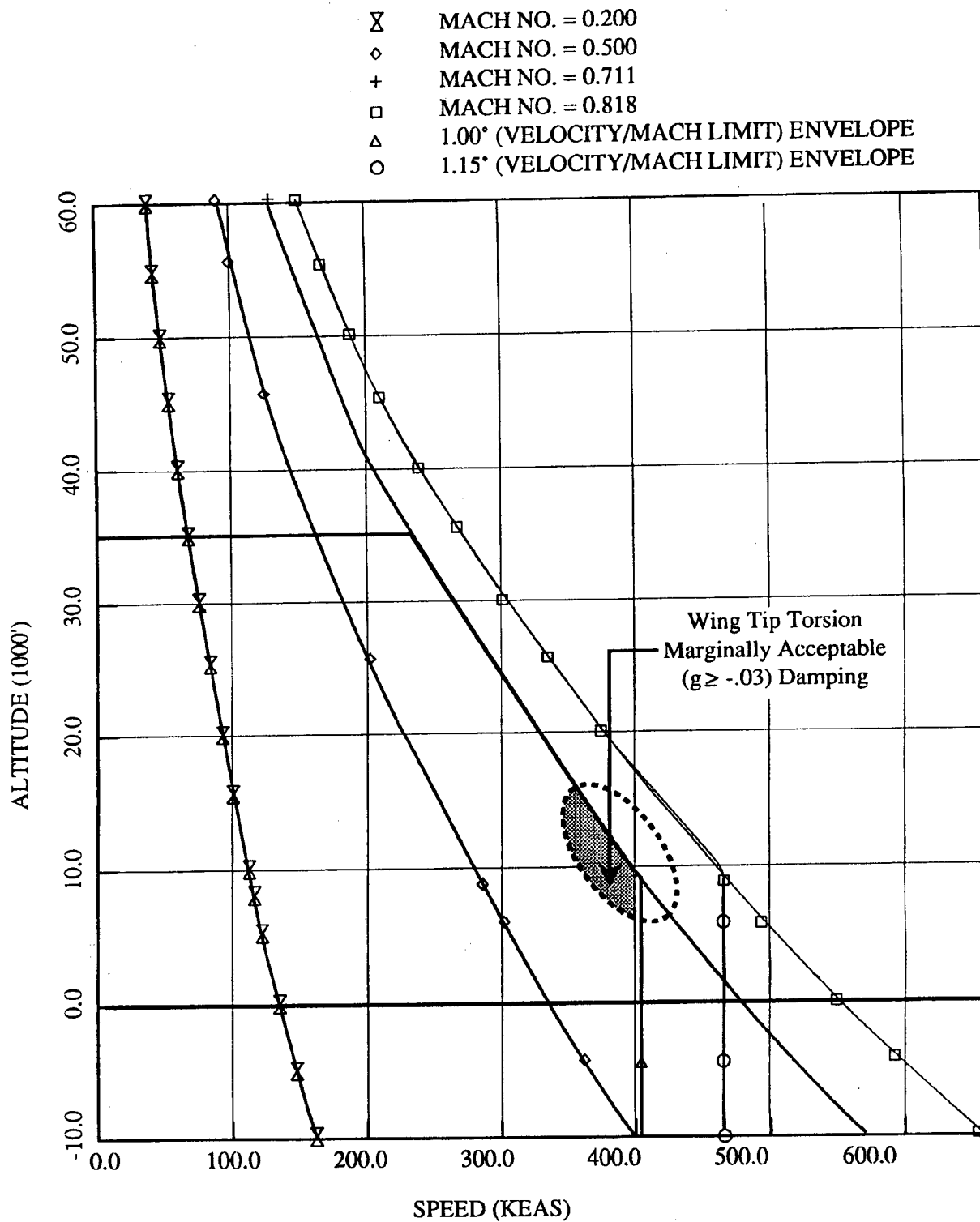
Figure 22: Marginally Acceptable Flutter Enclave For The New Aileron

Case 6: Elevon-Wing Torsion Flutter of a Delta Wing Model

This case, communicated to the authors by word of mouth, is included because of its similarity to Case 2. Both indicate the destabilizing effects of control surface aerodynamic balance.

Aircraft Description

A delta-wing wind tunnel model with its structure dynamically scaled to represent that of a full scale aircraft is the subject of Case 6. It had a single control surface per side that performed the functions of elevator and aileron. Such a surface is called an *elevon*.

The model was tested for flutter stability with the control surface, of constant size, hinged along the leading edge and along two chordwise positions aft of the leading edge.

Flutter Experience

Three tests were performed of elevons of the same size, i.e., the same percent chord. The hinge axis was progressively moved aft from the leading edge in succeeding tests. This was expected to have the effect of increasing the aerodynamic balance, by the distributed balance method, and to progressively reduce hinge moment per unit control surface deflection.

In addition to the effect expected, however, a progressive decrease in flutter speed was noticed. This occurred even though a zero static mass balance condition was maintained in the three tests.

Postulated Flutter Mechanism

It is suspected that the flutter mechanism is a coupling of an essentially wing-torsion mode with elevon rotation, and that an elevon rotation mechanical spring has been employed that raises the rotation-mode frequency to nearly that of the wing quasi-torsion mode.

The fact that the elevon is statically mass balanced does not uncouple the two modes, as is indicated in Case 5. The I_β coupling still exists.

With the progressive aft movement of the hinge axis, the aerodynamic spring-to-ground reduces, eventually to zero, and thus is ineffective in splitting the frequencies of the two modes. In addition the damping of the rotation mode also reduces with aft movement of the hinge axis to about 1/3 its value with the hinge at the control surface leading edge.

It is this reduction in damping that is suspected as the cause of the gradually reducing flutter speed with hinge-axis aft movement.

REFERENCES

1. Scanlan, R.H., and Rosenbaum, R., *Aircraft Vibration and Flutter*, Dover Pub., New York, 1951.

2. Rosenbaum and Vollmecke, *Simplified Flutter Prevention Criteria for Personal Type Aircraft*, U.S. Civil Aeronautics Administration, Airframe and Equipment Engineering Report No. 45 (USGPO, 1950).

William Roberts

Flutter Occurrence On Eighteen
High Performance Military Aircraft

Abstract

This paper records the concurrent development of flutter analysis, numerical modeling techniques, ground vibration testing and in-flight flutter testing at three companies. Airplanes of 18 distinct types serve as illustrative examples, covering subsonic, supersonic and hypersonic regimes. Of these, half showed flaws in flutter design and half did not. Initially, analysis was not supplemented with scale model testing. As soon as scaled model technology was brought into regular use, the risk attendant on full dependence on analysis-namely that flutter might appear after production had begun-was steadily reduced. Several examples are included. Other major developments were the finite element methods for both structural and aerodynamic analysis. Piston theory, once available, found immediate application in the X15 with its Mach 7 speed. Another significant development was the use of item by item structural scaling on a flutter model for the delta wing, Mach 3, F108, and its use on the Space Shuttle for development of a 1/4 scale model of the entire "stack" for early GVT. Three variables-stiffness, chordwise c.g. and control surface balance-were found to be the major determinants of success in preventing flutter. Satisfactory criteria based on this approach are given. The criteria show the great difficulty of building large airplanes with thin wings for use at high speed and show that accident rates are increased when the stiffness requirements are compromised.

The author's experience at the FAA sheds light on the distinct flutter prevention criteria applying to both military and civil aircraft. Civil transports are fail safe structures and in addition, damage identified by a Damage Tolerance Assessment is included in the flutter analysis. Flutter has nearly disappeared as a primary cause for an accident as a result of the complete program of flutter prevention. Because of its import on safety the stiffness criteria have also been useful in assessing new designs.

William Roberts

B.Sc. Aeronautical Engineering, U. of Cincinnati, 1943
M.Sc. Engineering, UCLA, 1953
Ph.D. Engineering, Columbia Pacific University, 1995
36 years industry experience as lead engineer and manager; 16 years FAA experience. Flutter responsibility at all times. Space Shuttle Dynamics Manager and Flutter Designer, North American Rockwell. Project Dynamicist and flutter analyst on 12 first flights of experimental airplanes at Edwards AFB. Accident Investigator. Established correlations between principal parameters such as speed, stiffness, and load amplification on close approach to critical speed.

Table of Contents

List of Tables

William Roberts

Flutter Occurrence On Eighteen High Performance Military Aircraft

INTRODUCTION

This research presents actual case histories specially chosen for their fundamental content. There are many ways to learn flutter: a mentor is one way, extensive analytic experience is another. Some companies focus on approving the strength design, while others set forth the flutter requirements directly during preliminary design. Many of the cases from the history of flutter occur at a time when the approach was different from that now used. Thus the lesson drawn from each case is drawn from a time period where the context is also needed. While GVT and FFT have always been part of the design process, the scaled wind tunnel flutter models have not. Prior to use of the scaled models in wind tunnel tests, exceptional reliance was placed on the analyses, since a product was built and essentially readied for flight prior to conducting the essential flutter tests. There was obvious risk in this approach, and many of the cases presented will demonstrate this risk. The scaled model technology was clearly a response to this risk and came along at a definite point in the time history where the need was great. This permitted experimental determination of the adequacy of the design at a point in time when the essential information could still be acted on.

In this same vein, the analytical techniques were changing to introduce the structural and aerodynamic influence coefficients. Conclusions drawn regarding the technology prior to these developments would not be the same as those drawn following that development. For example, throughout the consideration of each case it is desirable to ask where might the fault lie that allowed flutter to occur. Was it the structural analysis, the aerodynamics, the flutter theory or in the testing technology. A surprising conclusion from the research was that the fault generally lay in but one of these areas -- the portion of the flutter analysis devoted to the math model of structure. Unsteady aerodynamics was advanced via the influence coefficients appropriate for different flight regimes -- just in time for the Mach 3 B70 and the Mach 3 F108. Piston theory was developed just in time for the X15 (see Appendix B) with its Mach 7 performance. Another differentiation is to ask at what point was the design found to be not adequate and it was known that a change was required. This might occur following GVT or FFT or service experience. Each case answers these questions.

To the credit of the flutter designer, the experience of flutter has greatly diminished. Where 7 cases occurred to the F-100 in which one-half of the horizontal stabilizer was lost before control of the problem was obtained, experience in the civil transports has seen no such repetitive occurrences. Near total disappearance of flutter in transport category has occurred if one uses primary cause as a criterion. Flutter does occur as a result of instrumentation failure or as a result of structural failure but this means flutter is a secondary event, not the primary. Even these occurrences are very rare. In the general aviation fleet the picture is not as

encouraging. Less rigorous regulation, design practice, maintenance and inspection result in repetitive failures in some fleets. The design challenge in both transports and general aviation is increased by increased speeds and altitudes. Altitude adds to the risk because, once upset occurs, the extent of overspeed can increase with altitude prior to regaining control.

Many of the designs covered in this history were the exceptional design challenges that pioneered new flight regimes. Covered are the first supersonic fighters, the first supersonic bomber, the Space Shuttle, and a hypersonic missile interceptor that reached Mach 10 in the lower atmosphere. One of the design challenges is the inclusion of trailing edge control surfaces that are not ballasted to prevent flutter but do so by the different approach of increasing control surface stiffness and damping. Three of these early vehicles that prevented flutter without the use of ballast weights were the X15, B70 and the Space Shuttle.

At the FAA the essential function is to eliminate the fatal accidents. This is a practical goal since in 5 of the recent 10 years the number of fatalities was very nearly zero. To determine the root cause of the fatal accidents, many dynamic phenomena were identified and the question asked, what is their relationship to vehicle design. The most important of these relationships are described. In many cases it raises the question, is not flutter prevention a surrogate to prevention of many of these other phenomena. A possible answer to the question is provided in a plot (see Appendix A) showing an attempted correlation of accident rates with speed and two other aeroelastic variables: stiffness and span. The correlations were successful and draw attention to the relationship of the accidents to aeroelasticity. Since the vehicles shown were certified as flutter free the correlation is presumably drawing attention to the difference between stiffness, airplane to airplane, in the design for flutter prevention, or to other phenomena which are stiffness related. This preliminary result cannot be used to conclude that a correlation has been established. Although 8 million departures and 92 accidents were recorded for 5 transports in the time frame 1987 to 1991, this is a too small data sample to provide a convincing correlation. But since the data were sufficiently ordered, it would be worthwhile to add more cases and to search for other causes that could verify or refute the relationship.

The study covers three topics, the presentation of the flutter story for each of 18 designs, flutter related events at the FAA, and flutter criteria. The study as a whole directs one's attention to vehicle stiffness --

1. as the major determinant required for flutter prevention,

2. for its involvement in other wide ranging dynamic phenomena and

3. that the flutter program probably is acting as a surrogate for prevention of other undesirable dynamic phenomena not directly addressed otherwise.

Case 1: North American Aviation F-100

This Air Superiority Fighter was the first fighter with the capability to achieve supersonic speeds in level flight. When the design was first flown, it did not have this capability. It was entered against designs from three other companies in the century series fighter competition. Each company had promised supersonic capability in level flight but this promise proved unattainable in their initial designs. North American immediately proceeded on its own to redesign to meet the 600 knot, 1.3 Mach number requirement by drag reductions. The other three companies chose to wait to renegotiate their contracts. The redesign consisted of four improvements: cockpit canopy, lip of the inlet engine duct, and reduced thicknesses to the horizontal and vertical stabilizers. The airfoil thicknesses were reduced from 7% to 3.5%. The changes to the horizontal and vertical stabilizers were especially challenging since the original design met its flutter requirements along the 600 knot leg only by restrictions limiting the use of the afterburner. On takeoff and climb to 40,000 feet with afterburner followed by a dive to sea level with afterburner, the horizontal stabilizer would flutter. Either the right or the left half would separate from the airplane. This occurred on seven occasions. It was a result of afterburner heating that reached the horizontal stabilizer actuator, which provides actuation in pitch to control the all-moving surface. The heated hydraulic fluid was less stiff than fluid that was not heated. Fortunately the airplane could land safely with only 1/2 stabilizer.

Because of the obvious criticality of the configuration as first designed, the thinner horizontal stabilizer for supersonic speeds was subjected to further testing in a configuration expected to be flutter free. Testing was needed to the limit speed and also to the limit Mach number. Rather than model testing it was decided a more reliable answer could be obtained from full scale sled testing. Both critical dynamic pressure and critical Mach number could be reached by this test approach. The sled test was conducted at Edwards AFB on a full span surface with actuator and fairing and necessary support structure. The first test failed as a result of flutter, the model separated from the sled and, flying freely, reached an altitude of 500 feet above the desert before slowing and descending. But the occurrence of flutter was judged not to be related to the airplane design but to the manner of mounting the test structure on the sled. Following analysis and redesign of this unrelated case, subsequent sled tests substantiated freedom from flutter. A further requirement was to substantiate the test result with a flutter analysis. The initial flutter cases described above occurred in large part because the analysis for natural frequencies and mode shapes failed to match the ground vibration test results. A pitch mode appeared that had not been predicted. If a match could be obtained to the original ground test, then, taking that same analytical approach for the revised configuration, it could be expected that subsequently the ground test for the new configuration and the analysis would agree.

The configuration is presented in Figure 1 showing an all-moving stabilizer with no elevator. An actuator at the centerline controls the pitch motion. The primary structure joining the two halves of the stabilizer is the large torque tube shown. A very large afterburner interferes with joining the two halves so that the torque tube is obliged to curve under the afterburner. The horizontal tail design is also unique in having its pitch axis elevated 7 inches above the midplane of the surface. The entire horizontal tail assembly is suspended from the fuselage pivots by the hanger shown in Figures 2 and 3. The original analysis was a simplified bending torsion beam analysis with fixity assumed at the side of body. All the many deficiencies of this model were not suspected prior to the flutter cases. When the pitch mode showed up at a frequency significantly lower than the first torsion mode, this model was obviously invalid. The analysis had not attempted to describe the missing mode. The angle of attack amplitudes in both the pitch and torsion modes were large and accounted for both being unstable, Figure 4. The most significant deficiency concerned the local flexibilities identified in Figure 2 and Figure 3 -- such local flexibilities were not part of the state of the art of flutter analysis in the early 1950s. Conceptually, the local flexibilities must describe flexibilities not included in either horizontal stabilizer bending or torsion or fuselage bending or torsion. The analyst could normally ignore the detail flexibilities of local structures for the case where two primary structures are joined at right angles. Not so for this case, here the primary structural box of the horizontal stabilizer outboard of the root was of generous dimensions but was reduced to the dimensions of a single 6 inch tube inboard of the side of the body. Another complication requiring improved methodology was the large coupling between all the fundamental motions, bending, torsion, pitch and fore and aft or in-plane chordwise motion. Closely spaced pitch and torsion modes and an extensive flutter history were the result of the extra flexibility in the root structure.
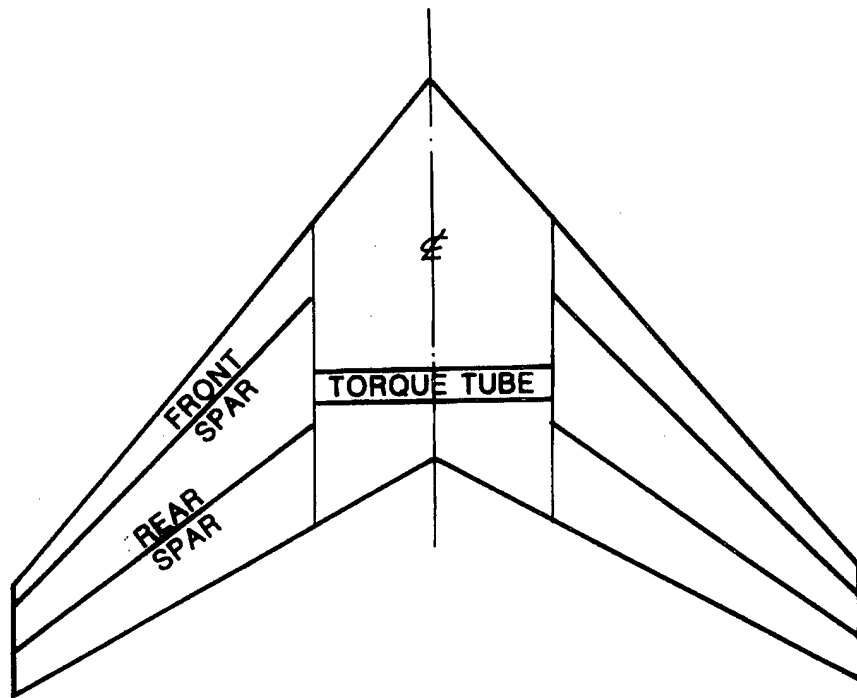
Figure 1: Plan View F-100 Horizontal Stabilizer

LOCAL FLEXIBILITIES SHOWN
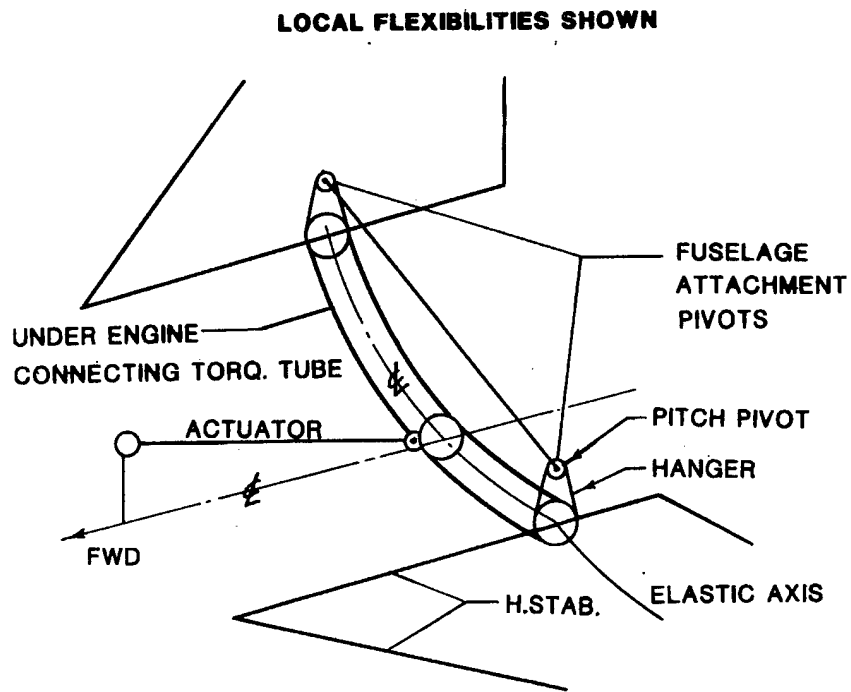
Figure 2: Three Dimensional Perspective (Perspective View)
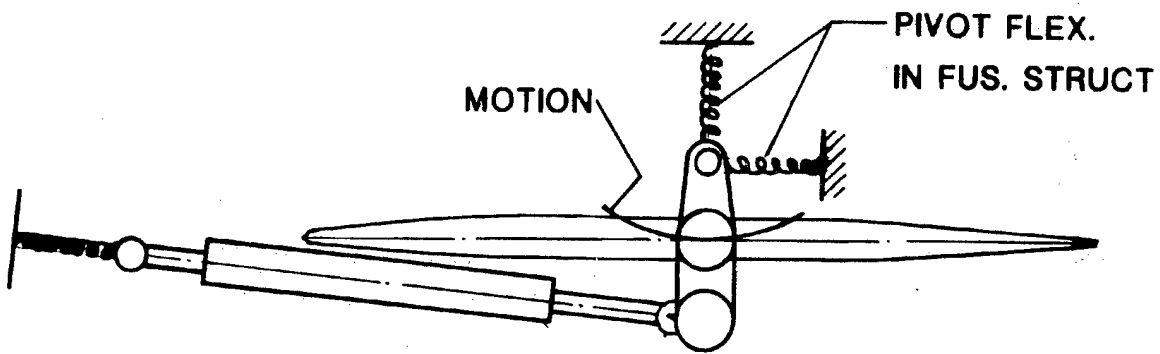
Figure 3: Local Flexibilities (Side View)

FLUTTER STABILITY
NORTH AMERICAN F-100
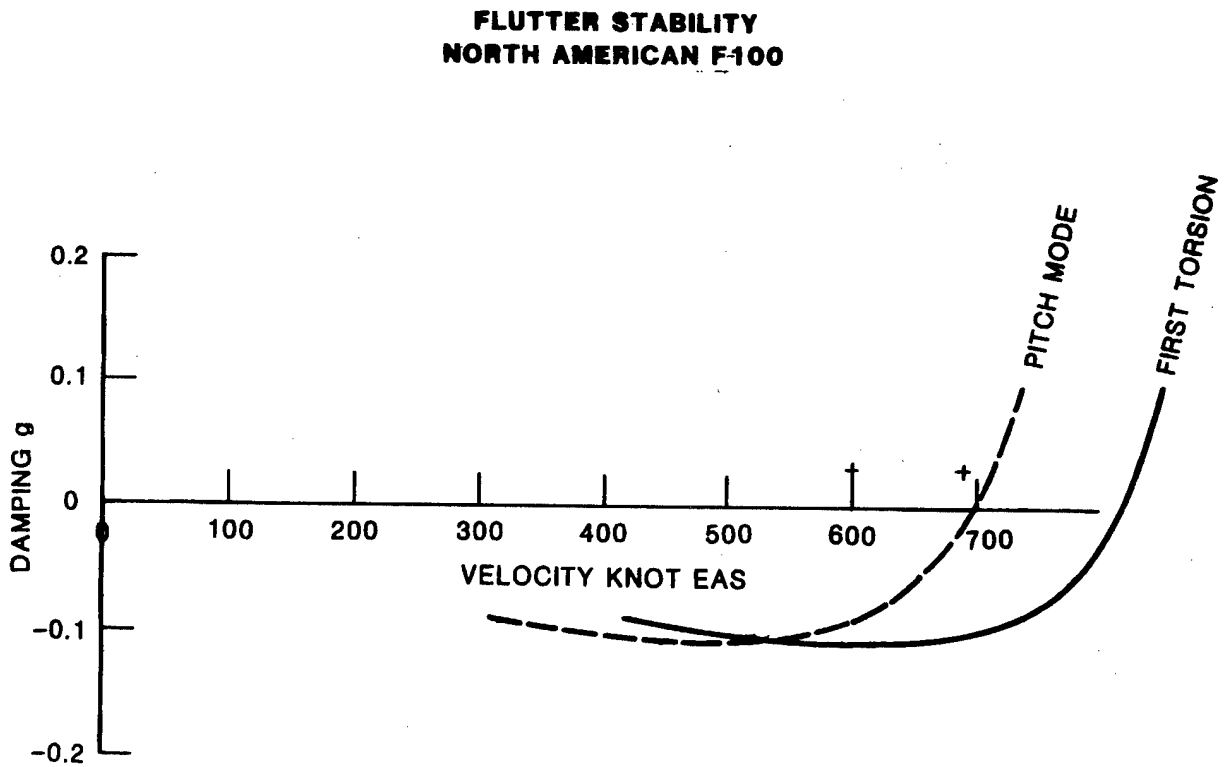
Figure 4: Damping vs Velocity, F100 Horizontal Stabilizer

An expediency was chosen to obtain these local flexibilities from the original ground test results by iterating the analysis until matching modes and frequencies were obtained. An agreement to 2 or 3% was sought but the close coupling between pitch and torsion required a dozen iterations before suitable agreement was obtained. The need for describing a fore and aft mode had been encountered only rarely. Thus guidance was taken from an experimental result already in hand to determine the quantitative values for the structural flexibilities.

North American was following their own successful methods developed during the 1940s in which correspondence between analysis and test was clarified by defining coupled modes. The strip theory flutter analysis of Technical Report 4798 had been augmented to be compatible with insertion of coupled modes of vibration rather than uncoupled modes. With this procedure a match can be seen directly in frequency and mode shape between analysis and ground test. Later the technology gravitated to component modes throughout the industry but in this later approach, clarity can be lost between analysis and test.

By the time this new design was to be frozen, a conservative procedure was chosen to provide an adequately stiff structure for the thin 3.5% thickness horizontal stabilizer. The original classical bending and torsion analysis was upgraded in parallel to the new analysis with bending, torsion, pitch and fore-and-aft modes. Whichever of these analyses provided the higher requirements was used at any location along the structural axis. The final result of the vibration and flutter analysis for the new configuration is seen in the g-V curve in Figure 4. This unique result shows two unstable modes just beyond the required flutter speed with the more critical being the one with the lower frequency, a coupled pitch and fore-and-aft mode. Because of pivot points above the plane of the surface, the fore-and-aft mode contains a large pitch component.

What Was Learned

The two important lessons were:

1) the development surrounding the concept of local flexibility and

2) the importance of rebuilding the analytical model to agree with the ground vibration test results. From the structural diagrams presented along with the description of the unique vibration modes, it can be seen immediately that no vague or approximate statement of the local flexibilities can possibly match the measured modes. All the local flexibilities must be precisely identified to obtain an accurate math model. An iterative method was developed whereby a correct set of vibration modes and frequencies could be defined using the results from the ground vibration test. This first example was based on 12 iterations which can be considered reasonable based on its importance to the design.

Case 2: North American F107
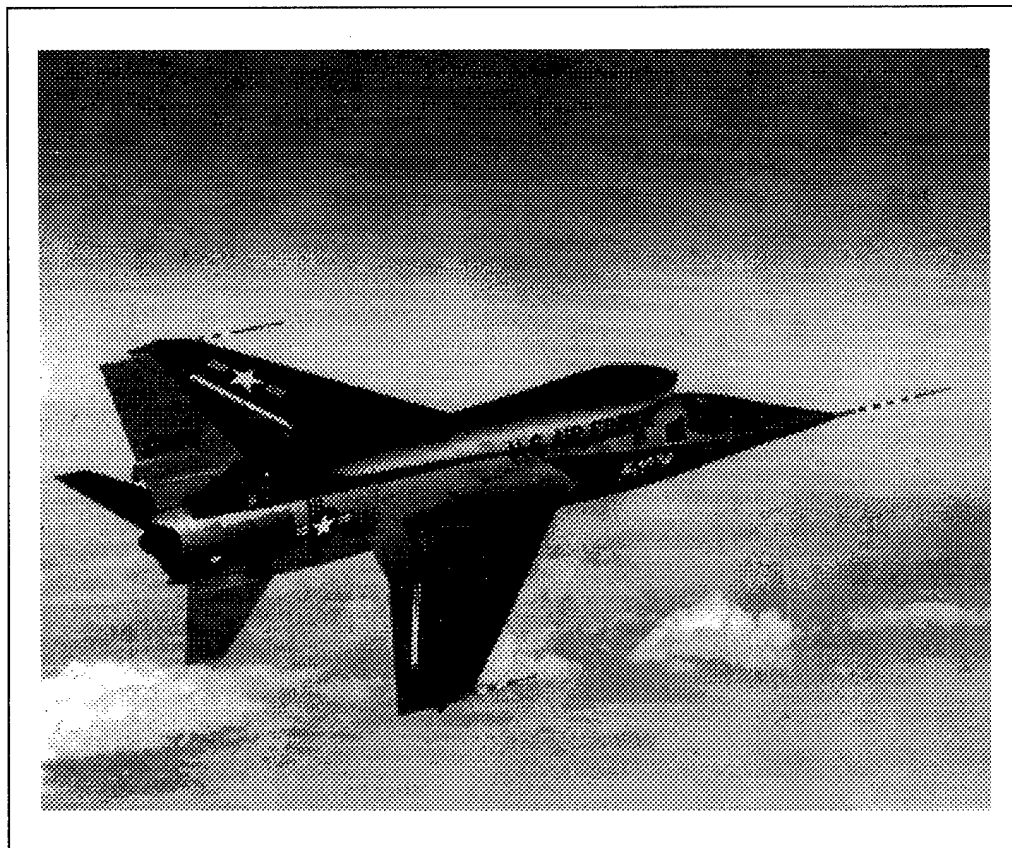
The F100 design was begun as a version of the F86; likewise the F107 was begun as a version of the F100. Wing and horizontal stabilizer were unchanged but the vertical was greatly enlarged as a result of a fatal accident to the F100 in which the large diameter of the fuselage had reduced the effectiveness of the vertical stabilizer in a pullup. During flight test, the airplane diverged in yaw at high angles of attack. Thus yaw stability dictated a larger vertical stabilizer. The challenge of the empennage design in this case was that both the horizontal and vertical stabilizers were all moving surfaces; i.e., no trailing edge control surfaces. The speed altitude design envelope of the new aircraft was very greatly enlarged, to Mach 1.2 at sea level and 2.0 at altitude which naturally required greater stiffness in the wing and empennage. Figure 5 shows the layout of the all moving vertical stabilizer illustrating its relatively small footprint for the three point root restraint. Points 1 and 2 shown are the top and bottom of the spindle and point 3 is the location for the actuator connection.

With the experience of the F100 all moving horizontal surface as a foundation, the design of the all moving vertical stabilizer could reasonably have been expected to proceed without problems. The program was supported with a new low speed wind tunnel flutter model. The stiffness requirements for the model were easily established based on a long history of quantifying both the surface stiffness requirements and separately the root stiffness
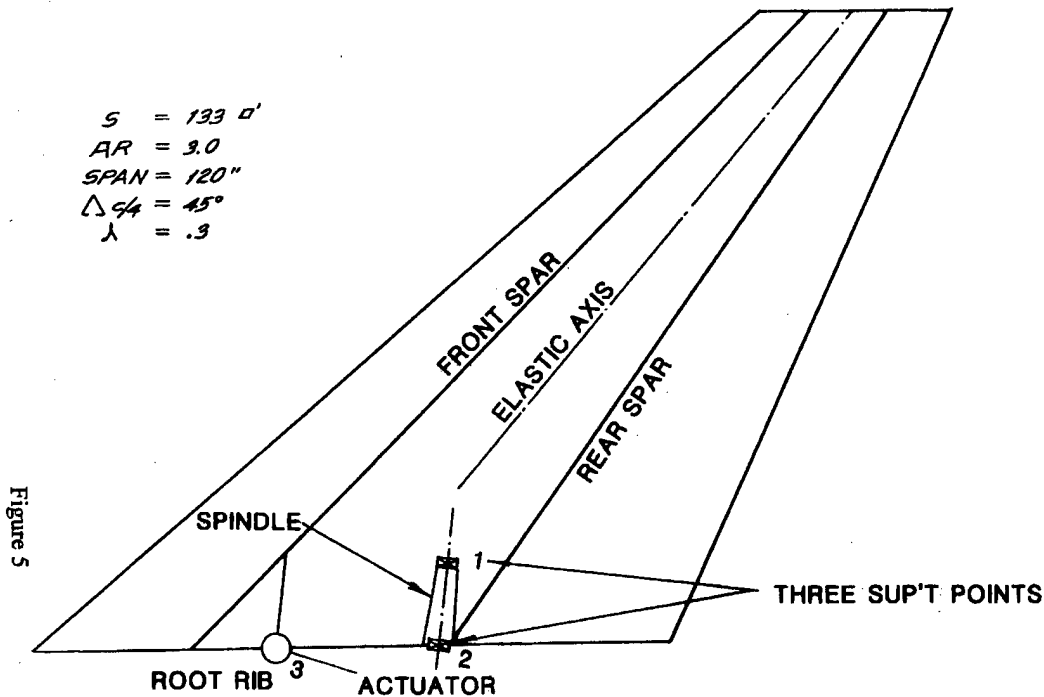
Figure 5: F107 Vertical Stabilizer

requirements. The wind tunnel program proceeded on the basis of the original stiffness requirements prior to the time that the ground vibration test was conducted. However the ground vibration test (GVT) showed the all moving surface failed to meet its design targets for the torsion frequency. It was in fact a repeat on the vertical stabilizer of the problem seen on the F100 all moving horizontal stabilizer. The design requirements had been implemented in two steps:

1. conventional beam model for EI and GJ, and

2. root stiffness requirements at the 3 support points.

The original design analysis showed the design met the requirements. The root flexibility from the three point support was analyzed with a sufficiently advanced math model that avoided one pitfall. The elastic center of the three springs (a point load provides translation but not rotation) was determined and the surface elastic axis was located to pass through this centroid. In addition, the maximum and minimum principal axes of inertia representing the stiffness properties of the three point support were determined and the flutter analysis was based on this description.

The low speed wind tunnel model was constructed only for the empennage. Flutter speeds obtained from the model showed that the flutter speeds were satisfactory in reaching the target flutter speeds of 1000 mph based on the chosen flutter design which included the 15% margin in speed.

The failure of the first flight article to reach the required natural frequency during GVT was a result of the additional local flexibility at the root beyond that described by the analytical model. Separate actuator stiffness tests had been conducted to verify the hydraulic actuator stiffness so that the areas questioned for the extra flexibility were either in the body supported 3 point restraint or in the surface locally in the vicinity of the three support points. Experience with the structural stiffness of the main box further out the span was not questioned as the torque box was of conventional design. In addition, allowance had been made for the shear lag reducing the dimensions in the transition zone from the main box to the much smaller dimensions at the 3 point support. Assessing the likely location of the extra flexibility as arising either in the body or in the surface at the root suggested that the nature of the structures problem was quite different between the two areas. In the body the structures were known, they were conventional, and the design group had excellent experience in meeting stiffness targets. Reviewing the root structure however showed that what had likely been missed was the ability of the covers to spread during bending and torsion as would be modeled by Figure 6.

VERTICAL CROSS SECTIONS

F107

Notes:

1. Spanwise bending acting on internal spindle generates prying action on cover plates.

2. Local Flexibilities shown were stiffened with a structural box lying on either side of spindle to tie covers together. Root RIB stiffened as it also serves same function.

SPINDLE

SCHEMATIC
LOCAL FLEXIBILITY

Figure 6: Local Flexibilities

The design group recognized immediately that the necessary structure was missing and stiffened the root rib and boxed in the bearing areas to tie the two covers together. (This was not a simplified structure without ribs -- just that the ribs and the structure surrounding the spindle did not meet the stiffness requirements.) The subsequent tests showed a return to the expected stiffnesses and agreement with the original design analysis.

The empennage flutter model represented a completely new design approach to the model structure. It was shown that a solid magnesium airfoil section would match both b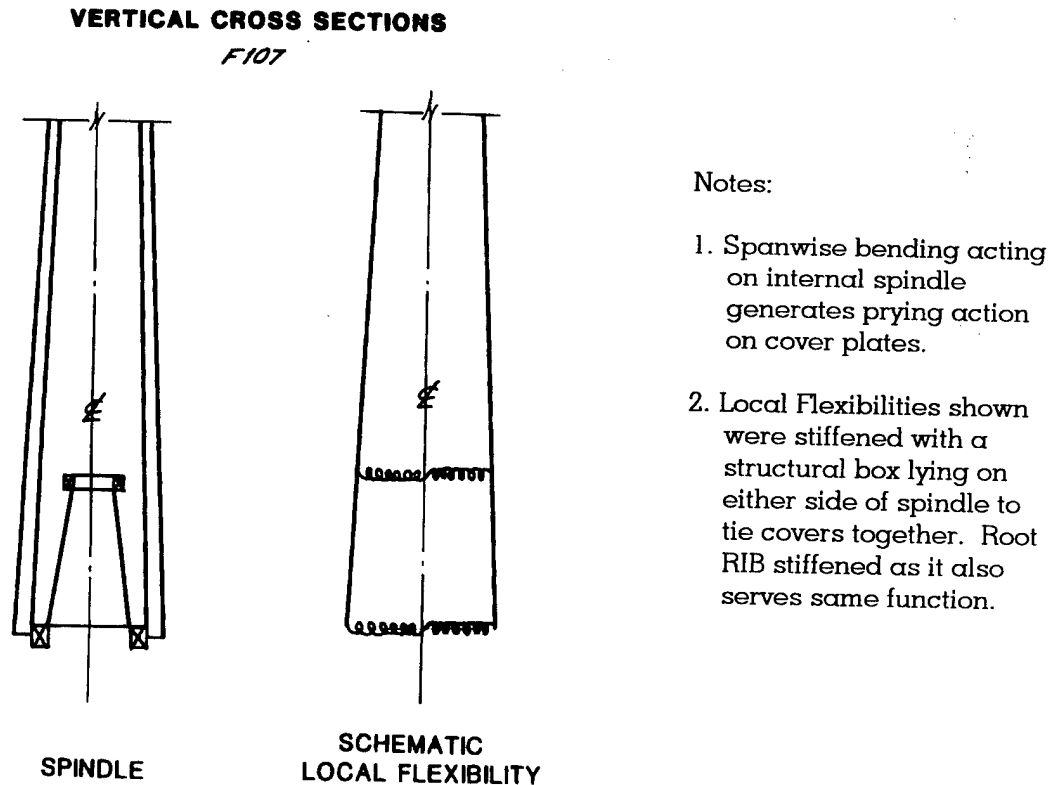ending and torsion stiffness of the full scale structure based on an appropriate choice of thickness to chord ratio. This made the task of flutter model construction much simpler. In addition the 3 point support was modeled. The model construction using a solid magnesium cross section provided an excellent match to the analytic math model of the full scale design. The vibration modes were unique in that the first torsion and second bending modes of the surface were close in frequency and had node line patterns that could only be measured during GVT by a special test procedure. It was necessary to locate the shaker on one node line at the position that gave maximum excitation to the other mode as would be shown by a moment arm chosen to maximize the distance to the other node. At that point in time the vacuum pads had been developed that allowed the shaker to be attached at any point on the surface. Without that special test procedure, modes and frequencies were not repeatable when other shaker positions were used to verify results. Indeed both the node lines and natural frequencies wandered excessively without this approach of simultaneously maximizing the response in one mode while minimizing the response in the closeby mode. The node lines are shown in Figure 7 and the necessary critical shaker locations are given. These had to be obtained by iteration so as to obtain stable modes and frequencies. It is a point of further interest that two close modal frequencies were also a feature of the F-100 horizontal stabilizer case described above. Although the wind tunnel model adequately covered this, the stiffness levels were the design values. Because the wind tunnel flutter model preceeded the GVT, the problem it would uncover was not yet exposed.

The F107 was faulted for a failure to match a new incompressible flutter speed requirement of 1000 knots. The customer had previously imposed a target of 1000 mph requirement for bypassing the subsonic compressibility dip near Mach 0.85, see Figure 8. The final wing flutter analyses had shown lesser flutter speeds than planned which was traced to a spoiler installation just forward of the flap. The addition to structural weight by the spoiler in a location far aft of the elastic axis was especially sensitive in reducing the flutter speed. A 1% further aft chordwise c.g. requires a 6% increase in wing stiffness to accommodate it. In this case the wing c.g. had moved from 40 to 46% of the chord in the region of the spoiler necessitating correspondingly large increases in wing stiffness. This sensitivity had not previously been included in the stiffness criterion. After validating the effect, it was added to the criterion. The argument was extended to chordwise c.g. forward of the reference 40% c.g. to show that the helicopter blade design solution of locating the chordwise c.g. at 25% chord canceled the normal flutter requirements for torsional stiffness, see Figure 9. Considerable optimization was completed to raise the wing flutter speed to the requested level for the least structural weight and it was found that relatively minor cover thickness increases in the outer 1/3 of the span would provide the increase requested.

NORTH AMERICAN F107 VERTICAL STABILIZER
NODE LINES FOR TWO CLOSELY SPACED MODES
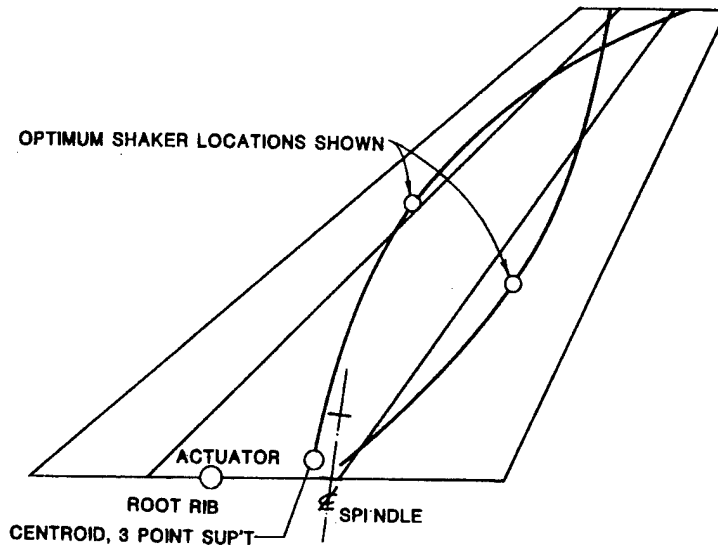
Figure 7: F107 Vertical Stabilizer Vibration Nodal Pattern

APPROXIMATION
INCOMPRESSIBLE FLUTTER SPEED WITH
SUFFICIENT MARGIN TO AVOID TRANSONIC DIP
F107
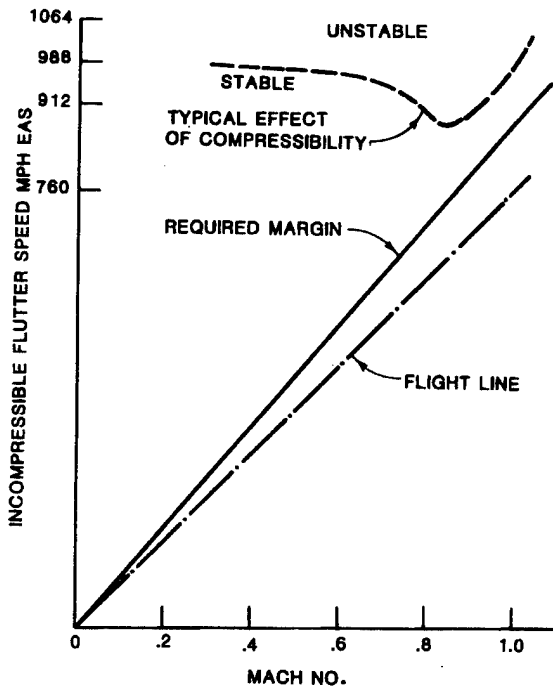
Figure 8: F107 Flutter Speed vs Mach
Number Showing Transonic Dip

SENSITIVITY OF STIFFNESS
REQUIRED TO SECTION C.G.
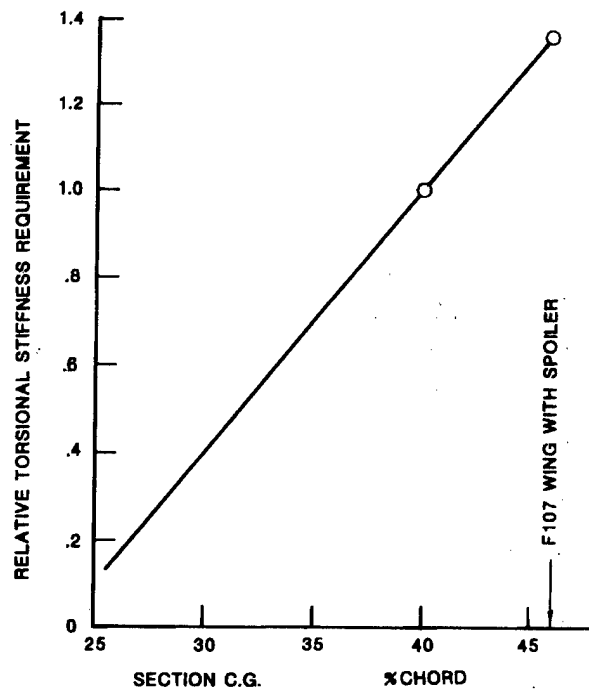
Figure 9: Stiffness Requirement vs
Chordwise Center of Gravity

3-14

Previous theoretical studies had already been completed to identify optimum placement of torsional stiffness spanwise. The results had been included in the stiffness criterion in the form of a weight equation that defined the weight of the torsion box needed for flutter, reversal or divergence. First attempts had been done merely by comparing several placements of additional material to find an optimum. The optimum result changes with taper ratio, the planform variable that measures the ratio of tip chord to root chord. But the task of optimizing each separate case was simplified when it was recognized that all cases could be defined by a constant stress-equivalent to constant strain energy. The optimum placement of torsional stiffness spanwise is illustrated by presenting the optimum mode shape in Figure 10 for the divergence case.

OPTIMUM TORSION MODE SHAPE
DEPENDENT ON TAPER RATIO
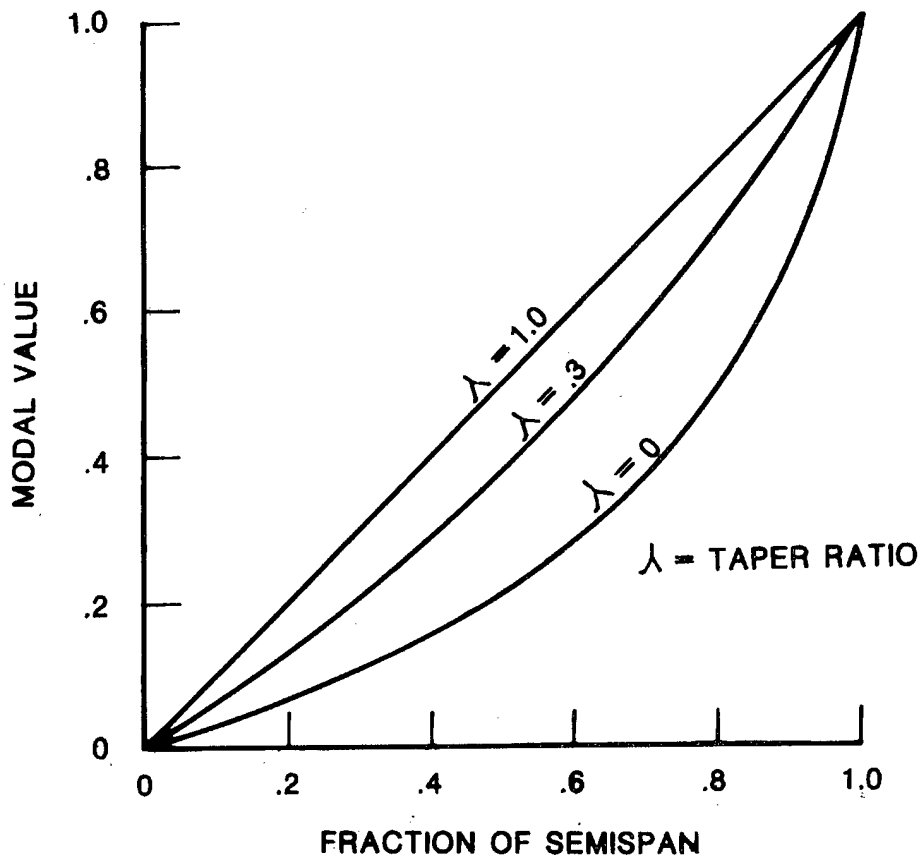
Figure 10: Optimum Mode Shapes

The presentation of the stiffness criterion will be done later in two forms, the theoretical development in the section "Simplified Criterion for Torsional Stiffness Required for Flutter", and its accompanying weight equation, Table 3. The latter form is especially useful for preliminary design. The criterion was also compared to the NASA flutter criterion and shown to correspond in the section "Similarities and Differences Between the Two Key Criteria." It makes an elegant alternative presentation with considerable insight to the overall aeroelastic design challenge.

What Was Learned

The lessons learned were much more numerous for this supersonic fighter with Mach 1.2 capability at sea level and 2.0 capability at altitude even though this design was a duplicate in much of the configuration and structural design to that of the F100.

1. To pass through transonic speeds and avoid the dip in flutter speeds at Mach 0.85 the customer would demand 1000 knot incompressible flutter speed instead of the previously accepted 1000 mph.

2. The sensitivity to an aft c.g. on a lifting surface was established and shown to be a dominant variable. A 6% increase in stiffness was needed to accommodate an aft shift by 1% in chordwise c.g. This result was validated and shown to be consistent with the helicopter rotor blade design where the c.g. at the 25% point is free of a stiffness requirement. An addition was made to the stiffness criterion to accommodate the effects of aft c.g.'s.

3. The missing element in the design of the all moving vertical stabilizer was the local flexibility surrounding each of the three restraints at the root. Structural loads on the surface could spread the covers on the structural box. Once the covers at the root were properly secured, one to the other, the measured stiffness returned to the predicted values called for in the original design. This deficiency in the approach occurred even though most of the design had been carefully validated step by step. The local flexibility at key points of the root restraint, the lesson learned in the case of the F-100 above, was of a different character from that of the previous case.

4. The structural analysis was improved by a method to describe the three point support by an elastic center and axes of minimum and maximum stiffness. Other axes do not account for the existence of a minimum value of stiffness.

5. A new procedure was developed for use in the GVT for separating closely spaced modes. If the shaker is located so as to minimize the excitation in one of the modes and maximize the excitation in the other, then a stable set of data can be obtained which can be validated by other shaker locations. Unless this is done, as the shaker is moved, mode shapes, node lines and natural frequencies can change radically. The state of the art for GVT had advanced to the point where the vacuum pads could be located at any point on the surface, a necessary development for this case.

6. Using aluminum for the structural material of choice was adequate for this Mach 2.0 design. Structural temperatures did not exceed 205 degrees farenheit at which point the loss in moduli did not exceed 5%.

7. A technique for flutter model construction using a solid magnesium cross section for the structural design of the lifting surface simplified the time and cost of construction. The dynamically scaled magnesium model was designed to match full scale stiffness by varying the thickness.

8. The optimum spanwise placement of torsional stiffness which had previously been solved, demonstrated its usefulness on the wing, horizontal and vertical stabilizers.

ASSESSING THE STATE-OF-THE-ART FLUTTER ANALYSIS IN THE 1940s & 1950s

During the decade of the 1940s and early 1950s prior to the widespread use of the scaled flutter models for low speed wind tunnel testing, the state-of-the-art consisted mainly of a stability analysis derived from energy methods using two dimensional unsteady aerodynamic derivatives in a strip theory format. Because all terms in the stability analysis were integrated spanwise the technique was referred to as three-dimensional, U.S. Army Technical Report 4798, Reference 4. The approach was supported by the ground vibration test (GVT) and the flight flutter test (FFT). Since the latter two tests occur at the end of the design verification, it means that reliance on the analysis engendered sizable risks. As we will show in this section, the hardware produced under these methods were generally successful. Between 1945 and extending all the way to 1950 North America successfully produced the following group of eight airplanes of mostly conventional designs: for the U.S. Navy, FJ-1, XSN2J, XAJ, XA2J; and for the USAF, F86, T28, B45 and later in the 1950 decade the Utility Transport UTX, later identified as the T39 and Sabreliner (see Appendix B). These airplanes featured wings without sweepback (with the exception of the F86 Sabrejet and the UTX), small wing spans, relatively thick airfoil sections that provided for adequate torsional stiffness, speeds that reached as high as Mach 1.0 on the F-86, but otherwise conventional layouts and straightforward structures. The flutter requirements were not very demanding because the configurations were such that extra structural material over and above the strength design was generally not required, although there were exceptions. The approach used during the 1940s and the early 50s continues in use up to the present, but starting in 1955 lifting surface theories and aerodynamic influence coefficients gradually supplanted strip theory for designs for the higher speeds.

One might ask why such a simple approach had the capability to produce flutter-free hardware. Was it reasonable to expect that the design process for flutter based on simple theory would be successful? The major factors that promoted success using this approach were:

1. Fundamental correctness of the underlying theory of unsteady aerodynamics was a proven technology,

2.   Structures technology adequate for uncomplicated structures, illustrated by the ability to calculate natural frequencies to the required 5% accuracy and

3.   NASA support for flutter that generally kept pace with the design requirements.

At North American the program for flutter prevention began in preliminary design by applying the criteria described later in this text.

   a.   Torsional stiffness appropriate to each candidate configuration

   b.   Chordwise c.g. control, a particularly sensitive flutter parameter for each of the lifting surfaces

   c.   ballasted control surfaces by elements

The approach supported design in all speed ranges if the incompressible flutter speeds were adjusted upward to avoid the transonic dip (see Figure 8). The F86 and F100 series airplanes illustrated the successful use of the basic theory in speed ranges that included the transonic and low supersonic speeds. The kinds of problems that arose and their source will be shown. Only the specific problems are described for each of the designs. The recurring problems were mostly deficiencies in structural stiffness.

Case 3:   F-86
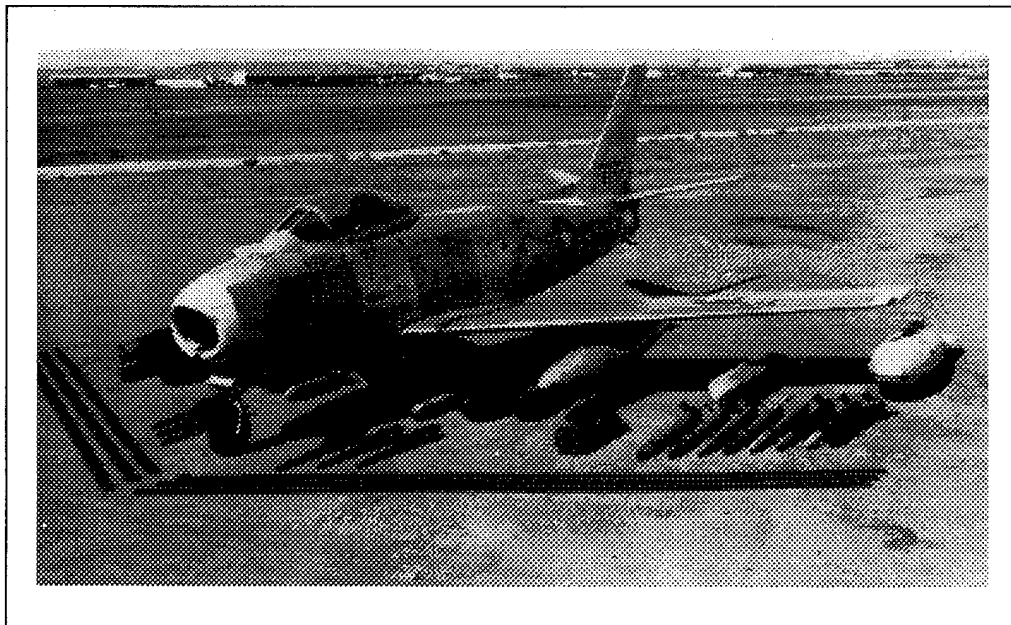
The swept wing and empennage configurations required a derivation of the aerodynamic terms specifically tailored to the alteration of the slipstream angle of attack resulting from bending and torsion. Bending was no longer free of angle of attack change and torsion about the elastic axis was different from the slipstream angle. The derivation of the aerodynamic terms was done by two different methods, a velocity component method and a direct solution for flow along the slipstream. By 1947 the F86 had reached sonic speeds in a dive without benefit of flutter analysis valid for that speed range. Both the design and its flight testing were ahead of the flutter substantiation. In reality the design was substantiated by flight testing with the analysis following as rapidly as possible.

The design quickly progressed to carry a wide variety of underwing stores. Many of these configurations would not show satisfactory calculated flutter speeds. Extensive design studies, both analyses and tests, were conducted to define required pylon stiffness, safe store locations and upper limits to the gross weights and chordwise centers of gravity. Part of the requirement for scaled flutter models was the result of the need to more quickly and efficiently approve the large number of configurations based on the variety of stores and their many combinations. Anyone familiar with the weight of armament carried under the wing will appreciate the challenge to flutter stability.

Case 4: B-45
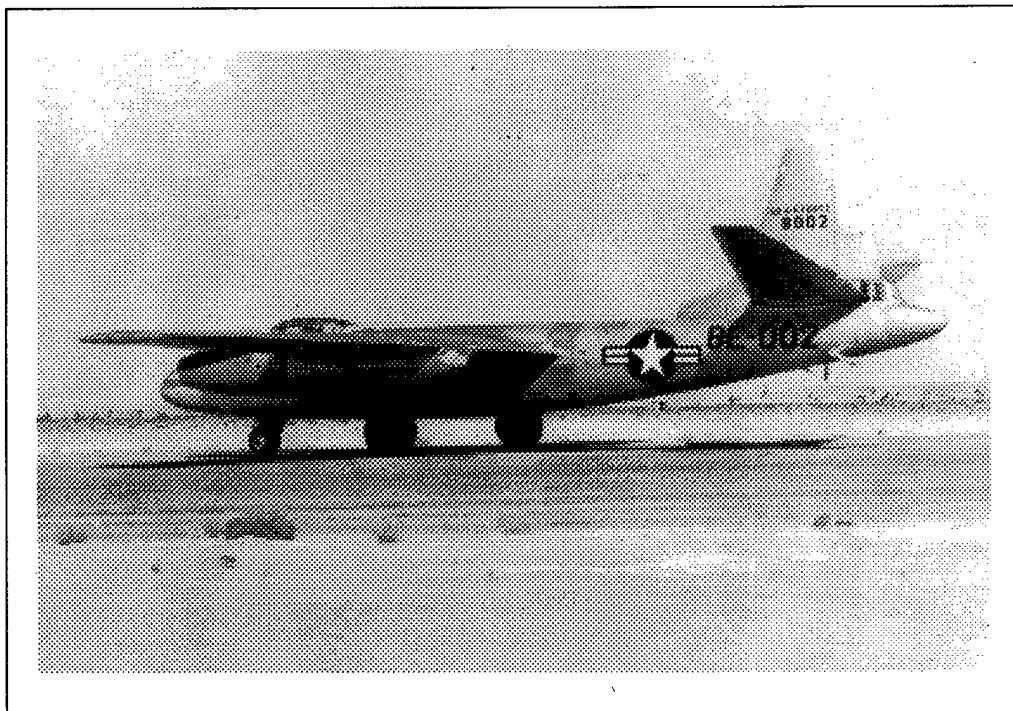
The ability to design a long range jet powered bomber is difficult technically. In order to reach the extended range needed for this bomber, ten thousand pound tip tanks were added to

each wing tip. These were designed and substantiated by state of the art methods in the late 1940s using analysis, ground vibration test and flight flutter test. Stiffness was added in the outer wing panel to accommodate the extreme weight of the fuel tanks and the chordwise location of the c.g. was carefully optimized and controlled by bulkheads internal to the tip tanks. Adequate control of the c.g. was obtained in this way for any amount of fuel remaining. With partial fuel loads, fuel produces aft c.g.'s that cause unacceptably low flutter speeds. The power of the existing flutter methods was shown by this challenging design configuration.

Case 5: UTX, Also T-39, Later Commercial Version Became Sabreliner

This design was a utility transport for carriage of premium parts needed for repair of USAF airplanes. It was also configured for transport of VIPs. The airplane is a small twin engined jet with swept surfaces. The initial design was unique in that a normal elevator ballast weight design would not provide the required flutter speeds for the horizontal stabilizer. Neither balance by elements nor ballast concentrated near the tip had acceptable flutter speeds. The combination of modes defining the problem were first and second horizontal stabilizer bending, first torsion and elevator rotation and torsion. The coupling term for parallel axes does not completely decouple the elevator inertially from the torsion mode even when the elevator has 100% static balance $S_\beta = 0$. The term in question is

$$I_\beta + b(c - a)S_\beta \tag{1}$$

The residual quantity I_β remains and can only be suppressed by an elevator that is overbalanced, i.e. negative S_β. Because of the sensitivity shown by the analysis, the analysis was extended to include the aerodynamic overbalance and the hinge flexibility as a further safeguard. The elevator design included aerodynamic balance forward of the hingeline which results in longer hinges which provide translation of the hingeline - a conceivable complication. Methods to describe these variables were contained in USAF TR 5153. Such overbalance is rarely required and, in addition, an optimum ballast location spanwise was also needed. Suitable flutter speeds were obtained once this was done. This problem was unscrambled during design with no schedule delay.

Case 6: XA2J-1 Navy Carrier Bomber
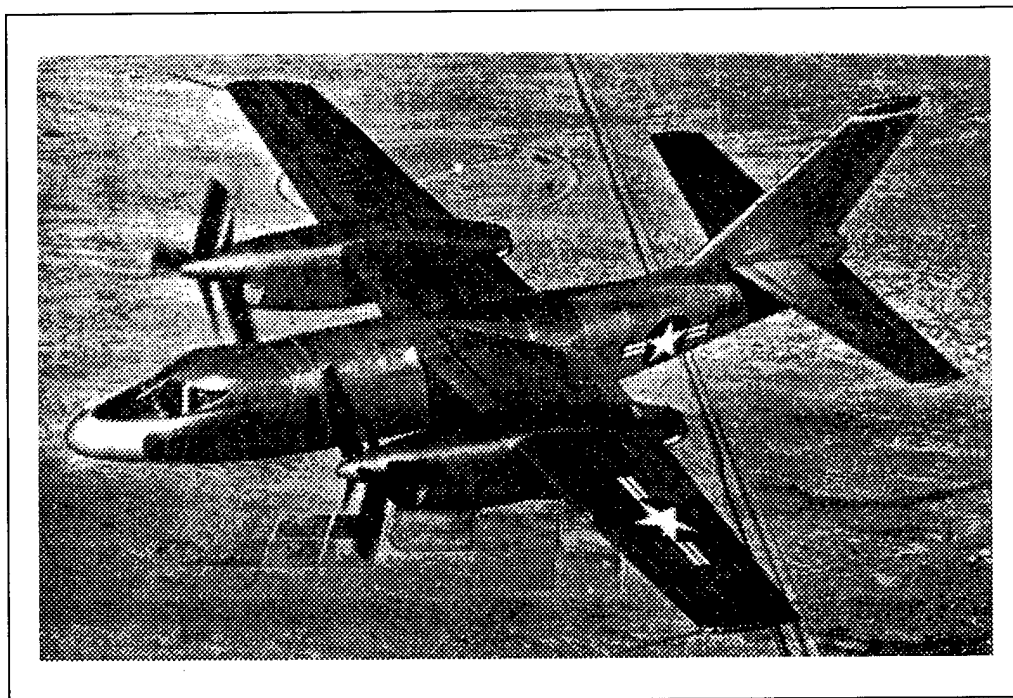
This jet powered turboprop was a heavy weight 52,000 pound bomber designed specifically for carrier operations. Large counter rotating propellers were required to absorb the 4000 horsepower from the jet engines. The design was unique in the extreme forward location of the propellers relative to the elastic axis. Flutter requirements could not be met based upon the results of the ground vibration test showing a low frequency for the stabilizer first torsion mode. The modal pattern indicated excess flexibility inboard of the root rib that arose from the ability to trim the complete horizontal stabilizer in pitch. Excess flexibility from the front spar carry through structure from left side to right side (see Figure 11). Trim was provided by

a vertical ball screw actuator of adequately stiff design but the front spar carrythrough introduced extra flexibility by the extra freedom for rotation at the centerline. Both the extra flexibility and the extra degree of freedom were removed by a full depth carrythrough structure for the front spar that extended across the centerline from root rib to root rib.

TRIMMABLE HORIZ. STAB, FRONT SPAR

XA2J-1
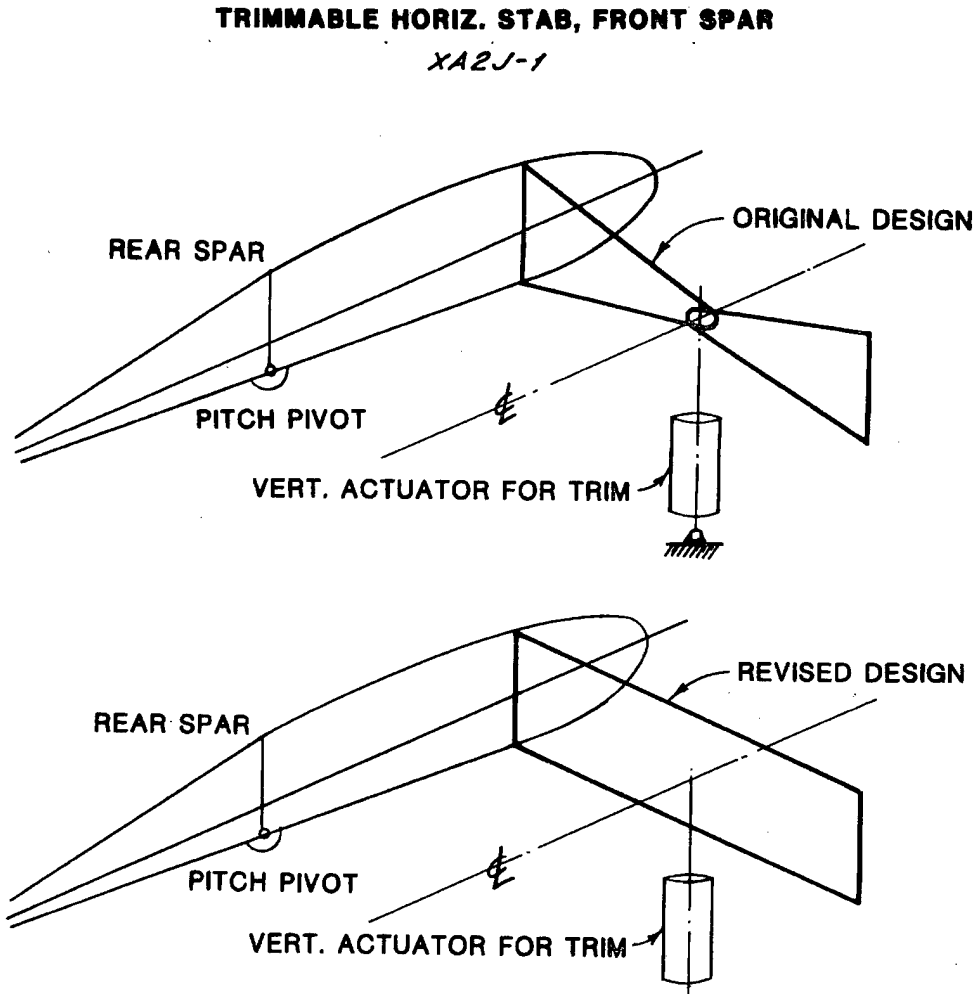
Figure 11: XA2J Trimmable Stabilizer Showing Front Spar Configurations

Lessons Learned

This large and significant sample size of eight totally new vehicle designs and configurations were cleared for flutter based on an analytical approach buttressed by the ground vibration test and the flight flutter test. Since the latter two tests occur at the end of the design period, it means that confidence in the analysis was sufficient to accept the obvious risks. The basic approach was that of U.S. Army TR 4798 and the strip theory it depends on. The reason for the success of this approach was partially a result of other aspects of the design that were accomplished prior to the flutter analysis:

a. appropriate torsional stiffness, knowable at design inception

b. ballasted control surfaces by elements

c. chordwise c.g. control of all masses in the lifting surfaces; wing, horizontal and vertical stabilizers

Thus each of these eight designs had met these flutter design criteria prior to the beginning of the flutter analysis as a result of the work done in preliminary design. This examination of the state of the art flutter design for the time period up to 1955 shows the validity and practicality of the overall approach. The most difficult and time consuming design problems were the underwing stores on the F-86 and the large tip tanks on the B-45.

SUMMATION: CAUSE OF THE ABOVE FLUTTER PROBLEMS

The difficulties reported were of two types: 1) in-flight flutter and 2) necessary redesign prior to flight when GVT results showed unacceptable structural flexibility. Using the state-of-the-art information in the paragraph above, it can be seen that, procedural or substantive flaws in the accepted methods were not the source of either problem. For example, the state-of-the-art dependence on strip theory had been shown to be adequate and conservative on numerous occasions for determining flutter speeds by analysis. This included surfaces with aspect ratios as low as 3.5. In fact, the expected errors in the technique were seen as conservative. But when structural analyses were critically examined, it became clear that the structural math models were the source of both the flutter problems in flight and were the source of the GVT problems when targeted frequencies were not met. While conceptually the methods were in every sense adequate, the initial plans for the math model were often incomplete and important details of structural flexibility were omitted.

For swept wings of low aspect ratio and for all moving surfaces, a compromise had been accepted in using beam technology with structures cantilevered from a fixed root. The compromise was the use of beam theory for wings even of low aspect ratio, for wings with abrupt transitions in the structural box and for use on swept wings. Beyond these compromises in beam theory, there were also large assumptions made that the cantilever beam was fixed at the root. For the all moving surface or for the trimmable horizontal stabilizers, these variable root structures introduced a dominant flexibility. Use of finite element structural modeling technology was needed but was not yet a part of standard practice in flutter. A carefully executed finite element model would have solved all of these problems under favorable circumstance but even this technique would have missed a goodly portion of the instabilities without some foresight for new problems. If the fore and aft mode were the unstable mode, as it was in the case of the F100, then a finite element model does not solve this problem unless the math model is sufficiently complete to contain this degree of freedom. The difficulty with including all the flexibility introduced by the all moving stabilizer is answering the question of what degree of local flexibility needs modeling in joining two beams, the fuselage with the stabilizer. Hydraulic actuator flexibility is also critical because it

concentrates load at a number of point elements. Framing these problems conceptually was needed to best exploit the added capability of FEM techniques. These flutter problems, mostly due to structures, suggested the following lessons learned:

For the F-100

1. The analysis of natural modes and frequencies must match those from GVT.

2. The GVT and the sled flutter test were needed to establish the critical mode: a coupled Mode combining pitch and fore and aft motion.

3. Matching the analysis to the measured modes depended on an accurate description of local root flexibility. Although not generally a part of the state-of-the-art these flexibilities could be determined by iteration and reverse engineering.

For the F-107

4. Structure surrounding the bearings that mount the vertical tail was inadequate to prevent excessive root flexibility caused by spreading of the cover plates. The root rib also functions to tie the covers together but initially was also too flexible. When corrected, the design then matched the analysis with no further change. Later the design was altered with greater thickness at the root to provide the necessary stiffness.

5. The flutter design criterion of 1000 mph incompressible flutter speed was upgraded by USAF just as the airplane was being readied for first flight. This required additional wing material. There were three other lessons attached to this portion of the problem:

   a. One reason for not achieving the new 1000 knot incompressible flutter speed requirement was the relatively far aft chordwise c.g. at the spanwise location of the spoilers. These roll devices are located in the vicinity of 55 to 60% of the chord, inboard of half span, immediately ahead of the flaps.

   b. The unique sensitivity of approximately 6:1, (6% increase in stiffness for 1% c.g. movement aft), was verified and added to the torsional stiffness criterion.

   c. These problems are stated correctly as stiffness -- not frequency problems.

For the XA2J-1

6. For the trimmable horizontal stabilizer, extra front spar flexibility was a result of an unnecessary structural pivot at the centerline. Torsional deformation in pitch was considerably amplified by this feature. When the front spar was joined side to side with a full depth beam this extra flexibility was removed.

The flutter cases in flight and the unsatisfactory outcomes of the GVTs lead to the conclusion that the analytic descriptions of primary structure contained in the flutter analyses were insufficiently accurate and complete.

Case 7: F-108
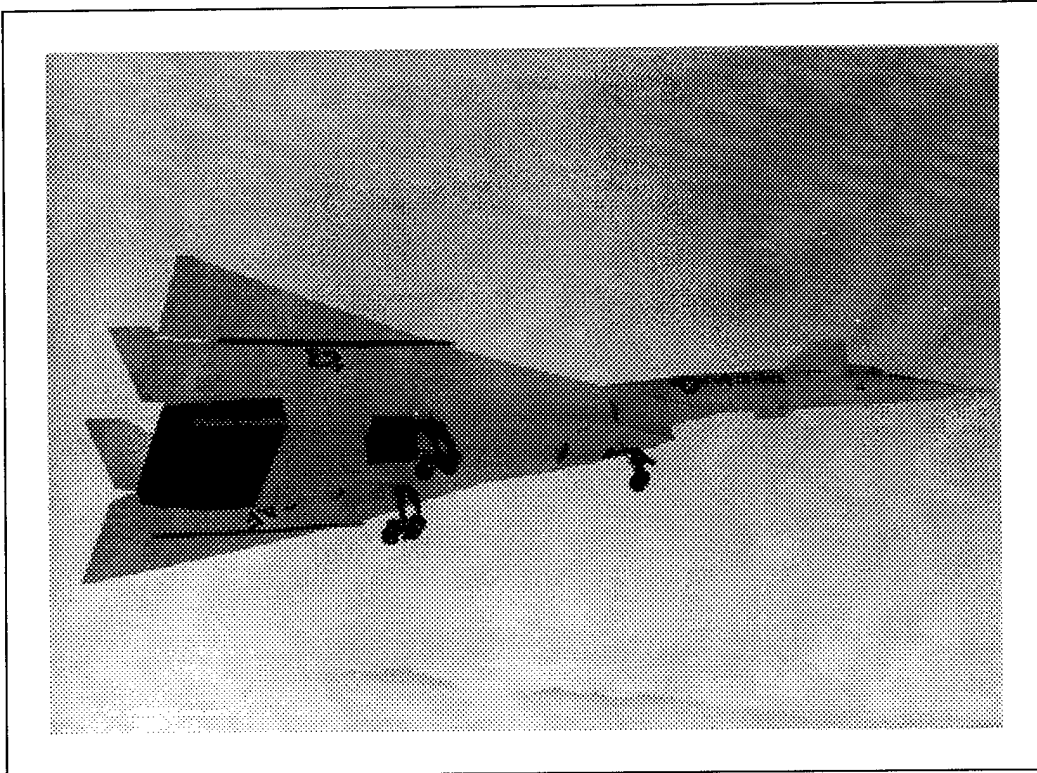
This Mach 3 interceptor was a smaller version of the B70, shown in the above picture. Configuration and structural design were quite similar: a $65°$ delta wing with a forward canard surface and a structure of brazed steel honeycomb sandwich. The surfaces were so exceptionally thin that no possibility existed for ballast weights, instead a frequency criterion was imposed to obtain a trailing edge control surface of satisfactory stiffness. In considering how to model the surface, the analysis was conceived as being based on aerodynamic and structural influence coefficients. But the flutter model technology existing at that time would be a very poor representation. The idea of concentrated stiffness at a single spar location was simply not acceptable. To model the diffuse structure on the other hand would require a new material were we to continue to use the more convenient low speed wind tunnel. First, it was desirable to set down a requirement without a presumed limitation to satisfy the desire to go with an accurate simulation. This approach led to a need to provide item-by-item simulation of the structure. And this in turn led to a need for a material with reduced moduli in tension

and shear so that practical thicknesses could be used for skin, ribs and spars. The ratio of the two moduli, E to G, must also match that of the full scale article. Lastly, introduction of a totally new material meant it must be qualified as a structural material with a usable range of stresses and appropriate fatigue properties for use in a flutter model.

A plastics specialist had a very clear picture of how to meet these requirements and suggested that a material constructed in such a way as to be orthogonal in a material sense would provide the required internal structural similarity needed for a dynamic model -- thereby providing the required ratio of E to G. The concept was implemented with microballs of bakelite which were joined with a plastic cement. The material had been developed to float on large reservoirs of petroleum to suppress evaporation of a volatile material. From the initial test, the material passed each requirement in turn. The material allowed the construction of a delta wing structure by item-by-item scaling of each individual component. In addition, it was shown to have usable fatigue properties and could be expected to provide a practical structure by permitting flutter amplitudes up to those that would be expected were flutter to occur near max expected amplitudes.

During qualification in the first low speed wind tunnel test, the model was lost at only half max tunnel speed while slowing the tunnel to test the ability to stop the flow. At approximately 55 mph the model rose to the ceiling of the wind tunnel, a distance of 3 feet, and was destroyed. The cause was the configuration of the flat plates designed to block the flow. Two plates at the level of the model, one on either side, are introduced to the flow by very rapid spring loaded "fly swatters." The centerline flow was not blocked but the flow further outboard was. The result was that the destabilizing canard near the tunnel centerline experienced increased flow and the stabilizing wing in the wake of the brakes experienced much diminished flow. This produced the pitchup that caused the model to rise and impact the tunnel ceiling. Cost at that time was a lost model worth $25,000. The model was immediately rebuilt and its performance as a flutter model met all requirements (following relocating the flat plates that partially block the flow). It was a pleasure to see full tip deflections occur during flutter without damage to the structure of the model. GVT tests results of the wind tunnel flutter model showed excellent match to those obtained analytically. Flutter speeds were found at the expected values and showed proper margin.

Lessons learned on the previous cases had shown the need for the scaled dynamic model and the delta wing showed the need for the item-by-item scaling. The material development needed to support the model allowed its use in a low speed tunnel.

Case 8: OV-10
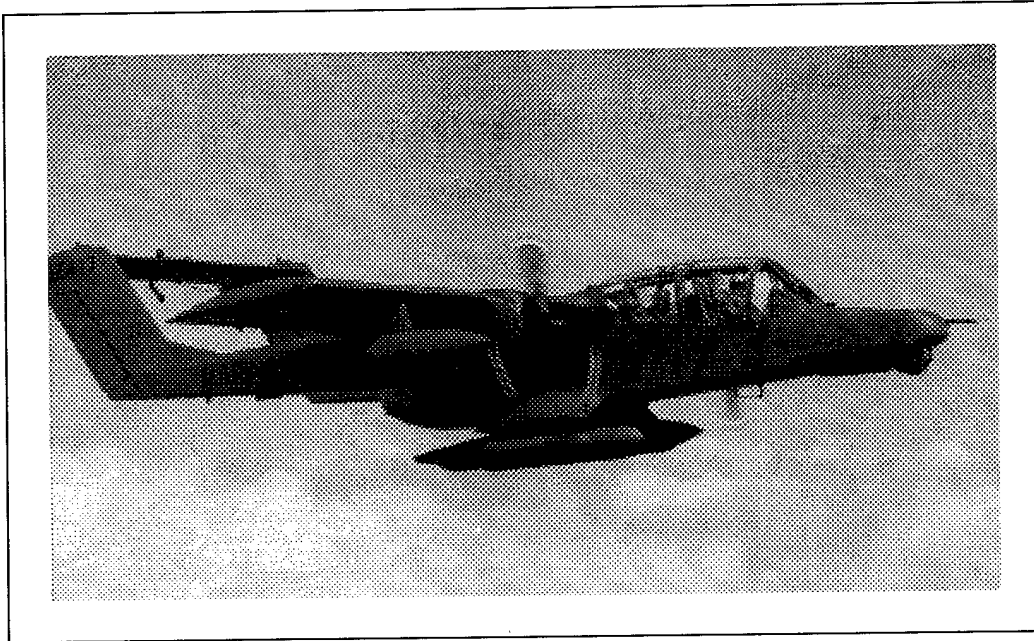
The counter insurgency fighter, the OV-10, experienced flutter in flight test on 3 different occasions over a three year period and the contract was on the verge of cancellation when the source of the problem was determined by analysis. The configuration for this special design was an unconventional twin boom arrangement supporting the empennage. The design was compromised by locating the horizontal stabilizer between the two vertical tails rather than a lower position between the tail booms. The two spars for the horizontal did not match the two spars for the vertical. As a result of the flutter instabilities in flight, flight measurements were made to determine the frequencies participating in the instability. These did not match those contained in the analytical model nor those from the ground vibration test. It was reasoned that the cause for different frequencies in flight relative to those measured on the ground was buckling of a panel at the root of the horizontal stabilizer where it attached to the vertical. The rear spar was not continuous due to the rear attach from the horizontal to the vertical stabilizer was forward of the horizontal rear spar location. Rear spar load was dumped into a skin panel for transfer to the eccentric attach. Further measurements showed this skin panel was buckled under flight loads resulting in a reduced stiffness to the key flutter mode, see Figure 12. During the initial ground vibration test, agreement was obtained between the calculated and measured frequencies because both were describing an unbuckled panel. With the right idea in hand, the explanation of the lower measured frequency when the horizontal was under load was straightforward.

In summary, the structural problem concerned the load path at the rear spar of the horizontal stabilizer where it connects to the vertical stabilizer. A direct tie was prevented by the mismatched locations of these two spars. A large eccentricity was present where the two rear

OV-10 HORIZONTAL STABILIZER

BUCKLED PANEL
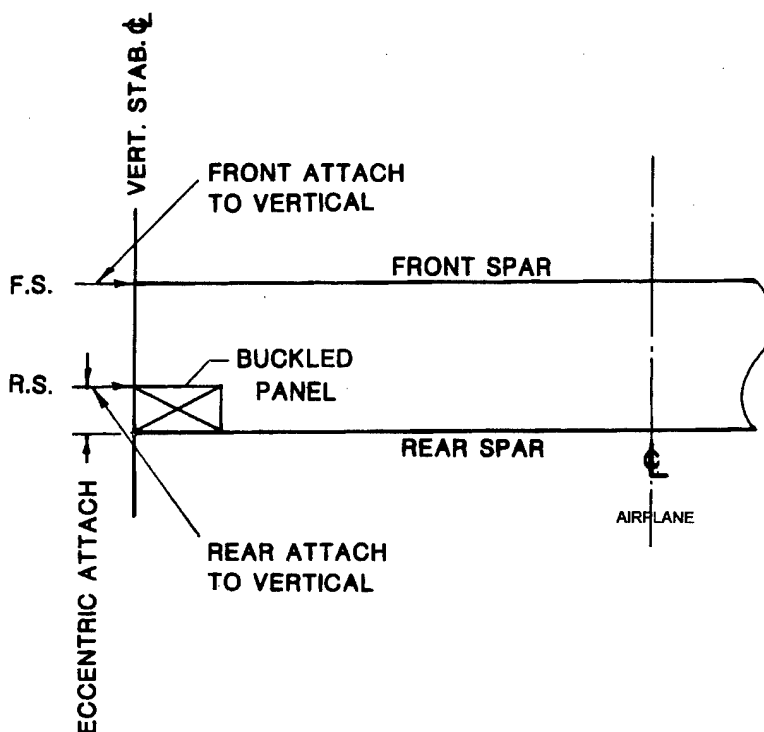
Figure 12: OV-10 Coin Buckled Panel

spars were joined. A shear panel transferred the load from the rear spar over to the attach point. Under load this panel would buckle; and its loss of stiffness was sufficient to cause flutter. It consumed nearly 3 years before the problem could be located.

DESIGNS WITH RADICALLY NEW CONFIGURATIONS

Three designs that departed radically from past practice were the F-108, B-70 and the Space Shuttle. B-70 was a long range Mach 3 strategic bomber with a 65° delta wing that lay inside the Mach 3 shock. The requirement for low drag resulted in a 3% wing thickness. Efficient structure required the use of a brazed steel honeycomb sandwich. Elevons serve for both roll and pitch control. To prevent bending across the large wing span, the elevons were segmented into 12 short segments. The full program included development of aerodynamic and structural influence coefficients and the construction of flutter models. Piston theory was also applied at the high Mach numbers. One problem common to all three designs centered on a major design improvement, trading increased control system restraint stiffness for ballast weights. The use

of lead ballast was an established design practice on the control surfaces for flutter prevention because it decouples bending and torsion from control surface rotation. However, there are three major disadvantages to the use of lead ballast.

1. A structure is needed forward of the hingeline to support the lead. Requirements for support include large load factors approaching 100 G limit load plus the test demonstration of the ability to carry 60 G for 500,000 cycles. These requirements apply to both civil and military airplanes, see References 2 and 3.

2. Control surface mass unbalance is matched with approximately equal mass unbalance forward of the hingeline. The weight of lead and the weight of structure are positioned far aft on the chord, a location that heavily penalizes flutter speeds.

3. Design direction for high speed flight required thin airfoils which no longer provided adequate space for lead weights within the confines of the airfoil lines.

Exploring the fundamental question, for the same weight used to provide the lead ballast, is there a possibility that the control system stiffness could be made essentially equivalent to that of trailing edge structure, i.e., effectively "rigidly attached." (Trailing edge structure does not exhibit buzz.) If not, could sufficient damping also be added to accommodate the stiffened control system for whatever unacceptable flexibility still remained. Although designs without the use of lead ballast would also carry severe design penalties, ballast forward of the hingeline was literally no longer possible for very thin airfoil sections. Thus, solutions without the use of ballast were required. It is worthy of note that the all moving horizontal and vertical stabilizers are also compromised design solutions to circumvent the use of ballast weights.

The history of this development is not totally recorded. But a list of airplanes using this stiffness approach would include: F108, B70, Space Shuttle, AMD Falcon jet, and the Boeing series, 757, 767, and 777. The approach must account for different flight regimes, either subsonic or transonic, and for the civil transports cited, must account for the Federal Air Regulations requirements for fail safety. Requirements in the different flight regimes are considerably different because of the transonic control surface buzz phenomenon. Space Shuttle and B70 met the requirement

$$\frac{c\omega}{V} = 2.0 \tag{2}$$

where c is the average control surface chord length (hinge line to trailing edge), ω is the natural frequency in rotation (in radians/second), and V is the true airspeed (in feet/second).

While the AMD Falcon Jet had only a 30 Hertz aileron first rotation mode to meet the flutter speeds needed for subsonic flight, the level required for suppressing transonic buzz per the above criterion would have been possibly 5 times greater. A careful explanation for this difference is required. The buzz phenomenon is best understood as oscillating shocks that move in opposite directions on the upper and lower surfaces (implying different locations).

Their different locations chordwise provide a large hinge moment that keeps the control surface oscillating constantly at high frequency. This phenomenon is seen generally at a very limited Mach range between 0.85 and 0.90. The variation from design to design is believed to be a function of the trailing edge angle between the straight lines of the upper and lower airfoil surface. The smaller the angle, the weaker the shock. Control surface buzz can be expected on any trailing edge control surface at transonic speeds and would normally reach such high amplitudes as to cause the flight to be immediately terminated. If the designer has chosen to proceed without damping added to the control surface, then the limit speed is set below the Mach number at which buzz begins and flight tests are conducted to demonstrate freedom from buzz. If the airplane limit speed includes Mach numbers greater than that for the onset of buzz, then dampers are incorporated in the design.

For Space Shuttle the buzz requirements were known as a result of the research completed on the B-70. Data had been assembled from known buzz cases, reduced to the dimensionless form shown in equation (1) and an envelope drawn to cover all the cases. In determining the stiffness in rotary motion of the control surface, the sketch shows the critical local structural flexibility at four points plus that of the actuator.
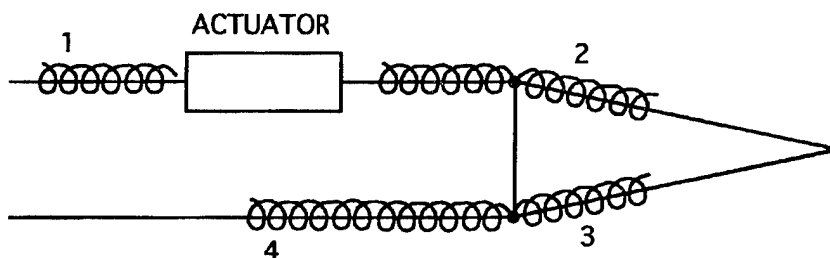
The extent of the structure brought into the calculation of local flexibilities is best determined from calculations in similar cases (supported by test data). Elevon supporting structure was extensively stiffened at all these locations and optimized for efficiency.

Space Shuttle also benefited from the torsional stiffness criterion presented in the paragraph "Simplified Criterion for Stiffness Required for Flutter." Space Shuttle wing and vertical tail were designed to this criterion and then extensively tested in five different wind tunnels for different Mach regimes to demonstrate freedom from flutter and buzz. At no point were changes made to the criteria or to the initial design. Thus these two design criteria were successfully applied to Space Shuttle.

Another application of lessons previously learned was utilized for Shuttle. NASA was concerned that the struts joining the four bodies led to large local flexibilities at their intersections with conventional structure. If a scaled model based on item-by-item scaling were built, the modal characteristics could be obtained much earlier. The vehicle dynamic characteristics pervaded many of the analyses on which safety depended. A 1/4 scale model was built and provided a 2 year lead time on the full scale GVT.

FAA FLUTTER REQUIREMENTS FOR UNBALLASTED CONTROL SURFACES

Overall system complexity may consist of the supercritical airfoil, fly-by-wire, multiple actuators for a single control surface, and a primary flight computer, each with dual or triple redundancy. In addition, load alleviation, flutter suppression, gust suppression, unique control laws, overspeed protection and stability augmentation systems may be part of the design. The civil requirements have been under development for more than ten years and have reached a high degree of refinement. FAA requirements are continuously improved and developed but in the latest cases the following have been used:

1. The loss of either stiffness or damping constraint needed to preclude flutter must be shown to be extremely improbable;

2. Failures, malfunctions, or adverse conditions must be considered in showing compliance, including any single failure, any combination of failures not shown to be extremely improbable, latent failures not detected in normal operation, and any single hydraulic or electrical failure in combination with one actuator disconnect;

3. Prior to every flight, conduct tests to expose latent actuator failures. During flight continuously monitor the primary flight control functions and monitor system configuration such as blocking and bypass modes;

4. Latent failures not identifiable in preflight tests require the inclusion of a maintenance and inspection program in the certification maintenance requirements;

5. Conduct hazard analysis to identify failure modes and latent failures;

6. Force fight between actuators must be eliminated;

7. Any damage or failure condition selected for investigation by FAR Part 25.571, 25.631, 25.671, 25.672 and 25.1309 must be considered. Failure modes from the primary flight computer (PFC), electrical, electronic, hydraulic and mechanical systems, their sensors and transducers, and feedback information to the PFC that could contribute to flutter must be considered. Failure probabilities must be based on previous experience.

8. If a free surface cannot be shown to be free from flutter, then assurance must be provided that the surface will not become free.

Lessons Learned -- Unballasted Control Surfaces

A major difference was shown between design at Mach numbers much less than transonic Mach numbers and design that requires penetration of the transonic region where buzz occurs.

Two criteria were used in the preliminary design stage for Space Shuttle, both of which were successful. If these had not been available, significant additional design time would have been

required. Space Shuttle also benefited from an advanced modeling technology that provided early GVT results. Civil requirements for unballasted control surfaces include fail safety, damage tolerance; and failures, malfunctions and adverse conditions.

FAA AND FLUTTER

The relationship of the FAA to flutter is best shown by relating some historical background, describing the applicable regulations and showing the extent each accident is covered, the corrective action and the overall depth of the many safety issues. Through in-depth study of the accidents a more thorough understanding of basic flight science has resulted. Topics to be covered include structural dynamics and flight dynamics, fail safety, reliability, maintenance with small flaws, flutter criteria including an Excel spread sheet, and the contrast in the required margins for the separate structural design tasks of stiffness and strength. The extent of the involvement of the various aeroelastic and dynamic phenomena has been far greater than expected with greatest involvement in the most serious accidents.

The history of the program to prevent flutter at the FAA is not consistent between transport category and general aviation. Because of the necessity to protect the passenger of an air carrier, requirements for transport category are extremely strict. This is not matched in general aviation because of the desire on the part of that community for greater design freedom and their desire to avoid burdensome regulations. So the history of occurrence of flutter between these classes of civil aviation is considerably different. History over the last 25 years shows freedom from whirl flutter that first appeared in 1955 in transport category was resolved very quickly. (Current regulations require evaluation of whirl flutter in both transports and general aviation.) Classical flutter has been observed in transport category on very rare occasions and then mainly as a result of a prior failure. Service difficulty reports required from air carrier operators provide only minimal information, and on the occurrence of flutter, a label "vibration" is used instead.

Serious flutter accidents do occur and have been catastrophic but almost always for the reason that another failure preceded flutter as the following cases will illustrate. Two examples are an Electra in Pennsylvania in 1983 and a Boeing 737 in Panama in 1991. In both cases the airplane was upset at high altitude due to a failure of the autopilot, direction finder or artificial horizon. The airplane entered a vertical dive and the flutter instability began as the airplane approached design dive speed. In both these cases flutter was so violent that the cockpit separated in flight. Another example, a Convair 580 elevator hinge pin failed leading to flutter of the horizontal stabilizer. This too was a catastrophic case in which the empennage separated in-flight and the airplane plunged into the North Sea. A catalog of flutter cases in the civil system would easily reach several dozen in transport category and many hundreds in general aviation.

The lesser regulation of the general aviation airplanes is best shown by the basic flutter requirements for the case where design dive speeds are less than 260 knots that lead only to the use of Report 45 "Simplified Flutter Prevention Criteria"; and for speeds greater than 260

knots that require only analysis or flight flutter test but not both. The higher accident rates and number of fatal accidents and number of fatalities in general aviation airplanes are all associated with the decision to impose lesser regulatory requirements. These lessened requirements lead directly to lesser safety. Various forms of dynamics that also depend on airframe stiffness would also help account for these lessened safety results. Reduced safety can be shown by the 2:1 difference in fleet safety depending on whether analysis *and* test were chosen to show compliance with freedom from flutter or analysis *or* test only. This choice is not available in transport category where a full flutter program is required: wind tunnel test, ground vibration test, flutter analysis and flight flutter test. The rigorous standards applicable to transport category likewise account for the excellent safety record achieved.

ACCIDENT INVESTIGATION

It would appear that no serious inroads on safety will occur without being grounded in the knowledge intentionally acquired from the fatal accidents. Current knowledge is faulted by the -
- repetitive occurrences of fatal accidents
- an unrecognized generic pattern with over 100 cases which has dominated the last several decades
- hidden dynamics because the accident investigations are shallow in this area
- new phenomena

Findings to date are of two kinds -
- the accident process itself. Once begun, the process tends to continue to completion, and
- fundamental additions to the aero sciences. This has been the most surprising part of the accident studies. The aero and structural instabilities interact with the weather, the vehicle and the pilot.

While there are many different components to the investigation itself -
- many failures, scattered debris
- a need to develop candidate scenarios from indirect evidence from the FDR, the ground marks and witnesses,

the main failure has been concentrating on the individual accidents without also integrating the whole of the body of knowledge. It is logical to breakdown the whole into several categories -
- propulsion, aerodynamics, systems and structures and
- those particular fleets with the highest number of accidents and the highest rates.

Thus the broadest possible role must be assigned to accident investigation -
- prevent repetitions of accidents of any one kind
- establish the involvement of structural and flight dynamics in the fatal accidents, currently estimated as 90% or more of the total number of cases

- using the label pilot error for primary cause in the majority of cases truncates the investigation short of determining vehicle deficiencies. In cases of repetitive accidents, it is only after the vehicle deficiencies are identified and corrected that the accidents stop.
- the on-site investigator must be trained to describe the important dynamics' clues.

IN-DEPTH SUBSTANTIATION OF FINDINGS

Findings from several decades of accident investigation provides a pretty good picture of the fundamentals. Data are given for the number of fatalities and the accident rates vs time, Figures 13 and 14. The flight dynamics and structural dynamics showed one underlying fundamental phenomenon was occurring. Beginning with Instrument Meteorological Conditions (IMC) and turbulence, upset occurred in pitch, roll or yaw, singly or in combination. As long as the pilot was alert and arrested the divergent motion, safety was assured; but if permitted to persist, then overspeed was the next step in a process that led to stall or ground contact. Fifteen degrees nose down pitch held until a terminal velocity was approached showed that speeds of 160 to 180% of cruise speeds were obtained. Such speeds are well beyond the flutter speeds that reside just beyond 1.15 to 1.2 V_d.
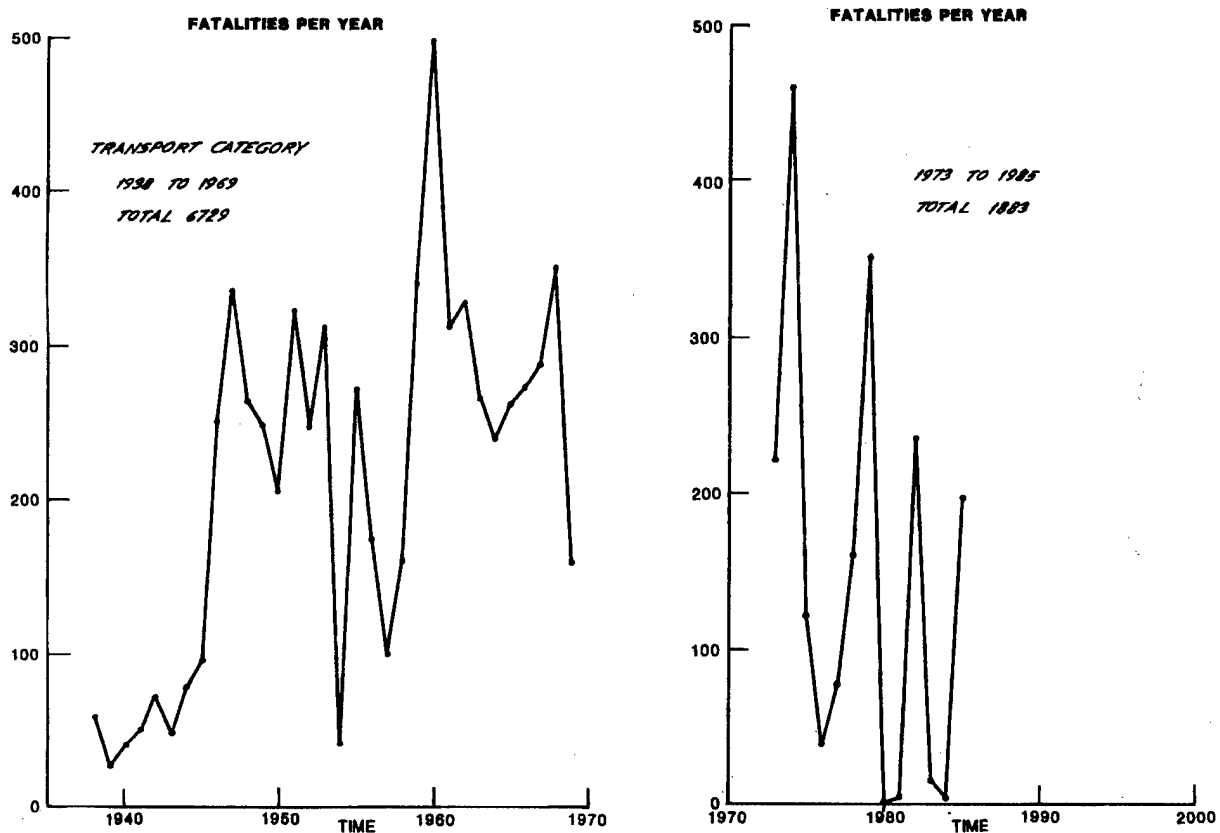
Figure 13: Number of Fatalities, U.S. Scheduled Air Carriers

TREND OF IMPROVEMENT IN ACCIDENT RATES

REFERENCE: 1992 YEAR IN REVIEW
F.A.A. AVIATION SAFETY JOURNAL
VOL. 3, NO.1
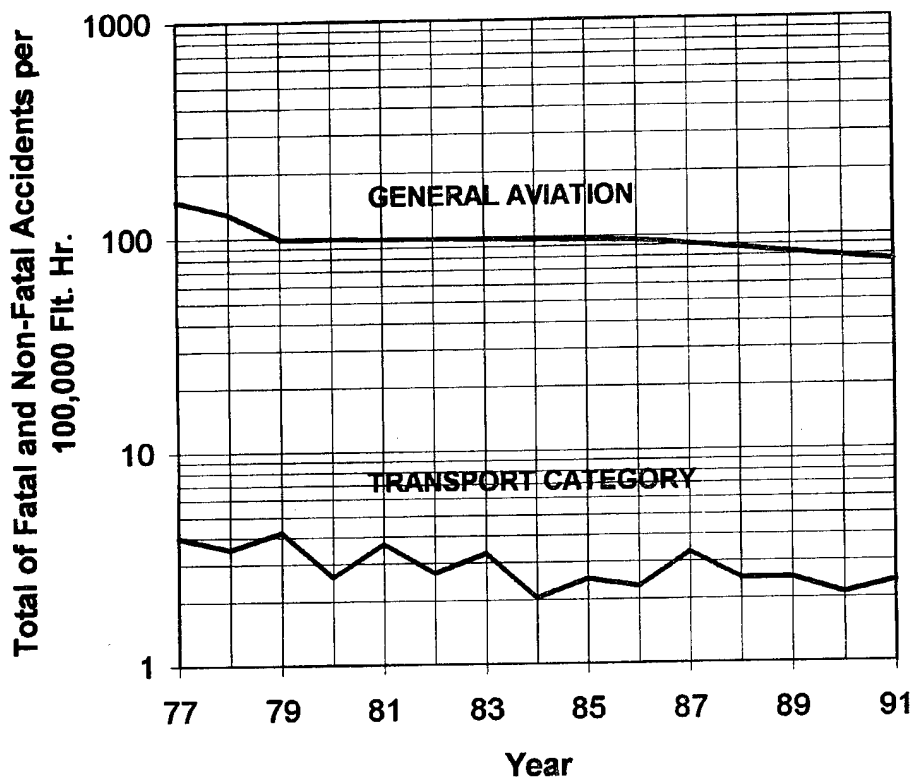
Figure 14: Accident Rates, U.S. Scheduled Air Carriers

This underlying process that leads to fatal accidents was not known and accounts for one reason the fatalities have remained constant. The process is specific:

1.   IMC and turbulence

2.   upset and overspeed

3.   stall or ground contact

Other dynamic instabilities were found. The two rigid body modes of flight dynamics are the phugoid and the short period mode. Singly or in combination, these modes offer instabilities in certain circumstances that are difficult for the pilot to deal with. The oscillation in the phugoid mode obscures the flight path angle and the short period mode obscures the angle of attack.

The above descriptions of events have been identified in over 100 cases. Another kind of repetition had occurred in one general aviation fleet with 915 fatal accidents over a period of 40 years. Partly these repetitions were a result of the dynamics that lay hidden for many decades. The accident investigators were not specialists in this area, had not identified either of the four failure modes nor chose to deal with the repetitive occurrences. The dynamics involved in these accidents arose from longitudinal instabilities, lateral instabilities, the processes defined above, and imperfect structural design that allowed the root rib of the v-tail to fail.

In another example, 21 similar fatal accidents with a unique wreckage pattern occurred in one general aviation fleet. First along the wreckage path were two separate wing panels and two separate elevators. This indicates symmetric in-flight airframe failure. It was reasoned that no likely combination of gust and maneuver loads would exceed the measured strength in 21 cases (static test of the airframe showed a capability for 8 G ultimate load). A load amplification factor was derived that reached very high values on approach to a critical speed, see Figure 15. The proof of concept was established both analytically and experimentally, Figure 16. Thus this was a pivotal case leading to the development of the underlying process defined above: upset and overspeed and an explanation for repetitive failure in a single fleet with demonstrated 8 G capability. This was a major finding from the accident investigations which led to a significant advance in understanding the impact of lifting-surface structural flexibility on load magnification.

LOAD AMPLIFICATION FACTOR

$$1/\left[1 - q/q_D\right]$$
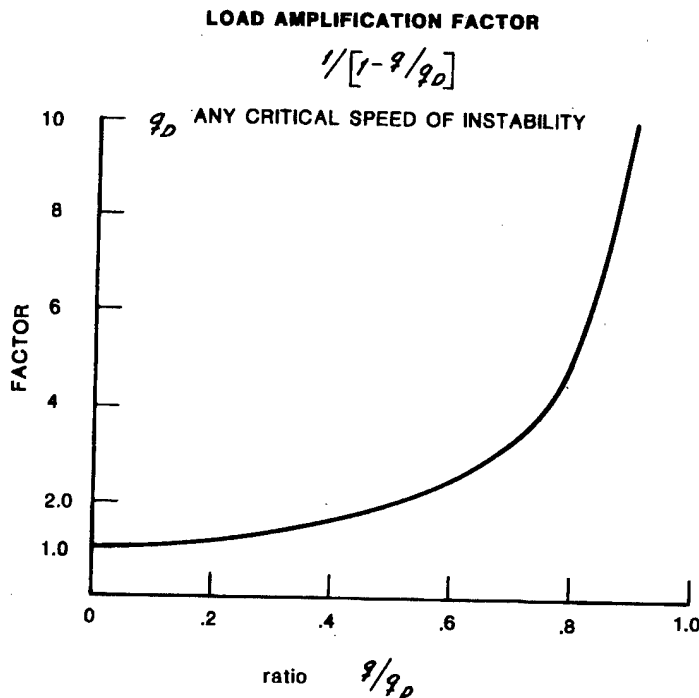
Figure 15: Load Amplification Factor on
Close Approach to a Critical Speed
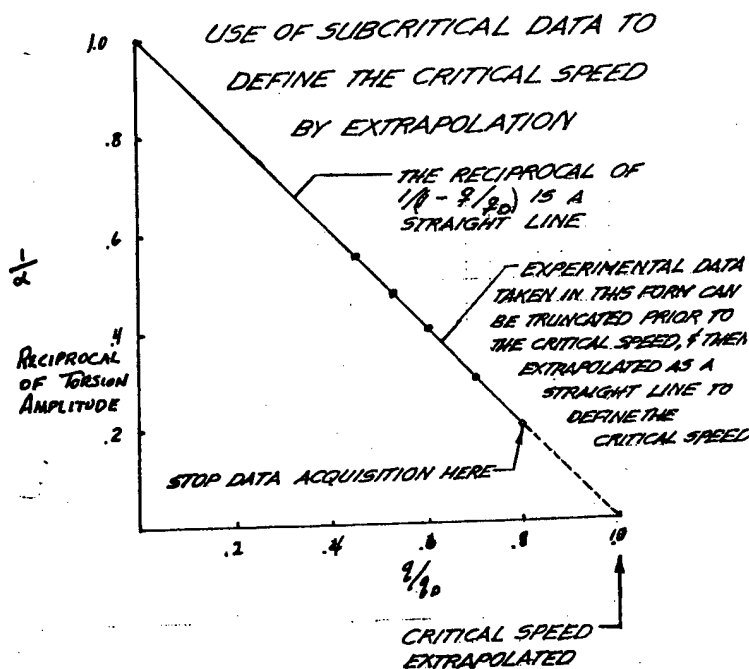
Figure 16: Load Amplification Measured
During Experimental Flutter Testing

Accident reviews show two new flight phenomena. General aviation straight wing airplanes, on being upset in yaw, experience wing failure due to bending torsion divergence. This is compounded in those designs with slight sweepforward of the structural elastic axis. General aviation straight wing airplanes experience in-flight airframe failure when upset at high roll rates. Rapid roll tends to occur about the axis of minimum inertia in roll. In those airplanes where the axis is low at the nose and high at the tail, complete rollover finds the airplane at much higher angle of attack (AOA) inverted than the initial angle of attack. The much greater AOA inverted leads to IFAF.

Flutter design that meets the regulatory requirements may be acting as a surrogate for other stiffness related phenomena involved in fatal accidents. As a class fatal accidents exhibit more extreme loads and maneuvers than nonfatal accidents. The flexible airframe allows these loads to be amplified as previously discussed and generally suggest minimum margins. Repetitive accidents have featured each of the flagship fleets of the major general aviation manufacturers. It is suggested that the various dynamic phenomena are not recognized in the on-site investigations, that they lie hidden and that the repetitive accidents are a further indication of minimum margins.

Although the accident process was described, only in-depth substantiation is usable requiring a much longer investigation. It is not in the nature of complex relationships between owners, operators, manufacturers and government regulators that a simple unfolding of the events

would suffice. The process of substantiation is moved forward in three steps, engineering findings, satisfactory explanations and development of consensus.

FLUTTER CRITERIA

Several flutter criteria have been developed by the British, by NASA, by USAF, through a Navy contract and probably by each company separately as proprietary data. The objective of the criteria is to act as a surrogate for the flutter analysis, to cover all the key variables and to do so in the shortest possible time. Analysis of the criteria show several types exist:

1. torsion influence coefficient at a strategic location spanwise, say 0.75 span

2. torsion natural frequency expressed as a dimensionless variable

3. torsional stiffness, a three dimensional measure of stiffness from root to tip

4. for all moving surfaces, a stiffness criterion was developed that provides a

5. balance between root flexibility and flexibility in the lifting surface

The two principal criteria are items 2) and 3) above. Both are torsional stiffness criteria but criteria that differ in the nature of their construction. The torsional frequency criterion is a measure of the important torsional stiffness of the main structural box extracted from the mode shape in the first torsion vibration mode. It measures a root to tip stiffness in a mode derived from an inertial load obtained from the mass moment of inertia distribution about the elastic axis. The torsional stiffness criterion by contrast is also a measure of the important torsional stiffness of the main structural box but it is extracted from the mode shape obtained in the calculation of the torsional divergence speed. It measures the root to tip stiffness in a mode derived from an aerodynamic load obtained from the aero moments that produce divergence.

The latter has proved effective for the following reasons:

1. no need to change an original estimate up to the point of the completed design

2. divergence mode shape used in the estimate is similar to the flutter mode shape

3. the mode shape for flutter is determined by the aero moments more than by the inertial moments

4. variables needed to determine required stiffness appear in the torsional stiffness criterion but not in the frequency criterion

The experience level associated with the stiffness criterion above has covered five decades of every conceivable design configuration. It is especially easy to apply. Solutions for optimum

mode shape have been developed using the stiffness criterion to fulfill a need for an optimum solution for the flutter problem. Precise definition of permissible root flexibility for an all moving surface were accomplished using a variant of the stiffness criterion. Were a flutter program to produce an unsatisfactory result, the criterion has been reexamined and upgraded as needed. At the end of the presentation of this successful flutter criterion, a spread sheet is presented, Table 2. It also contains a new technique for matrix iteration, a unique plus available from the spread sheet format. The result shortens the calculation.

The design process is optimized by incorporating loads, flutter, strength, twist and camber solutions simultaneously into wing design. An optimum design is found by iteration. This was possible based on enhanced computer capability. It is almost mandatory for composite structure design as the design direction moved away from isotropic materials to anisotropic embedded fibers. Fibers in composite structures are subject to orientation in any direction and layered in such a way that sophisticated solutions could be found for each detail design requirement. It is a feature of this approach that a flutter analysis is incorporated in each design iteration. That analysis is sensitive as always to the torsional stiffness of the lifting surface and for a composite material this is provided by + and - 45 degree fibers. The stiffness criterion provides a means to check the result at a tiny fraction of the time spent on iterating for the optimum, a process covered in preliminary design.

SIMPLIFIED CRITERION FOR TORSIONAL STIFFNESS REQUIRED FOR FLUTTER

This criterion was constructed to include each known and significant flutter variable. The accuracy target for the criterion is to provide at initiation of a new design a level of stiffness required by the flutter phenomenon that would not require change during production design. For already completed designs, it directly measures the torsional stiffness built into that design. It permits an assessment of the design approach as executed by different design teams. When flutter occurs, it allows one to answer the question: was flutter due to a deficiency in stiffness. Using this measure of stiffness for both transports and general aviation airplanes, values of the effective eccentricity, e_e, are shown to increase proportionate to the dynamic pressure defined by the limit design speed. The starting point for the theoretical development is the work of Alexander Flax, The Influence of Structural Deformation on the Airplane Characteristics, Journal of Aeronautical Sciences, January 1945. The divergence formula from this reference is:

$$q = \frac{\int GJ\theta'^2 dx}{\int c^2 \theta^2 C_{l_\alpha} e\, dx} \tag{3}$$

where

q = dynamic pressure, psi

GJ = torsional stiffness of the wing cross section

θ = torsion mode shape, a function of span

θ' = first derivative of the modal parameter

C_{l_α} = lift curve slope

e = chordwise eccentricity between aerodynamic center and elastic axis

c = wing chord, inches

$\int dx$ = indicates spanwise integration

Put the aerodynamic variables on the left and the structural variables on the right.

$$C_{l_\alpha} e\, q = \frac{\int GJ\theta'^2 dx}{\int c^2 \theta^2 dx} \tag{4}$$

A label, the effective eccentricity, e_e, is attached to either grouping. For a completed design, the structural variables on the right-hand side result in a single number, a measure of the torsional stiffness of a lifting surface. This number defines the value of the criterion, a torsional stiffness index. Table 1 contains a list of 50 of these including most of the airplanes discussed in this paper. For preliminary design, the aerodynamic variables on the left side are also useful in defining a requirement.

The chordwise eccentricity for different aeroelastic problems is illustrated:
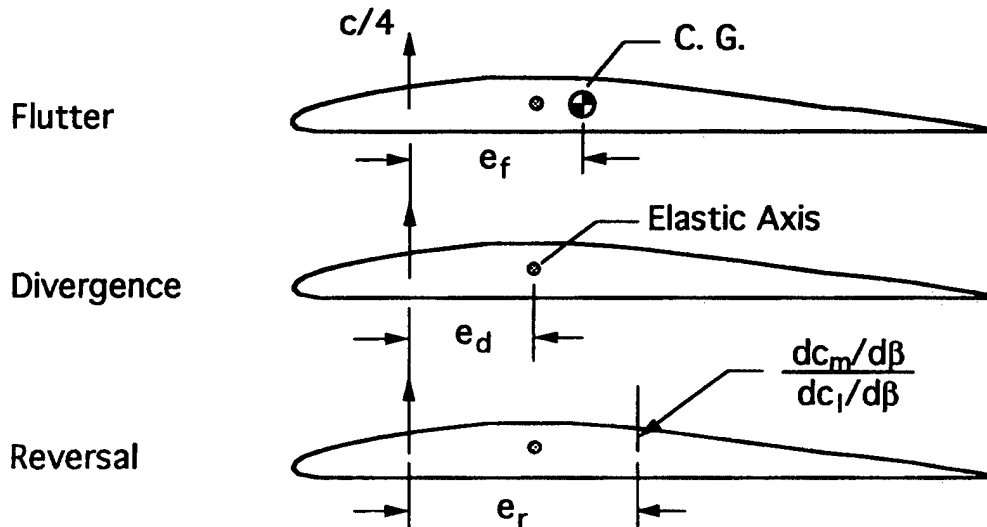
Their similarity is apparent. As the aerodynamic center moves aft from the quarter chord on approach to transonic and supersonic speeds, the eccentricity, *e*, identified in each figure is greatly diminished. For all three phenomena, both the aerodynamic center (a.c.) and the elastic axis (e.a.) remain the same. Flutter is sensitive to the c.g. position, divergence involves only the a.c. and the e.a.; and reversal depends on the center of pressure for trailing edge control surface movement. For a trailing edge control surface, however, the center of pressure for incremental lift moves to the midpoint of the control surface greatly increasing the eccentricity for reversal and effectively preventing the use of trailing edge controls at supersonic speeds for their normal spanwise position near the wing tip. The sensitivity to the eccentricity may not be immediately apparent, but an increase in eccentricity from a c.g. position at 40% chord to 46% chord resulted in a requirement for a 36% increase in stiffness. This describes an actual case that resulted from addition of a spoiler just forward of the trailing edge flap at midspan. The relatively heavy weight of the spoiler moved the c.g. significantly further aft on the chord. The sensitivity is shown in Figure 9. In the original development of the torsional stiffness criterion it was necessary to extend the work beyond that of Reference 1. A broad review of available flutter data was undertaken to find and quantify other variables important to flutter: area, aspect ratio, taper ratio, airfoil thickness, and the effect of aerodynamic heating on modulus. These variables naturally divide into those affecting the stiffness requirement directly and those affecting the structure and the resulting weight of the torque box. The two variables affecting stiffness are sweep, and the chordwise location of the sectional center of gravity. Variables affecting structural geometry and the weight of material in the torque box include thickness ratio, taper ratio, span, material, temperature environment and torque box efficiency. These variables are expressed in a form most easily used by preliminary design. To clarify the contributions of the many variables to either stiffness or weight, the variables are listed under the parameter affected:

Stiffness	Weight
lift curve slope	taper ratio
chordwise eccentricity	airfoil thickness/chord ratio
dynamic pressure	structural span
sweep angle at c/4	torque box efficiency, defined as the (dimensionless) torque box area divided by the (dimensionless) torque box perimeter

Thus the stiffness requirement in the form of the effective eccentricity becomes:

$$e_e = C_{l\alpha} \, e \, q \times f\left(\Lambda_{c/4}\right) \tag{5}$$

where

$$f\left(\Lambda_{c/4}\right) = 0.4 + 0.7\ cos\ \left(\Lambda_{c/4} - 10°\right)$$

The extended definition of required stiffness is seen in the weight equation, Table 3.

An extensive list of the stiffness indices has been kept as an historical accounting for a period of 5 decades. Although designs have been built on both jumbo jets and general aviation airplanes by different design teams that were later clearly seen as deficient in stiffness, the process is often self correcting as design teams encounter service difficulties and return to stiffness levels defined by the flutter community as a whole. A method was developed to measure the underlying fundamental requirement for flutter, torsional stiffness. An Excel spreadsheet example calculation is given in Table 2.

The Space Shuttle preliminary design was prepared in this way. After flutter analysis, flutter model tests at subsonic, transonic and supersonic Mach numbers in five different wind tunnels, the design did not require change. The lifting surface on the SPRINT hypersonic missile interceptor with a dynamic pressure of 100,000 psf was also prepared from this criterion and, likewise, was proven successful at Mach 10 and elevated temperature in the lower atmosphere.

A recent calculation for wing, horizontal and vertical stabilizers of a new large jet transport showed the following values for the stiffness index:

wing	8.84
horizontal stabilizer	8.81
vertical stabilizer	9.7

The design currently certified and flying showed relatively constant stiffness indices.

To apply the stiffness requirement to a particular wing design in a preliminary design proposal, 1000 candidates may be examined to locate an optimum design. Requirements from all disciplines are combined, summarized in terms of weight and using weight and configuration, performance is determined. The weight equation developed for flutter is thus one of many similar expressions developed for other disciplines.

SIMILARITIES AND DIFFERENCES BETWEEN THE TWO KEY CRITERIA

The frequency criterion developed by NASA and used by USAF will be reformulated to allow comparison to the stiffness criterion presented above.

Square the frequency criterion:

$$\left[\frac{b\omega_\alpha}{V}\sqrt{\mu r_\alpha^2}\right]^2 = \frac{b^2\omega_\alpha^2\mu r_\alpha^2}{V^2} \tag{6}$$

Substitute $\dfrac{m}{\pi e b^2}$ for μ: $\qquad \dfrac{\omega_\alpha^2 m\, r_\alpha^2}{\pi\rho V^2}$

Substitute I_α for mr_α^2: $\qquad \dfrac{\omega_\alpha^2 I_\alpha}{\pi\rho V^2}$

Substitute K_α for $\omega_\alpha^2 I_\alpha$ and q for $\dfrac{1}{2}\rho V^2$: $\qquad \dfrac{K_\alpha}{2\pi q}$

These kinds of simplified flutter criterion are used to assure an adequate level of torsional stiffness, the key design variable which places these aeroelastic instabilities well beyond the flight speeds. With all other conditions and requirements equal, designs of different size and configuration can be defined using the same value for the stiffness index used in a previous design. In the above comparison of the two criteria it was shown that the NASA frequency criterion requires that the torsional stiffness be increased proportionately to an increase in the dynamic pressure. Since it omits all other flutter variables it is insufficient and incomplete, as shown by the stiffness criterion in equation 2 and 3 and in Table 3.

LIFTING SURFACE STRENGTH VS STIFFNESS REQUIREMENTS

A comparison between strength requirements and stiffness requirements shows that in the normal design process for general aviation airplanes the strength requirements will also generally fulfill requirements for stiffness up to approximately 200 mph. Beyond that speed, stiffness requirements will likely exceed strength requirements and the design process must recognize the requirement for adequate torsional stiffness and what other flutter requirements may be needed. Margins of safety attached to strength and stiffness vary considerably. A long-standing factor of safety for strength requirements has been a factor of 1.5, but the civil stiffness requirements have recently been reduced and now require only a flutter speed with a 15% margin above design dive speed. This equates to a stiffness factor of safety of only 32% ($1.15^2 - 1.0$). Consideration of the load amplification shown in Figure 15 suggests there is no justification for this difference. Consideration of the correlation of accident rates with stiffness would also suggest a larger margin is needed on the stiffness related aspects of the design.

Examination of the weight equation for flutter given in Table 3 shows three variables, squared or cubed, plus the velocity squared term included in the effective eccentricity. Each of these four exponents is to a one greater power than the corresponding exponents that would be used in a weight equation for strength.

Three quite different aspects of the regulatory standards will be presented next, the fail safety requirement applicable to flutter, the reliability standard and the effect of less than perfect maintenance characterized by small flaws.

FAIL SAFETY

Flutter requirements are unique in requiring both fail safety and damage tolerance. Fail safety is a requirement that on the occurrence of any structural failure, no flutter will result. "Failure of any single element of structure ... any single failure in any flutter damper system must be considered ..., any other combinations of failures ... not shown to be extremely improbable" Reference FAR Part 25.629.

DAMAGE TOLERANCE

Under FAR Part 25.629(d) Failures, Malfunctions and Adverse Conditions, "Any damage or failure conditions required or selected for investigation by 25.571 must be considered ... and any damage, failure, or malfunction considered under 25.631, 25.671, 25.672, and 25.1309 ... and discrete source damage conditions of 25.571(e)".

RELIABILITY

The general requirement for reliability is that systems, equipment and components whose functioning is required must be designed to ensure:

1. they perform their intended function under any foreseeable operating condition

2. that the occurrence of any failure which would prevent continued safe flight and landing is extremely improbable.

The reliability standard is interpreted to mean that the probability of failure shall be less than 10^{-9} per flight hour. This standard of quality and excellence accounts for the safety in transport category, Reference FAR Part 25.1309. Deviation from this standard shows the consequences of maintenance with small flaws.

MAINTENANCE WITH SMALL FLAWS LEADS TO FATAL ACCIDENTS

A math model was constructed of a process of accruing small maintenance flaws over a period of time for the purpose of examining the question what size flaws and what number of flaws would account for two fatal accidents in a fleet of 500 transports in one year, a real case. A probabilistic approach based on normal distributions of loads and strength was used. Since propulsion, electrical, electronic, hydraulic, fuel and control systems are involved, it was assumed that the structural model could be used to represent failures in all systems. The following assumptions were made to start the system and the variable to be finally determined would be the size of the maintenance flaws:

1. flaws accrue for a period of 6 years

2. for a vehicle of 2,500,000 parts, 10% or 250,000 parts were capable of generating a fatal accident

3. 1% of the maintenance actions were flawed. The number of maintenance actions (including inspection) covered 4,000 parts per 10,000 flight hours. If 1% were flawed, it meant 40 items were flawed in 10,000 hours of flight.

4. 1 G static load plus gust and maneuver loads are normally distributed about 1 G. Strength is normally distributed about a mean to be determined

5. actually two solutions are developed, one for the healthy airplane and one for the airplane with flaws, their difference defining the reduction in mean strength that would account for the two accidents.

6. utilization of each airplane was 2400 hours per year, a total of 7,200,000 hours for 500 airplanes over 6 years. For two fatal accidents in the 6 years, this leads to an accident rate of 1 per 3,600,000 hours.

7. the number of bad parts derived from the above data is 28,800 bad parts in 6 yrs. The part failure rate derived from the above two numbers is 10^{-11} per hour.

The results are graphed in Figures 17 and 18. These two previously calculated failure rates are transformed into the number of standard deviations from the mean where the two distributions overlap. Failure rates are determined from Figure 18 and their meaning is presented by the graph in Figure 17 to show the extent of the overlap (where the two distributions overlap, the area formed is a measure of the probability of failure). As can be seen from Figure 17, the area of overlap is so small that it is less than the width of the line representing the horizontal axis of the graph. The two distributions overlap where the standard deviation for each is 6.67, determined from Figure 18. For comparison, the required failure rate for the original healthy airplane was also estimated in the same way. The number of good parts was 250,000 and the failure rate was taken exactly as the reliability standard, 1 fatal accident per 10 exponent 9 hours. In this case the part failure rate is the division of these two

numbers, 1 per 2.5×10^{-14} hours. The math model provides an analysis that combines safety and maintenance. A too coarse screen to either instigate or withhold maintenance, determines whether the product will meet the reliability standard or fall short, and whether fatal accidents will occur that would not otherwise have occurred. The total process is out of the range of perception and buried in numbers so small as to obscure their meaning. Thus effective maintenance depends on the mathematics of extremely remote events.

PROBABILITY OF FAILURE FOR FLAWED & GOOD PARTS
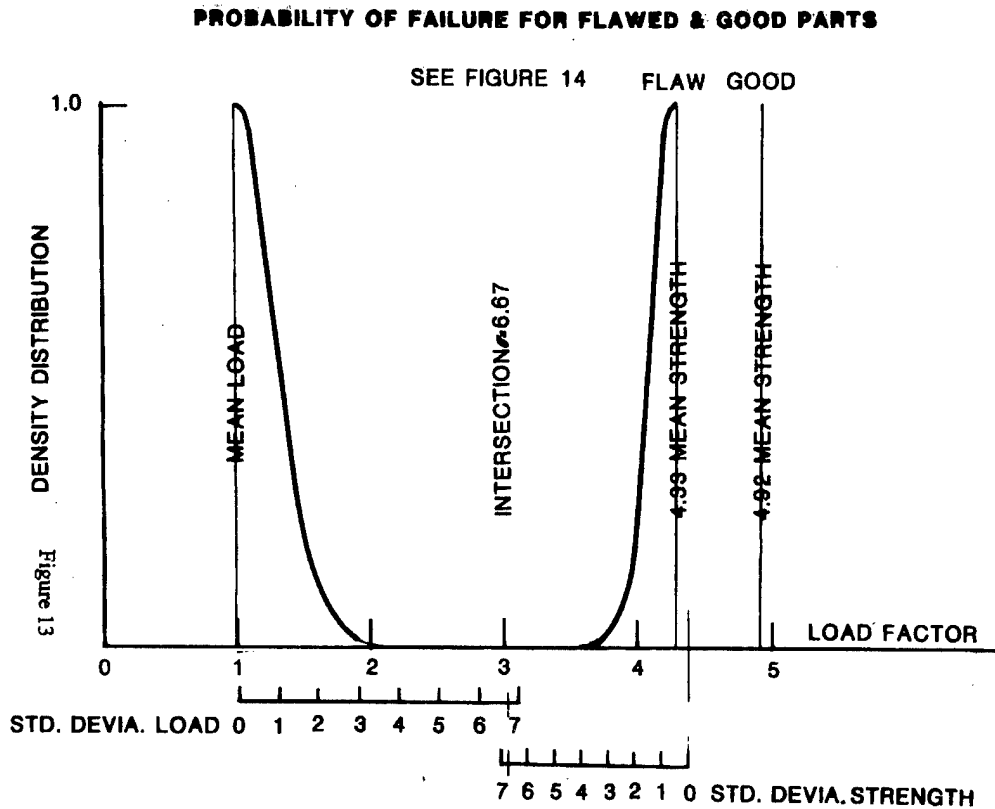
Figure 17: Maintenance with Small Flaws

The analysis shows that a reduction of 12% in mean strength led to an increased probability of the occurrence of the two fatal accident from 10^{-9} per flight hour to 10^{-6} per flight hour. Only a small loss in mean strength from 4.92 to 4.33 g for 28,800 bad parts produced a 1000 fold increase in risk. The exercise was supported by other analyses:

1. analysis of the accidents and incidents in this 500 airplane fleet,

2. a comparison of causes of fatal accidents in other major domestic fleets, and

3. a critique by a recognized professional engineer for probability analyses

3-46

Figure 18: Normal Probability Curves at Large Values
of Standard Deviation

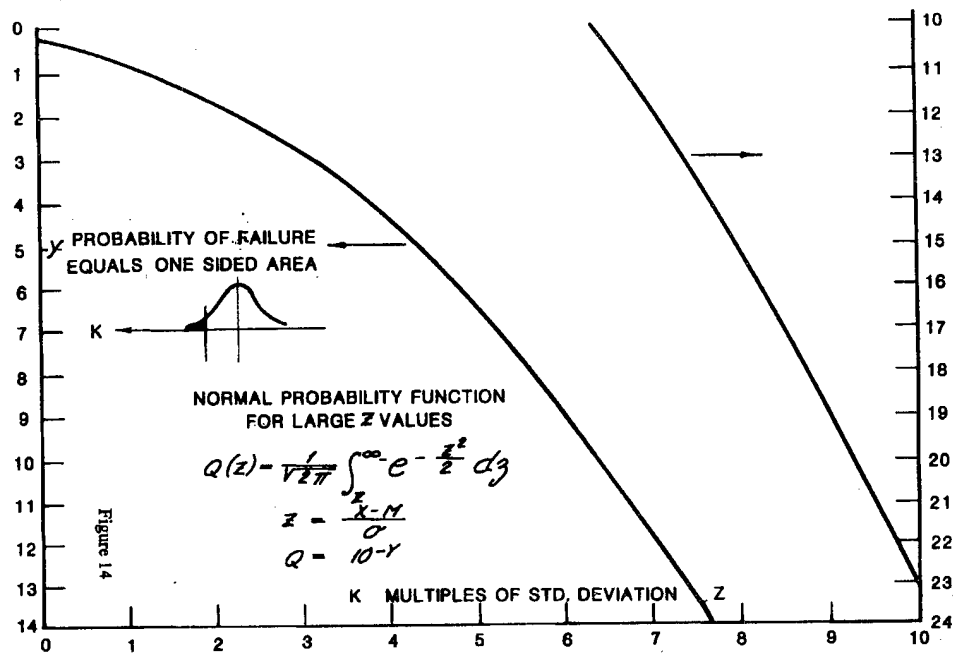The analysis shows system safety depends on operations at the very limits of human perfection. Maintenance with small flaws greatly increases the probability of failure. The model was constructed with plausible inputs and subsequently checked as indicated. The analysis also suggests the system currently in operation in transport category lies far beyond what most engineers might have expected in terms of ruggedness and durability.

The analysis was a test of the ability to describe the source of two accidents in one fleet of 500 airplanes in a one year period -- an actual case. The nature of the accidents were such as to identify the two accidents as maintenance related.

CONCLUSIONS

1. The status of airplane flutter as it relates to the many safety issues has been reviewed. By the 1940s the method for conducting a flutter analysis had proven itself in many key high speed airplane developments. Prior to the time that the ground vibration test and the flight flutter test could be conducted, the design had been completed. In-service experience on these airplanes by the 1950s showed that sufficient problems arose that large risks were present that originated in the initial design and it was necessary to validate the design prior to manufacture and flight. The ability to build dynamic models and subject these to wind tunnel test has been demonstrated as early as 1940. This-off-

the-shelf capability was considered the missing link therefore and the military customer pressed for its inclusion in each program.

2. The flutter analysis depended on very accurate descriptions of unsteady aerodynamics and flexible structure of the special character needed for flutter prevention. In addition to dynamic scaled models using beam technology, finite element structural models and aerodynamic influence coefficients were developed during the 1950s to fulfill a need for improved techniques. The scaled models in low speed tunnels have proved to be a durable technology and when coupled with the full knowledge of the transonic dip, results from low speed tunnel tests were used to qualify airplanes for supersonic speeds.

3. These two developments, the scaled dynamic model and the improvements in the flutter analysis, allowed the design and construction of advanced airplanes for all speed regimes free of flutter both in the initial flight testing and the later in-service usage.

4. The cause of the flutter problems given were due mainly to a failure to completely describe local structural flexibilities at locations in primary structure where transitioning occurred to small local structures where loads became concentrated.

5. An attempted correlation between accident rates and three aeroelastic variables, stiffness, span and speed suggested a relationship exists. The correlation is enticing but a solid physical relationship is not known. More work is needed to verify or refute the attempted correlation.

6. Computing capability following the Fridens and the Marchants depended on IBM mainframes with their cost burden -- a new model every year and the need to adapt all the programs with new software. At North American the computer was initially used 8 hours every day on optimizing new designs by Latin Squares for competitive bids on new contracts. The flutter equations played a key role in providing an optimum design with flutter requirements already incorporated.

Table 1: Table of Stiffness Measure, Effective Eccentricity

NORTH AMERICAN AVIATION
REPORT NA-54-619   DATE 6-8-54   *EXTENDED*
TABLE OF STIFFNESS MEASURE, EFFECTIVE ECCENTRICITY

WING		HORIZ. TAIL	
XF86	10.9	XF86	18.0
T-28	10.0	T-28	17.4
XAJ-1	8.6	XAJ-1	17.7
XA2J-1	8.8	XA2J-1	7.5
B45A	12.3	B45A SMALL	11.5
B45C	15.0	B45A EXTNDD	15.6
		ALL MOVING HORIZ TAIL	
F100A	16.0	YF100 (7%)	11.6
F100B	14.4	F100A (3.5%)	8.2
F107 ORIG	15.3	F100A REDES	11.7
F107 TIP DBLR	21.0	F107	12.0
XFJ-1	12.7		
FJ-2	13.0	T-38	10.0
FJ-4	13.4		
B47	10.0	ALL MOVING VERT. TAIL	
B51	6.3		
XF91	3.1	F107 ORIG DES	15.3
F84	15.7	F107 AS BUILT	11.6
XF3H1-1	14.5	F107 ROOT STIFFND	13.37
CONSTITUTION	3.7 (XR60-1)	F107 REDESIG 5 3/4% THICK @ROOT	
SNARK	13.8		17.6
DC-10	6.67		
B747	4.4		
B707-320	6.0		
L1011	9.13	L1011	5.7
DC-8	6.95		
AERO COMMANDER 680F			
	10.0		
SHUTTLE	10.0		
N156F	14.4		

Notes:
1.   These stiffness measures can be used by reference to a vehicle in the same speed range.
2.   These stiffness measures will correlate best if arrayed against their design limit speeds; in civil parlance, design dive speeds.
3.   These stiffness measures were defined using strip theory. This would be characterized by a relatively more outboard load. It thereby emphasizes tip stiffness. A strip theory flutter analysis would do the same.
4.   The variability is a result of the many different design groups controlling the design and the many different design limit speeds.
5.   In some cases the flutter group has participated in the stiffness design and in some cases it has not.

Table 2: Torsional Divergence

	CHORD		MODE	MOMENT	TORSION CONSTANT	$\Sigma M/J \uparrow$	
	c inch	c^2	α_1	$\Sigma c^2 \alpha_1 \downarrow$	J inch^4	α_2	α_1/α_2
Tip	106.5	11342.25	1	11342.25	1256	32.06613	0.031186
	129.5	16770.25	0.718	23383.29	3271	23.03568	0.031169
	152.5	23256.25	0.4954	34904.44	6804	15.88701	0.031183
	175.5	30800.25	0.3354	45234.84	13085	10.75702	0.03118
	198.5	39402.25	0.2275	54198.85	22768	7.300022	0.031164
	221.5	49062.25	0.1534	61725.00	27218	4.919539	0.031182
	244.5	59780.25	0.08268	66667.63	57051	2.651738	0.03118
	267.5	71556.25	0.04624	69976.39	96829	1.483176	0.031176
	290.5	84390.25	0.0237	71976.44	159637	0.760496	0.031164
Root	313.5	98282.25	0.00965	72924.87	235530	0.30962	0.031167

0.031174 Avg.$=K_D$

STRIP THEORY:

$$L = 2\pi \alpha q c \, \Delta x$$

$$M = 2\pi \alpha q c^2 \, \Delta x \, \frac{(1/2 + a)}{2}$$

$$\Delta x = constant, \ = 102 \ inches$$

$$K_D = \pi q \, (\Delta x)^2 (1/2 + a) / G = Avg.$$

$$V_D = \frac{262,670}{\Delta x} \sqrt{\frac{K_D}{(1/2 + a)}} = 829 \ mph, \ indicated \ incompressible$$

$$e_e = \frac{3.45 \times 10^6 \times K_D}{(\Delta x)^2} = \frac{3.45 \times 10^6 \times 0.031174}{(102^2)} = 10.3$$

Note: Using Excel spreadsheet, convergence was easily obtained by continually adjusting α_1 to produce a constant value in the last column.

Table 3: A Weight Equation for Flutter

$$W = 1.1 f(\lambda) \frac{L^3}{(t/c)^2} e_e \frac{0.3845^2}{(a_0/k)^2} f(\Lambda) f(T) \frac{1+0.06g}{1.36}$$

W = weight of structural material around torque box, pound

$f(\lambda) = 0.124 + 0.432\lambda$ variation with taper ratio, λ

e_e = effective eccentricity, $C_{l_\alpha} e\ q$

L = structural semispan, along swept axis, ft.

t/c = structural thickness to chord ratio, structural direction, percent

a_o = dimensionless torque box area relative to rectangle enclosing airfoil

k = dimensionless torque box perimeter relative to chord

$f(\Lambda) = 0.4 + 0.7\ cosine\ (\Lambda_{0.25} - 10°)$ sweep correction

$f(T) = 39 \times 10^6 \times \sigma/G$ modulus correction due to material or temperature

g = chordwise location of the section center of gravity, measured aft from a reference at 40% chord, as percentage chord.

G = shear modulus

σ = material density

Table 4: Special Case for Determining Effective Eccentricity at Root Arising From Root Flexibility

$$e_e = \frac{Kroot}{\overline{C}^2 L} \qquad \overline{C} = AVG\ CHORD \perp e.a.$$

Table 5: NTSB Accident Brief

BRIEFS OF ACCIDENTS

FILE DATE	LOCATION	AIRCRAFT	INJURIES	FLIGHT	PILOT
			F S MN	PURPOSE	

2-1134 9/11/66 NR MITCHELL OREG BEECH A35 CR- 1 0 0 NON COMMERCIAL PRIVATE
TIME-0920 N745B PX 3 0 0 PLEASURE, PERSONAL AGE29
DAMAGE-DESTROYED 28 HOUR IN TYPE
NONINSTRU.RATED

TYPE OF ACCIDENT   PHASE OF OPERATION
  AIRFRAME FAILURE IN FLIGHT   INFLIGHT - NORMAL CRUISE
    COLLISION WITH GROUND/WATER   INFLIGHT UNCONTROLLED DESCENT
PROBABLE CAUSES
PILOT IN COMMAND - CONTINUED VFR FLIGHT INTO ADVERSE WEATHER CONDITIONS
PILOT IN COMMAND - SPATIAL DISORIENTATION
AIRFRAME - WING SPARS
MISCELLANEOUS ACTS, CONDITIONS - OVERLOAD FAILURE

FACTORS
  WEATHER - LOW CEILING
  WEATHER - TURBULENCE, ASSOCIATED W/CLOUDS AND THUNDERSTORMS
WEATHER BRIEFING - NO RECORD OF BRIEFING RECEIVED
WEATHER FORECAST - WEATHER SLIGHTLY WORSE THAN FORECAST

SKY CONDITION   CEILING AT ACCIDENT SITE
  OVERCAST   300
VISIBILITY AT ACCIDENT SITE   PRECIPITATION AT ACCIDENT SITE
  UNKNOWN/NOT REPORTED   NONE
OBSTRUCTIONS TO VISION AT ACCIDENT SITE TYPE OF WEATHER CONDITIONS
  NONE   IFR
TYPE OF FLIGHT PLAN
  NONE
REMARKS - RIGHT WING AND LEFT RUDDERVATOR FAILED IN FLIGHT

See notes on next page on how to interpret the above NTSB Accident Brief.

Table 5: NTSB Accident Brief (continued)

Note: This authentic reproduction should be interpreted as follows:

File:	2-1134	type accid:	airframe failure in flight
Date:	9/11/66		collision with ground
location:	Mitchell OR	phase of operation	inflight-normal cruise
aircraft:	Beech A35		inflight-uncontrolled descent
Injury:	fatal/serious/minor	probable cause	continued visual flight rules
	cr 1 0 0		into adverse weather
	px 3 0 0		spatial disorientation
flight	non commercial		airframe wing spars
purpose	pleasure		overload failure
pilot	private pilot	factors	low ceiling, turbulence
	age 29		no briefing
	28hr in type		wx worse than forecast
	non instru. rated		overcase, ceiling 300
time	0920	type of weather	Instru. Flt. Rules
I.D.#	N745B	Remarks	Right Wing and Left Ruddevator failed in flight

REFERENCES

1. Alexander Flax, "The Influence of Structural Deformation on Airplane Characteristics," *Journal of the Aeronautical Sciences*, January 1945.
2. Military Specification MIL-A-8870.
3. Federal Air Regulations, Parts 23 and 25.
4. U.S. Army TR-4798.
5. U.S. Army TR-5153.
6. G. Harris, Flutter Criteria for Preliminary Design, BuWps Contract NOw 61-1072c, Chance Vought, Sept., 1963.

APPENDIX A

CORRELATION OF ACCIDENT RATES WITH SPEED AND OTHER AEROELASTIC VARIABLES
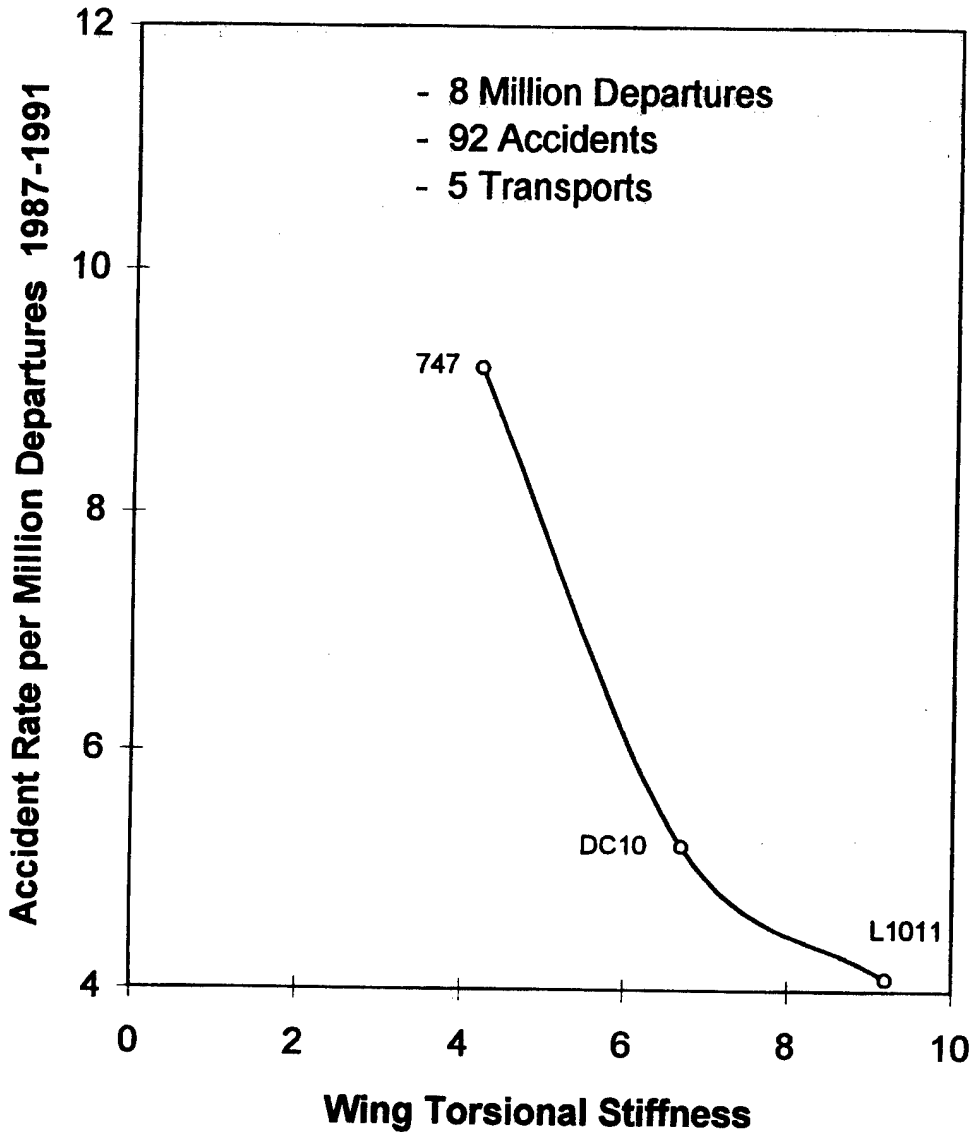
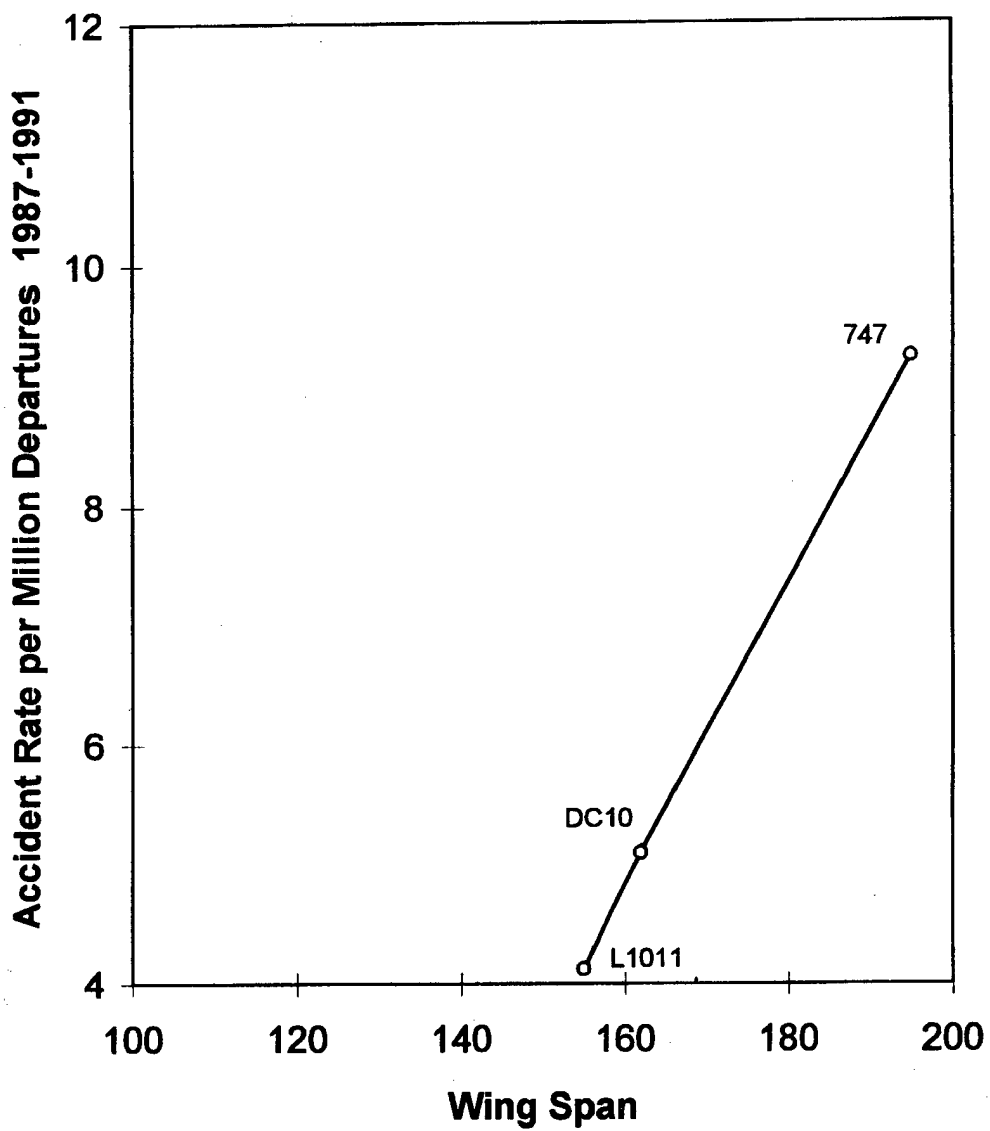Figure A-1: Correlation Accident Rate vs. Wing Stiffness
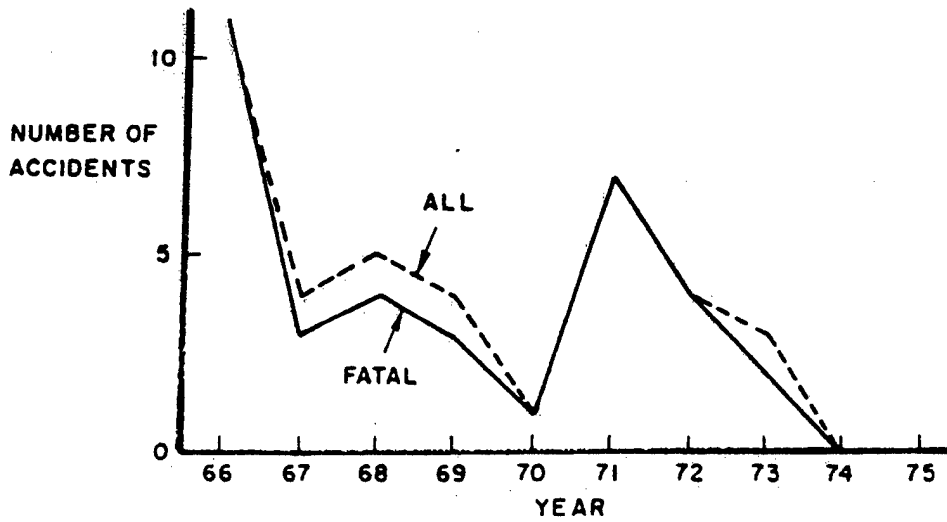
Figure A-2: Correlation Accident Rate vs. Wing Span
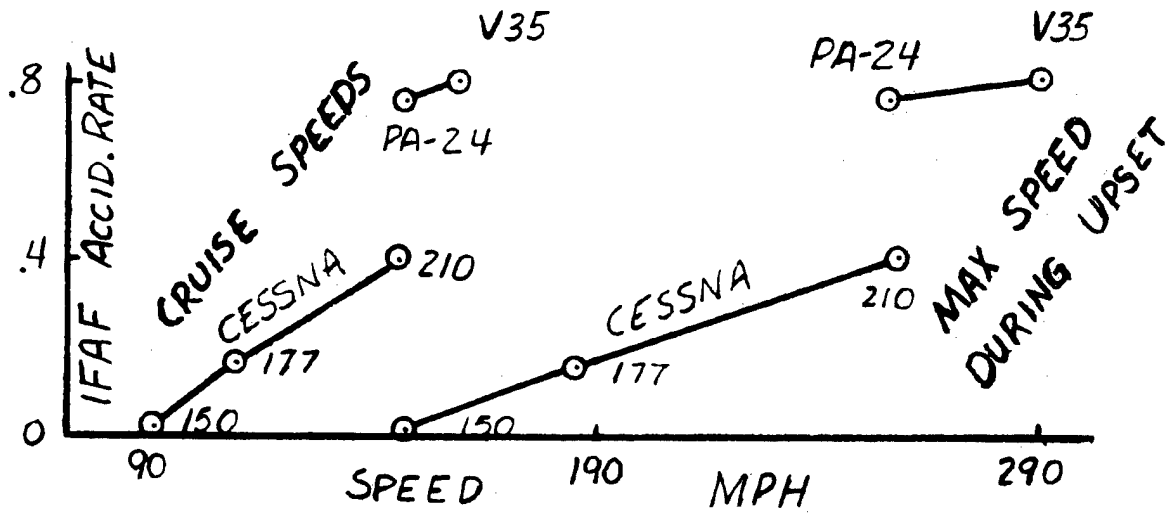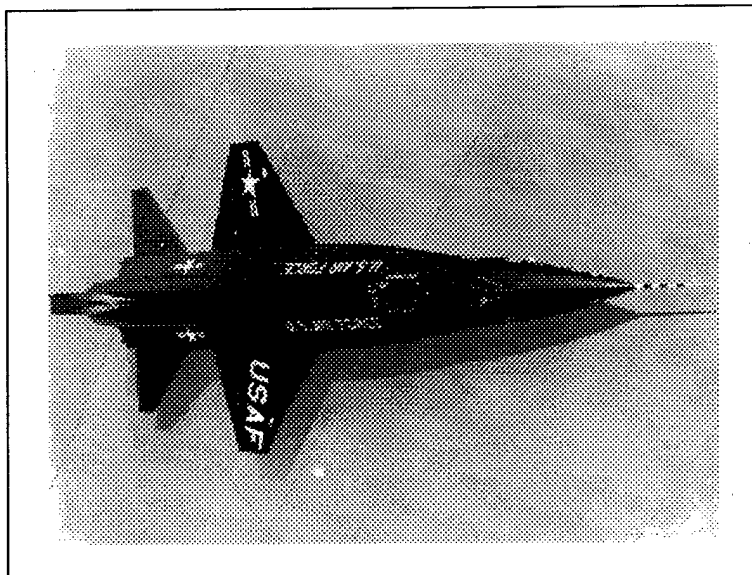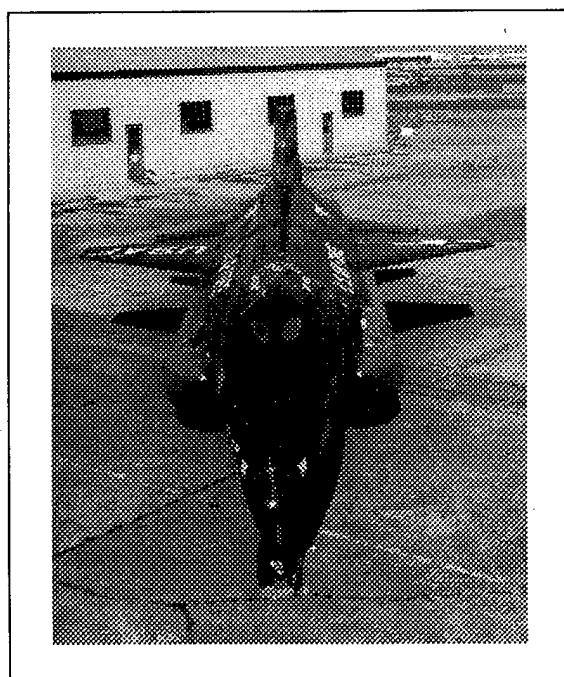
Figure A-3: IFAF Accident History PA-24
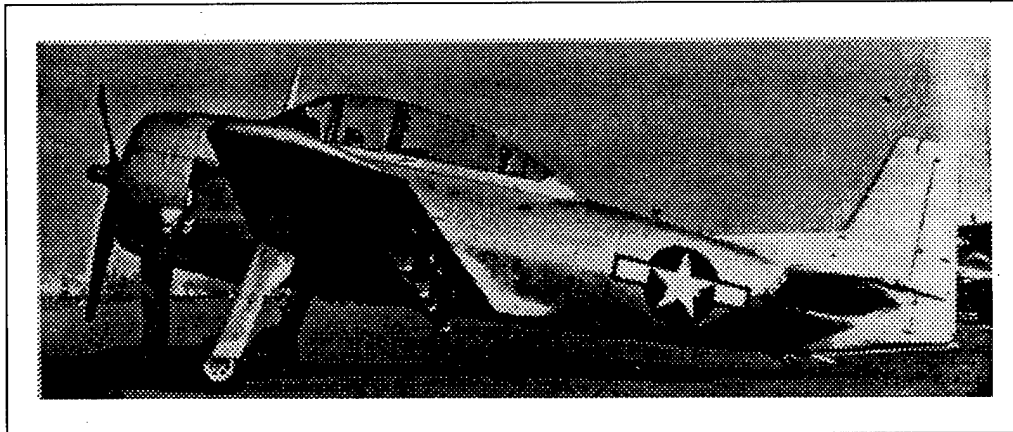
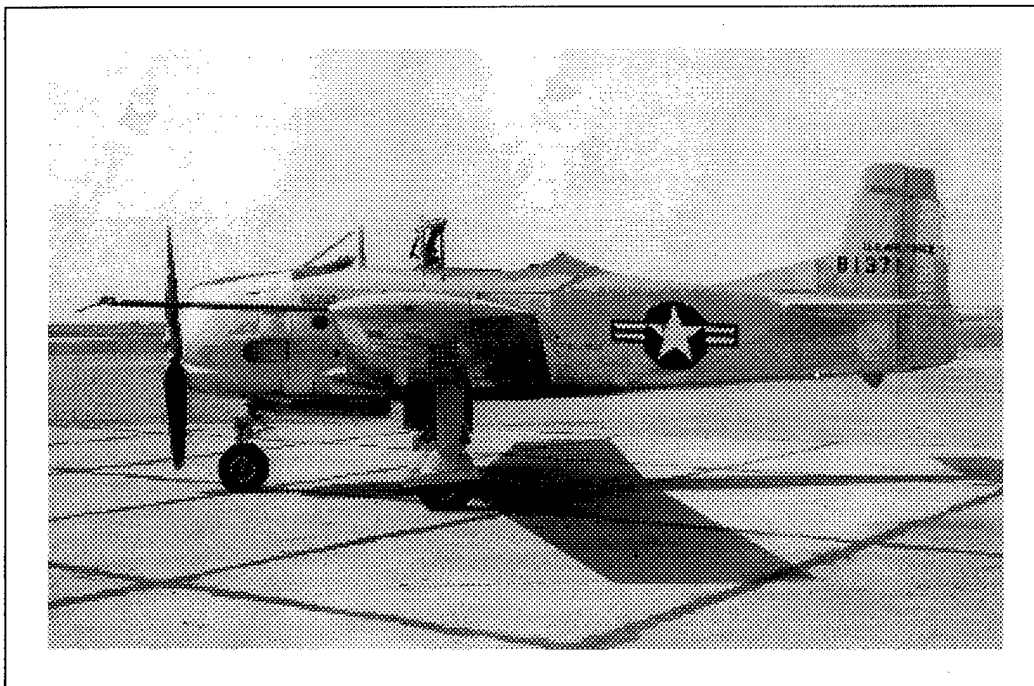Figure A-4: Effect of Speed on Accident Rates for Five Fleets
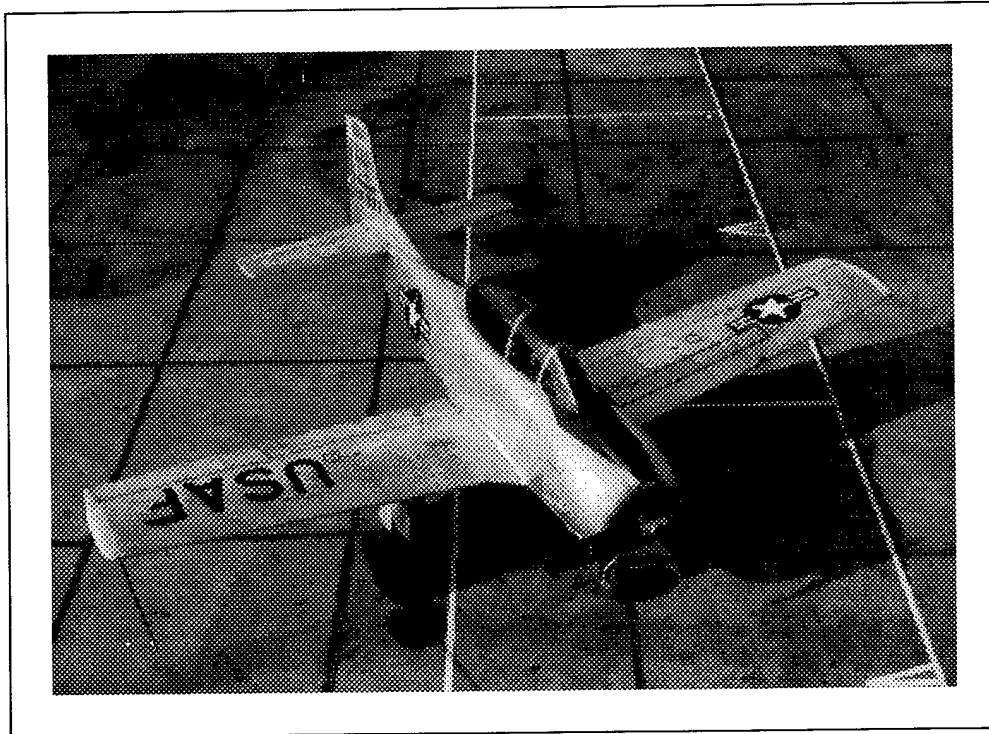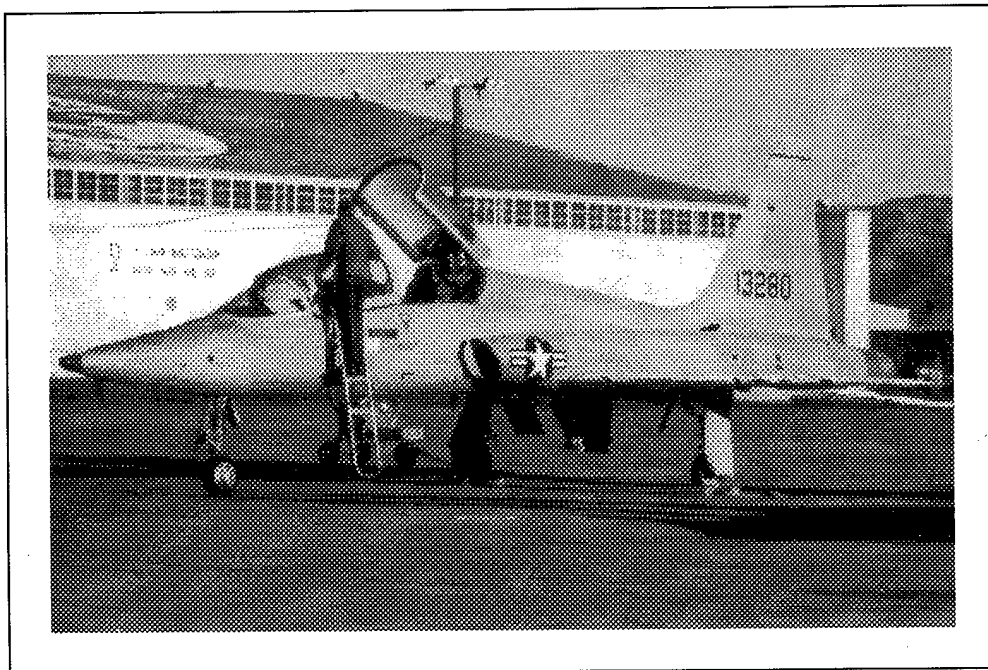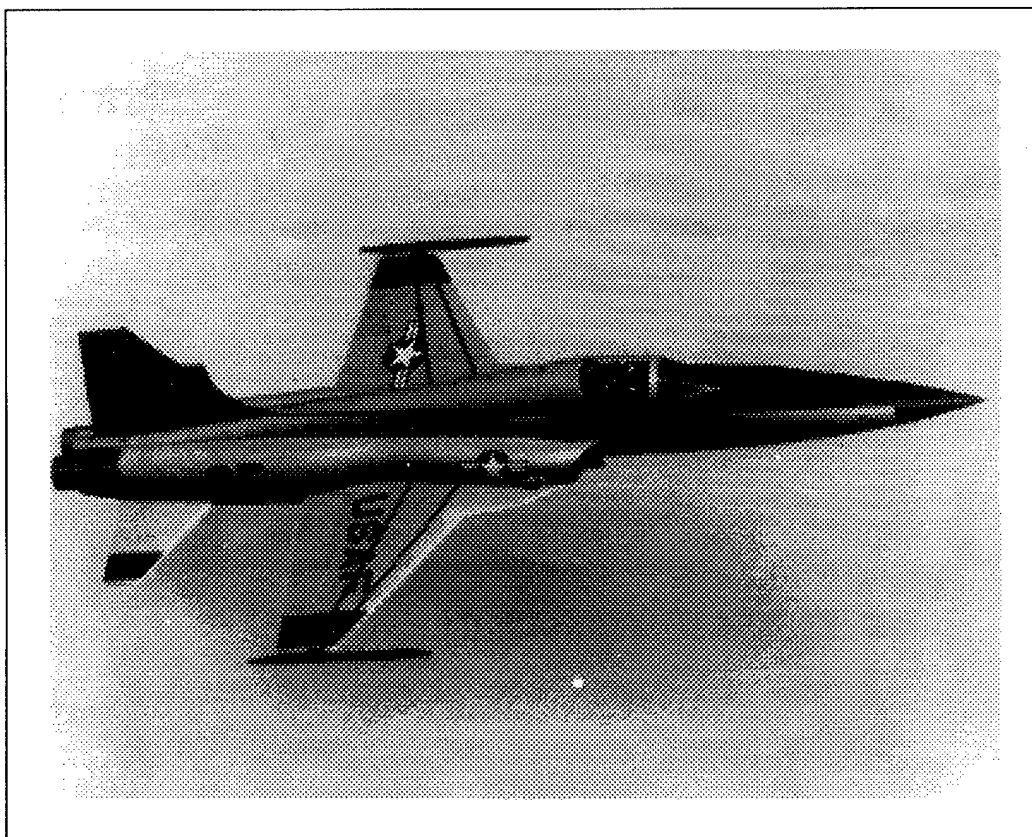
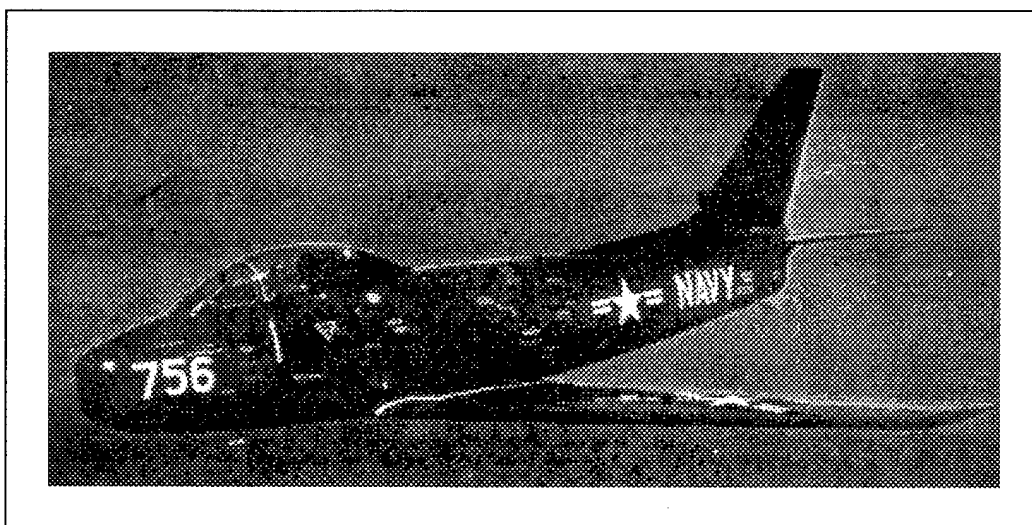# APPENDIX B

AIRCRAFT PHOTOS

X-15

X-15A

XSN2J

T28 (Side View)

T28 (Perspective)

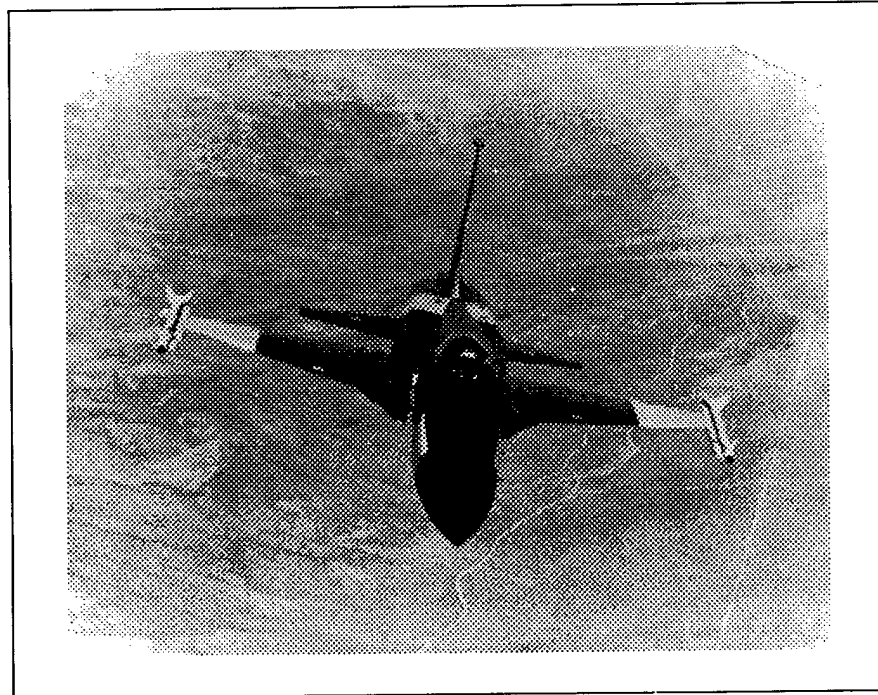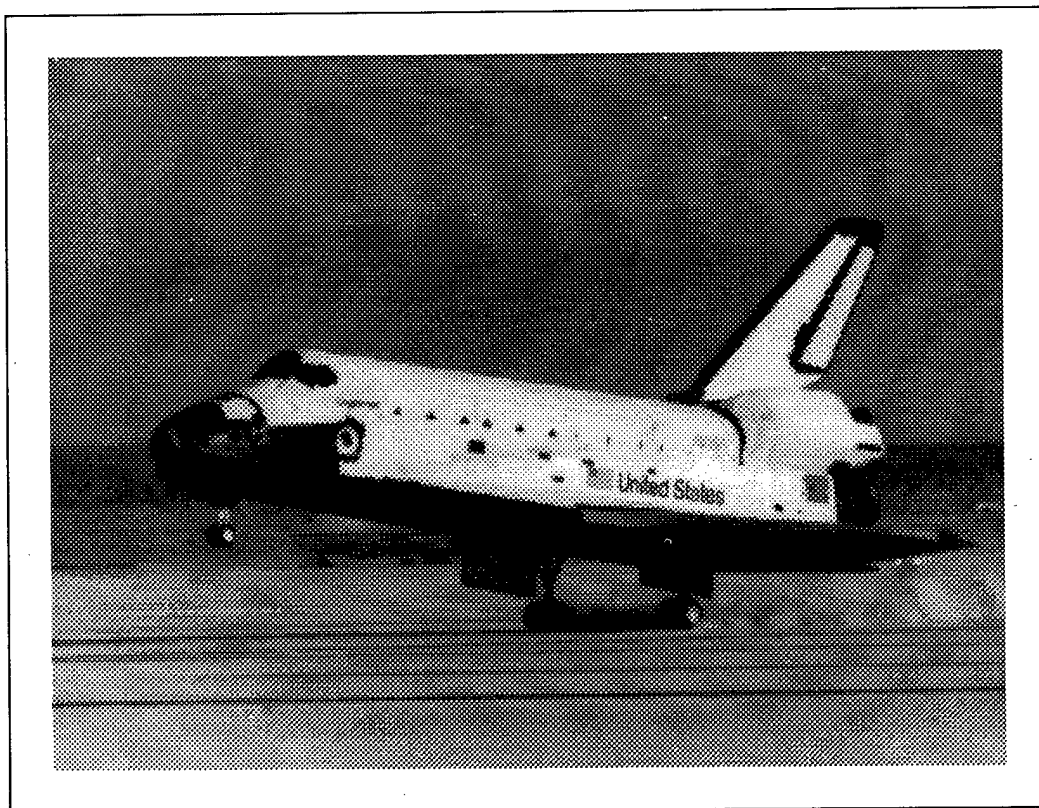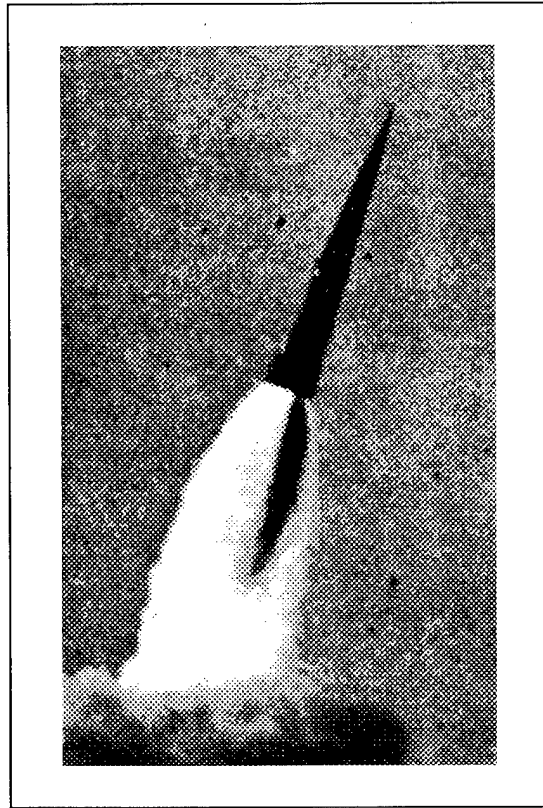

T38

F-5E

XFJ-2B Fury

N-156F

Space Shuttle

Sprint Missile

Raymond P. Peloubet, Jr.

Aeroservoelastic Instability, Case Study A

Abstract

The author presents two cases of aeroservoelastic instability, in which configurations that were flutter-stable without their flight control systems becomes unstable at certain regimes with the control systems engaged.

Part A discusses a high performance fighter with fly-by-wire control which showed antisymmetric oscillation in early flight tests. Flutter analysis and wind tunnel tests showed the aircraft minus flight control system was stable. The Nyquist Criterion was used to calculate the stability of the airplane with the control system engaged; it showed an unstable antisymmetric oscillation mode very close in frequency to that observed in flight. Calculated control loop gain adjustments were tested in flight and found to correct the problem.

Part B concerns a fighter prototype with fly-by-wire control which showed a pitching motion in a narrow range of high-subsonic Mach numbers, at a frequency well below that of the first symmetric vibration mode of the structure and well above the rigid-body short-period mode. Subsequent flight tests showed that reducing the pitch loop gain eliminated the problem. Although the immediate problem was solved, two methods for measuring the open-loop frequency response function of the flight control system without actually opening the feedback loops were applied during flight tests. Both methods are explained and discussed.

Raymond P. Peloubet, Jr.

BSME, Louisiana State U., 1949; MSAE, Ohio State U., 1953 Flutter and Vibration Engineer, Wright Aeronautical Development Center 1949-54. Senior Structural Engineer, Convair Fort Worth 1954-63. Supervisor, Structural Dynamics Group 1963-88. Staff Specialist, 1988, Division Specialist 1989. Retired 1994.

Mr. Peloubet is the author and co-author of numerous papers in the fields of flutter, vibration, gust response, unsteady aerodynamics, flutter suppression, aeroelasticity and the subject of the present contribution, aeroservoelasticity.

Table of Contents

Raymond P. Peloubet, Jr.

Aeroservoelastic Instability, Case Study A

INTRODUCTION

Flutter is an instability that is caused by the interaction of aerodynamic, elastic and inertia forces. The addition of servomechanism forces as a fourth set of interactive forces can cause a flutter stable configuration to become unstable. This type of instability has been labeled as an aeroservoelastic (ASE) instability.

The servomechanism forces are usually generated by control surface deflections which are produced by hydraulic actuators controlled by servo valves. The input to the servo valves is the sum of the inputs from the pilot and the feedback from flight control sensors which have been passed through flight control laws. The control laws can be mechanized either by analog or by digital systems. However, other types of servo mechanism forces, such as vectored thrust systems, can produce ASE instabilities.

An appreciation for the cause of ASE instabilities can be obtained by considering a typical design process. First, flight control laws are designed to cause the airplane to respond in the desired manner to pilot inputs throughout the airplane's operational envelope. These control laws are usually developed with the airplane considered to be rigid. Initially, the only flexibility effect considered is the modification of the stability derivatives due to aeroelasticity. The flight control law designer might take several steps to reduce the likelihood of encountering an ASE instability.

- Sensors might be located to minimize their response to certain natural modes of vibration. For example, vertical accelerometers might be located on the fuselage centerline close to a node line for the first fuselage bending mode. Similarly, pitch rate gyros might be located on the fuselage centerline near the maximum deflection on the first fuselage bending mode, where the slope would be zero and the pitch rate would be near zero.

- The flight control designer might select hydraulic actuators that have a low band pass. That is, the hydraulic actuator produces one degree of control surface deflection for one degree of command to the actuator for frequencies from zero to some cut-off frequency (for example, 3 Hz). Above the cut-off frequency, the actuator produces lower deflection which continues to decrease as the frequency increases.

- The flight control law designer can incorporate low pass filters in the control law which diminish the feedback signal for frequencies above some selected cut-off frequency, and/or notch filters which reduce the feedback signal in selected frequency bands.

However, in spite of these precautions, the response of one or more of the flight control sensors to the excitation of a structural natural mode of vibration might produce a feedback signal of sufficient magnitude and with the right phase angle to cause an ASE instability.

Sometimes it is difficult to determine if an instability encountered in flight is caused by flutter or ASE. That is, if the unstable boundary is approached at constant altitude by slowly increasing airspeed from the stable side of the boundary, the instability might first appear as constant amplitude oscillations for either type of instability. It is important to distinguish which type of instability is involved because the type of correction needed is different. If the instability is caused by flutter the needed correction might be to modify the structure, or the mass distribution, or the aerodynamic configuration (by adding vortex generators or fences, for example). If, on the other hand, the instability is an ASE instability, the solution is usually to modify the flight control system or control law.

If the flight control system lowers the flutter boundary by a small increment, modifications to the flight control system might only restore that small increment. Further incremental increases to the flutter boundary might well require "flutter type" modifications. If the flight control system increases the flutter boundary by a small increment, further increases in the boundary might best be achieved by flutter type modifications. Sometimes, however, a modification to the flight control system or the addition of a separate independent control system can increase the flutter boundary substantially or remove it entirely. In these cases the control system is called a **flutter suppression system.**

A direct means of determining whether an instability encountered in flight is caused by flutter or ASE is to disengage the flight control system. This is a viable option if the ASE instability is caused by an autopilot and the pilot can override the autopilot with the basic flight controls. If, on the other hand, the instability is caused by a closed-loop flight control system in which small forces applied by the pilot to the flight controls produce large control surface deflections if the feedback loop is opened, disengaging the flight control system is not a viable option. That is, with the loop open, the pilot would be in danger of over controlling and subsequently losing control of the airplane. Furthermore, aircraft that are statically unstable and rely on the flight control system for stabilization would be statically unstable if the feedback loop were opened.

Methods used to distinguish a flutter instability from an ASE instability include:

(1) Comparing flutter analyses with ASE analyses,

(2) Conducting flight tests with a gradual reduction in flight control system gains (subject to flight control safety limitations) and

(3) Measuring the open-loop frequency functions in flight (without actually opening the flight control loop) at a sequence of flight conditions that approach the unstable boundary (this is discussed in Part B).

Case Study A Airplane Description

This case study is about a prototype of a highly maneuverable fighter aircraft that made its initial flight tests during the early part of the 1970 decade. One of the advanced technology concepts that it employed was the fly-by-wire flight control system. The connection between the cockpit controls and the servo valves for the hydraulic actuators for each control surface was electrical rather than mechanical. The conventional control systems of the time transferred pilot-commanded deflections of the stick and rudder pedals via mechanical linkages to deflect the servo valves. The fly-by-wire system transformed pilot applied-stick and rudder forces into electrical signals which were sent to the servo valves by means of electrical lines. Pilot-applied stick forces produced deflections that were so small as to be virtually imperceptible, so the stick was called a **force stick**. The airplane was statically unstable over part of its operational envelope and the flight control system was used to stabilize the airplane.

The airplane with missiles mounted on the wing tip launchers is shown in Figure 1. Control surfaces included flaperons on the wings, all-movable horizontal tail surfaces and a rudder. The locations of the servos that commanded the control surface actuators are shown. Electrical signals from the pilot controller and rudder pedals and the air data computer were input to the flight control computer which implemented the flight control laws. Electrical signals from the flight control computer were sent to the servos which commanded the control surface actuators. The airplane response to the control surface movement was sensed by the flight control sensors and the outputs of those sensors were returned to the flight control computer to close the loop. The flight control system had three primary loops:

FLY-BY-WIRE FLIGHT CONTROL
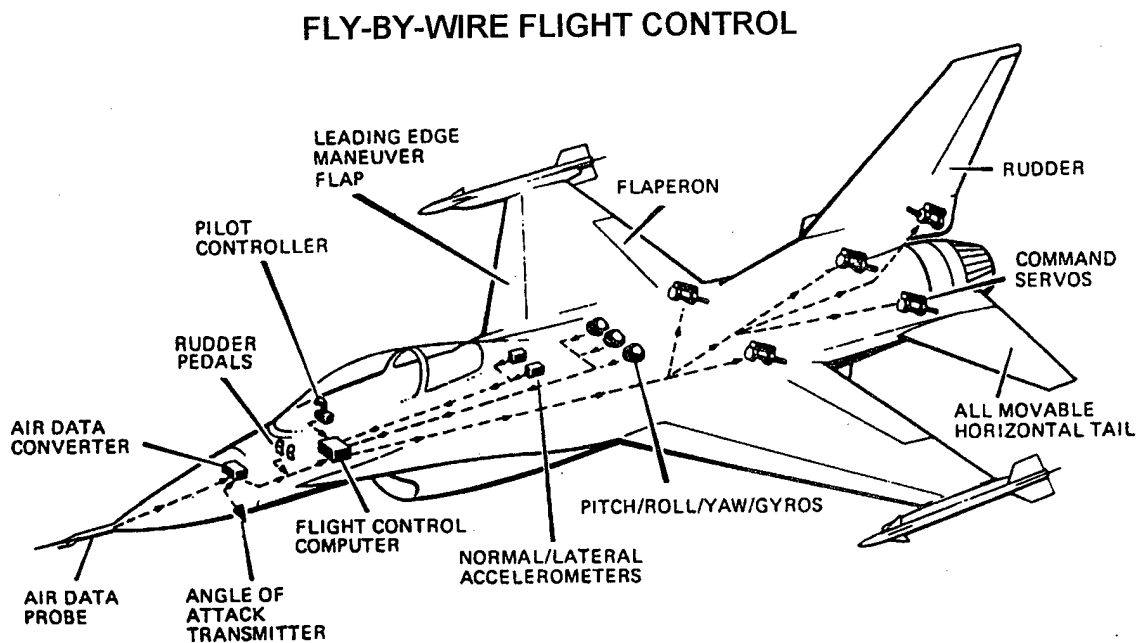
Figure 1: Case Study A Airplane Configuration

- The longitudinal loop commanded the horizontal tail surfaces to move symmetrically; airplane response was sensed by the normal accelerometer, the pitch rate gyro and the angle of attack sensor.

- The roll loop commanded antisymmetric deflections of the flaperons and of the horizontal tail surfaces in the ratio of 1.0 degree flaperon to 0.25 degree horizontal tail; airplane response was sensed by the roll rate gyro.

- The yaw loop commanded the rudder and the airplane response was sensed by the roll rate gyro, the yaw rate gyro and the lateral accelerometer.

Pre-Flight-Test Analyses and Tests

Flutter analyses were conducted without the flight control system. Analyses were conducted over a range of Mach numbers and altitudes. Several configurations of the airplane were analyzed, including configurations with and without wingtip missiles, for several fuel load conditions. These analyses indicated that the unaugmented (without the flight control system) airplane had at least a 20 percent flutter margin throughout its flight envelope.

Ground vibration tests were conducted with the airplane held by a soft suspension system. Hydraulic power was supplied to all control surface actuators but the feedback loops for all flight control system sensors were left open. With the tip missiles installed, the first two antisymmetric modes that were obtained by the ground vibration tests are shown in Figure 2.
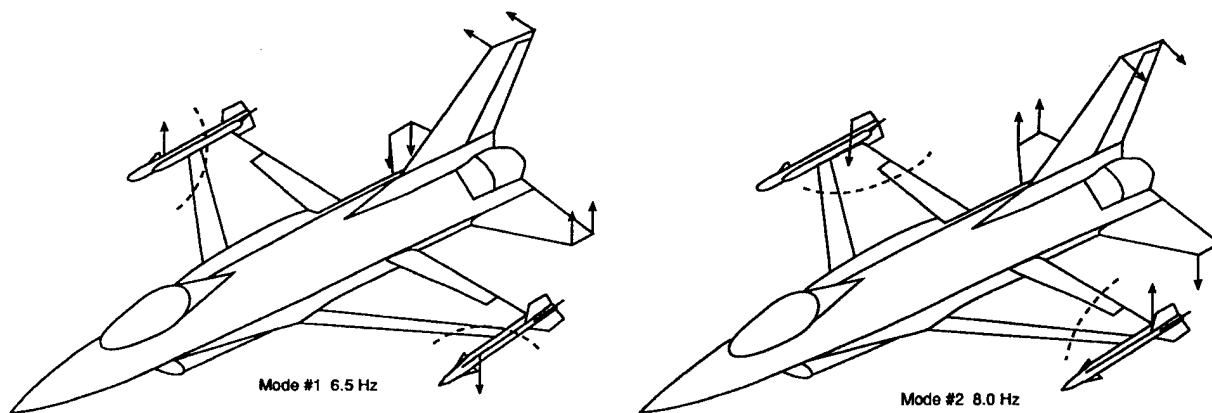
Figure 2: Missiles On: Missile Pitch and First Wing Bending Modes

After the ground vibration tests, the finite element stiffness matrix of the airplane was modified to improve the correlation between computed and measured natural modes of vibration. Flutter analyses were repeated and they continued to show the unaugmented airplane to have at least a 20 percent flutter margin throughout its flight envelop.

A one-quarter scale flutter model of the airplane was tested on a cable system in the NASA Langley Transonic Dynamics Tunnel. The flight control system was not included in the model. The wind tunnel tests indicated that the unaugmented airplane with and without the tip missiles had at least a 20 percent flutter margin throughout its flight envelope.

Stability analyses of the airplane were conducted with the airplane considered to be a rigid body and with the flight control system engaged. Stability derivatives used in these analyses were modified to include the effects of static aeroelasticity. These analyses indicated that the augmented airplane was stable. Hence no aeroservo instabilities would be expected at any point in the flight envelope if the airplane were rigid.

Ground tests of the airplane were conducted with the airplane resting on its landing gear. An oscillatory input signal was applied to each set of control surfaces and the frequency of the input was varied over a broad range. Each control loop was opened, one at a time, and the open-loop frequency response function (the ratio of feedback response to control surface input as a function of input frequency) was measured. Previous experience with this type of ground testing supported the belief at that time that if the magnitude of the measured frequency response function did not exceed 0.5 regardless of the phase angle, then the airplane would not experience any ASE instabilities in flight. These tests were conducted with the flight control system gains varied to simulate a large number of Mach-altitude flight conditions. These tests indicated that the airplane should be free of ASE instabilities throughout its flight envelope.

An ASE analysis was conducted at one high Mach number, low altitude flight condition that was thought to be the most critical point. The results of these analyses indicated that the aircraft would be free of ASE instabilities at this flight condition. Subsequent post flight test analyses indicated that this flight condition was beyond the back side of the unstable region as predicted by analysis.

Flight Tests

Initial flights of the airplane were made with the wing tip missiles. In this configuration an antisymmetric oscillation at approximately 6.5 Hz was first experienced during flight number 8. The oscillation was experienced at the three flight conditions shown in Figure 3. The airplane was being accelerated slowly at a constant altitude when the oscillation first began. The pilot climbed and reduced speed to get out of the unstable region. Then he climbed and increased Mach number until the instability was repeated. This operation was then repeated a third time.
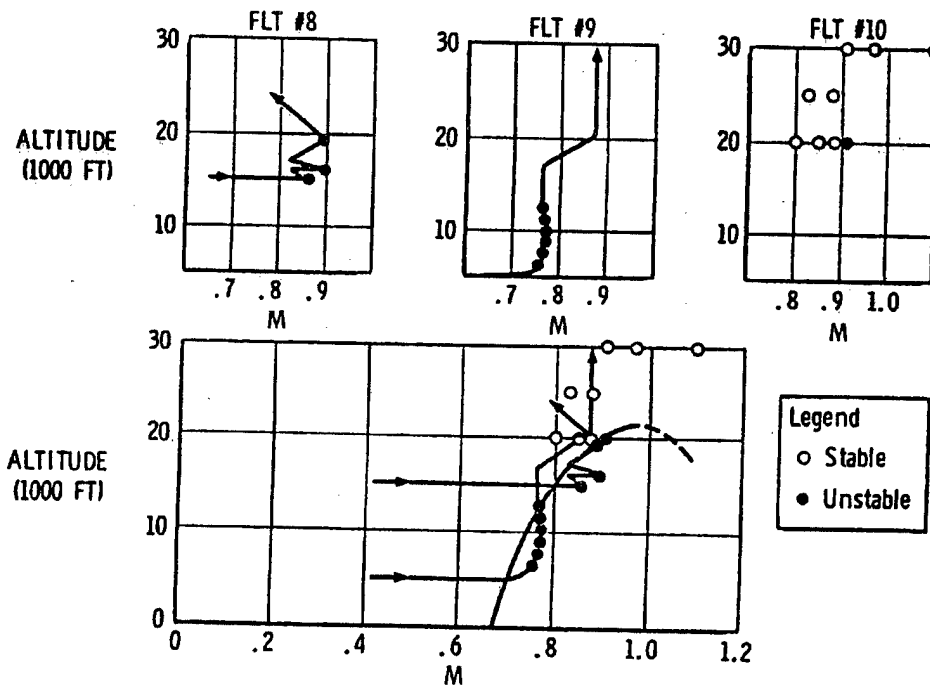
Figure 3: Missile On Flight Tests Results with Reference Control System

The oscillation was again encountered during a sustained climb over a large altitude range on flight number 9, as shown in Figure 3.

The instability was probed in a systematic manner on flight number 10. The airplane was flown at selected combinations of Mach number and altitude. These flight conditions were held constant while control surface pulses were applied. The roll pulse was the most effective in exciting the lowly damped response at 6.5 Hz as the unstable boundary was approached. But no excitation was required when the boundary was reached or exceeded. The unstable boundary at 20,000 feet was established. At 30,000 feet, however, the instability did not occur even for much higher Mach numbers.

A composite of the stability data that was obtained during the three flights is shown in the lower part of Figure 3. A line was drawn through the unstable points that were thought to be near the boundary of the instability and which divided all known stable flight conditions from all known unstable flight conditions. Since the instability did not exist at higher altitudes, the unstable boundary was expected to have a top and perhaps a back side as indicated by the dashed line continuation of the unstable boundary line.

During the 6.5 Hz antisymmetric oscillations, the output of the accelerometers mounted on the wing tip launchers, the horizontal tail tips and the vertical tail tip were consistent in magnitude and phase angle with the 6.5 Hz, first antisymmetric mode of vibration measured during the ground vibration tests and shown in Figure 2.

Initially there was some uncertainty about whether the oscillations were caused by flutter or ASE. However, after a series of ASE analyses were conducted at 0.9 Mach number and sea level that indicated that the roll loop was causing an ASE instability, additional flight tests were conducted with systematic gain reductions in both the roll and yaw channels. These tests indicated that the instability no longer existed when the roll loop gain was reduced by 50 percent. There was no appreciable difference in the results when the yaw loop gain was reduced.

Post-Flight Analyses

To conduct the ASE analyses, it is desirable to add the flight control system equations to the equations of motion used to conduct flutter analyses. It is desirable because any change in stability can be attributed to the addition of the flight control equations and not be confused by the possibility that the change resulted from using a different method of analysis or a different modeling of the stiffness, mass or unsteady aerodynamics.

Unsteady aerodynamics are most conveniently expressed as a function of reduced frequency. Conventional V-g flutter analyses are conducted by constraining the equations of motion to harmonic motion, selecting a value of reduced frequency, computing the aerodynamic terms for the selected reduced frequency and then solving for the roots of the determinant of the equations of motion in the form of frequency and structural damping pairs. Using the selected reduced frequency, each frequency root can be used to compute a velocity associated with that root. The structural damping root can be plotted versus the velocity. By repeating this process for several selected reduced frequencies, each point on that curve can be interpreted to be the required structural damping to produce flutter at the associated frequency. The point on the curve where the required structural damping agrees with the real structural damping is called the flutter point.

The flight control equations are usually expressed as a function of the Laplace variable. Hence, these equations can also be expressed as a function of frequency by substituting $i\omega$ for the Laplace variable s. For a selected velocity, frequency could be converted to reduced frequency so that the flight control equations could be expressed as a function of the reduced frequency to be compatible with the unsteady aerodynamics in the flutter equations. However, since velocity is an unknown variable in the flutter equations, only roots with velocity identical to the assumed velocity in the flight control equations would be valid solutions. Iterative methods would have to be applied in order to determine solutions that were compatible with the assumed value of velocity for the flight control equations.

A method for determining ASE stability characteristics was selected for the study airplane which employs the same equations of motion used in the flutter analysis. It requires selection of a velocity (Mach number, altitude and speed of sound) so the analyses can be conducted in the frequency domain. The flight control equations are combined with the flutter equations in the frequency domain. The stability of the closed loop system is determined by computing

frequency response functions at selected flight conditions. The frequency response functions have a physical meaning and can be measured on the airplane.

The method of analysis is explained by referring to the block diagram of a closed loop single-input-single-output system shown in the upper left of Figure 4. For the present application,

$$\frac{X_0}{X_I} = \frac{G}{1 + GH}$$

$$s - PLANE$$

$$1 + GH$$

$$\underline{GH}$$

$$Z - P = N$$
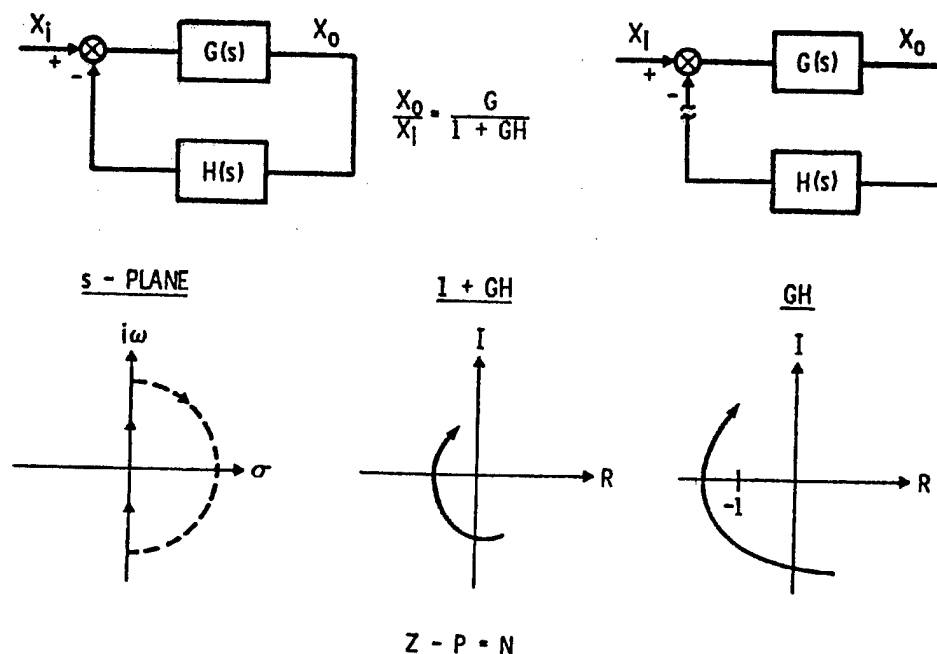
Figure 4: Nyquist Criteria

consider an airplane with a flight control system consisting of only a roll loop and a single roll rate sensor. In the diagram, x_i would be the pilot commanded roll input signal. The symbol G would represent the transfer function relating roll rate response, x_o, to aileron deflection for the unaugmented airplane. The symbol H would represent the transfer function for the roll loop relating feedback response to the roll rate gyro input. The sensor response, x_o, to the pilot input for the closed loop system, expressed as a function of the Laplace variable, is

$$\frac{x_o}{x_i} = \frac{G}{1 + GH}$$

(1)

The stability of this closed-loop system can be assessed by determining whether the denominator $(1+GH)$ has any zeros on the right hand side of the Laplace plane. If it has one or more zeros on the right-hand side, it is unstable. If it has no zeros on the right-hand side, it is stable. If a function of the Laplace variable is infinite at a value of the Laplace variable, it is said to have a pole at that value. Hence, if the function $(1+GH)$ has a zero at some value of

s on the right hand side of the Laplace variable plane, then the function $G/(1+GH)$ has a pole at the same value of *s*.

The Nyquist criterion states that if a function of the Laplace variable is evaluated over a closed clockwise path that encloses the entire right hand side of the Laplace plane, the number of times (N) this function encloses the origin in the clockwise direction is equal to the difference between the number of zeros (Z) and the poles (P) on the right-hand side of the Laplace plane.

$$N = Z - P \qquad (2)$$

The evaluation path is illustrated on the lower left part of Figure 4. The path extends from the origin up the frequency axis to plus infinity. Then it follows a path that would be traced by a vector of infinite magnitude rotating from +90 degrees, to zero degrees, to -90 degrees. The path is then closed by following the frequency axis from minus infinity to zero. For this application the function $(1+GH)$ would be evaluated for values of the Laplace variable along this path and plotted as illustrated by the lower center part of Figure 4. In practice the function $(1+GH)$ would be plotted over a finite path along the frequency axis from zero to some selected positive upper frequency. The characteristics of the plot for higher frequencies and for the infinite magnitude part for the plot can usually be deduced. Also, since poles and zeros of the function $(1+GH)$ are either real or appear as complex conjugate pairs, the plot of the function $(1+GH)$ for negative frequencies is the mirror image of the plot for positive frequencies. The lower right part of Figure 4 illustrates that the equivalent criteria is to determine the number of clockwise enclosures of the minus one point by the function GH. And the upper right part of Figure 4 illustrates that the physical interpretation of GH is the open-loop frequency response function relating the feedback to the pilot input. This is a measurable function.

By plotting the function GH, the number of enclosures of the minus one point can be determined. Hence, the number of zeros on the upper right quadrant of the Laplace plane can be computed

$$Z = N + P \qquad (3)$$

The number of poles in GH is equal to the sum of the number of poles in G and H. If the unaugmented airplane is stable, G has no poles on the right-hand side of the Laplace plane. The number of poles on the right-hand side of H can be determined by inspecting the block diagram of the flight control system and usually there are none. So in practice, if the plot of GH shows no clockwise enclosures of the minus one point, the closed-loop system is stable. If the plot of GH shows one or more clockwise enclosures of the minus one point, the closed-loop system is unstable.

ASE stability was determined by computing the open-loop frequency response function over a frequency range from near zero to a selected upper frequency. The equations of motion

employed rigid body side translation, roll and yaw and antisymmetric modes of vibration as generalized coordinates.

$$[A_{rs}]\{q_s\} = -\{A_{r\delta}\}\delta \qquad (4)$$

where

$$A_{rs} = \left[1 - \left(\frac{\omega_r}{\omega}\right)^2 (1 + ig_r)\right] M_{rs} + Q_{rs} \qquad r = s$$

$$= M_{rs} + Q_{rs} \qquad r \neq s$$

$$A_{r\delta} = M_{r\delta} + Q_{r\delta}$$

In order to put the equations in the form usually employed in flutter analyses, they have been divided by $-\omega^2$.

$$Q_{rs} = \frac{1}{\omega^2} \int \phi_r \Delta p_s dS$$

$$\qquad (5)$$

$$Q_{r\delta} = \frac{1}{\omega^2} \iint \phi_r \Delta p_\delta dS$$

where S indicates the area of integration.

In Equation (4) the structural damping in each mode can be assumed to be the same in every mode and treated as an unknown variable for the purpose of conducting flutter analyses. Setting the determinant of the left-hand side to zero and solving for the roots yields the variables that are plotted in the V-g type of flutter analysis.

Alternatively, the velocity, Mach number and altitude can be held constant and the determinant of the left-hand side of Equation (4) can be computed as a function of frequency and plotted. The stability can be determined by the method of Landahl.

These analyses were conducted for the case study airplane at Mach 0.9 for several altitudes. The analyses indicated that the unaugmented airplane was stable.

A block diagram of the roll and yaw channels of the flight control system are shown on Figure 5. The control system was an analog system. It had several gains that could be
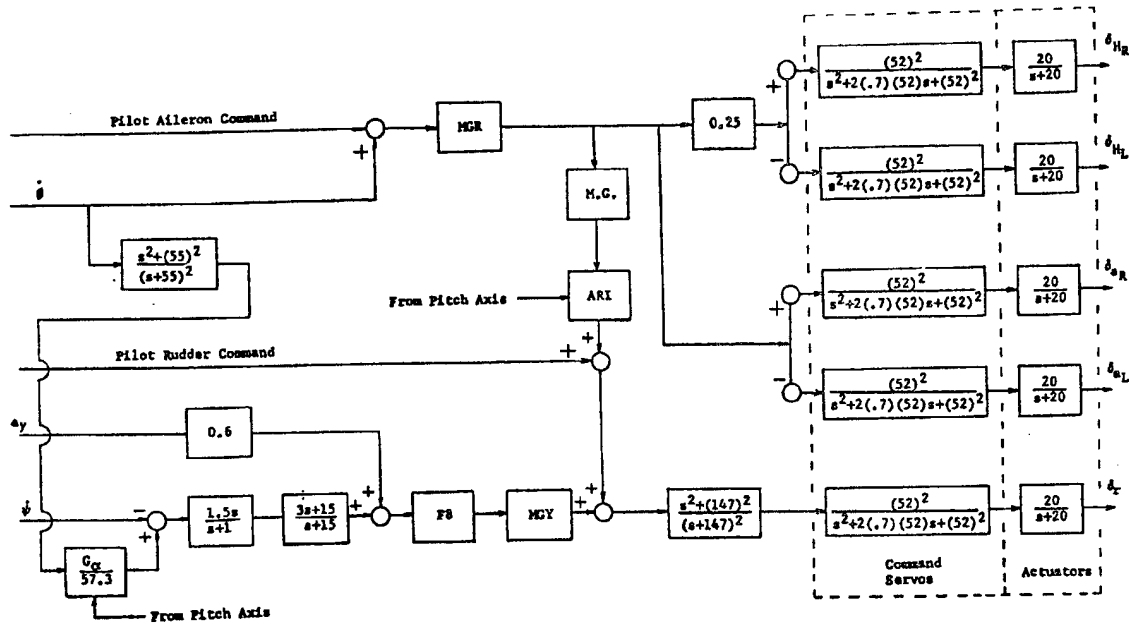
Figure 5: Reference Flight Control System

changed manually on the ground and it had gains that were computed as a function of the flight condition and changed automatically. The roll and yaw channels were essentially decoupled from the pitch channel. Two of the gains were varied as a function of the angle of attack and hence coupled with the pitch channel. However, these gains varied as a function of the steady angle of attack and provided virtually no dynamic coupling. The block labeled MGR is a manual gain in the roll channel; it was initially set at a value of 0.2. The block labeled M.G. is a manual gain in the aileron-rudder-interconnect; it was set a value of 1.0. The blocks labeled G_{ARI} and $G_\alpha/57.3$ are variable gains that are a function of the angle-of-attack. The block labeled F8 is a gain that varied as a function of the flight condition. The gains that varied as a function of the flight condition are tabulated on Figure 6.

The actuator was represented by a no-load, no-flow transfer function. The transfer function is different when the actuator is operating against a load and when high hydraulic flow rates are required. The no-load, no-flow transfer function was used because of its simplicity and because it was thought to be appropriate for predicting the onset of low amplitude ASE oscillations.

Similarly, the actuator stiffness was treated as a spring with constant stiffness. It was computed at a high frequency where the stiffness of the dynamic actuator approaches the stiffness of the hydraulic fluid. It appears in the equations of motion by way of the natural

H=0.9				
ALT.	S.L.	5K	15K	20K
F8	0.5	0.5	0.5	0.5
G/57.3	-.0105	-.0157	-.0262	-.0262
G_{ARI}	-.305	-.282	-.24	-.237
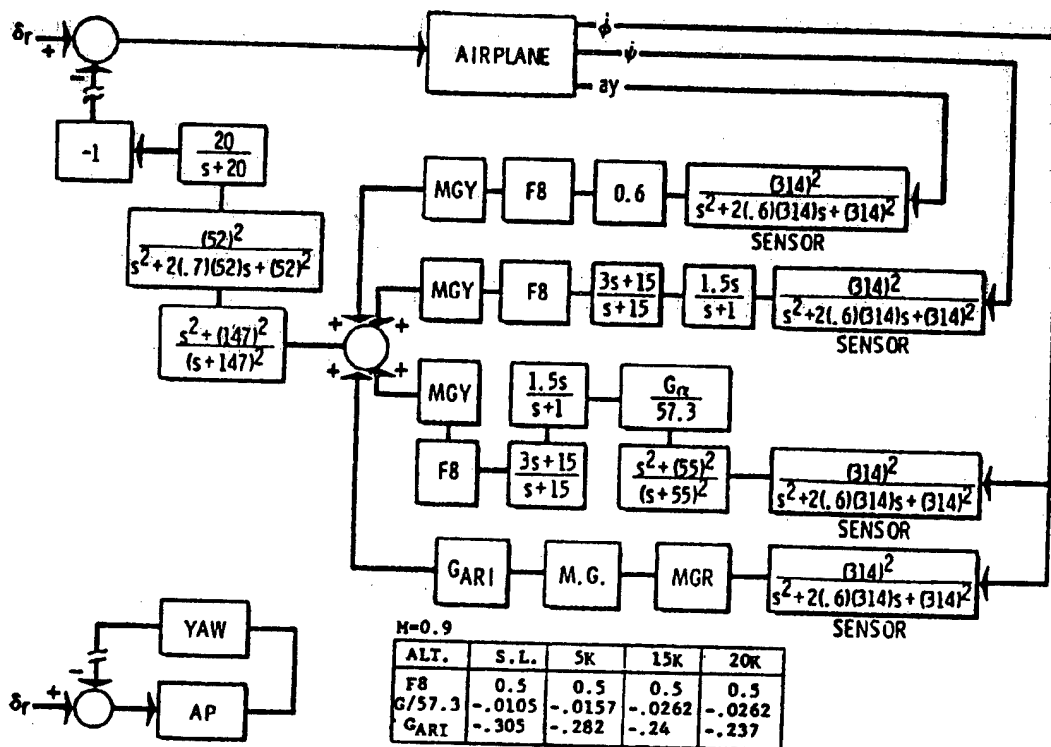
Figure 6: Yaw Loop

modes of vibration which were computed with a stiffness matrix in which each actuator spring was represented by a finite element.

The block diagram of the airplane with the yaw loop is shown in Figure 6. Note that the sensor transfer functions have been added to the feedback loop. These transfer functions relate the sensor outputs to the airplane motion at the sensor locations. Note also that a minus one has been added so that the feedback signal subtracts from the pilot input. The flight control system block diagram on Figure 5 shows the feedback signal adding to the pilot output. However, the negative sign is embedded in the feedback system or in the signs associated with control surface deflection.

The roll loop as used in the frequency response analyses is shown on Figure 7. One degree of pilot commanded aileron produces one degree of aileron deflection plus 0.25 degrees of differential horizontal tail deflection.
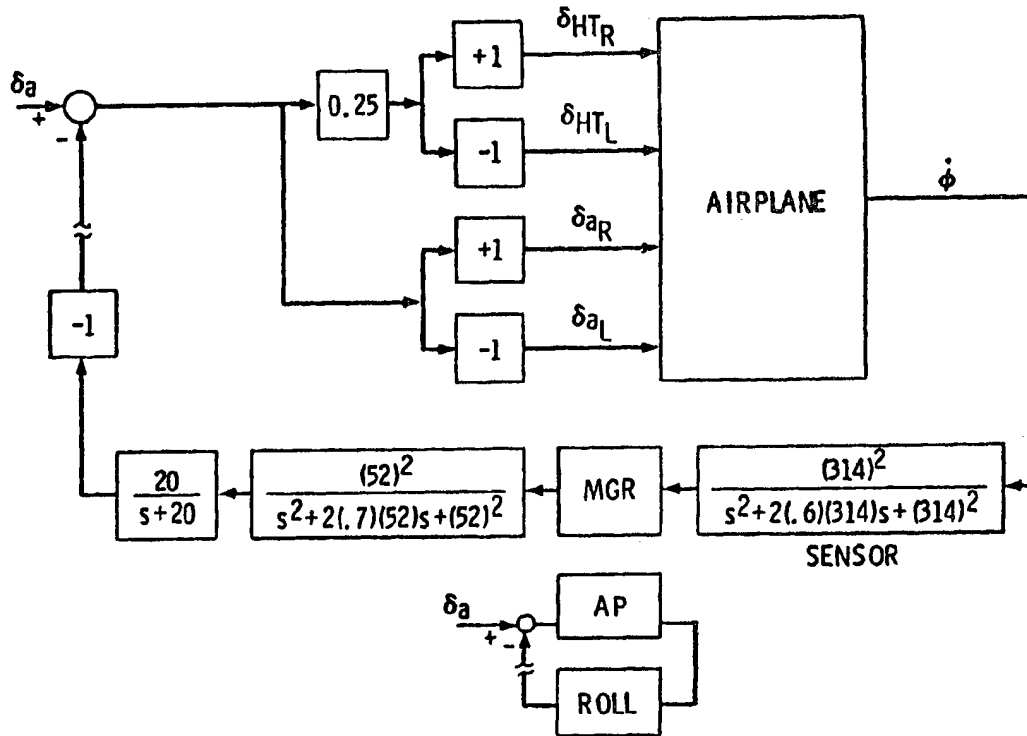
Figure 7: Roll Loop

Equation (4) was used to compute the response of the generalized coordinates to rudder excitation.

$$\left\{\frac{q_s}{\delta_r}\right\} = -\left[A_{rs}\right]^{-1}\left\{A_{r\delta_r}\right\} \tag{6}$$

The frequency response function for each of the yaw loop sensors was computed as follows:

$$\frac{a_y}{\delta_r} = -\omega^2 \lfloor h_s \rfloor \left\{\frac{q_s}{\delta_r}\right\}$$

$$\frac{\dot{\psi}}{\delta_r} = i\omega \lfloor \psi_s \rfloor \left\{\frac{q_s}{\delta_r}\right\} \tag{7}$$

$$\frac{\dot{\phi}}{\delta_r} = i\omega \lfloor \phi_s \rfloor \left\{\frac{q_s}{\delta_r}\right\}$$

where h_s is side deflection at the lateral accelerometer location,

         ψ_s is yaw deflection at the yaw rate gyro location,

         φ_s is roll angle at the roll rate gyro location, for unit amount of generalized coordinates q_s.

The feedback at the point where the yaw loop is broken, shown in Figure 6, can be expressed in the following form by substituting $i\omega$ for the Laplace variable s.

$$\frac{Feedback}{\delta_r} = T_{a_y}(\omega)\left(\frac{a_y}{\delta_r}\right) + T_{\dot\psi}(\omega)\left(\frac{\dot\psi}{\delta_r}\right) + T_{\phi_r}(\omega)\left(\frac{\dot\phi}{\delta_r}\right)$$

(8)

Substituting Equation (7) into Equation (8) yields the frequency response function relating the feedback in the yaw loop to rudder excitation with both the yaw and roll loops open. This function is plotted in polar form of the left side of Figure 8 for Mach 0.9 sea level flight condition. The upper left part shows the function when only the three rigid body degrees of freedom (DOF) are used. This figure has two scales. All data plotted inside the unit circle have a scale from zero to unity. Outside the unit circle, the scale is from unity to 11.4. This figure shows no enclosures of the minus one point. It is concluded that if the yaw loop were closed, the rigid body representation of the airplane would have no ASE instabilities.

The figure on the lower left part of Figure 8 shows the same frequency response data that was computed for a 9 DOF representation of the airplane. This representation has the same three rigid body DOF along with six natural modes of vibration DOF. The two antisymmetric modes of vibration shown in Figure 2 are included in this analysis. This figure indicates that if the yaw loop were closed, the 9 DOF representation of the airplane would be stable. The stability margins of an airplane with a flight control system are usually expressed in terms of gain margin and phase margin. The gain margin requirement is usually 6 dB, which means that the overall gain in the open-loop FRF could be increased by a factor of 2 before the closed-loop system became unstable. This requirement is equivalent to the requirement that the maximum allowable magnitude of the open-loop FRF (with all other loops closed) where it crosses the negative real axis on a Nyquist plot, shall not exceed 0.5. The magnitude of the maximum negative axis crossing is tabulated in Figure 8 along with the frequency at which the crossing occurs. The phase margin is defined as the angle between the negative real axis and the phase angle of the open-loop FRF where it crosses the unit circle. The phase margin requirement for a flight control system is usually ±60°. This means that the open-loop FRF phase angle (with all other loops closed) could be increased or decreased 60° before the closed-loop system became unstable. The phase margins can be estimated from the plots on Figure 8.
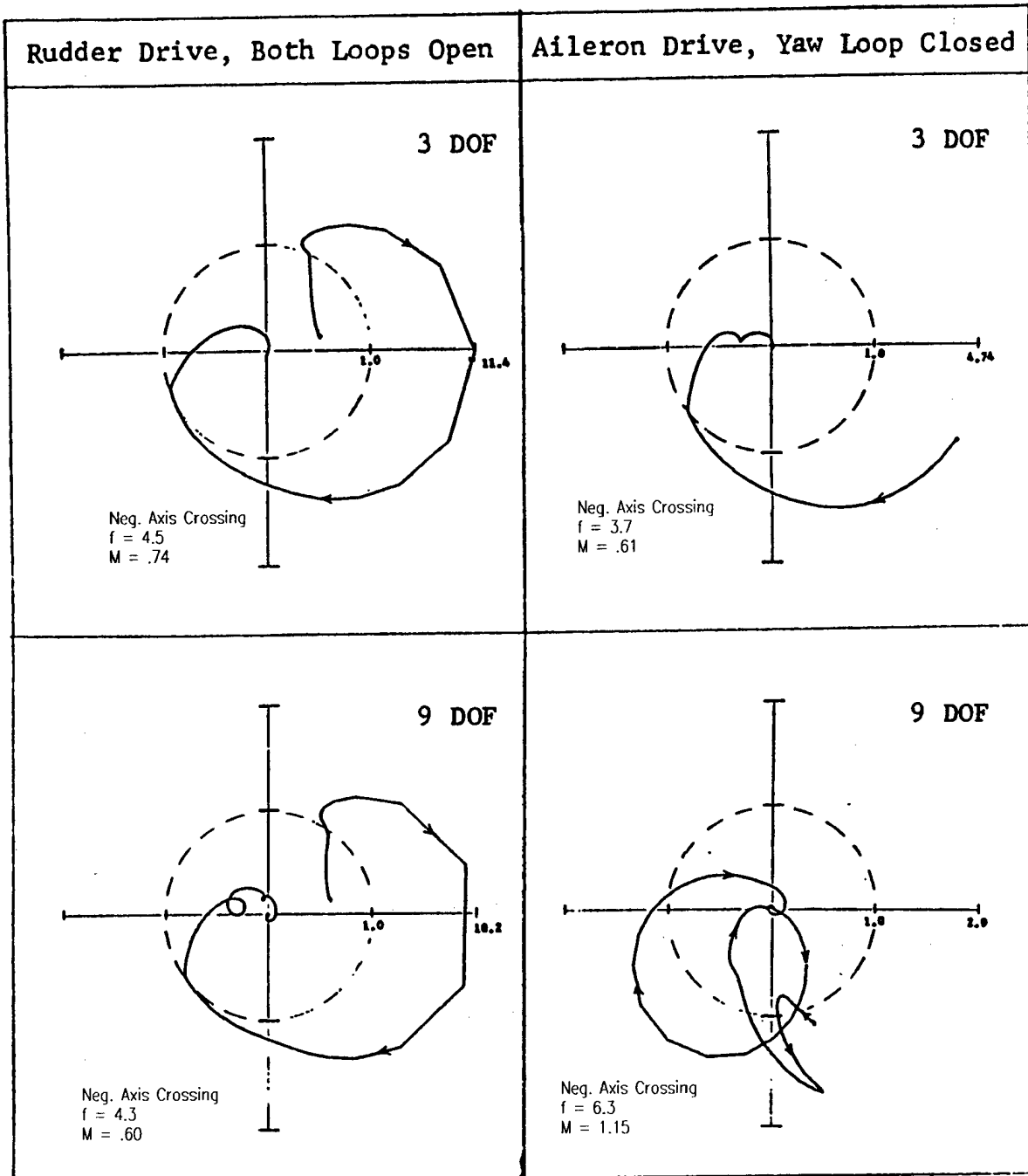
Figure 8: Nyquist Plots with Yaw Loop Closed First, M=0.9,
Sea Level, Missiles On, "Flexible" Stability Derivatives, Truncated GVT Modes

The next step in the analysis is to close the yaw loop. The numerator of the left hand side of Equation (8) is the rudder signal that was fed back and the denominator was the rudder signal that was input. Hence, the rudder signal that is fed back due to the sensor input, including the sign change at the summer, can be expressed as follows.

$$\delta_r = -T_{a_y}(\omega)a_y - T_{\dot\psi}(\omega)\dot\psi - T_{\dot\phi_r}(\omega)\dot\phi \tag{9}$$

Expressing the lateral acceleration, yaw rate and roll rate in terms of the generalized coordinates, as indicated by Equation (7) yields the following expression.

$$\delta_r = -T_{a_y}\lfloor -\omega^2 h_s \rfloor \{q_s\} - T_{\dot\psi}\lfloor i\omega\psi_s \rfloor\{q_s\} - T_{\dot\phi_r}\lfloor i\omega\phi_s \rfloor\{q_s\} \tag{10}$$

$$= \lfloor T_{\delta_r} \rfloor\{q_s\}$$

Substituting Equation (10) into (6) yields the equations of motion for the airplane with the yaw loop closed.

$$[A_{r_s}]\{q_s\} = -\{A_{r\delta_r}\}\lfloor T_{\delta_r} \rfloor\{q_s\} = -[A_{\delta_r}]\{q_s\} \tag{11}$$

$$[A_{rs} + A_{\delta_r}]\{q_s\} = 0 \tag{12}$$

The Nyquist plots shown on the left side of Figure 8 indicate that the airplane with the yaw loop closed would be stable at the Mach 0.9, sea level flight condition. Therefore, the closed loop system indicated by Equation (12) is stable.

The equations of motion for the airplane with the yaw loop closed and excited by an oscillatory aileron command are as follows.

$$[A_{rs} + A_{\delta_r}]\{q_s\} = -\{A_{r\delta_a}\}\delta_a \tag{13}$$

where δ_a means aileron plus horizontal tail differential deflection in the ratio of one degree aileron to 0.25 degrees horizontal tail.

The generalized coordinate response per δ_a can be computed from equation (13) and used to compute the roll rate at the sensor location per δ_a.

$$\frac{\dot\phi}{\delta_a} = i\omega\lfloor \phi_s \rfloor\left\{\frac{q_s}{\delta_a}\right\} \tag{14}$$

Using Figure 7, the ratio of aileron feedback, at the point where the loop is open, to the aileron command can be expressed as

$$\frac{Feedback}{\delta_a} = T_{\dot{\phi}_R}(\omega)\frac{\dot{\phi}}{\delta_a} \tag{15}$$

Substituting Equation (14) into Equation (15) yields the expression for the open loop feedback in the roll loop with the yaw loop closed. This frequency response function was computed and is shown plotted in polar form on the right side of Figure 8.

The plot on the upper right-hand side of Figure 8 is for the airplane represented with 3 DOF. This plot shows no clockwise enclosures of the minus one point. This plot indicates that the rigid airplane with both the yaw and roll loops closed would be stable.

The plot on the lower right-hand side of Figure 8 is for the airplane represented with 9 DOF. This plot shows one clockwise enclosure of the minus one point. The negative axis crossing has a magnitude of 1.15 at a frequency of 6.3 Hz. The direction of increasing frequency is shown by arrow heads on each of the plots of Figure 8. The plot on the lower right-hand side of Figure 8 indicates that the 9 DOF representation of the airplane is unstable when both the yaw and roll loops are closed and that the frequency of the instability is near 6.3 Hz. This frequency is very close to the frequency of the instability that was observed during flight tests. The large loop on the plot with its maximum magnitude centered near a phase angle of -135 degrees, is associated with the response of the mode one in Figure 2. This antisymmetric mode has a large component of fuselage roll to balance the large inertia roll moment produced by the wing and tip missile motion.

Additional information can be obtained from the plot on the lower right-hand side of Figure 8. Since the negative axis crossing has a magnitude of 1.15, a gain reduction in the roll channel of 1/1.15 would cause the open-loop frequency response to pass through the minus one point. Hence, neutral stability would occur for this reduced gain at this flight condition. That gain and any higher gain would cause the instability to occur. To reduce the gain so that the magnitude of the negative axis crossing was 0.5 (6 dB gain margin), the gain in the roll loop would have to be reduced by a factor of 0.5/1.15 or 44 percent.

The analysis was repeated with the control loops closed in the reverse order. The same conclusions with respect to ASE instability should be obtained. Only additional gain and phase information should be obtained. Plots of the open-loop frequency response function with the roll loop closed first are shown on Figure 9. Referring to the lower left-hand side plot (9 DOF), it can be seen that the open-loop frequency response for the roll loop with both loops open shows a clockwise enclosure of the minus one point. The magnitude of the negative axis crossing is 1.06 and the frequency is 6.3 Hz. This plot indicates that closing the roll loop with the yaw loop open would still cause the ASE instability.
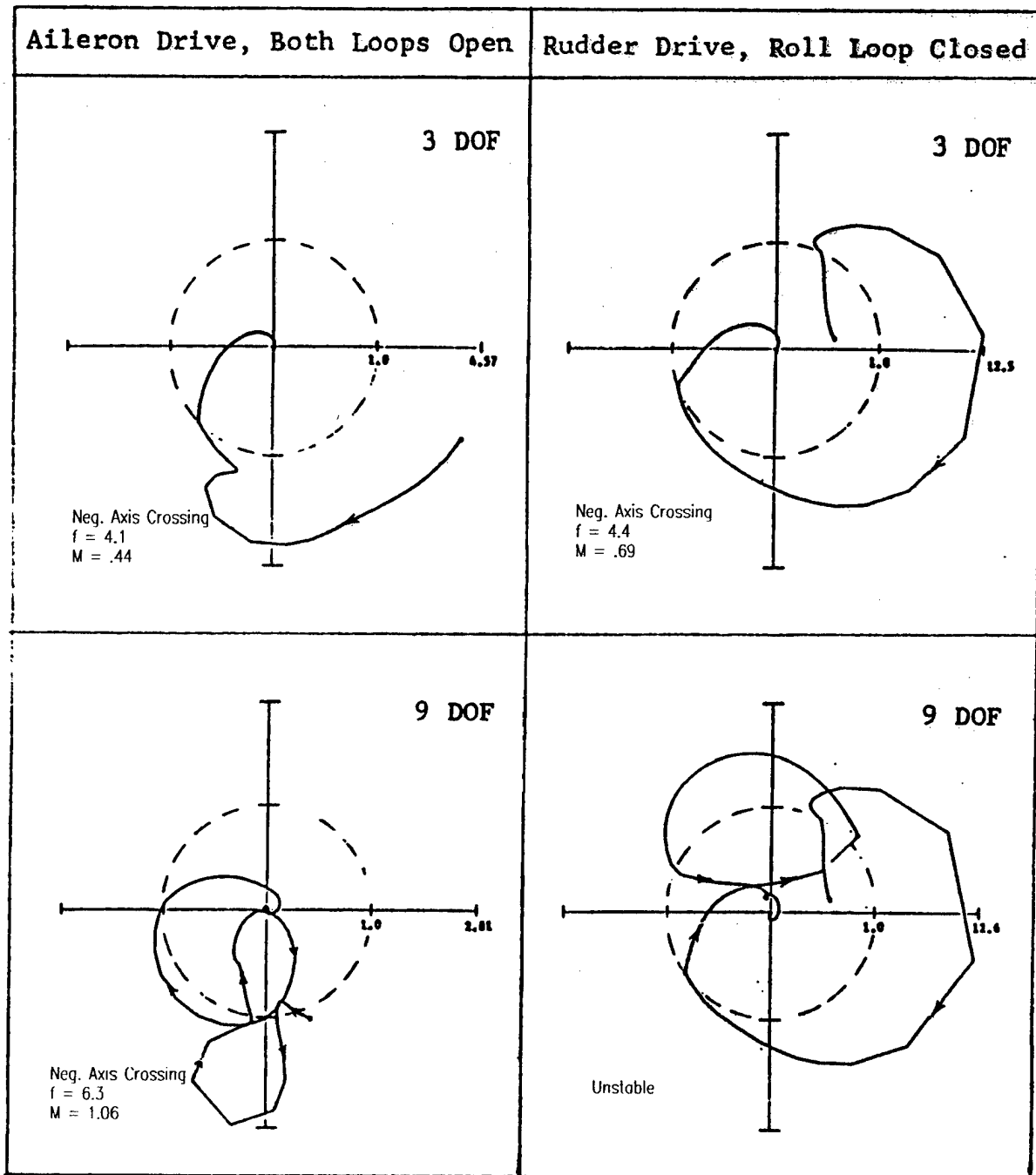
Figure 9: Nyquist Plots with Roll Loop Closed First, M=0.9,
Sea Level, "Flexible" Stability Derivatives, Truncated GVT Modes

The plot on the lower right-hand side of Figure 9 is the open-loop frequency response for the yaw loop with the roll loop closed. Since the left-hand plot shows the system to be unstable with the roll loop closed, the forward loop, G, (airplane with the roll loop closed) has one pole on the right-hand side of the Laplace plane. Substituting P equal one into the right-hand side of Equation (3), it can be seen that N has to equal minus one in order for the number of zeros on the right hand side of the Laplace plane to be zero. That is the plot of the open-loop frequency response function for the yaw loop, with the roll loop closed, would have to produce one counterclockwise of the minus one point in order to conclude that the airplane with both loops closed was ASE stable. If it did not produce one counterclockwise enclosure of the minus one point, the airplane with both loops closed would be unstable.

Returning to Figure 9, the plot in the lower right hand side does show a counterclockwise loop but it does not enclose the minus one point. The counterclockwise loop has its maximum magnitude centered near a phase angle of approximately 100 degrees. Since a reduction in the yaw loop gain would reduce the magnitude of each point along radial lines from the origin, it can be seen that no amount of reduction of the gain in the yaw loop would cause the counterclockwise loop to enclose the minus one point. This plot confirms the conclusion that this airplane could be stabilized by reducing the gain in the roll loop but it could not be stabilized by reducing only the gain in the yaw loop. This conclusion was consistent with flight test results.

The two plots on the upper part of Figure 9 show that the 3 DOF rigid body representation is stable with both loops closed. Therefore, regardless of the order in which the roll and yaw loops are closed the 3 DOF rigid representation indicates that the rigid airplane with both loops closed is stable and the 9 DOF representation indicates that the flexible airplane with both loops closed is unstable.

Although the analysis predicted the ASE instability which occurred during flight tests, the analysis did not predict as large a region of instability as was determined by flight tests. ASE analyses were conducted at Mach 0.9 at three altitudes, namely, sea level, 5,000 feet and 20,000 feet. Hence, the analysis indicated that the top of the unstable region was near 5,000 feet and the flight test data indicated that the top of the unstable region was at least as high as 20,000 feet.

Part of the unconservative characteristic of the analysis is attributed to the manner in which the computed aerodynamic terms for the rigid body DOF and the control surface aerodynamics were modified to agree with wind tunnel measured rigid stability derivatives corrected for aeroelastic effects. These stability derivatives were called flexible stability derivatives. The unsteady aerodynamic terms that were computed for the 3 DOF rigid body equations of motion were modified to agree with the flexible stability derivatives near zero frequency. When the 9 DOF analyses were conducted, six generalized coordinates representing six natural modes of vibration were added to the 3 DOF rigid body representation. All of the unsteady aerodynamic terms associated with the 3 DOF analysis were the same as they were in the 3 DOF analysis (that is, corrected to agree with the flexible stability derivatives). No change

was made to the computed unsteady aerodynamic terms that were produced by adding the six natural mode generalized coordinates. Hence, the six natural modes produced additional aeroelastic effects on the rigid body stability derivatives.

Later ASE analyses were conducted using the residual flexibility method. This method computes the residual flexibility that exists when a truncated set of natural modes are used in the equations of motion. The aeroelastic effects produced by the truncated set of natural modes plus the effect produced by the residual flexibility method provided the correct total aeroelastic effect. Hence, the computed unsteady aerodynamics for the rigid body DOF need only to be corrected to agree with wind tunnel based rigid stability derivatives.

A second method which approximated the residual flexibility method was also used. The aeroelastic effect contributed by the truncated set of natural modes was computed. This effect was subtracted from the total desired aeroelastic effect and the difference was applied to the rigid body stability derivatives. Hence, the sum of the modified rigid body aerodynamic terms plus the contribution produced by the truncated set of modes produced approximately the desired aeroelastic effect.

Later ASE analyses using these two methods for applying aeroelastic effects to the rigid body stability derivatives plus other refinements in the parameters used in the analyses improved the correlation between analysis and flight test data.

The ASE analysis conducted immediately after the ASE instability was encountered during flight tests provided assurance that the instability was an ASE instability, rather than flutter, and indicated that reducing the gain in the roll channel would restore stability. Although flight test experience indicated that a 50 percent reduction in the roll channel gain would stabilize the airplane, the selected correction consisted of reducing the roll channel gain to 60 percent of its original value and adding a notch filter to the roll channel. The notch filter was centered near 6.5 Hz and provided an additional gain reduction in a frequency band centered near 6.5 Hz.

Source of Additional Information

For a more in-depth description of the flight test experience, as well as a more detailed description of the ASE analyses that were conducted to improve the correlation between analysis and flight test results, the interested reader is directed to Reference 1, from which most of the figures in the present work were taken. Subsequent ground testing that was conducted for the purpose of improving the ASE mathematical model is reported in Reference 2.

The ASE instability for the Case Study A airplane was also reported in Reference 3 at the 16th Structures, Structural Dynamics and Materials Conference. At the same meeting a similar ASE instability on a different airplane was reported in Reference 4.

Recent ASE encounters through 1978, earlier close encounters, ASE analysis techniques, testing techniques, and design requirements are discussed in Reference 5.

Aeroservoelastic Instability, Case Study B

INTRODUCTION

Most ASE instabilities occur near the frequency of a structural natural mode of vibration. The frequency of the ASE instability for the Case Study A airplane with wing tip missiles, was very close to the frequency of the first antisymmetric natural mode of vibration of the structure. At or near the frequency of a structural natural mode, a small amount of oscillatory control surface deflection can cause a large response in the natural mode and a large output from the flight control sensors. The flight control system designer is usually successful in designing the system so that it does not destabilize one of the airplanes rigid body natural frequencies.

However, the instability for the Case Study B airplane occurred at a frequency that was considerably below the lowest structural natural frequency and above the frequency of the rigid body short period mode. The frequency at which the instability occurred can be explained as the frequency at which the phase lag in the open-loop FRF increased to 180° and the magnitude equaled or exceeded unity.

Case Study B complements Case Study A in that it demonstrates the use of one method of distinguishing a flutter instability from an ASE instability which was not applied in Case Study A. Specifically, Case Study B describes the measurement of the open loop frequency response function (FRF) in flight.

Case Study B Airplane Description

The Case Study B airplane was a fighter prototype with a cranked delta wing planform. The configuration is shown on Figure 10.

It had two sets of wing trailing edge control surfaces. The outboard control surfaces were called ailerons. They extended from an over-wing fairing that housed the aileron actuators to the wing tip missile launchers. The inboard surfaces, called elevons, could be actuated differentially as ailerons and symmetrically as elevators. The elevon actuators were located at the inboard end of each elevon in the fuselage. The airplane had a vertical tail with a full span trailing edge control surface called the rudder. The rudder actuator was located at the lower end of the rudder.

Flight control was provided by an analog fly-by-wire system. Pilot inputs to the controller and the rudder pedals were transmitted electrically to the actuator servo valves. The servo valves and the actuators were combined into units called integrated servo actuators (ISAs), allowing the hydraulic fluid flow path between servo valves and actuators to be considerably shortened.
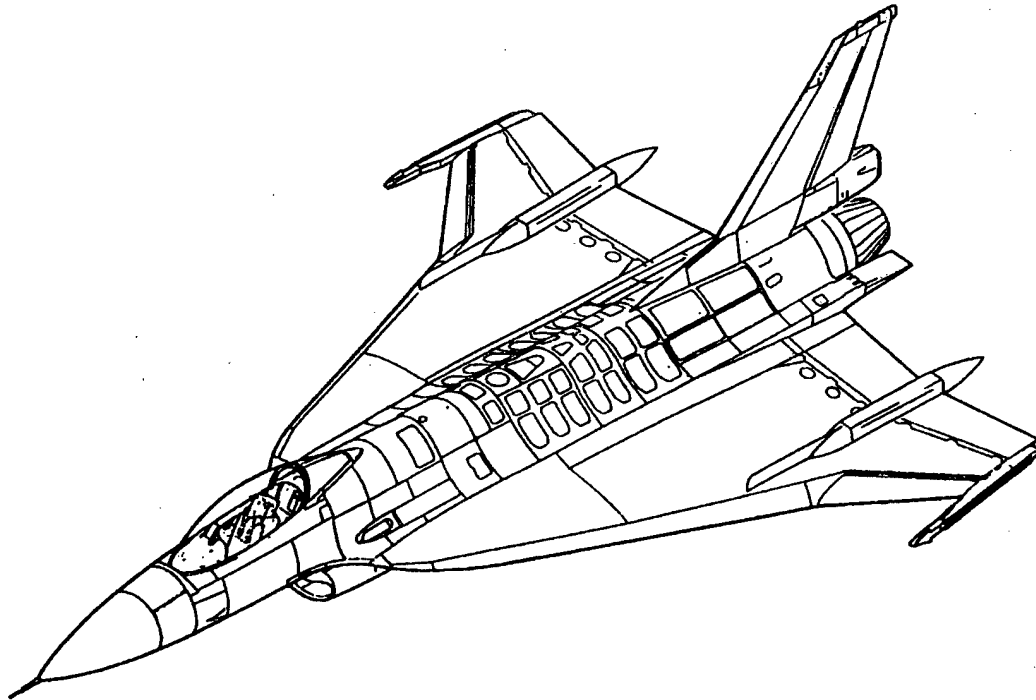
Figure 10: Case Study B Airplane Configuration

The airplane also had two sets of wing leading edge flap surfaces; these were not used for flight control.

The configuration carried missiles on wing tip launchers. Additional external stores were carried under the wing. Fuel was carried in the fuselage and in the wings.

Pre-Flight-Test Analyses and Tests

Flutter analyses, without the flight control system, were conducted with and without the tip missiles, for a wide range of fuel conditions and for many underwing store configurations. These analyses indicated that the airplane had at least a 20 percent flutter margin throughout its flight envelope.

Flutter model tests of the complete configuration without the flight control system were conducted in the NASA Langley Transonic Dynamics Tunnel. These tests indicated that the airplane without the flight control system had at least a 20 percent flutter margin through the transonic and low supersonic regions (to the wind tunnel limits).

Flight simulation studies indicated the airplane, with the flight control system engaged, to be stable throughout its flight envelope. These studies were conducted with the airplane

considered to be a rigid body. Stability derivatives were determined by wind tunnel tests conducted with rigid models. The wind tunnel based stability derivatives were modified to account for aeroelastic effects.

ASE analyses were conducted. These analyses indicated that no ASE instabilities should be expected throughout the flight envelope. The symmetric ASE analyses for the basic configuration without underwing external stores, indicated that the lowest gain and phase margins occurred in a frequency range between 2.5 and 3.0 Hz. This frequency range is below the first symmetric structural natural mode frequency which was 5.6 Hz, and considerably above the airplane's short period mode frequency.

Flight Tests

During flight tests the pilot reported feeling a pitching motion of the airplane. It occurred in a narrow Mach number range between 0.9 and 0.95. It was experienced at all altitudes up to 40,000 feet. The oscillations were either constant amplitude oscillations or lowly damped oscillations. The frequency of the oscillations ranged from 2.0 to 2.5 Hz.

Several flights were conducted in an effort to find an aerodynamic oscillatory excitation mechanism as an explanation for the pitch oscillations. After these flight tests proved to be unsuccessful in determining the source of the oscillations, a decision was made to measure the open loop FRF in the flight control pitch channel, in flight. However, while preparations were being made to make these measurements, a second decision was made to reduce the gain in the pitch channel by 25 percent. Subsequent flight tests showed that a 25 percent reduction in the pitch channel gain eliminated the pitch oscillations. At this point the need to measure the open loop FRF in flight was considerably reduced. However, the plan to make the measurements was continued in order to obtain better visibility for other potential corrective actions.

The objective of measuring the open loop FRF is to determine the stability of the closed loop system, as illustrated in Figure 11. A block diagram of a single input, single output closed loop system is shown on the upper left part of this figure. For this application, $G(s)$ represents the airplane transfer function and $H(s)$ represents the flight control pitch channel transfer function. The ratio of the feedback signal, $X_i(s)$, to the input signal, $X_i(s)$, is shown in the equation in the upper part of Figure 11.

The open-loop FRF can be measured by physically opening the feedback loop at the point at which it would subtract from the input signal. By applying an oscillatory input signal and measuring the oscillatory feedback signal, the open loop FRF relating the feedback signal to the input signal can be obtained, as illustrated by the block diagram and equation in the lower left part of Figure 11.
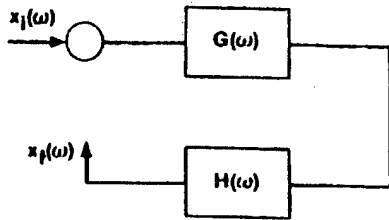
It is not feasible to physically open the loop during flight tests because of the associated risks of losing control of the airplane. However, the open-loop FRF can be measured without physically opening the loop. Two methods for measuring the open-loop FRF with the loop
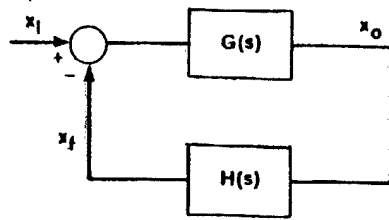
$$\frac{X_o(s)}{X_i(s)} = \frac{G(s)H(s)}{1 + G(s)H(s)}$$
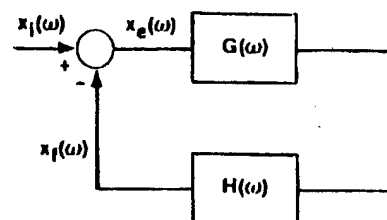
Measuring Open-Loop Frequency Response Function

With Loop Open   *Or*   **With Loop Closed**

$$G(\omega)H(\omega) = \frac{X_f(\omega)}{X_i(\omega)}$$

$$G(\omega)H(\omega) = \frac{X_f(\omega)}{X_e(\omega)} \quad \textbf{Direct Method}$$

$$G(\omega)H(\omega) = \frac{T(\omega)}{1-T(\omega)} \quad \textbf{Indirect Method}$$

$$T(\omega) = \frac{X_f(\omega)}{X_i(\omega)}$$

Figure 11: Open-Loop Frequency Response Measurements

closed are illustrated by the block diagram and the equations in the lower right part of Figure 11.

To obtain the open-loop FRF by the direct method, an oscillatory input signal is applied and the FRF for the ratio of the feedback signal to the error signal x_e is measured. The error signal is the difference between the input signal and the feedback signal. This method is called the direct method because the open-loop FRF is measured directly and requires no subsequent algebraic operation.

To obtain the open-loop FRF by the indirect method, an oscillatory input signal is applied and the FRF for the ratio of the feedback signal to the input signal is measured. This closed-loop FRF is called T. By substituting frequency for the Laplace variable for the closed-loop transfer function equation at the top of Figure 11 and substituting T for the left hand side of the equation, the equation can be solved for the product GH. This result is shown in the lower right part of Figure 11 as T divided by 1-T and is labeled the Indirect Method. This method is called the Indirect Method because the closed-loop FRF T is measured and the open-loop FRF is obtained as the algebraic ratio $T/(1-T)$.

Both the direct and indirect methods were used to measure the open loop FRF with the loop closed, in flight. A block diagram of the pitch channel is shown in Figure 12. The airplane block shows that the input to the airplane is the combined symmetric deflections of the elevons and the ailerons. The outputs of the flight control sensors were fed back through the pitch channel to produce the feedback signal. The flight control sensors were the angle of attack sensor, α, the vertical accelerometer, A_n, and the pitch rate gyro, Θ. During the FRF measurements, the excitation signal was applied through the autopilot while the pilot supplied input to maintain straight and level flight conditions at constant altitude and constant Mach number. The input signal was measured as the sum of the excitation signal and the pilot signal. The feedback signal was measured at the point before it was subtracted from the input signal to produce the error signal. The locations of the three signals that were measured are shown on the upper left part of the block diagram in Figure 12 and labeled as x_i, x_e, and x_f.
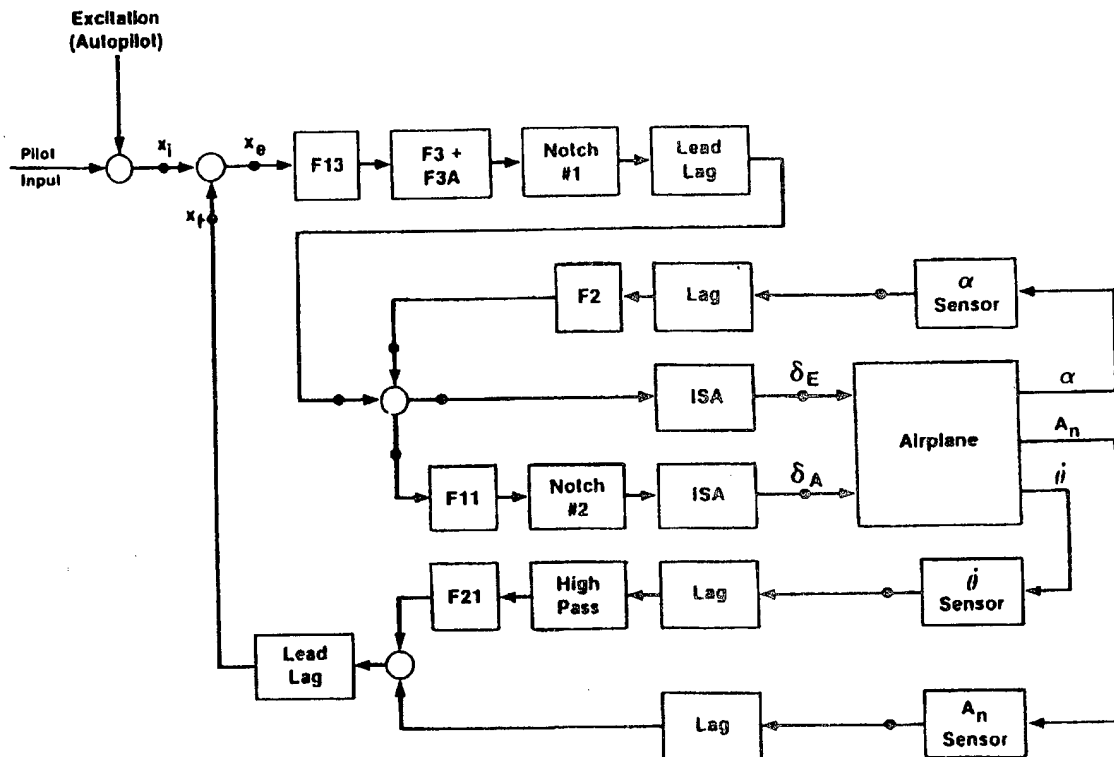
Figure 12: Case Study B Flight Control System Pitch Channel

The blocks in Figure 12 that are labeled with an alphanumeric symbol beginning with the letter F are gains; both fixed and variable. The blocks labeled notch, lead lag, lag and high pass, indicate transfer functions for notch filters, lead lag functions, lag functions, and high pass filters. The blocks labeled ISA are the transfer functions for the integrated servo actuators.

The blocks labeled sensors are the transfer functions for the angle-of-attack sensor, the pitch rate gyro sensor and the normal accelerometer sensor. The numerical value of the gains and the transfer functions are not given because the purpose of Case Study B is to show the results of measuring FRFs in flight; not to compare computed and measured FRFs. All gains were constant over the Mach number range from 0.85 to 1.0. Also, there was no variation in the transfer function blocks.

The FRF could be measured by applying the excitation at a discrete frequency and measuring the desired ratios at the discrete frequency. By repeating the measurements at a sufficient number of points the open-loop FRF could be produced. A more efficient method of measuring the FRF is by the use of a harmonic analyzer that employs the Fast Fourier Transform (FFT) algorithm. The FFT algorithm computes the discrete Fourier transform of a sequence of measurements equally spaced in time in a very efficient manner (minimum number of mathematical operations) if the number of time measurements is equal to a power of two (for example, 512 or 1024). A harmonic analyzer of this type was used to process the flight test data. This harmonic analyzer could accept 1024 measurements at equal time intervals and compute the FRF for the ratio of the two signals at 512 positive frequency points in approximately 0.03 second after the last of the two sets of data had been received. Hence, the FRF could be computed in virtually real time. Therefore, the excitation signal through the autopilot did not need to be a discrete frequency. Any type of input signal could be used and the harmonic analyzer could compute the FRF.

Two types of excitation are commonly used to measure FRFs. One is commonly called sine sweep excitation and the other is called random excitation. Sine sweep excitation applies an excitation signal at a discrete frequency and the frequency is slowly changed by sweeping from a selected minimum frequency to a selected maximum frequency or vice versa. The random excitation method was selected for the Case Study B airplane. One reason for this selection is because the random excitation produces airplane motion that feels to the pilot as if he is flying in random turbulence. Hence, the ride comfort (or discomfort) and the degree of difficulty in maintaining straight and level flight appears to the pilot to be approximately the same from the beginning to the end of the applied excitation period. Whereas, during the sine sweep excitation the airplane response at the pilot station can vary to large degree as the frequency is slowly changed. Hence, the pilot feels like he is on a roller coaster ride with varying degrees of difficulty in maintaining straight and level flight throughout the frequency sweep.

The harmonic analyzer that was used, processed the data supplied to it in blocks called records. Each record consisted of 1024 measurements, for each of two signals, at equal time intervals. For this application the time intervals or sampling rate was set such that a record length was approximately 25 seconds. Hence the time interval was approximately 25/1024 or 0.0244 seconds. The FRF frequency increments were 1/25 or 0.04 Hz. Since 1024 data points are transformed into 512 positive frequency increments, the frequency range was from 0.04 Hz to (512)(0.04 Hz) or approximately 20 Hz. To improve the statistical accuracy the process was repeated for many records and the FRF data were averaged. To reduce the total time that the excitation was applied and to obtain better statistical accuracy, a new record was analyzed when 25 percent of new data had been added to the previous record and the oldest 25

percent of the previous record had been discarded. Using this 75 percent overlap on successive records, 32 records could be processed and averaged in a total excitation time of 220 seconds. These data are tabulated in Figure 13.

Direct   **Indirect**

f = 2.25 Hz   f = 2.28 Hz

Mach = 0.95   No. of FRF Averages = 32
Altitude = 40K ft   75% Overlap
Frequency Range = 0 to 20 Hz   Total Record Length = 220 sec.
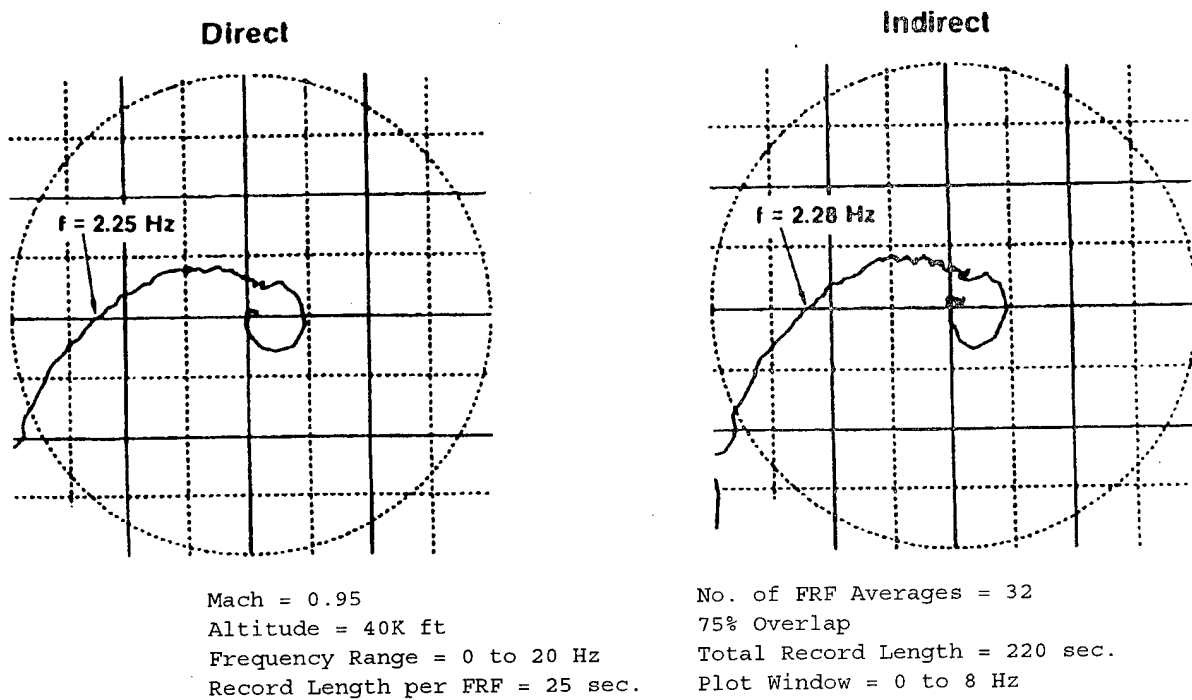Record Length per FRF = 25 sec.   Plot Window = 0 to 8 Hz

Figure 13: Comparison of Direct and Indirect Methods for Measuring Open-Loop FRF

A comparison of the open-loop FRF as obtained by the direct and indirect methods for one flight condition is also shown on Figure 13. The FRFs are plotted in polar form or as Nyquist plots. The dotted circle on each plot is the unit circle. Although the frequency range was normally from zero to 20 Hz, the data are plotted up to 8 Hz. The data are plotted for negative feedback systems so the minus one point is the critical point. To describe the direction of the plot with increasing frequency it is noted that the magnitude of the plot at the low frequency end is greater than the unit circle and as the frequency is increased the magnitude of the plot approaches the center of the unit circle. Hence, the direction of the plot with increasing frequency is clockwise. It can be seen that the two methods for obtaining the open-loop FRF, with the loop closed, produce results that are very nearly the same. In particular, both methods show a negative axis crossing with a magnitude of approximately 0.63, at a frequency near 2.25 Hz. Since the measurements were made with the gain in the pitch channel reduced to 75 percent of the value that it had when the pitch oscillations were experienced, the magnitude of all points would be expected to be increased by the ratio of 1/0.75 or 4/3 if the measurements had been made before the gain reduction had taken place. Hence, the magnitude of the negative axis crossing would have increased from 0.63 to 0.84.

This magnitude is very close to unity and would indicate that the closed-loop system would be stable but lowly damped.

The flight conditions at which the open-loop FRF was measured are shown in Figure 14. Measurements were made at three Mach numbers for each of the three altitudes and at six Mach numbers for one altitude.
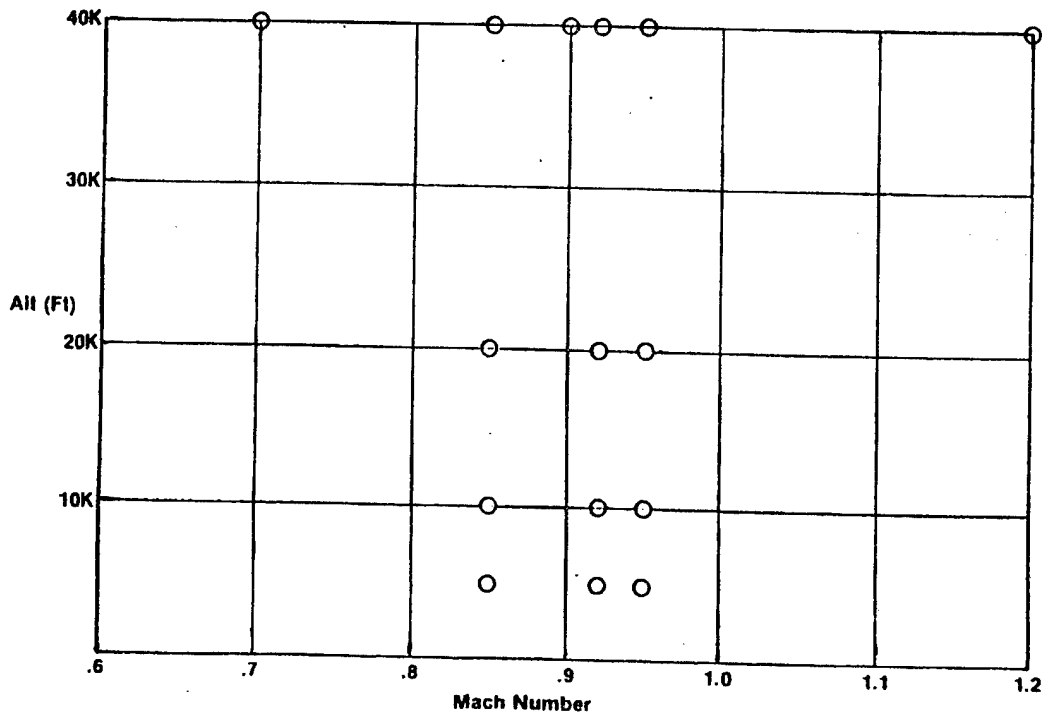

Figure 14: Flight Conditions at which Open-Loop FRF was Measured

Plots of the open-loop FRF obtained by the direct method at 40,000 feet for each of six Mach numbers are shown on Figure 15. It can be seen that the negative axis crossing has the largest magnitude at 0.95 Mach number and that the magnitudes at lower Mach numbers are progressively lower. The magnitude of the crossing at the higher Mach number is also significantly lower. Hence, these plots show that the closed-loop system would be the closest to unstable at 0.95 Mach number.

The magnitude of the negative axis crossings, or the crossings with 180 degree phase angle, are plotted versus Mach number at 40,000 feet on Figure 16. The measurements were made with various levels of excitation input that are identified as low, intermediate and high levels. The measurements that were made with and without wing fuel are identified on the plot. The scale on the left indicates the magnitude of the crossings with the pitch channel gain reduced to 75 percent of its original value. The scale on the right has been increased by a factor of 4/3 to

Direct Method, 40,000 Ft
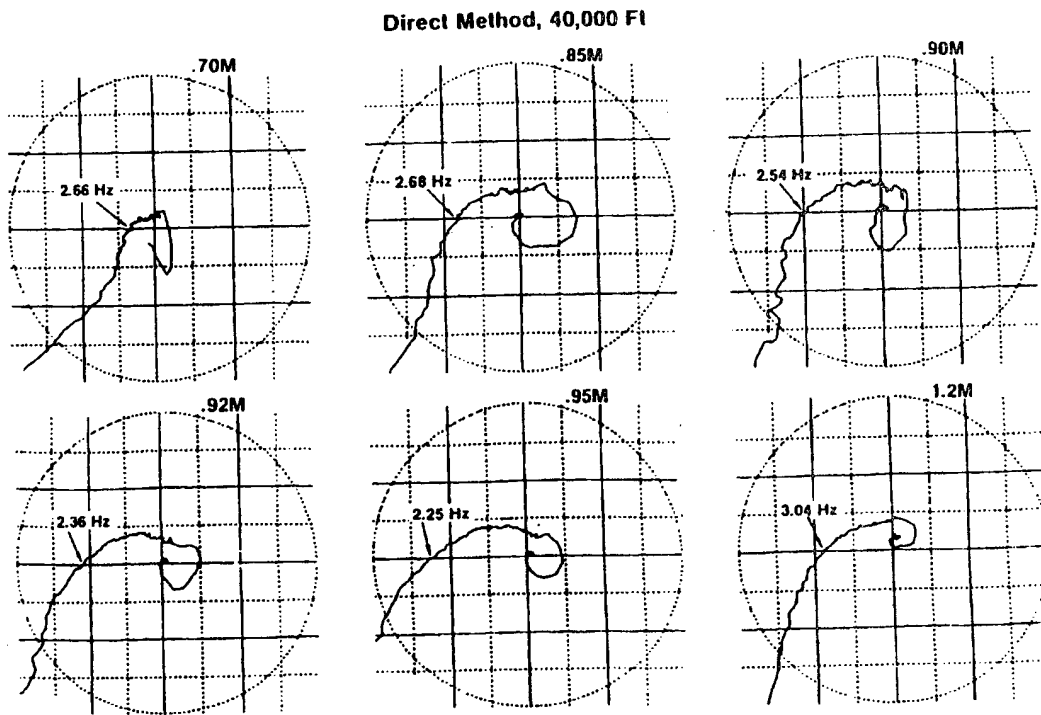
Figure 15: Direct Method FRF Measurements at 40,000 ft
Showing Maximum Negative Axis Crossing Near Mach 0.95

40,000 Ft

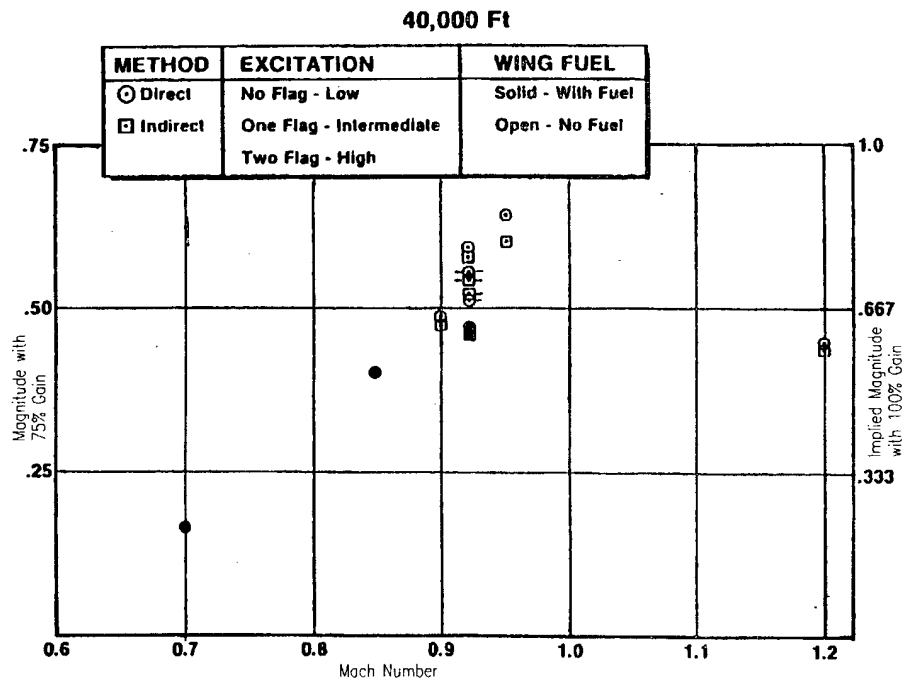| METHOD	EXCITATION	WING FUEL
⊙ Direct	No Flag - Low	Solid - With Fuel
⊡ Indirect	One Flag - Intermediate	Open - No Fuel
	Two Flag - High	

Figure 16: Magnitude of Negative-Axis Crossing
vs. Mach Number at 40,000 ft, Showing Maximum Near Mach 0.95

show the magnitude of the crossing that would have existed, by implication, before the gain was reduced. It can be seen that the implied negative axis crossing was very close to unity at 0.95 Mach number before the gain was reduced. Since the measured negative axis crossing does not equal or exceed unity for the 100 percent gain implies that measurement error accounted for the short fall or that the measurements were not made at the critical Mach number. That is, if the measurements had been made for smaller Mach number variations near 0.95 Mach number, a Mach number might have been found that produced a negative axis crossing that equaled or exceeded unity. However, the data that were obtained were in agreement with the original observations that the pitch oscillations occurred in a narrow Mach number range between 2.0 and 2.5 Hz.

The magnitude of the negative axis crossings at 20,000 feet and 10,000 feet versus Mach number are shown in Figures 17 and 18. These plots indicate the minimum stability occurred at 0.92 Mach number at these two altitudes.

Summary

The objective of measuring the open-loop FRF for the pitch channel, in flight, was to help diagnose the source of the pitch oscillations experienced by the pilot during flight testing in a narrow Mach number range between 0.9 and 0.95, in a frequency range between 2.0 and 2.5 Hz. Before the open-loop FRF was measured, flight tests were conducted with the pitch channel gain reduced to 75 percent of its original value. The pitch oscillations no longer occurred after the gain was reduced. Hence, the need for measuring the open-loop FRF in flight was highly reduced. However, the planned measurement of the open-loop FRF in flight was continued with the pitch channel gain reduced to 75 percent of its original value.

By looking at Figure 15 and visualizing what the sequence of open-loop FRFs would look like if the magnitude of each point was increased by a factor of 4/3, it can be seen that the measurements with the original pitch channel gain would have shown the minus one point to be very nearly enclosed by a clockwise enclosure. It would have been clear that the pitch oscillations were caused by the flight control system and that a reduction of the pitch channel gain would have stabilized the pitch oscillations. These plots would also have shown that the lowest gain margins occurred in the Mach number range between 0.90 and 0.95 and that the frequency ranged from 2.54 Hz at Mach 0.9 to 2.25 at Mach number 0.95.

It would also have been clear from the sequence of plots in Figure 15 that the pitching oscillations were not likely to be caused by flutter. If flutter were the source of the instability, a clockwise loop near a structural mode frequency would have been expected at a low dynamic pressure flight condition, such as Mach number 0.7 at 40,000 feet. If flutter were the source of the pitch oscillations, the magnitude of the structural mode loop would have increased and the frequency at which the largest magnitude in the loop occurred would have approached the 2.0 to 2.5 Hz range as the flutter boundary was approached. Figure 15 does not show these characteristics. One can therefore conclude that flutter was not the likely source of the pitch oscillations.
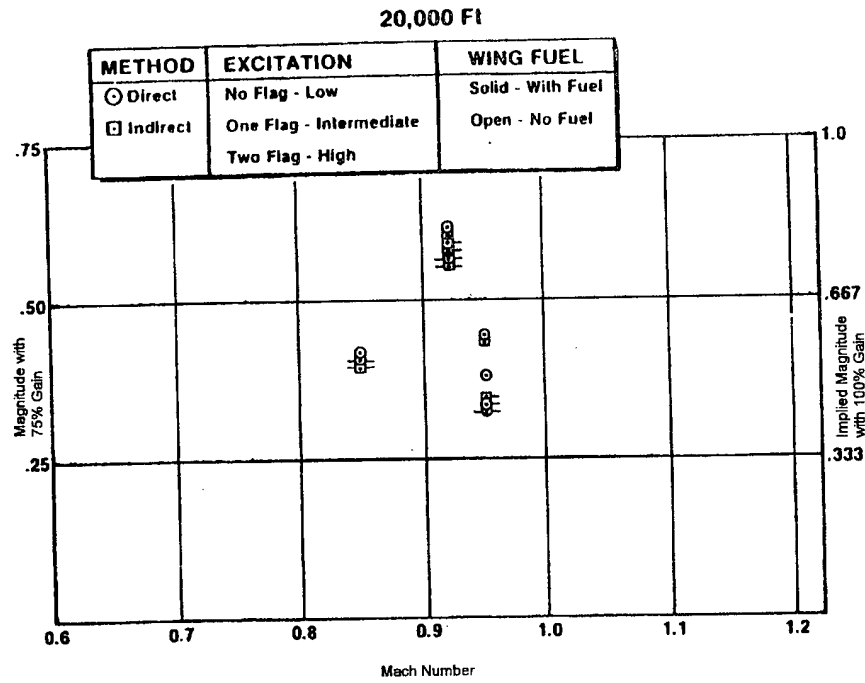
Figure 17: Magnitude of Negative-Axis Crossing
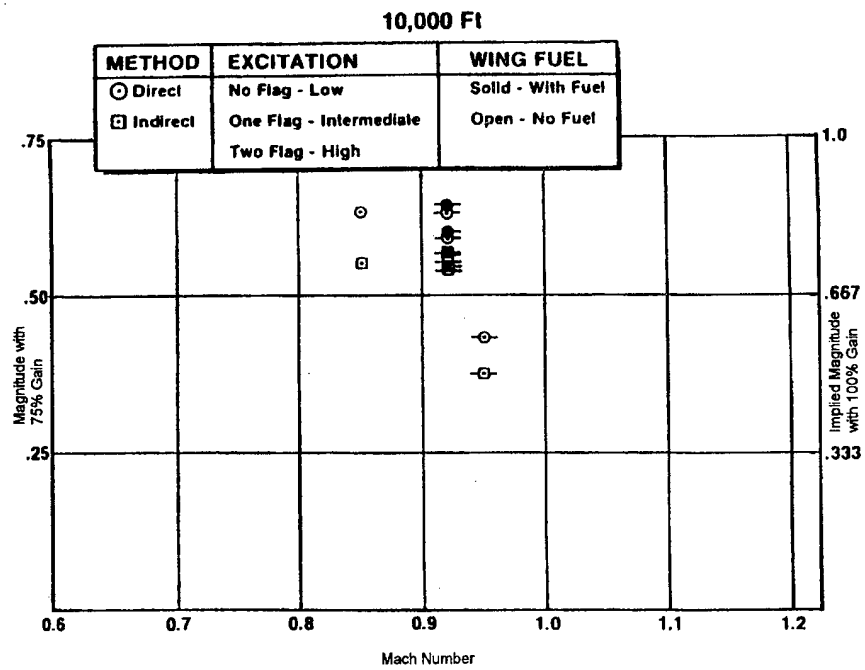vs. Mach Number at 20,000 ft, Showing Maximum Near Mach 0.92

Figure 18: Magnitude of Negative-Axis Crossing
vs. Mach Number at 10,000 ft, Showing Maximum Near Mach 0.92

The ASE analyses that were conducted prior to the flight tests showed open-loop FRFs that were similar to the ones shown in Figure 15 in that the negative axis crossing with the largest magnitude occurred in the frequency range between 2.5 and 3.0 Hz. However, the magnitude of the negative axis crossing was not sufficiently high to expect an instability in flight. The ASE analyses might have under predicted the magnitude of the negative axis crossing because the reduction in the control surface effectiveness due to aeroelasticity in the transonic range, might have been over predicted. If the control surface effectiveness, in the transonic region, was predicted to be lower than it actually was, this under prediction would lead to the ASE analyses predicting lower negative axis crossings. It would also encourage the flight control system designer to increase the gain in the pitch channel gain to compensate for the reduction in the control surface effectiveness.

As the frequency increases from zero to approximately 2.25 Hz, the phase lag in the pitch channel open loop FRF increases to 180 degrees. The phase lag is produced primarily by the ISA and the pitch channel. The oscillations were not caused by a rigid body natural frequency, such as the short period mode, or by a natural structural mode. Instead, they occurred because the gain in the open loop FRF was too high when the phase angle was 180 degrees. The frequency of the oscillation was determined by the frequency at which the phase angle reached 180 degrees.

It was demonstrated during these flight tests that the open-loop FRF can be measured without actually opening the loop. Both the direct and indirect methods were used. For this application, the two methods yielded virtually the same open-loop FRF measurement.

Source of Additional Information

The Case Study A airplane, without the tip missiles, encountered an instability in flight that was similar to the instability encountered by the Case Study B airplane. With the tip missiles removed from the Case Study A airplane, the first antisymmetric natural mode of the structure is 8.0 Hz. The Case Study A airplane without the tip missiles encountered an instability at a frequency near 3.5 Hz. This frequency is far below the first natural frequency of the structure and above the rigid body natural frequency. This instability is reported in References 1, 2 and 3.

Techniques for measuring the open-loop FRF without physically opening the loop were developed and demonstrated during wind tunnel tests of a flutter model with a flutter suppression system. These techniques and the results obtained by applying them are described in References 6, 7 and 8. To the author's knowledge, the first time these techniques were applied to an airplane in flight was when these techniques were applied to the Case Study B airplane.

LESSONS LEARNED

Some of the lessons learned from the experience gained from the Case Studies A and B are discussed.

- **Conduct ASE Analyses at Multiple Flight Conditions**

  It is generally not sufficient to conduct ASE analyses only at maximum flight conditions. Flight control systems frequently employ variable gains that are scheduled to change as a function of flight conditions. Stability derivatives for a rigid airplane when plotted versus mach number frequently peak in the transonic region. Aeroelastic effects modify the stability derivatives for each flight condition. Hence, ASE analyses should be conducted for a sufficiently large number of flight conditions to ensure that the entire flight envelope has been adequately investigated.

- **Conduct ASE Analyses for Multiple External Store Configurations**

  If the airplane carries external stores mounted on the wings, the natural modes of vibration can change with each store configuration. ASE instabilities can occur at different frequencies and at different flight conditions for different external store configurations. ASE analyses should be conducted for a sufficient number of store configurations to ensure that all possible external store configurations, including take-off store loadings and downloadings, have been adequately investigated.

- **Flight Control System Ground Tests**

  Open-loop FRF tests which are conducted on the airplane on the ground, should not be used, in lieu of ASE analyses, as a means of inferring ASE stability characteristics in flight. These tests are directly applicable only to the stability of the airplane on the ground. Open-loop FRF tests of the airplane on the ground (preferably supported by a soft suspension system to remove the effects of the landing gear) should be used to improve the correlation between the ASE mathematical model (without the aerodynamic representation) and the test data. One reason that ground tests are important is because flight control sensors are frequently located on the airplane where the response of the sensor is very low for one or more of the natural modes with the lowest frequencies. Hence, small errors in the computed mode shape at the sensor locations can make large percentage differences in the FRF.

- **Aeroelastic Effects on Stability Derivatives**

  The flight control system designer frequently conducts analyses with the airplane considered to be a rigid body. Stability derivatives are frequently obtained from wind tunnel tests of a rigid model. Hence these stability derivatives are sometimes called rigid stability derivatives. Aeroelastic effects are frequently computed by using a stiffness matrix representation of the airplane structure. The rigid stability derivatives modified by aeroelastic effects are sometimes called flexible stability derivatives. The flexible stability derivatives are used by the flight control designer.

When ASE analyses are conducted, the unsteady aerodynamic terms are computed. If only rigid body DOF (degrees of freedom) are to be used in the analysis, the computed unsteady aerodynamic terms should be modified so that they agree with the flexible stability derivatives as the frequency approaches zero.

If both rigid body DOF and natural modes of vibration DOF are included in the ASE analysis, the modification of the rigid body unsteady aerodynamics varies with the number of natural modes included in the analysis. The same stiffness matrix that was used to conduct the static aeroelastic analysis should be used to compute the natural modes. If a lumped mass is located at each of the aerodynamic loading points used in the aeroelastic analysis, then the stiffness matrix is loaded with inertia loads in the vibration analysis at the same loading points used in the aeroelastic analysis. The maximum number of modes that can be computed is equal to the number of mass points. If all of the natural modes are included in the ASE analysis then the computed unsteady aerodynamic terms for the rigid body DOF should be modified to agree with the rigid stability derivatives as the frequency approaches zero. That is, the complete set of natural modes produces the same aeroelastic effect, as the frequency approaches zero, as the stiffness matrix produced in the aeroelastic analysis.

When a truncated set of modes (subset of the total number of modes) is used in the analysis (to reduce computational costs), only part of the stiffness effect is represented. If a truncated set of modes is used in the ASE analysis, the computed unsteady aerodynamic terms for the rigid body DOF should be modified, such that the sum of the aeroelastic effects in the modified rigid body aerodynamic terms plus the aeroelastic effect produced by the truncated set of modes, equals the correct total aeroelastic effect, as the frequency approaches zero. It should be noted that control surface aerodynamic terms are included when modifying computed unsteady aerodynamic terms for the rigid body DOF. Methods for making aerodynamic modifications are discussed in Reference 1.

- **Measure Open-Loop FRF Without Physically Opening the Loop**

  If an instability is encountered during flight tests the source of the instability is frequently in doubt. The measurement of the open-loop FRF at a series of speeds approaching the speed at which the instability was encountered, can be an effective means of determining whether the instability is caused primarily by ASE of flutter. It is also useful in determining the changes needed to eliminate the instability.

REFERENCES

1. Peloubet, R.P. Jr., Haller, R.L, Cunningham, A.M., Cwach, E. E. and Watts D., "Application of Three Aeroservoelastic Stability Analysis Techniques," AFFDL-TR-76-89, September 1976.

2. Peloubet, R.P. Jr., Haller, R.L., McComb, C.N., and Bolding, R.M., "Ground Vibration Testing of Fighter Aircraft With Control Systems," AFFDL-TR-76-110, December 1976.

3. Peloubet, R.P. Jr., "YF-16 Active-Control-System/Structural Dynamics Interaction Instability," presented as Paper 75-823 at the AIAA/ASME/SAE 16th Structures, Structural Dynamics and Materials Conference, Denver, Colorado, May 27-29, 1975.

4. Authors, T.D. and Gallager, J.T., "Interaction Between Control Augmentation System and Airframe Dynamics on the YF-17," presented as Paper 75-824 at the AIAA/ASME/SAE 16th Structures, Structural Dynamics and Materials Conference, Denver, Colorado, May 27-29, 1975.

5. Felt, L.R., Huttsell, L.J., Noll, T.E., and Cooley, D.E., "Aeroservoelastic Encounters," *Journal of Aircraft*, Vol. 16, Number 7, July 1979, pp. 477-483.

6. Peloubet, R.P. Jr., Haller, R.L. and Bolding, R.M., "F-16 Flutter Suppression System Interaction Feasibility Study and Wind Tunnel Tests," *Journal of Aircraft*, Vol. 19, Number 2, Feb. 1982, p. 169.

7. Peloubet, R.P. Jr., Haller, R.L. and Bolding, R.M., "Wind Tunnel Demonstration of an Active Flutter Suppression System Using F-16 Model with Stores-Adaptive Studies," AFWAL-TR-83-3046, Vol II, August 1984.

8. Peloubet, R.P. Jr., Haller, R.L. and Bolding, R.M., "Recent Developments in the F-16 Flutter Suppression With Active Control Program," *Journal of Aircraft*, Vol. 21, Number 9, Sept. 1984, p. 716.